# UNDERSTANDING THE DIFFERENT RESPONSES OF DIURNAL SURFACE AND AIR TEMPERATURES TO EVAPORATION ACROSS VEGETATION TYPES

## Dissertation
(kumulativ)

zur Erlangung des akademischen Grades

Doctor rerum naturalium
(Dr. rer. nat.)

vorgelegt dem Rat der Chemisch-Geowissenschaftlichen Fakultät der Friedrich-Schiller-Universität Jena

von Annu Panwar, M. Sc. (Atmosphere and Ocean Science)
geboren am 14. Februar 1993 in Uttarakhand, India

**Gutachter:**

1. Prof. Dr. Christiane Schmullius, Friedrich-Schiller-Universität, Jena, Germany
2. Dr. PD Axel Kleidon, Max-Planck-Institut für Biogeochemie, Jena, Germany

Tag der Verteidigung: 26.01.2022

*Have a look at these great blessed trees, who live only for the welfare of others, themselves facing the severity of stormy winds, heavy showers, heat and snow, all the while protecting us from them. The birth of trees is the most blessed in the world, as they contribute unreservedly to the well-being of all creatures. Just as no needy person ever returns disappointed from the house of a benevolent individual, similarly do these trees do for those who approach them for shelter. All of their many parts - leaves, flowers, fruits, shadow, roots, bark, wood and fragrance, are useful to others. . . A tree does not withdraw its cooling shade even from the one who has come to cut it. -Bhagavata Purana 10.22.32-35*

# Contents

# Acknowledgments

The research presented in this Thesis benefited from the efforts of many people who I want to mention here. Most importantly, I am extremely thankful to Axel Kleidon, Christiane Schmullius and Maik Renner, without their guidance this work would have been impossible. I express my deep sense of gratitude to Axel Kleidon for believing in me and offering me a position as a doctoral candidate. He is also the person who provided me most of the guidance, freedom to pursue my own ideas and positive energy that kept me enthusiastic for great research. Countless productive discussions with him and Maik Renner led to interesting findings.

Weekly writing meetings organized in group helped immensely to shape my manuscripts. I want to thank all of my colleagues, Luigi Conte, Muye Du, Jonathan Minz and Sarosh Alam Ghausi for their useful suggestions on my manuscripts. A special thanks to Richard Nair for proofreading my thesis and Sinikka Paulus for helping me with the German translation of the thesis summary. I am also grateful to Kasun Gayantha who guided me on the process of thesis submission.

A special thanks to Christiane Schmullius and Christoph Gerbig, who were in my PhD Advisory Committee (PAC) and provided useful inputs that helped structuring my manuscripts. Organization of regular PAC meetings was possible with the help of Steffi Rothhardt, a sincere thanks to her. She kept me encouraged during my PhD and directed me to participate in relevant courses. My earnest gratefulness is extended to Ulrike Schleier and John Kula, who managed my administrative procedures and provided constant moral support. I also want to show my sincere gratitude to Ulrich Weber who directed and supported me with useful data. My sincere thanks to Guido Salvucci from Boston University for hosting my research stay. Our discussion on boundary layer dynamics shaped my ideas for future outlooks.

My deep and sincere gratitude to my family and friends for their unparalleled love, help and support. I am grateful to my parents, my mother Sampurna Panwar and father Rajendera Singh Panwar, for giving me opportunities and experiences that have made me who I am. My sisters, Swati Negi, Manisha Panwar and brother Ayush Panwar showed their curiosity about my research. They have always being there for me as a friend.

x

Exciting discussions with my family about life and science kept me thrilled during this period. My Jiju, Naresh Negi, for supporting me during my masters. Also thanks to my little niece, Harshali, my lucky charm. Finally, I want to express my profound gratitude to my partner, Jose Cortes, for proofreading this thesis and for his unconditional love and support throughout my journey.

# Summary

Temperature is one of the most important meteorological variables in the field of natural science. Most commonly, Earth's temperature is measured either as air temperature at about 2 meters above the surface, or as surface temperature by the balance among the various energy flows at the surface. Air temperature is regularly monitored by meteorological stations and is a crucial indicator of global change. However, its observations are confined to a limited number of weather stations, therefore, use of surface temperature has been encouraged ever since the arrival of remote sensing techniques.

Surface and air temperatures are driven by the heating and cooling of the land atmosphere system. The main heating source of Earth's temperature is solar radiation absorbed at the surface. The absorbed solar radiation is then subdivided into different forms of energy, depending on the evaporative condition and vegetation characteristics of the surface. Usually, higher evaporation and taller vegetation induce cooler temperatures, however, responses of surface and air temperatures to these processes are still unclear. Previous studies have shown that surface and air temperature potentially carry similar information on the surface energy partitioning in their mean state, but limited number of studies pursue to understand the plausible contrasting information their diurnal variations contain. Proper knowledge of their differences would lead towards better understanding of the feedbacks of heat and moisture exchange on the land-atmosphere system.

Diurnal variation of surface and air temperatures is mainly caused by the diurnal variation of solar radiation. The maximum of surface and air temperatures occur around the solar noon and the minimum during early morning. Generally, the diurnal amplitude of surface and air temperature are found lower in forests than in short vegetation. Often the lower warming of temperatures in taller vegetation are linked to their high rate of evaporation. However, in order to determine the individual cooling effect of vegetation and evaporation a novel approach to analyse their impacts is needed. One of the major challenges to identify these contributions is the inadequate evidence of the underlying physical processes. For instance, evaporation is a surface process but it also influences the planetary boundary layer (PBL) dynamics and its heat content. Furthermore, high aerodynamic conductance of tall vegetation cools the surface temperature but also builds on the heat in the atmosphere that might lead to warmer air temperature. To quantify for

these effects, one potential approach is to utilize their tendencies at different evaporative and vegetation conditions. For that, the contribution of solar radiation shall be accounted for, and representative attributes of evaporative and vegetation conditions should be determined.

My overarching goal is to determine if and how, surface and air temperature respond differently to evaporation and what is the role of vegetation in altering these responses. In order to achieve this goal, three primary unknowns are identified, that are 1) Does diurnal surface and air temperature variation respond differently to changes in evaporative conditions, if so, why?, 2) How do these responses vary across vegetation types? and, 3) What are the dominant physical constraints that shape the diurnal variation of surface and air temperatures? To quantify for these responses I develop a novel index called warming rate that normalizes the warming effect of solar radiation. Warming rate is the slope of linear regressions of morning to noon time half hourly values of temperatures and solar radiation. In this thesis evaporative condition is represented by the evaporative fraction and vegetation characteristics by their aerodynamic conductance. My analysis is based on observations from multiple FLUXNET sites across different evaporation and vegetation regimes along with continental scale of ERA5 reanalysis data.

This thesis is divided into six chapters. Chapter 1 provides a general description of association and distinction of surface and air temperatures, followed by an overview on the main factors responsible for their diurnal variations. In chapter 2, main approaches to quantify and explain different processes shaping surface and air temperature are described. These approaches include firstly, the description of warming rate of temperatures from morning to noon time. Following which, two physically constrained models, one for air temperature and the other for surface temperature are developed based on atmosphere and surface energy balance. Chapters 3, 4 and 5 uses these approaches and gradually lead towards the main goals of this thesis.

The primary objective of chapter 3 is to examine the first order responses of surface and air temperatures to evaporation. This study uses FLUXNET measured energy fluxes and PBL height observations for a cropland field in the United States. The analysis shows that the daytime warming of surface temperature reduces strongly on evaporative days. However, the daytime warming of air temperature does not. The weaker responses of air temperature are hypothesized to link with the diurnal growth of the PBL height, that is also evident in the observations. To demonstrate this I develop a simplified PBL heat storage model that shows that the PBL height's response to sensible heat flux compensates for the daytime warming of air temperature. Based on these findings it can be concluded

that diurnal variation of air temperature is not a good indicator of evaporative condition but surface temperature is, especially for a surface covered by short vegetation.

In chapter 4, the main focus is on surface temperature and its link to vegetation's aerodynamic conductance. One of the secondary goal is also to determine the generality of the findings of chapter 3. To do so, additional FLUXNET sites across short vegetation, savanna and forest are used. Similar to chapter 3, chapter 4 shows strong responses of surface temperature to evaporative conditions for short vegetation. Similar weak responses of air temperatures are also found in all types of vegetation, which verify the generality of PBL compensating effect reported in chapter 3. Contrary to short vegetation, in forest the diurnal warming of surface temperature is found weakly affected by the changes in evaporative conditions. These results are then explained by a simplified surface energy balance model, that can quantify the individual contribution of evaporative fraction, aerodynamic conductance and solar radiation in influencing diurnal variation of surface temperature. Overall, chapter 4 shows the dominant role of aerodynamic conductance in cooling surface temperature in forests. These findings imply that in forest the diurnal variation of air temperature as well as surface temperature contain weak imprints of evaporation.

Chapter 5 encapsulates the major processes that shape diurnal variation of surface and air temperatures with insights on their continental scale responses. Here, in addition to multiple FLUXNET sites, ERA5 reanalyses is used due to its global estimates of meteorological variables and PBL height data. The responses are quantified in terms of diurnal temperature range ($DTR$) that is in principle the product of maximum solar radiation and warming rate. Based on this simplification, models introduced for air temperature (in chapter 3) and surface temperature (in chapter 4) are further developed into a simple atmospheric boundary layer model (SABL) and simplified surface energy balance model (SSEB), respectively. Modeling and observational study shows that solar energy input and PBL dynamics are crucial in explaining diurnal variation of air temperature. Surface temperature, on the contrary, mainly represents aerodynamic conductance of vegetation, evaporative conditions and solar radiation. ERA5 and FLUXNET are different in aspects of their resolution and methods of data constructions. This chapter discusses that ERA5 temperatures responses to evaporation are rather stronger than of FLUXNET's that are linked to its DTR bias on dry and wet conditions. Based on this chapter, it is concluded that the diurnal variation of surface and air temperature can be simply reproduced from the fundamental surface and atmosphere energy balance approach.

Overall, the findings from chapters 3, 4 and 5 demonstrate evident differences between surface and air temperatures in their daily scale and in regards to their global patterns. Remarkably, the diurnal variation of surface and air temperatures simply relies on the surface and atmosphere energy balance. Chapter 6 outlines these findings and their implications for the climate system. My research work provides valuable insights on the information that surface and air temperature carry on land atmosphere processes. These findings have implications when quantifying the impact of deforestation and water stress in the ecosystem, using surface and air temperatures. Differences between surface and air temperature during daytime and their physical interpretation should be considered when using them as proxy of each others. Discerning these differences could benefit the understanding of the land atmosphere system's responses to global change, such as drought and deforestation.

# Zusammenfassung

Die Temperatur ist eine der wichtigsten meteorologischen Größen im Bereich der Natur-
wissenschaften. Meistens wird die Temperatur der Erde entweder als Lufttemperatur in
etwa 2 Metern über der Erdoberfläche oder als Oberflächentemperatur durch die Bilanz
der verschiedenen Energieströme an der Oberfläche gemessen. Die Lufttemperatur wird
regelmäßig von meteorologischen Stationen überwacht und ist ein wichtiger Indikator
des Globalen Wandels. Ihre Beobachtungen beschränken sich jedoch auf eine begrenzte
Anzahl von Wetterstationen, weshalb die Verwendung der Oberflächentemperatur seit
dem Aufkommen der Fernerkundungstechniken gefördert wird.

Oberflächen- und Lufttemperaturen werden durch die Erwärmung und Abkühlung
des Systems Land-Atmosphäre angetrieben. Die Haupterwärmungsquelle für die Tem-
peratur der Erde ist die an der Oberfläche absorbierte Sonnenstrahlung. Die absorbierte
Sonnenstrahlung wird dann in verschiedene Energieformen aufgeteilt, je nach Verdun-
stungszustand und Vegetationscharakteristik der Oberfläche. Meistens erzeugen höhere
Verdunstung und höhere Vegetation kühlere Temperaturen. Dennoch sind die Reaktio-
nen der Oberflächen- und Lufttemperaturen auf solche Prozesse bis heute größtenteils
unklar. Frühere Studien haben gezeigt, dass die Oberflächen- und Lufttemperaturen in
ihrem mittleren Zustand potenziell ähnliche Informationen über die Energieverteilung an
der Oberfläche enthalten. Doch nur eine begrenzte Anzahl von Studien beschäftigt sich
mit den gegensätzlichen, aber plausiblen Informationen, die ihre täglichen Variationen
enthalten. Eine genaue Kenntnis ihrer Unterschiede würde zu einem besseren Verständnis
der Bedeutung des Wärme- und Feuchtigkeitsaustauschs im System Land-Atmosphäre
führen.

Die tägliche Variation der Oberflächen- und Lufttemperaturen wird hauptsächlich
durch den Tagesgang der Sonneneinstrahlung verursacht. Das Maximum der Oberflächen-
und Lufttemperaturen tritt um die Mittagszeit auf und das Minimum am frühen Mor-
gen. Meistens sind die täglichen Amplituden der Oberflächen- und Lufttemperatur
in Wäldern geringer als in kurzer Vegetation. Oft wird die verringerte Erwärmung
der Temperaturen bei höherer Vegetation mit ihrer relativ höheren Verdunstungsrate in
Verbindung gebracht. Um jedoch die individuellen Kühlungseffekte von Vegetation und
Verdunstung zu bestimmen, ist ein neuartiger Ansatz zur Analyse ihrer Auswirkungen

erforderlich. Eine der größten Herausforderungen bei der Identifizierung ihrer individuellen Beiträge ist der unzureichende Nachweis der jeweiligen zugrunde liegenden physikalischen Prozesse. Zum Beispiel ist die Verdunstung ein Oberflächenprozess, aber sie beeinflusst auch die Dynamik der planetaren Grenzschicht (PBL) und deren Wärmeinhalt. Darüber hinaus kühlt die hohe aerodynamische Leitfähigkeit hoher Vegetation die Oberflächentemperatur, staut aber auch die Wärme in der Atmosphäre, was zu einer Erwärmung der Lufttemperatur führen kann. Um diese Effekte zu quantifizieren, ist ein möglicher Ansatz, ihre Tendenzen bei unterschiedlichen Verdunstungs- und Vegetationsbedingungen zu nutzen. Dazu ist der Beitrag der Sonneneinstrahlung zu berücksichtigen, und es sollten repräsentative Eigenschaften der Verdunstungs- und Vegetationsbedingungen bestimmt werden.

In dieser Arbeit verwende ich Beobachtungen von mehreren FLUXNET-Standorten aus verschiedenen Verdunstungs- und Vegetationsregimen. Das übergeordnete Ziel ist es, zu bestimmen, ob und wie unterschiedlich die Oberflächen- und Lufttemperatur auf die Verdunstung reagieren und welche Rolle die Vegetation bei der Veränderung dieser Reaktionen spielt. Um dieses Ziel zu erreichen, werden drei grundlegende Fragen identifiziert: 1) Reagieren die täglichen Variationen der Oberflächen- und Lufttemperatur unterschiedlich auf Veränderungen der Verdunstungsbedingungen? Wenn ja, warum? 2) Wie unterscheiden sich diese Reaktionen zwischen verschiedenen Vegetationstypen? und 3) Was sind die dominanten physikalischen Bedingungen, welche die tägliche Variation der Oberflächen- und Lufttemperaturen beeinflussen? Um diese Reaktionen zu quantifizieren, wird ein neuer Index namens Erwärmungsrate verwendet, der den Erwärmungseffekt der Sonnenstrahlung normalisiert. Die Erwärmungsraten werden durch lineare Regressionen der halbstündlichen Werte von Temperaturen und Sonneneinstrahlung von morgens bis mittags quantifiziert. Der Verdunstungszustand wird durch den Verdunstungsanteil und die Vegetationseigenschaften durch ihren aerodynamischen Leitfähigkeit dargestellt.

Die vorliegende Arbeit ist in sechs Kapitel unterteilt. Kapitel 1 gibt eine allgemeine Beschreibung der Assoziierung und Unterscheidung von Oberflächen- und Lufttemperaturen, gefolgt von einem Überblick über die Hauptfaktoren, die für ihre täglichen Schwankungen verantwortlich sind. In Kapitel 2 werden die wichtigsten Ansätze beschrieben um Prozesse, welche Oberflächen- und Lufttemperatur beeinflussen, zu quantifizieren und zu erklären. Zuerst wird die Erwärmungsrate der Temperaturen von morgens bis mittags eingeführt. Anschließend werden zwei physikalisch begrenzte Modelle entwickelt, eines für die Lufttemperatur und das andere für die Oberflächentemperatur, basierend auf der Energiebilanz der Atmosphäre und der Oberfläche. In den

Kapiteln 3, 4 und 5 werden diese Ansätze dann angewendet und führen schrittweise zu den Hauptzielen dieser Arbeit.

Das primäre Ziel von Kapitel 3 ist die Untersuchung von Reaktionen erster Ordnung von Oberflächen- und Lufttemperaturen auf Verdunstung. Diese Studie wurde mit Hilfe von FLUXNET gemessenen Energieflüssen und PBL-Höhenbeobachtungen an einem Ackerland Standort in den Vereinigten Staaten durchgeführt. Es wurde festgestellt, dass die Erwärmung der Oberflächentemperatur tagsüber an verdunstungsintensiven Tagen stark abnimmt. Die Erwärmung der Lufttemperatur tagsüber tut dies jedoch nicht. Es wird angenommen, dass die schwächere Reaktion der Lufttemperatur zusammenhängt mit dem Wachstum der PBL-Höhe tagsüber. Dies zeigt sich auch in den gemessenen Beobachtungen. Um diese Annahme zu bestätigen, wird ein einfaches PBL-Wärmespeichermodell verwendet, welches zeigt, dass die Reaktion der PBL-Höhe auf den fühlbaren Wärmestrom die tägliche Erwärmung der Lufttemperatur kompensiert. Basierend auf diesen Erkenntnissen wird gefolgert, dass die tägliche Variation der Oberflächentemperatur ein guter Indikator für den Verdunstungszustand ist, im Gegensatz zur Lufttemperatur. Dies gilt insbesondere bei kurzer Vegetation.

Der Schwerpunkt von Kapitel 4 liegt auf der Oberflächentemperatur und ihrem Zusammenhang mit der aerodynamischen Leitfähigkeit der Vegetation. Eines weiteres Ziel war es, die Allgemeingültigkeit der Ergebnisse aus Kapitel 3 zu bestimmen. Dazu wurden zusätzliche FLUXNET-Standorte mit kurzer Vegetation, Savanne und Wald verwendet. Die Ergebnisse dieser Auswertung bestätigen die starke Reaktion der Oberflächentemperatur auf Verdunstungsbedingungen bei kurzer Vegetation. Außerdem wurden ähnliche, schwache Reaktionen der Lufttemperaturen in allen Vegetationstypen gefunden, was die Allgemeinheit des in Kapitel 3 berichteten kompensierenden PBL-Effekts belegt. Im Gegensatz zu kurzer Vegetation wird die tägliche Erwärmung der Oberflächentemperatur in Wäldern nur schwach von den Änderungen der Verdunstungsbedingungen beeinflusst. Diese Ergebnisse wurden dann durch ein vereinfachtes Oberflächen-Energiebilanzmodell erklärt. Dieses quantifiziert die individuellen Beiträge des Verdunstungsanteils, der aerodynamischen Leitfähigkeit und der Sonnenstrahlung zur täglichen Variation der Oberflächentemperatur. Insgesamt zeigt Kapitel 4 die dominante Rolle der aerodynamischen Leitfähigkeit bei der Kühlung der Oberflächentemperatur in Wäldern. Diese Ergebnisse implizieren, dass in Wäldern sowohl die tägliche Variation der Lufttemperatur als auch der Oberflächentemperatur nur schwach von Verdunstung geprägt sind.

Kapitel 5 fasst die wichtigsten Prozesse zusammen, welche die täglichen Schwankungen der Oberflächen- und Lufttemperaturen formen, und gibt Einblicke in ihre Reaktionen auf kontinentaler Ebene. Zusätzlich zu mehreren FLUXNET-Standorten werden hier ERA5-Reanalyse Daten aufgrund ihrer globalen Schätzwerte meteorologischer Variablen und PBL-Höhendaten verwendet. Die Reaktionen werden als tägliche Temperaturspannen ($DTR$) quantifiziert, die im Grunde das Produkt aus maximaler Sonneneinstrahlung und Erwärmungsrate sind. Basierend auf dieser Vereinfachung werden die für die Lufttemperatur (in Kapitel 3) und die Oberflächentemperatur (in Kapitel 4) eingeführten Modelle zu einem einfachen atmosphärischen Grenzschichtmodell (SABL) bzw. einem vereinfachten Oberflächenenergiebilanzmodell (SSEB) weiterentwickelt. Die Auswertungen von Modell und Beobachtungen zeigen, dass der solare Energieeintrag und die PBL-Dynamik entscheidend für die Erklärung der tageszeitlichen Variation der Lufttemperatur sind. Die Oberflächentemperatur hingegen bildet hauptsächlich die aerodynamische Leitfähigkeit der Vegetation, die Verdunstungsbedingungen und die Sonneneinstrahlung ab. Zusätzlich zeigt dieses Kapitel auch die Unterschiede zwischen den Temperaturreaktionen von ERA5 und FLUXNET. Es wird über stärkere Reaktionen in ERA5 berichtet, die mit DTR-Bias bei trockenen und feuchten Bedingungen zusammenhängen. Basierend auf den Ergebnissen dieses Kapitels wird gefolgert, dass die tageszeitliche Variation der Oberflächen- und Lufttemperatur im Wesentlichen aus der Oberflächen- und Atmosphären-Energiebilanz reproduziert werden kann.

Insgesamt zeigen die Ergebnisse aus den Kapiteln 3, 4 und 5 deutliche Unterschiede zwischen Oberflächen- und Lufttemperaturen auf täglicher Skala und in Bezug auf ihre globalen Muster. Bemerkenswert ist, dass die tageszeitlichen Schwankungen der Oberflächen- und Lufttemperaturen einfach auf der Energiebilanz der Oberfläche und der Atmosphäre beruhen. Kapitel 6 umreißt diese Erkenntnisse und ihre Auswirkungen auf das Klimasystem. Diese Arbeit liefert wertvolle Erkenntnisse über die Informationen, die Oberflächen- und Lufttemperaturen über die Prozesse in der Landatmosphäre tragen. Diese Erkenntnisse spielen eine Rolle wenn Auswirkungen von Abholzung und Wasserstress im Ökosystem unter Verwendung von Oberflächen- und Lufttemperaturen quantifiziert werden. Die Unterschiede zwischen Oberflächen- und Lufttemperaturen während des Tages und ihre physikalische Interpretation sollten berücksichtigt werden, wenn sie als Proxy für die jeweils anderen verwendet werden. Das Erkennen dieser Unterschiede kann das Verständnis der Reaktionen des Land-Atmosphäre-Systems auf globale Veränderungen, wie z.B. Trockenheit und Abholzung, verbessern.

# Chapter 1

# General Introduction

## 1.1  Motivation

Temperature is one of the fundamental variables that makes Earth habitable. Appropriate temperatures provide comfort in our everyday lives by regulating land surface processes such as evaporation, respiration and photosynthesis (Xu, Baldocchi, and Tang, 2004). Besides, it is a vital meteorological variable used in the field of climate research, agriculture, ecology, and human well-being (Pecl et al., 2017). According to the World Meteorological Organization (WMO, 2020) temperature is among the seven global climate indicators. Presumably, near surface air temperature is the foremost used meteorological variable to detect global and regional effects of climate change (Barnett et al., 1999).

Most of the studies in climate science utilize observations of air temperature that has benefited the humankind in every aspect. However, these observations have limitation in space, leading to poor global coverage, therefore, greater attention is shifted towards remotely measured surface temperature (Jin and Dickinson, 2010). Currently, active discussions (ESA, 2020) are ongoing to comprehend the capability of current surface temperature products and their records to meet the challenging GCOS, n.d. requirements for climate applications. Indeed, surface temperature observations have facilitated global analysis nonetheless it is also intriguing to know by what means and why it is different than the air temperature. Discerning the dominant factors that shape surface and air temperatures would improve the understanding of their distinct responses to global changes, for instance deforestation, drought and global warming, and their consequences on the climate system.

In particular, changes in land cover type alter surface energy partitioning to which surface and air temperature might respond differently. Some Earth system models have assessed the impact of deforestation on surface temperature (Shukla, Nobre, and Sellers, 1990; Pongratz et al., 2010; Boisier et al., 2012; Li et al., 2015; Devaraju et al., 2018)

with a focus on forest's biogeophysical effects like albedo, roughness and evaporation. Other studies focus on air temperature (Findell, Knutson, and Milly, 2006; Pitman et al., 2009; Noblet-Ducoudré et al., 2012) because of its relevance to human living conditions. Few studies demonstrate the different sensitivities of surface and air temperature and these have found that surface temperature increase is twice as strong as the increase in air temperature during the event of deforestation (Dickinson and Henderson-Sellers, 1988; Winckler et al., 2019). Although, warming of temperatures are expected but quite contrary, some models also reveal cooling effects of deforestation on summer daily maximum temperature (Lejeune, Seneviratne, and Davin, 2017). Therefore, climate model experiments are insightful but often inconsistent with each other mainly due to differences in parameterization schemes (Pitman et al., 2009; Noblet-Ducoudré et al., 2012). These findings are also usually not in agreement with observations (Wickham, Wade, and Riitters, 2013; Schultz, Lawrence, and Lee, 2017) and lack an explicit explanation on the underlying physical processes.

An alternative to sophisticated climate models is to exploit observations of surface and air temperatures and their relation to vegetation properties. Observations show that taller vegetation results in lower surface and air temperature (Mildrexler, Zhao, and Running, 2011). Mostly it is attributed to the evaporative cooling and therefore lower temperatures are considered as a proxy to evaporation (Jackson et al., 1999; Kustas and Norman, 1999; Anderson et al., 2012). However, it is still unclear if tall vegetation cools mainly through evaporation or by means of their high aerodynamic conductance. A few studies have attempted to resolve these unknowns using decomposed temperature metrics but remain confined to surface temperatures (Juang et al., 2007; Luyssaert et al., 2014; Chen and Dirmeyer, 2016). Moreover, in such approaches the role of diurnal changes in heat storage of the land atmosphere system has not been examined well. More research on their diurnal variation is needed since the diurnal changes in heat source and sinks might be linked to the diurnal asymmetrical sensitivities (Schultz, Lawrence, and Lee, 2017) of surface and air temperatures to global change.

In this thesis, my overall goal is to investigate the differences between the responses of diurnal surface and air temperatures to changes in vegetation and evaporative conditions. To capture these responses in observations, instead of tracking land cover change events over time, the days are segregated for different evaporative conditions. Thereafter, these responses are analysed for different vegetation types. Using this space for time approach one can also approximate the responses of temperatures to land cover change by segregating these responses for different vegetation types. To further understand the underlying physical processes and their first order effects on surface and air temperatures

I propose two fundamental physical models based on surface and atmosphere energy balance constraints. The model for surface temperature estimates that surface temperature is a function of solar radiation, evaporative conditions and aerodynamic conductance of vegetation. Air temperature, however, also represents the atmosphere's response to evaporative condition. On dry days, the planetary boundary layer height increases, this thesis examines the extent to which increases in PBL height reduces the diurnal warming of air temperature.

This chapter first discusses the relationship of surface and air temperature in terms of their monthly, daily and sub-diurnal scales. Then, I further delve into explaining the major factors that shape the diurnal variation of surface and air temperatures. These factors are evaporative conditions, vegetation types and planetary boundary layer (PBL) dynamics. It is important to identify the differences between surface and air temperature while using and interpreting them for meteorological phenomenons associated to the variability of moisture, energy and vegetation.

## 1.2    Air temperature versus surface temperature

### 1.2.1    Generic description

Regular global air temperature records predate the year 1880 and has facilitated the understanding of the climate system (Wang et al., 2018). Typical weather stations measure air temperature with thermometers placed at a height of 1.4 meters to 2 meters above the ground (Pulliainen, Grandell, and Hallikainen, 1997). The height of the measurement of air temperature is based on average human height. If the thermometer is placed too close to the ground, it receives excess heat from the ground and if it is too high it shows cooler temperatures. Furthermore, the thermometer must be shaded from direct sunlight, covered to avoid precipitation, and should be adequately ventilated. Official weather stations around the world follow these standards to ensure inter compatibility between air temperature measurements. Air temperature measured by eddy-covariance networks are the representative temperature of atmosphere above the vegetation canopy. Thereby avoiding cooling effect of shading due to vegetation canopy. The distance between sensor and canopy is site specific, and depends on vegetation height, wind velocity and the frequency response of the sensor (Olson et al., 2004).

Despite being easy to gauge, in practice, observations of air temperature are sparse and unevenly distributed in space (Parker, 2016). Limited observations of air temperature is an obstacle for climate science community that relies on global temperature trends analyses. The point scale observations of air temperature are not often suitable for regional studies due to high variability in their spatial patterns (Rigor, Colony, and Martin, 2000; Kloog et al., 2014). In modelling, air temperature is diagnosed empirically by integrating the vertical profile of temperature from the surface, usually 2 meters above the apparent sink of sensible heat flux (Oleson et al., 2010). Such methods hold some limitation in complex surfaces such as tall vegetation due to variability of energy components within and over the canopy (Lee and Black, 1993; Lee, 1998). Therefore, when using modelled air temperatures for forests, uncertainties within forest canopies should be considered (Flerchinger et al., 2015).

Advances in space based observations (Tomlinson et al., 2011; Li et al., 2013) has provided a substitute to air temperature. Weather satellites retrieve thermal radiance emitted from the surface and atmosphere using Planck's law. The effects of atmospheric attenuation on satellite measured radiance are removed (Saunders, 1967) and the surface radiance is then mathematically inverted to obtain land surface temperatures. Over vegetated regions, surface temperature is similar to the canopy top temperature (Jin and Dickinson, 2010). Surface temperatures obtained from remote sensing are available for remote areas which are not otherwise easily accessible. Surface temperature can also be approximated from the ground based observation of upwelling longwave radiation ($R_{l,up}$) and surface emissivity ($\epsilon$) using Stefan–Boltzmann law ( $R_{l,u} = \epsilon \cdot \sigma \cdot T_s^4$, $\sigma$ is the Stefan–Boltzmann constant). Unavailability of surface emissivity, specially in regional scale (Jin and Liang, 2006) is one of the limitations, but usually for simplification, one can assume Earth as a blackbody surface with an emissivity of one (Wilber, 1999).

Different data sources use different terminology for surface and air temperature. Global Climate Observing system data product services (Copernicus, 2019), refers to air temperature as surface air temperature, that is simply because they provide air temperatures at multiple pressure levels. Likewise, surface temperature is occasionally available as skin temperature (skt) and land surface temperature (LST). In this thesis I will be using term surface temperature ($T_s$) for the temperature of the vegetation canopy and air temperature ($T_a$) for temperature measured $\approx$ 2 meters above the vegetation canopy .

## 1.2.2 Association and distinction

Surface temperature and air temperature are often considered as proxies for each other. Their strong relationship is used in climate science to approximate air temperature from surface temperature and vice versa. For example, regular values of air temperature are used as an important atmospheric forcing for weather forecasts and climate models (Collins, 1995) but its global coverage is inadequate. To overcome this challenge, global values of air temperatures are retrieved from remotely sensed surface temperature (Prihodko and Goward, 1997; Benali et al., 2012; Zhu, Lű, and Jia, 2013) using several statistical (Good, 2015; Benali et al., 2012; Janatian et al., 2017), machine learning (Ho et al., 2014; Emamifar, Rahimikhoob, and Noroozi, 2013; Jang, Viau, and Anctil, 2004), energy balance (Sun et al., 2005; Zhang et al., 2015), and temperature-vegetation index (Prihodko and Goward, 1997; Vancutsem et al., 2010; Zhu, Lű, and Jia, 2013) approaches. However, previous studies also show that these estimates are much more suitable for seasonal to monthly time scales but less accurate for daily to sub-daily scales (Oyler et al., 2016; Zhang et al., 2011).

Surface and air temperatures are associated but not exactly the same. Surface temperature is strongly related to the surface properties that mainly include vegetation cover and soil wetness (Lambin and Ehrlich, 1996). Consequently, surface temperature is spatially heterogeneous by higher degree compared to air temperature (Morrison et al., 2021). In contrast, air temperature is more sensitive to the mixing of heat in the planetary boundary layer via turbulent heat and moisture exchanges. The association of surface and air temperature also depends on the heat exchange between surface canopy and atmosphere. Rougher vegetation canopy facilitates stronger heat exchange and results in similar surface and air temperatures (Huete, Justice, and Liu, 1994). Moreover, the relationship of surface and air temperatures depends on the regional geography (Stoll and Brazel, 1992; Eliasson, 1990) and seasons (Kawashima et al., 2000).

The relationship between surface and air temperature also varies in different time scales. To illustrate this, figure 1.1 shows the correlation of their observed monthly (figure 1.1a) and daily (figure 1.1b) mean values in a cropland ecosystem of the Southern Great Plains in the United States (Biraud et al., 2016). The blue data points correspond to winter months (December, January and February) and red points to summer months (June, July and August). The monthly and daily means are constructed for 12 years of observations. It is notable that monthly means of surface temperature and air temperature have higher correlation compared to their daily means. Additionally, surface temperature is warmer than the air temperature specially in summer months. There are high variances in their daily relationship that reflect their sub-daily variation that were otherwise averaged
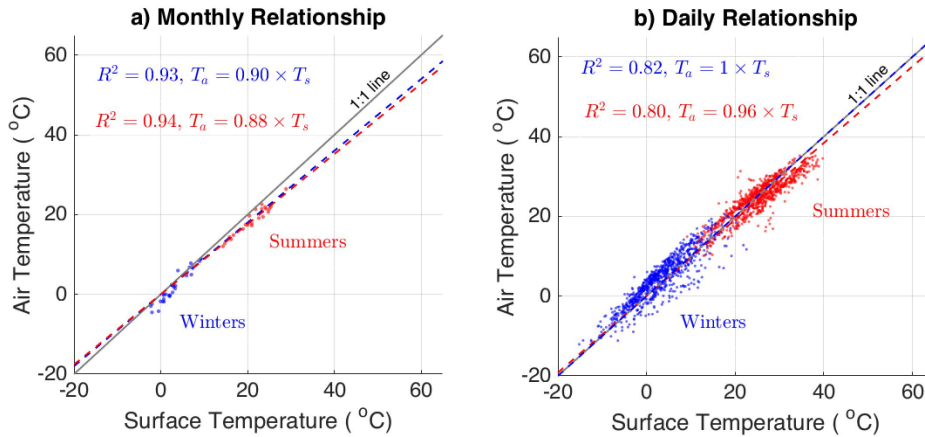
FIGURE 1.1: The relationship between mean values of surface($T_s$) and air temperature($T_a$) in monthly and daily basis for summer and winter months. Grey line is the 1:1 line and dotted lines are the slopes of surface and air temperature with zero intercept. Data source: FLUXNET site at Sebastien, 2016 Southern Great Plains Lamont

out in their monthly relationship (Good et al., 2017). Diurnal variation of surface and air temperatures have distinctive sensitivities to meteorological processes like vegetation-atmosphere interaction, turbulent heat partitioning and boundary layer dynamics that are further discussed in the next section.

### 1.2.3   Diurnal temperature variations

The mean values of temperature are primarily used to examine present climate and climate change. However, beside the mean values of temperature most of the phenomenons also depend on its diurnal variability and extremes during the day (Karl et al., 1991). The daily means hold additional information on the meteorological processes that occur in sub-daily time scales (Braganza, Karoly, and Arblaster, 2004). Moreover, information on diurnal temperature variation benefits research in the fields of agriculture and ecology to evaluate its impact on crop yield (Lobell, 2007; Nicholls, 1997) and mortality of humans, endangered plants and animal species (Kan et al., 2007; Lee et al., 2017; Yi et al., 2018).

Diurnal temperature variation is usually quantified as diurnal temperature range (DTR) that is the difference between maximum and minimum temperatures of the day. Maximum temperature generally occurs during the afternoon and minimum temperature in the early morning, similar to the diurnal variation of solar radiation (Bristow and Campbell, 1984). To illustrate this, figure 1.2 a shows the diurnal variation of solar radiation, surface temperature and air temperature for a cropland site in the Southern Great Plains of the United States (data: Biraud et al., 2016). Surface and air temperature
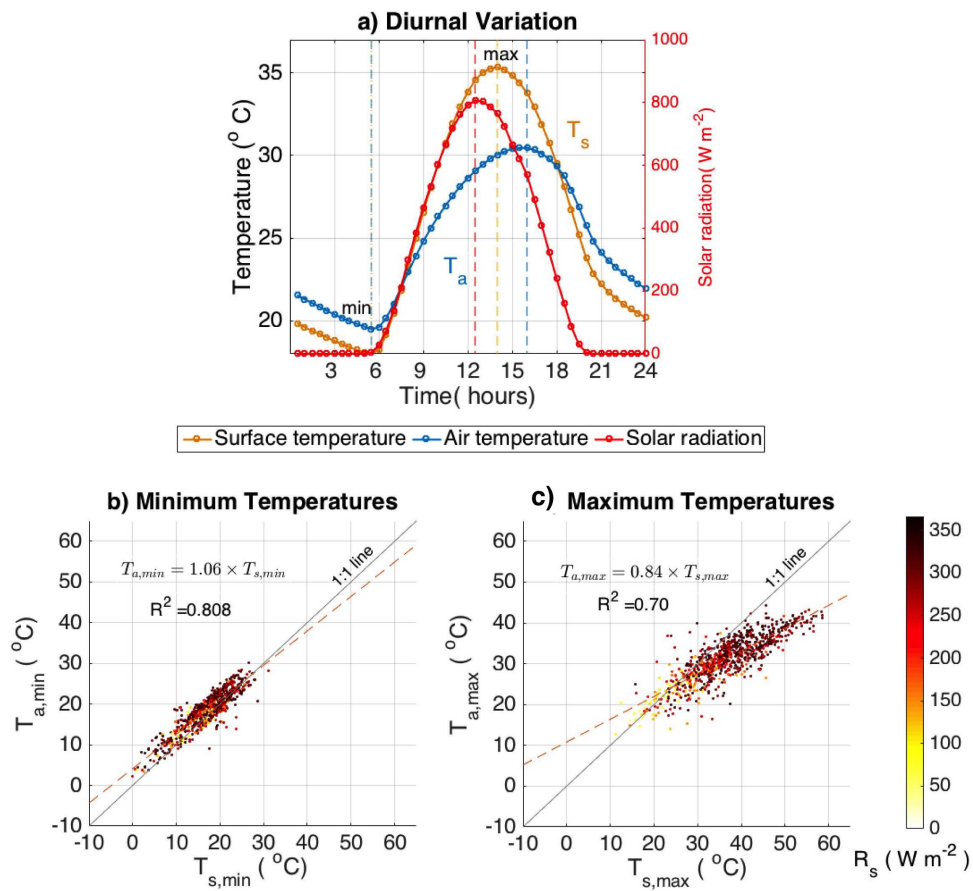
FIGURE 1.2: a) The mean diurnal variation (half hourly) of solar radiation (red), surface ($T_s$, orange) and air temperature ($T_a$, blue) for summer season in a cropland ecosystem. The dashed lines in the morning and afternoon represent their minimums and maximums, respectively. b) The relationship between daily minimums of surface and air temperatures c) the relationship between daily maximums of surface and air temperatures. Grey line is the 1:1 line and the color bar represents the value of mean solar radiation. Data source: FLUXNET site at Sebastien, 2016 Southern Great Plains Lamont.

follow the diurnal changes in solar radiation with their maximums slightly lagging behind to the maximum of solar radiation. This phase lag is larger for air temperature compared to surface temperature. The phase lag in temperatures is the outcome of the the heating and cooling of the land atmosphere system (Prescott and Collins, 1951; Hassan et al., 2016). Earth's surface is primarily heated by the solar radiation and cools by emitting infrared or longwave radiation to space. Temperature is minimum when solar radiation exceeds the outgoing longwave radiation and maximum when the outgoing longwave radiation exceeds solar radiation (Bonan, 2015). Earth's surface is a better radiator than the atmosphere so maximum surface temperature occurs earlier than the maximum air temperature. Additionally, variation in land surface properties like emissivity and albedo

alter surface temperature differently than the air temperature (Jackson, Idso, and Otterman, 1975; Sailor, 1995; Krayenhoff and Voogt, 2010; Federer, 1968).

The relationship between surface and air temperature differs over the period of a day. Figure 1.2 b and figure 1.2 c show the relationship of their maximum and minimum values for summer time. During early morning, minimum values of surface temperature and air temperature are similar and have a consistent relationship irrespective of the variation in the daily mean solar radiation. In the afternoon when maximum temperatures occur, the surface temperature is warmer than the air temperature, especially on days with higher mean value of solar radiation. Certainly, variation in solar radiation alone does not explain the differences in surface and air temperature. If similar surface moisture conditions are present then the higher solar radiation perhaps corresponds to a shift of surface energy partitioning towards sensible heat flux (Cellier, Richard, and Robin, 1996). Alternatively, for similar solar radiation the surface soil moisture condition can vary within season due to past occurrence of rainfall (Eltahir, 1998) in response to which surface and air temperature might respond differently. Last but not least variation in these relationships are subject to differences in biophysical properties of vegetation type.

## 1.3   Factors shaping diurnal temperatures

Besides solar radiation, diurnal variation of temperature is influenced by many other geographical constraints and meteorological processes. Temperature reduces with altitude because of the pressure drop (Barry, 1992). Clouds can reduce daytime temperatures by reducing surface solar radiation, however at nighttime clouds increase downward longwave radiation and hence increase the temperatures (Dai, Trenberth, and Karl, 1999). Similarly, atmosphere with high humidity or greenhouse gases enhances the downward longwave radiation and can influence daytime and nightime temperatures differently (Wang and Dickinson, 2013). Surface properties can also influence diurnal variation of surface and air temperature. Surface covered with tall vegetation like forest is generally cooler; this is often linked to the role of evaporative cooling (Bonan, 2008). However, the rougher surface of forest also enhances heat and moisture mixing and can influence surface and air temperature differently. The temperature of the atmosphere also represents the changes in heat storage that corresponds to the boundary layer height and its response to surface energy partitioning (Koster et al., 2006; Guo et al., 2006). The main objective of this section is to understand the role of vegetation, evaporative conditions and boundary layer dynamics in the diurnal variation of surface and air temperature.

### 1.3.1 Role of evaporation

Evaporation is a vital component of the water cycle. Liquid water molecules absorb heat from the surface to evaporate. It requires about 2458 kilo Joules ( at 18 ˚C) of energy to evaporate one litre of water (Monteith, 1972). The processes of evaporation at the surface consumes about 50 % ($88 \pm 10 \ Wm^{-2}$) of the Earth's net surplus solar radiant energy ($165 \pm 6 \ Wm^{-2}$) and leads to total cooling of the Earth system (Trenberth, Fasullo, and Kiehl, 2009; Stephens et al., 2012). In a model based experiment Shukla and Mintz, 1982 shows that the temperature of the Earth could be higher by 25 K in the absence of evaporative cooling.

The process of evaporation depends on available energy at the surface and surface moisture. The net surface available energy that is the sum of net solar radiation ($R_s$) and longwave radiation ($R_{l,net}$) is partitioned into latent heat flux (LE), sensible heat flux (H) and ground heat flux (G), see equation 1.1.

$$R_s + R_{l,net} = LE + H + G \qquad (1.1)$$

Latent and sensible heat denoted with negative sign indicates their direction from the surface to the atmosphere, meaning they consume the surface energy and transport it to atmosphere. Latent and sensible heat flux utilize solar energy absorbed at the surface that eventually cool the surface. Some energy remains in the surface, also called as ground heat flux that keeps the surface warm. Ground heat flux is a positive quantity because it travels from the surface to the soil and represents surface heat storage. In general the ground heat flux constitutes only 10 % of the net radiation, subsequently majority of energy is consumed by turbulent heat fluxes (Santanello Jr and Friedl, 2003). In a non-energy limited scenario the partitioning of turbulent heat flux into latent and sensible heat flux depends on the water availability. Latent heat flux is the measure of energy absorbed at the surface for the process of evaporation. Latent heat is then moved by the water vapour to the higher atmosphere where it is then released by the process of condensation (Pauluis and Held, 2002). In a non-energy limited scenario, a wet surface consumes high latent heat flux that results in overall cooling of the surface and adjacent air. Contrarily, over a dry surface there is additional heat that warms the surface and the adjacent air (Stewart et al., 1994).

Figure 1.3 illustrates the mean values of turbulent heat partitioning for dry and wet conditions in a cropland ecosystem and its influence on surface and air temperatures. To keep the background conditions comparable I have chosen wet and dry days with similar incoming solar radiation. It is clearly noticeable that for similar solar radiation,
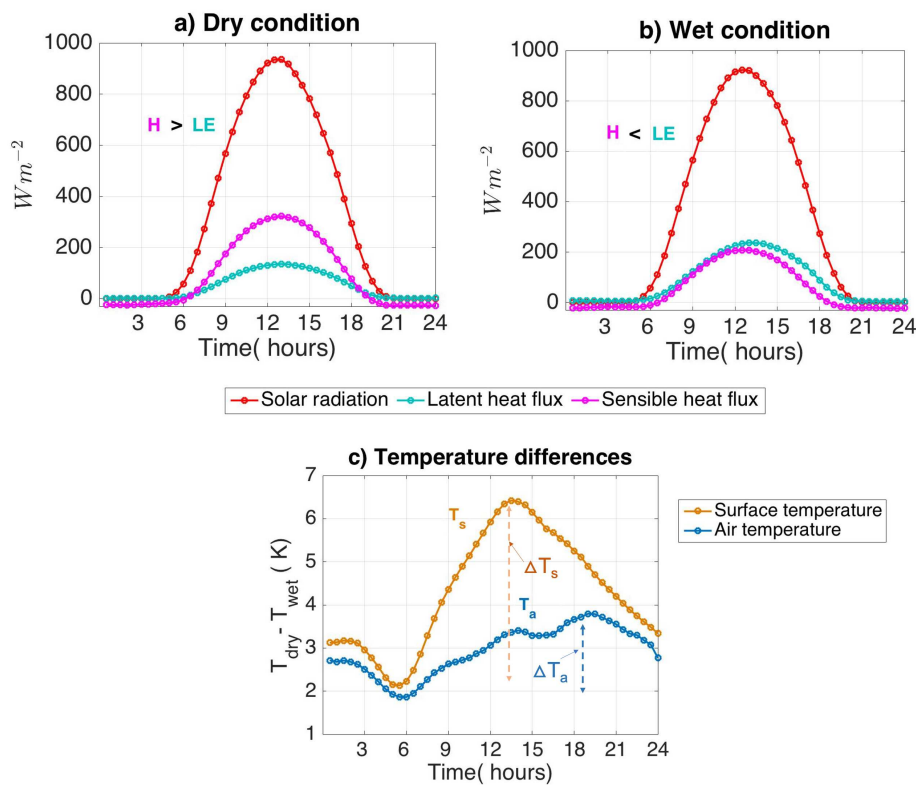
FIGURE 1.3: Diurnal variation of sensible heat flux (SH) and latent heat flux (LE) on a dry (a) and on a wet (b) day. The solar radiation input is similar in dry and wet days (in red). c) The surface ($T_s$) and air temperature ($T_a$) differences of dry and wet days. $\Delta T$ is higher for surface temperature during daytime but lower for air temperature. This represents that the turbulent heat partitioning mainly impact surface temperature, in a short vegetation. This might look different for a forest site. Data source: A cropland FLUXNET site US-ARM at Southern Great Plains Lamont

dry condition has less surface latent heat flux ($H > LE$) than the wet conditions. Turbulent heat fluxes are higher during the daytime and their partitioning predominantly influence the daytime temperatures, see figure 1.3c. Interestingly, the difference is higher for surface temperature and lower for air temperature ( indicated by $\Delta T$). This indicates the stronger response of surface temperature to energy partitioning than air temperature. These relationships might look different in the forests that is different than a cropland in many bio-physiological aspects.

## 1.3.2   Role of vegetation

Earth's land surface is predominantly covered by diverse vegetation types that include croplands, grasslands, forests and heterogeneous vegetation like savannas. Vegetation

cover influences the temperatures and local climate by altering the energy and moisture exchange between land and atmosphere. The importance of forest for curbing climate change is well recognized after the period of extensive deforestation in 21st century (Brovkin et al., 2006; Buma and Wessman, 2013). Forest take up the carbon dioxide and cools the Earth system (Law et al., 2002). The other main mechanisms that enable forests to moderate the temperatures comprise their considerable amount of evaporation, aerodynamic effects and reflectance properties (Jackson et al., 2008). Furthermore, the contribution of these mechanism can vary in tropical and temperate climate system (Li et al., 2015; Ellison et al., 2017; Zhang et al., 2020).

The impact of vegetation on temperatures can be accounted by modification of surface energy balance components. Forests usually have low albedo that enables them to absorb more solar radiation (Betts and Ball, 1997; Culf, Fisch, and Hodnett, 1995; Lutz and Howarth, 2014). In a typical forest the absorbed energy is mostly dominated by the latent heat flux, due to their deep root system. The extent of rooting zone or rooting depth maintains vegetation functioning even during dry episodes (Nepstad et al., 1994; Kleidon, Axel and Heimann, 2000; Feddes et al., 2001). Contrarily, land covered with short vegetation have higher albedo and tend to reflect more solar radiation (Lobell, Bala, and Duffy, 2006; Irvine, Ridgwell, and Lunt, 2011). Additionally, due to shorter root depth of short vegetation most of the absorbed radiation is utilized by sensible heat flux leading to overall warming.

Besides the cooling effect of evaporation, vegetation also alters temperatures through their aerodynamic properties. Rougher vegetation facilitates strong turbulence in the atmosphere that enhances the exchange of heat and moisture. The coupling of surface and air temperature is primarily determined by the aerodynamic conductance of the vegetation. The relationship between sensible heat flux ($H$), aerodynamic conductance of heat ($g_a$), surface temperature and air temperature is given by equation 1.2

$$H = c_p \cdot \rho \cdot g_a \cdot (T_s - T_a) \tag{1.2}$$

Here, $c_p$ and $\rho$ are the specific heat capacity and density of the atmosphere, respectively. Note that, $g_a$ also has a diurnal cycle, usually with the maximum values during noon (Takagi, Tsuboya, and Takahashi, 1998). Therefore the difference between surface temperature and air temperature ($T_s - T_a$) depends on $H$ and $g_a$.
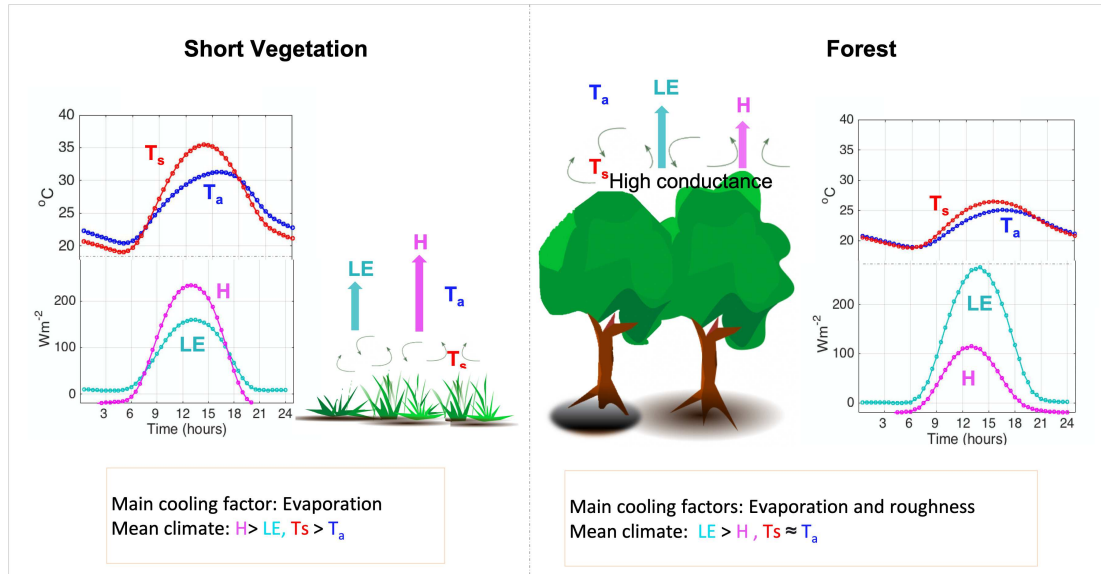
FIGURE 1.4: The mean diurnal variation of surface tempearture ($T_s$), air temperature ($T_a$), latent heat flux ($LE$) and sensible heat flux ($H$) for the summer season in a typical short vegetation and forest ecosystem. Data: A cropland FLUXNET site, US-ARM (Southern Great Plains site Lamont) and a deciduous broad leaf forest FLUXNET site, US-MMS (Morgan Monroe State Forest) in Indiana in the United States. Both sites have similar background climate condition.

As an illustration, figure 1.4 shows the summer time mean diurnal variation of sensible and latent heat flux and their impact on the relationship of surface and air temperature for a cropland site in the Southern Great Plains (data: Biraud et al., 2016) and a forest site in Morgan Monroe state forest (data: Philip and Novick, 2016). These two sites are located in similar geography and therefore receive similar solar energy input during the summer season. Clearly, in forest latent heat flux dominates the energy partitioning. In the cropland however, sensible heat flux is higher than the latent heat flux. One might relate the lower surface and air temperatures in the forest to stronger evaporative cooling. But it should be considered that the high aerodynamic conductance of forest plays an important role in lowering the surface temperature and raising the air temperature that might lead to their similar values, as indicated in equation 1.2. Conversely, surface temperature in short vegetation tends to be warmer than the air temperature due to lower heat exchange with the atmosphere and higher sensible heat flux. In an irrigated cropland the latent heat flux can be comparable to sensible heat flux. In general, evaporative cooling is the main cooling factor in the short vegetation but in forest, aerodynamic conductance's contribution to cooling can be greater. To quantify for different contributions of evaporative cooling and aerodynamic conductance, analysis of surface and air temperature in different vegetation and evaporative regimes is required.

The other aspect that might influence air temperature is its relation to boundary layer heat storage. Eventually, sensible heat flux released from the surface is stored in the planetary boundary layer. Nonetheless, the diurnal growth of planetary boundary layer is also shaped by the sensible heat flux. What remains unclear is to what degree the boundary layer growth adjusts the diurnal warming of temperature and if its response to sensible heat flux is similar for short vegetation and forest.

### 1.3.3   Role of planetary boundary layer

The planetary boundary layer (PBL) is the region in the lower troposphere that is directly influenced by surface forcing such as heating, cooling, friction and influxes of dust, water vapour and pollutants. It is best described in meteorology as the well mixed layer that has little variation in vertical profile of potential temperature and humidity (McBean et al., 1979). PBL height is usually diagnosed from the radiosondes soundings that are launced twice a day (Sugita and Brutsaert, 1991; Wang and Wang, 2014). Currently, Lidar based approaches are used to provide continuous observations of PBL height (Träumner et al., 2011). A typical PBL can vary from 500 to 2000 meters during the day. PBL observation is vital to understand processes that control the near surface climate. For example, air quality forecast requires boundary layer height to analyse air pollution dispersion (Davies, Middleton, and Bozier, 2007).

Similar to solar radiation and temperatures, PBL undergoes a diurnal variation (Stull, 1988). At night, surface temperature cools by emitting longwave radiation that results in weak turbulent exchange and shallow PBL. The nighttime radiative cooling causes surface inversion within 100 to 500 meters of the PBL. In the early morning, upward exchange of sensible heat flux erodes the inversion layer and develops a shallow PBL. Then, boundary layer grows rapidly against the potential temperature lapse rate of free atmosphere, see figure 1.5 . With increase in solar radiation and surface heating, convection strengthens and pushes the air parcels all the way up to the point where potential temperature is greater than the temperature of the air parcel. Alongside, heavy cold air sinks around the rising parcel to form a well mixed convective PBL. The maximum height of the PBL is achieved during the afternoon. Near the sunset, longwave cooling overtakes the solar heating that creates the surface inversion and prevents further mixing.

The growth of the PBL is also sensitive to soil moisture and turbulent heat partitioning that ultimately controls the diurnal variation in PBL's temperature. PBL develops during the day in response to energy and moisture exchange in the land atmosphere interface
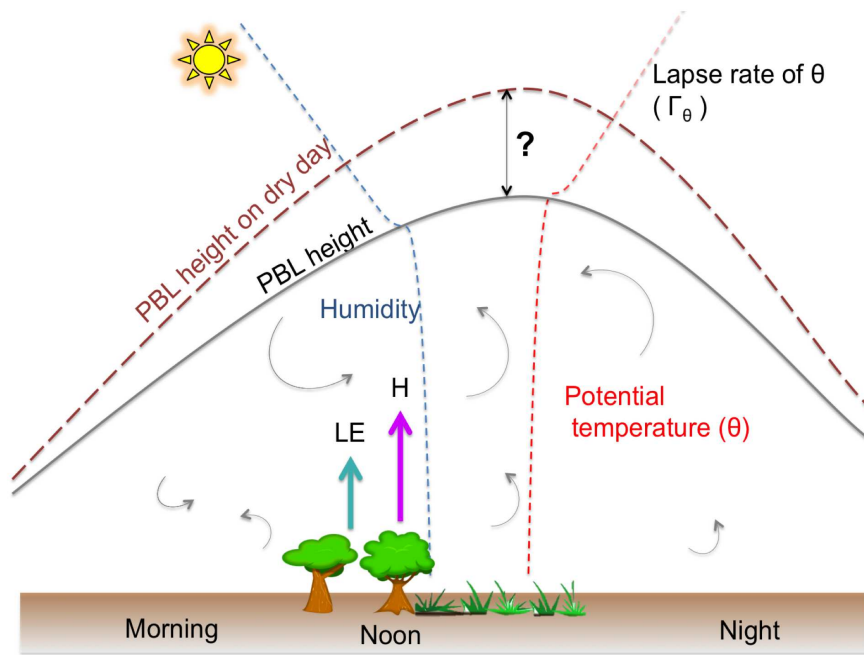
FIGURE 1.5: A schematic diagram of diurnal variation in planetary boundary layer height. PBL grows during the afternoon in response to strong convection due to high sensible heat flux. On dry day (less evaporation) PBL growth is stronger than on a wet day (more evaporation). Response of PBL height to evaporative conditions, as shown by the question mark(?) is unknown. In this thesis, the link of this response to diurnal variation of air temperature is examined.

(Camillo, Gurney, and Schmugge, 1983; Findell and Eltahir, 2003). The growth of the PBL is caused by buoyancy of the light and warm air parcel mixing from the surface to the atmosphere. Over a drier surface high sensible heat creates strong convection and subsequently increases PBL height as illustrated in figure 1.5. Surface temperature and PBL potential temperature tends to be warmer on dry day. Over wet surface more moisture is transferred to the PBL than the sensible heat that results in shallower, cooler and moist PBL (Sandeep et al., 2014). In this thesis, I further investigate how the PBL response to turbulent heat partitioning shapes diurnal surface and air temperature differently, and if these effects are similar for different vegetation types.

To conclude, surface solar radiation is the main source of heat but the diurnal amplitude of surface and air temperature is determined by its partitioning into latent and sensible heat flux. In taller vegetation, latent heat flux dominates over sensible heat flux that should cool the temperatures. On the other hand, the cooling effect of higher aerodynamic conductance of tall vegetation might dominate over the evaporative cooling. Contrary to surface temperature the diurnal variation of air temperature also depends on

the diurnal boundary layer growth and its response to sensible heat flux.

# Chapter 2

# Research Approach

## 2.1 Research objectives

The main objective of my thesis is to examine and understand the role of surface evaporative conditions and vegetation types in shaping the diurnal variation of surface and air temperature. More specifically, my objectives are to find the following unknowns:

- Does diurnal surface and air temperature variation respond differently to changes in evaporative conditions, if so, why?

  To answer this question I hypothesize that the diurnal growth of the boundary layer height reduces the diurnal warming of air temperature. Therefore, one would expect stronger imprints of evaporative cooling in surface temperature and weaker in air temperautre.

- How do these responses vary across vegetation types?

  Suppose the boundary layer height responds similarly to sensible heat flux, one would expect similar responses of air temperature in different vegetation types. Following the finding of first objective the role of PBL in shaping air temperature is tested for multiple FLUXNET sites. Unlike air temperature, surface temperature is mainly related to vegetation and evaporative conditions. Our second objective is to find to what extent, the aerodynamic conductance and evaporation cools the surface temperature in different vegetation types.

- What are the dominant physical constraints that shape the diurnal variation of surface and air temperatures?

  Diurnal variation of surface temperature and air temperature are shaped directly by absorbed solar radiation. It is further speculated that surface energy partitioning feeds convection in the boundary layer that should reduce the warming of air temperature. Using land atmosphere energy approaches and I develop fundamental physical models that provide insights on diurnal surface and air temperature

variation and their main controls. These models are tested for multiple FLUXNET sites and ERA5 reanalysis data at continental scale.

## 2.2 Methods

To quantify for the diurnal variation of temperature their daytime warming rates and diurnal temperature range ($DTR$) are used. Follow the arrow in the direction of morning to night time. The evaporative conditions are represented by evaporative fraction and vegetation types by their aerodynamic conductance. Next, two simple models are presented that demonstrate how the diurnal variation of surface and air temperature relates to solar radiation, evaporative fraction, boundary layer dynamics, and aerodynamic conductance of vegetation.

### 2.2.1 Diurnal warming rates
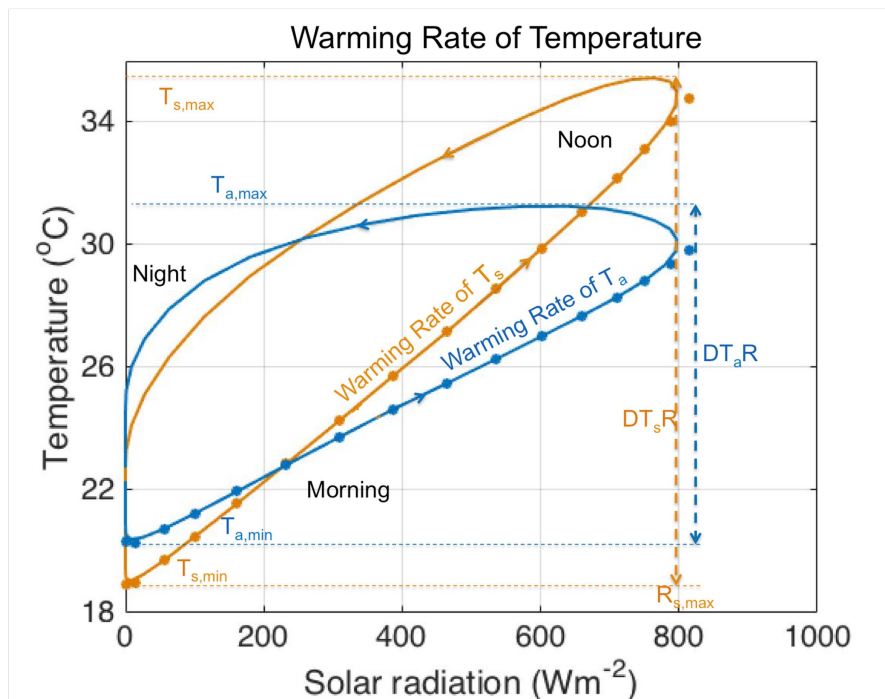


FIGURE 2.1: The morning, noon to night time relationship between diurnal temperature and solar radiation variation depicted from the diurnal hysteresis obtained on plotting their half hourly values against each other. The morning to afternoon slopes of the hysteresis are called warming rate. The dashed horizontal lines show minimum and maximum values of surface (orange) and air (blue) temperatures. The vertical lines show the diurnal temperature range and its relation to warming rates. Data source: A cropland FLUXNET site at Sebastien, 2016 Southern Great Plains Lamont

Diurnal warming of temperature is mainly driven by the absorbed solar radiation. This is apparent on plotting diurnal temperatures against solar radiation, see figure 2.1. In course of morning to afternoon, surface as well as air temperature increases linearly in response to increase in solar radiation. Solar radiation warms but vegetation and evaporation cool the temperature. To quantify the cooling effect of vegetation and evaporation, the warming effect of solar radiation is normalized by taking the linear regression of the morning to noon values of temperature and solar radiation. This value corresponds to the steepness of the slope and is called as warming rate with a unit of $K(Wm^{-2})^{-1}$. In this thesis the warming rate of surface and air temperature are expressed as $dT_s/dR_s$ and $dT_a/dR_s$, respectively. In general surface temperature warming rate is greater than the air temperature warming rate, however they might change for vegetation types. Calculation of warming rate requires high frequency (half hourly to hourly) values of temperature and solar radiation.

In climate science the diurnal temperature variation is usually quantified by diurnal temperature range ($DTR$). Warming rate of temperature has advantage over $DTR$ since it normalizes for the effect of solar radiation. This indicates that regions receiving different solar radiation but similar environmental (specially, vegetation and evaporation) conditions should have similar warming rates but different $DTR$. $DTR$ is basically the product of solar radiation and warming rate or in other terms when lacking frequent data, warming rates can be approximated from the ratio of diurnal temperature range ($DTR$) and maximum solar radiation ($R_{s,max}$).

### 2.2.2 Classification of vegetation and evaporative conditions

**Vegetation types**: In this thesis vegetation types are broadly classified in three categories, first is the short vegetation type that comprises croplands, shrublands and grasslands, second is the heterogeneous savannas and third is forest that includes mixed, evergreen needleleaf, evergreen broadleaf and decidous forests. The distinction between vegetation is based on the vegetation height and general roughness that is more in forest than in the short vegetation. For vegetation classification, the dominant vegetation class provided by International Geosphere-Biosphere Programme (IGBP) are used, more information on this product is available at Loveland et al., 1999.

**Evaporative conditions**: To account for the evaproative conditions an index called evaporative fraction ($f_e$) is used. Evaporative fraction is the ratio between the latent heat flux and total turbulent heat flux, such that $f_e = LE/(LE+H)$. Evaporative fraction is derived from the linear regression of the morning values (half-hourly) of LE and LE+H

and is assumed to be constant over the day, as demonstrated by Crago, 1996. For simplicity, conditions with lower evaporative fraction are termed as dry and conditions with high evaporative fraction as wet.

The higher value of evaporative fraction implies greater consumption of energy for the process of evaporation and lower warming rates of temperatures are expected. To measure for these sensitivities a range in evaporative fraction is required. Variation in evaporative fraction can be obtained by sampling data either over time or space. Here, the sensitivities of warming rates are obtained for summer months when evaporation is not energy limited. For consistency summer months are described as June, July and August in the northern hemisphere, and December, January and February in the southern hemisphere. These sensitivities are quantified based on the linear regression of daily values of warming rates and evaporative fractions. One can also interpret temperature's sensitivity to evaporative conditions in terms of $DTR$ that is computationally inexpensive.

## 2.3 Formulating diurnal temperature variations

Diurnal variation of surface and air temperature are physically constrained by different sets of processes which are driven by surface energy partitioning. The release of turbulent heat flux ($LE + H$) cools the surface temperature and eventually the heat released gets stored in the the boundary layer. For a non cloudy condition, it is generally the sensible heat flux that contributes to boundary layer heat storage and influences air temperature. Sensible heat flux also relates to aerodynamic conductance ($g_a$), the combination of the two controls the difference between surface and air temperature, as described in equation 1.2. Here, I provide two simple models that show how the release of sensible heat flux from surface and its storage in the boundary layer shapes the diurnal variation of surface and air temperature differently.

### 2.3.1 Surface temperature and surface energy balance

In equation 1.1 the surface temperature term can be obtained from the linearization of $R_{l,net}$, such that $R_{l,net} = R_o + k_r(T_s - T_{ref})$. Here $R_o$ is the net radiation at a reference temperature $T_{ref}$ and $k_r = \sigma T_{ref}^3$, $\sigma$ is the Stefan–Boltzmann constant ($5.67 \times 10^{-8} Wm^{-2}K^{-4}$). Based on this $T_s$ is given as

$$T_s = T_{ref} + \frac{R_s - R_o - LE - H - G}{k_r} \qquad (2.1)$$

The term $LE + H$ can be written as $LE + H = H/(1 - f_e)$. On taking the derivative of equation 2.1 with respect to solar radiation ($R_s$), the warming rate of temperature is expressed as the follow

$$\frac{dT_s}{dR_s} = \frac{1 - f_e}{c_p \cdot \rho \cdot \overline{g_a}} + \frac{dT_a}{dR_s} + \frac{\overline{T_s - T_a}}{\overline{g_a}} \cdot \frac{dg_a}{dR_s} \tag{2.2}$$

See more information on this derivation in chapter 4. On multiplying maximum solar radiation ($R_{s,max}$) with equation 2.2 (more details in chapter 4 and chapter 5) $DT_sR$ is given as follow

$$DT_sR \approx DT_aR + \frac{1.4 \cdot (1 - f_e)}{c_p \rho \cdot (1.4 \cdot \overline{g_a} + \Delta g_a)} \cdot R_{s,max} \tag{2.3}$$

Here it is assumed that maximum of surface and air temperature occurs at the same time as maximum of solar radiation. Equation 2.3 suggests that the $DT_sR$ depends on solar radiation, evaporative fraction, mean aerodynamic conductance ($\overline{g_a}$) and its diurnal amplitude ($\Delta g_a$). $DT_sR$ will be similar to $DT_aR$ if $f_e$ is close to one. The sensitivity of $DT_sR$ to $f_e$ can be obtained by taking the derivative of equation 2.3 with respect to $f_e$ as follows

$$\frac{d(DT_sR)}{df_e} \approx \frac{d(DT_aR)}{df_e} - \frac{1.4}{c_p \rho \cdot (1.4 \cdot \overline{g_a} + \Delta g_a)} \cdot R_{s,max} \tag{2.4}$$

Figure 2.2 summarizes the factors influencing $DT_sR$. Based on equation 2.3 the aerodynamic conductance of vegetation and evaporative fraction are the two major factors that reduce $DT_sR$. Solar radiation increases $DT_sR$, however higher solar radiation ($R_{s,max}$) also increases aerodynamic conductance ($\Delta g_a$) during the day, that should enhance thermal mixing and reduce $DT_sR$. Here it is assumed that evaporative fraction is independent of solar radiation but it should be noted that variation in solar radiation via clouds can influence evaporative conditions. Clouds can also alter the soil wetness via precipitation and eventually influence the evaporative conditions (Hartmann and Short, 1980). Also, high evaporation can lead to the formation of clouds that can reduce solar
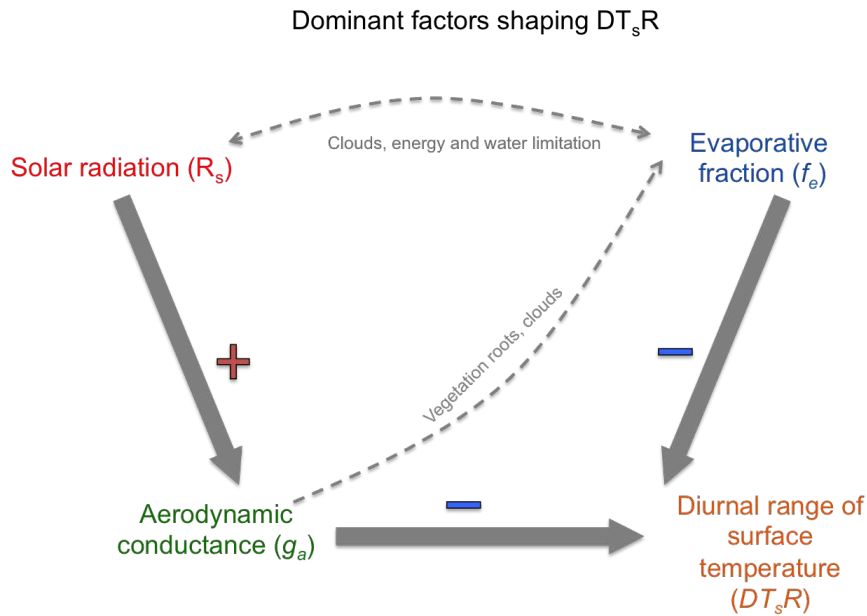
Dominant factors shaping DT$_s$R



FIGURE 2.2: An overview diagram for the response of diurnal surface temperature to solar radiation, evaporative fraction and aerodynamic conductance of vegetation based on equation 2.3

radiation (as shown by the dashed double arrow). Evaporation is also linked to the mean aerodynamic conductance ($\overline{g_a}$) of vegetation. Forests have higher aerodynamic conductance and a deeper root system that supports higher evaporation and formation of clouds (Sheil and Murdiyarso, 2009). These associated relations are incorporated in the model indirectly. Based on this model I further investigate how the cooling effect of the aerodynamic conductance compares to the cooling effect of evaporation in different vegetation types.

### 2.3.2 Air temperature and boundary layer dynamics

The diurnal warming of air temperature or $DT_aR$ mainly depends on the change in heat storage in the boundary layer. From early morning to afternoon the boundary layer grows and accumulates the sensible heat released from the surface. The diurnal boundary layer growth depends on the background lapse rate of the potential temperature ($\Gamma_\theta$) that is usually independent of the evaporative conditions unless there is a warmer residual layer from an earlier day (Santanello Jr, Friedl, and Kustas, 2005). The diurnal increase in boundary layer height ($\Delta z$) also increases the heat capacity of the boundary layer ($\Delta U$) that is approximated as

$$\Delta U = c_p \cdot \rho \cdot DT_a R \cdot \frac{\Delta z}{2} \tag{2.5}$$

Here, $c_p$ is the specific heat capacity of the atmosphere. A depiction of this simple relationship is given in figure 2.3.
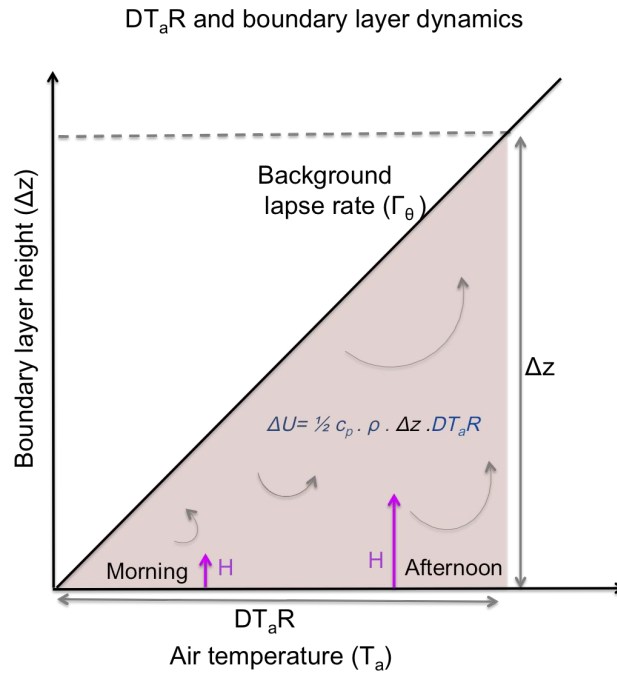


FIGURE 2.3: An overview diagram explaining diurnal air temperature ($DT_a R$) response to boundary layer growth and sensible heat flux ($H$) from morning to afternoon. The relationship of heat stored in the boundary layer($\Delta U$), boundary layer height ($\Delta z$) and $DT_a R$ is depicted in the figure

It is assumed here that $DT_a R$ is similar to diurnal amplitude of potential temperature of the boundary layer. Diurnal boundary layer growth ($\Delta z$) can be estimated by $DT_a R$ and $\Gamma_\theta$ such that $\Delta z = DT_a R / \Gamma_\theta$. Hence, $DT_a R$ depends on the heat stored in the atmosphere but not on the aerodynamic conductance of the vegetation. As per Kleidon and Renner (2017) the optimal turbulent heat flux ($J_{opt}$) relates to the mean solar radiation ($R_s$) and heat storage change by $J_{opt} = 0.5 \cdot (R_s + dU/dt)$. For a non-cloudy condition it is mainly the sensible heat flux that constitutes the change in heat storage($dU/dt$) in the boundary layer and can be given as (more details in chapter 5)

$$\Delta U = \frac{2 - f_e}{2 + f_e} \cdot \Delta U_0 \qquad (2.6)$$

Here $\Delta U_0$ is the heat storage in the boundary layer in absence of evaporation and is related to average solar solar radiation by $\Delta U_0 = 2/\pi \cdot R_{s,max} \cdot \Delta t_{day}$ with $\Delta t_{day}$ being the daylight length. Putting these simplifications in equation 2.5 and equation 2.6, $DT_a R$ can be expressed in terms of $f_e$ as the following

$$DT_a R = \left( \frac{2 - f_e}{2 + f_e} \right)^{1/2} DT_a R_0 \qquad (2.7)$$

Here $DT_a R_0$ is the DTR in absence of evaporation ($f_e = 0$) and is given by $(DT_a R_0)^2 = (2 \cdot \Gamma_\theta \cdot R_{s,max} \cdot \Delta t_{day})/(\pi c_p \rho)$. Equation 2.7 suggests that $DT_a R$ depends on $f_e$ and solar radiation. Here the term $((2 - f_e)/(2 + f_e))^{1/2}$ is about 0.6 for wet ($f_e=1$) conditions. This indicates that $DT_a R$ reduces by 60 % on wet conditions when compared to dry conditions. On taking the derivative of equation 2.7 with respect to evaporative fraction one gets the following

$$\frac{d(DT_a R)}{df_e} = -\frac{2}{((2 - f_e)/(2 + f_e))^{1/2} \cdot (2 + f_e)^2} \cdot DT_a R_0 \approx -0.4 \cdot DT_a R_0 \qquad (2.8)$$

The first term of equation 2.8 is close to 0.4 for different values of $f_e$ ( 0 to 1). Overall, $d(DT_a R)/df_e$ is a negative value that predominantly depends on the solar energy input. Unlike $d(DT_s R)/df_e$, $d(DT_a R)/df_e$ does not depend on aerodynamic conductance of vegetation. As per equation 2.7 $DT_a R$ in all vegetation types is strongly constrained by the solar energy input in the boundary layer.

## 2.4 Data

### 2.4.1 FLUXNET observations

To investigate the responses of diurnal surface and air temperature to evaporative conditions I use observations from multiple FLUXNET sites (Pastorello et al., 2020). FLUXNET is a global network of micrometeorological tower sites that use eddy covariance techniques to provide the routine observations of local atmospheric state variables and surface energy balance components. In this thesis, observations of diurnal air temperature, radiations and energy fluxes from FLUXNET sites are used. It should be noted that FLUXNET does not provide observations of surface temperature. Here surface temperature is estimated from the upward longwave emission using Stefan–Boltzmann's law. The key attribute of FLUXNET observations is the ability to measure in-situ fluxes at a spatial scale of hundreds of meters and on finer time scales of half hourly over a period of decades (Baldocchi et al., 2001). This is particularly important for my work since I am interested in partitioning of turbulent heat flux and their impact of temperatures.

FLUXNET network is dispersed over the continents of North, Central and South America, Europe, Asia, Africa and Australia. My research is based on FLUXNET's single site to multiple sites analyses. Single site analysis is designed to determine the first order differences of surface and air temperature in a typical cropland site of the Southern Great Plains. To link the findings based on this study to boundary layer height response to evaporative conditions we use boundary layer height data from Atmospheric Emitted Radiance Interferometer (AERI) for the Southern Great plains (Ferrare, 2012; Turner, Mlawer, and Revercomb, 2016). To understand how common these findings are and how these responses differ for different vegetation types. Then the study is further extended to multiple FLUXNET sites. Overall, this thesis uses 163 FLUXNET sites belonging to short vegetation, savanna and forest. These sites were selected because they have more than two years of observations, that is required to sample adequate number of dry and wet days.

### 2.4.2 ERA5 reanalysis

ERA5 is the reanalysis product that combines historical observations into global estimates using advanced modelling and data assimilation systems (Copernicus, 2019). It is the fifth generation of of reanalysis product provided by European Centre for Medium Range Weather Forecasts (ECMWF). ERA5 reanalysis was released in year 2019 and is an

improvised version of the older ERA5-Interim reanalysis product (Hoffmann et al., 2019).

In this thesis I use ERA5 at its finest resolution of 31 km (0.25 degree Latitude-Longitude grid) covering the years 2000 to 2015. Here, daily temperature products, surface energy balance components and the boundary layer height of ERA5 are used.

There are two main objectives of using ERA5 data. Firstly, unlike FLUXNET observations, ERA5 reanalysis provides continuous data in space, including PBL height that is otherwise not necessarily measured at FLUXNET sites. Relating PBL height to different components of surface energy balance is useful for obtaining insights on land atmosphere interaction. Secondly, to highlight the plausible biases in ERA5 temperature products by comparing ERA5 and FLUXNET findings (see details in chapter 5) .

## 2.5   Overview of publications

The next three chapters (3, 4 and 5) are research published in the international peer-reviewed journals. The overall structure of the three chapters is illustrated in figure 2.4.

Chapter 3 explores the different responses of surface temperature and air temperature warming rates to evaporative conditions in a cropland FLUXNET site. Here the main focus is to understand the role of boundary layer in compensating air temperature's response to evaporative conditions. In chapter 4, similar analysis is extended to multiple FLUXNET sites with a focus on diurnal variation of surface temperature. Here a surface energy balance model is developed to quantify the sensitivity of diurnal surface temperature to evaporative conditions, aerodynamic conductance and solar radiation. In chapter 5, the research is developed to continental scale by using additional FLUXNET sites and ERA5 reanalysis data. The main focus of chapter 5 is to establish simple physical models that can diagnose the factors shaping the diurnal variation of surface and air temperature. The findings of chapters 3, 4 and 5 are then concluded in chapter 6 along with the main limitations, interpretations, implications and future prospects of this thesis.
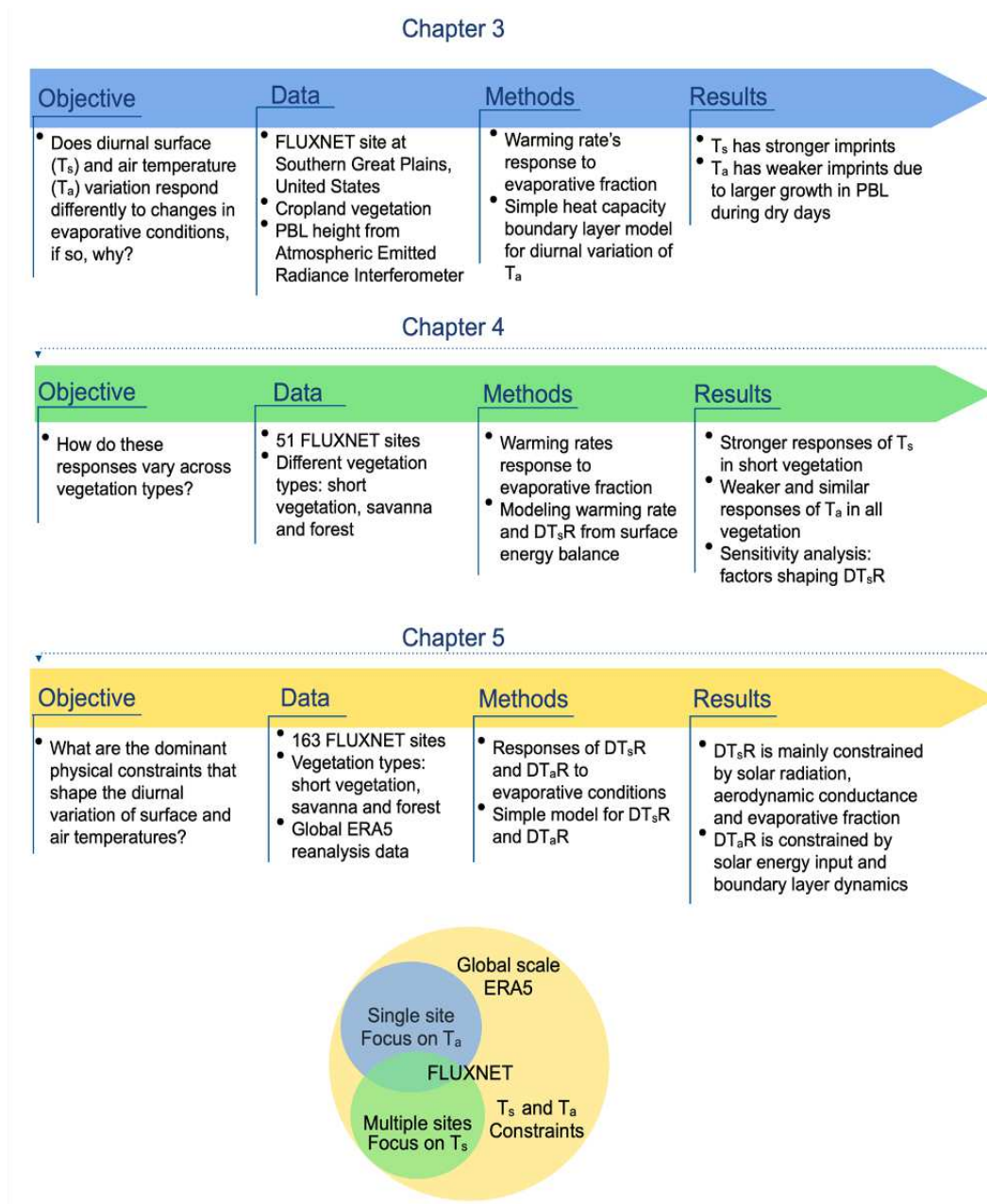
FIGURE 2.4: A flow diagram of publications of the thesis.

# Chapter 3

# Do Surface and Air Temperatures Contain Similar Imprints of Evaporative Conditions?

This chapter is originally published in

# Geophysical Research Letters

**Key Points:**
- Diurnal variations in surface temperature respond more strongly to water limitation than air temperature
- This is shown by the rate at which daytime temperature increases with solar radiation using data from the Southern Great Plains site
- The weaker response of air temperature is explained by the compensating effect of stronger boundary layer growth

**Supporting Information:**
- Supporting Information S1

**Correspondence to:**
A. Panwar,
apanwar@bgc-jena.mpg.de

## Do Surface and Air Temperatures Contain Similar Imprints of Evaporative Conditions?

**Annu Panwar[1]** [iD], **Axel Kleidon[1]** [iD], and **Maik Renner[1]** [iD]

[1]Biospheric Theory and Modelling Group, Max Planck Institute for Biogeochemistry, Jena, Germany

**Abstract** Generally, surface and air temperatures seem closely related but we show that they respond differently to evaporative conditions. We evaluate the temperature increase in response to solar radiation for different evaporative fractions, using observations from the Southern Great Plains. The warming rate of air temperature decreases only by $1.7 \times 10^{-3}$ K/(W m$^{-2}$) from dry to moist conditions compared to a stronger reduction by $14 \times 10^{-3}$ K/(W m$^{-2}$) for surface temperature. The weaker response of air temperature to evaporative fraction is explained by the larger growth of boundary layer on drier days, which suppresses the warming of air. Estimates based on this explanation reproduce the warming rate of air temperature in observations. Our results show that diurnal variations of surface temperatures contain imprints of evapotranspiration while air temperatures do not. These findings appear important to be considered when using, analyzing, or interpreting temperature data in studies dealing with climate change, hydrology, or land-atmosphere interactions.

**Plain Language Summary** Surface and air temperatures are measured just 2 m apart, so it might seem that they carry the same information. Here we show that these temperature measurements respond rather differently to whether the surface evaporates or not. To show this, we use data from a well-equipped measurement site in the Central United States and calculate the rates by which the surface and the air warm in response to solar radiation. We found that the surface temperature responds about 8 times stronger to evaporation than air temperature. We explain this weaker response of air temperature by the stronger growth of the boundary layer without evaporation. This results in a deeper, well-mixed boundary layer that does not warm as strongly. What our results imply is that evaporation may be inferred from surface temperatures, but not from air temperatures.

## 1. Introduction

Evapotranspiration uses three fifths of the net radiation at the surface, strongly affecting the Earth's land surface temperatures. Shukla and Mintz (1982) showed that in absence of evapotranspiration, the Northern Hemisphere would be 15 to 25 K warmer than the present-day climate. The direct relationship between reduced temperature and evapotranspiration is well known and described by the concept of evaporative cooling. Therefore, temperature is used as a critical parameter to derive evapotranspiration estimates. However, approaches can differ in terms of whether these use surface or air temperature.

Air temperature is generally used in empirical methods to estimate potential evapotranspiration (Hargreaves & Samani, 1985; Langbein, 1949; Thornthwaite, 1948) which is convenient because air temperature is typically easily available from routine measurements at meteorological stations. Few studies (Betts & Ball, 1995; Gentine et al., 2016; Santanello et al., 2009) use the diurnal evolution of air temperature in combination with humidity to estimate the share of evaporation in the total turbulent heat flux. Surface temperature, however, is not measured frequently at meteorological stations, but it is directly related to energy and moisture flux exchange between the land surface and the atmosphere (Idso et al., 1975; Jin & Dickinson, 2010; Sellers et al., 1988). With advances in remote sensing, data sets of radiometric surface temperature have become available, which are used for evapotranspiration estimates as well (Kalma et al., 2008; Kustas & Norman, 1996; Price, 1982; Seguin & Itier, 1983). Although remote sensing-based methods are applicable for large-scale estimates, some limitations in remote sensing products (Li et al., 2009) encourage the use of routine observations of air temperature at the local scale. So far, the retrieval of air temperature from remotely sensed surface temperature shows a robust relationship (Benali et al., 2012; Kawashima et al., 2000; Schwarz et al., 2012; Stisen et al., 2007; Sun et al., 2005; Zhu et al., 2013). Since surface and air

temperatures are measurements taken only 2 m apart, it may seem that these temperatures carry similar imprints of evapotranspiration.

Here we show that although surface and air temperatures are strongly coupled, they respond rather differently to evaporative conditions in their diurnal evolution. The daytime increase in surface temperature is strongly affected by the partitioning of the turbulent heat fluxes. This partitioning can be expressed by the evaporative fraction as the ratio of the latent to the total turbulent heat fluxes. Under wet conditions and high evaporative fraction, the increase in surface temperature is suppressed, while under dry conditions or low evaporative fraction, surface temperature increases much more strongly, yielding highest maximum surface temperatures. Air temperature is linked to both the surface and the lower atmosphere. Under daytime conditions, air temperature reflects essentially the potential temperature of the convective boundary layer (Oke, 1987; Stull, 1988). The height of this boundary layer is, however, not constant, but increases with the influx of sensible heat (Tennekes, 1973). Thus, an increased partitioning toward the sensible heat flux (or a lower evaporative fraction) results in a deeper growth of the boundary layer (Troen & Mahrt, 1986). We hypothesize that the greater boundary layer height enlarges the volume of the well-mixed boundary layer and hence its effective heat capacity. Consequently, the heating of the boundary layer is distributed over a greater vertical height, resulting in a suppressed warming of air temperature and a lower sensitivity to the evaporative fraction.

To demonstrate this, we use observations from the Southern Great Plains cropland site in Lamont, Oklahoma. We analyze the diurnal coupling of surface and air temperatures and show that their minima strongly correlate, whereas their maxima correlate less, especially on drier days. To evaluate their different responses to the evaporative conditions, we evaluate their morning to daytime evolution. This is done by comparing the temperature increases from morning to noon in response to surface solar radiation, which we refer to here as their warming rates. We refer to these warming rates as the derivative $dT_s/dR_s$ and $dT_a/dR_s$ for simplicity, noting that the strongest influence on daytime warming is the heating by solar radiation ($R_s$), although other factors also affect their variation. After presenting our results, we demonstrate with a simple calculation that the compensating effect of stronger boundary layer growth during drier conditions can reproduce the lack of sensitivity of the warming rate of air temperature inferred from observations and support our explanation.

## 2. Methods and Data

### 2.1. Definition of Warming Rates

We define the warming rate as the rate of temperature increase in response to a unit increase of surface solar radiation before solar noon, in units of $K/(W\,m^{-2})$. We express it as the derivative of temperature ($T$) to surface solar radiation ($R_s$), $dT/dR_s$. The use of solar radiation is justified by its dominant role in driving the diurnal course of temperatures (e.g., Bristow & Campbell, 1984). It is the main input of energy to the land surface and also a forcing which is largely independent of surface conditions provided clear-sky days.

To illustrate the use of surface solar radiation as a reference variable, we compare two different ways to show the diurnal changes in temperature. Figure 1a shows the common way to illustrate the diurnal cycle, with the mean diurnal variation of surface temperature, air temperature, and solar radiation plotted against time for clear-sky days in summer observed at Lamont, Oklahoma (see section 2.2 for data details). The temporal changes in the two temperatures mirror the change in solar radiation but it does not convey much information about their functional dependency. However, when plotting the two temperatures against solar radiation directly, this typically results in counterclockwise hysteresis (e.g., Renner et al., 2019) as shown in Figure 1b. These hystereses show a remarkable linear relationship to surface solar radiation during the time between sunrise and solar noon. This linear relationship is used here as a justification to infer the warming rate of temperature from observations by linear regression (shown by the stars in Figure 1b). Note that our approach to describe the diurnal cycle does not inform us about nighttime conditions. This is justified because turbulent fluxes on land are typically very small during nighttime.

### 2.2. Data and Analysis

We use observations of the surface energy balance components, temperatures, and boundary layer height from the Southern Great Plains cropland site at Lamont, OK (36° 39′N, 97° 37′W; elevation of 312 m), a
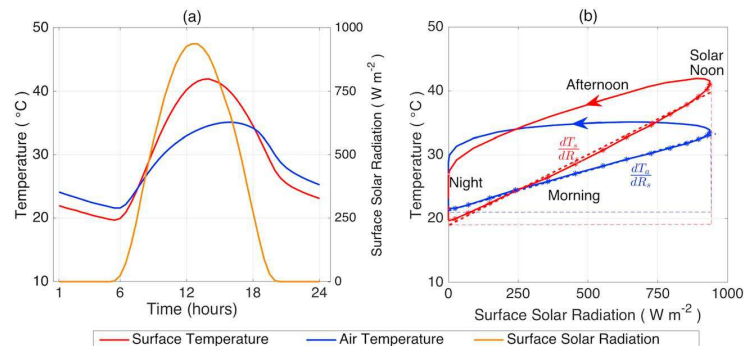
**Figure 1.** (a) Mean diurnal variation of surface temperature, air temperature, and incoming surface solar radiation observed at Lamont, OK, for clear-sky days during summer months of 2003–2012. (b) Same data as shown in (a), but temperatures are plotted against surface solar radiation. Arrows show the direction of the hysteresis from morning to afternoon. We define the warming rates ($dT_s/dR_s$ and $dT_a/dR_s$) as the slopes of temperatures ($T_s$, $T_a$) to incoming solar radiation ($R_s$) after sunrise and before solar noon (dashed lines in (b)).

recognized hot spot of land-atmosphere coupling (Koster, 2004). This site is one of the world's largest climate research facility, and is very well equipped for monitoring surface and atmospheric data (Sisterson et al., 2016). The site is reasonably homogeneous, covered mostly by cropland. We use half-hourly surface meteorological data obtained by an eddy covariance station from the FluxNet network for the years 2003 to 2012 (Fischer et al., 2007). Surface temperature is derived from outgoing longwave radiation at the surface using the Stefan-Boltzmann law. The 2-m air temperature is assumed to be equivalent to the potential temperature of boundary layer. To obtain boundary layer heights, we use hourly measurements from the surface-based Atmospheric Emitted Radiance Interferometer, which is available for the years 2009 to 2011 (Ferrare, 2012).

For our analysis, only clear-sky days of the summer months (June–August) are selected to keep the incoming solar radiation comparable. To identify clear-sky days, surface solar radiation is compared to the potential radiation (i.e., the incoming solar radiative flux at the top of the atmosphere). A day is classified as a clear-sky day if the aggregated surface solar radiation from morning to solar noon is greater than 65% of the aggregated potential radiation. We define morning as the time when surface solar radiation is greater than 20 W/m$^2$ and solar noon when solar radiation is at its maximum. In total, 44% of the summer days of the time period are clear-sky days (404 of 920 days).

Data are then stratified based on the daily mean evaporative fraction. The evaporative fraction is calculated as the ratio of the latent heat flux to the total turbulent heat flux using the eddy covariance observations. This ratio ranges from 0 to 1, corresponding to dry and moist conditions, respectively. Next, we calculate how the warming rates of surface and air temperatures are affected by the evaporative fraction. This is determined by linear regression. Similarly, linear regression is used to relate the growth of the boundary layer height to evaporative fraction.

## 3. Results and Discussion

### 3.1. Analysis of the Observations

To illustrate the different responses of surface and air temperatures to evaporative fraction we first examine the relationships of their minimum and maximum temperatures at the site. Figure 2a shows a strong linear relation between minimum temperatures with high correlation ($r^2 = 0.74$) and with a slope close to the 1:1 line irrespective of the evaporative condition of the day. Minimum temperatures are observed at the end of the night near sunrise and turbulent fluxes are essentially absent. Hence, no clear effect of the evaporative fraction on minimum temperature can be seen. Maximum temperatures are achieved in the afternoon when solar radiation fuels the turbulent heat fluxes and causes the growth of boundary layer. Figure 2b shows that maximum surface and air temperatures correlate much less ($r^2 = 0.53$) with a clear shift from the 1:1 line,
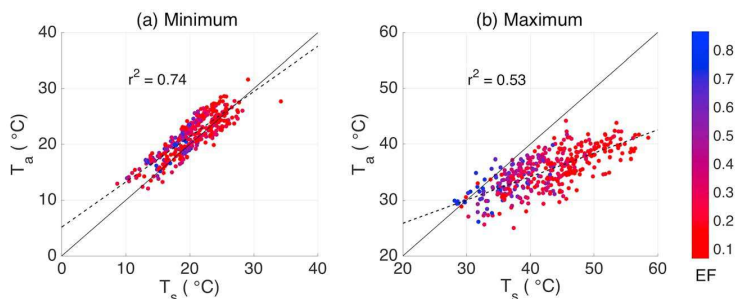
**Figure 2.** Relationship between observed (a) minimum and (b) maximum surface ($T_s$) and air temperatures ($T_a$) for clear-sky days in the summer season at the Southern Great Plains site in Lamont, OK. The color scale depicts the evaporative fraction (EF). The solid black line is the 1:1 line and the dashed line is the linear fit.

representing a weaker daytime warming of air temperature compared to surface temperature. However, on days with a high evaporative fraction (blue points in Figure 2b), surface and air temperatures show similar magnitudes.

To explain this difference in response of surface and air temperatures, we next looked at their warming rates. Figure 3a shows the relationships between the warming rates of the two temperatures and evaporative fraction. The magnitude of the warming rate in surface temperature is found to be much higher than that of air temperature especially on dry days, which is consistent with the deviation from the 1:1 line shown in Figure 2b. The warming rate of surface temperature decreases significantly to about half its value from low to high evaporative fractions with $r^2 = 0.4$. The warming rate of air temperature, however, decreases only weakly from low to high evaporative fractions with $r^2 = 0.05$. The linear regression equations for both warming rates as a function of evaporative fraction are shown in Figure 3a. What these regressions imply is that surface temperature increases more strongly on drier days with low evaporative fraction, represented by a greater warming rate $dT_s/dR_s$, than on wet days with a high evaporative fraction. Air temperature, however, increases almost independently of water availability during the day as its warming rate, $dT_a/dR_s$, shows a much weaker variation with evaporative fraction.

### 3.2. Interpretation by Boundary Layer Growth

We hypothesize that the weaker response of the warming rate of air temperature to evaporative fraction is the consequence of the compensating effect of stronger diurnal boundary layer growth. This hypothesis is supported by observations of boundary layer growth ($\Delta z$), taken as the difference in boundary layer height between its maximum height and early morning (Figure 3b). Although the correlation is comparatively weak ($r^2 = 0.2$, $p$ value <0.01), the observations show that $\Delta z$ decreases by more than a factor of 2 from dry to moist conditions.
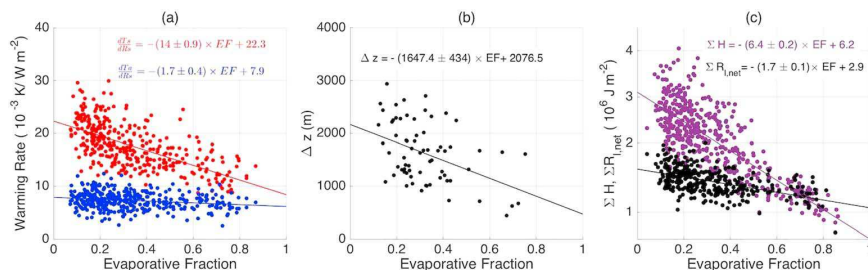


**Figure 3.** (a) Relationships of the warming rates of surface ($dT_s/dR_s$, red) and air temperatures ($dT_a/dR_s$, blue) with evaporative fraction (EF) in observations. (b) Relationship of observed boundary layer height growth from its minima to maxima ($\Delta z$) and EF. (c) Relationships of morning to solar noon accumulated fluxes of sensible heat (H, purple) and net longwave radiation ($R_{l,net}$, black) with EF in observations. Solid lines represent the linear best fit with equations provided in the plots.
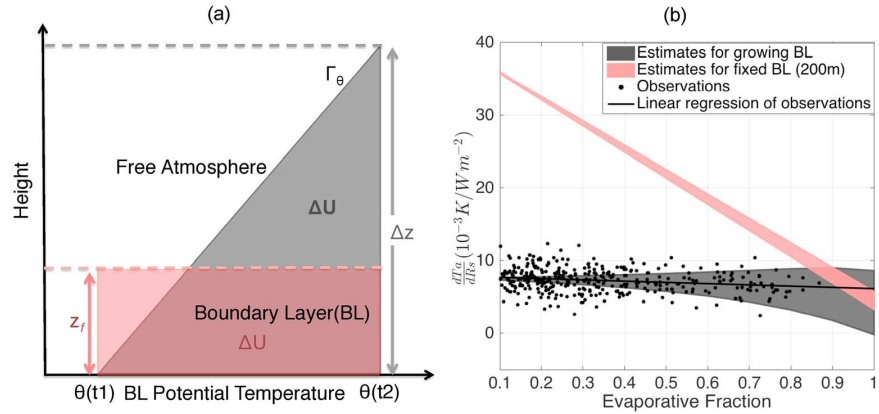
**Figure 4.** (a) A simple description of heat storage change in the boundary layer (BL) to estimate the sensitivity of the warming rate of air temperature to evaporative fraction. The increase in near-surface air temperature corresponds to an equivalent increase in the potential temperature $\theta$ of the lower atmosphere. The gray shaded area shows the heat storage change $\Delta U$ in the lower atmosphere due to a growing boundary layer that grows by $\Delta z$ from early morning (temperature $T_a = \theta(t_1)$) to solar noon (temperature $T_a = \theta(t_2)$) against a background lapse rate $\Gamma_\theta$ in potential temperature. The red box represents the heat storage change $\Delta U$ for a boundary layer with a fixed height $z_f$. (b) Estimated sensitivity of the warming rate for air temperature, $dT_a/dR_s$, for a growing (gray) and a fixed (red) boundary layer to evaporative fraction. The black points show the warming rate obtained from observations, with the black line representing the best linear fit to evaporative fraction.

The compensating effect due to stronger boundary layer growth is likely caused by the greater sensible heat flux on dry days (corresponding to a lower evaporative fraction), resulting in a deeper boundary layer and higher convective mixing. Since near-surface air temperature is approximately equivalent to the potential temperature of the boundary layer, it is not only linked to surface temperture but also represents the heat stored in the boundary layer. The heat stored in the boundary layer depends on its effective heat capacity, which is a function of its height. With a lower evaporative fraction and a greater sensible heat flux, the growth in boundary layer height represents a greater heat storage, which then supresses the warming of air temperture.

To demonstrate this explanation, we estimate the warming rate in air temperature as a function of the effective heat capacity of the boundary layer and the total heat stored in the system. The change in heat storage is calculated following the approach of Kleidon and Renner (2017) by accounting for the heating by the sensible heat flux $H$ and the net longwave radiation $R_{l,net}$. To isolate the effect of different rates of boundary layer growth, we compare the sensitivity of the warming rate to the evaporative fraction for two cases, one in which the boundary layer height is fixed and another in which it is allowed to grow (Figure 4a).

### 3.2.1. Fixed Boundary Layer

We first consider the case of a boundary layer with a fixed height, $z_f$. This case is shown by the red shaded area in Figure 4a. For this case, the change in heat storage within the boundary layer, $\Delta U$, is

$$\Delta U = c_p \, \rho \, \Delta\theta \, z_f \qquad (1)$$

where $c_p = 1,005$ J/kg K is the specific heat capacity of air and $\rho = 1.23$ kg/m$^3$ is the air density, which is assumed to be constant. We assume that the boundary layer height is $z_f = 200$ m, which is close to the observed boundary layer height in the morning. We further assume that the increase in potential temperature, $\Delta\theta$, is equivalent to the increase in near-surface air temperature, $\Delta T_a$.

The increase in heat content, $\Delta U$, is also given by the fluxes that heat the boundary layer during the day, which are the sensible heat flux, $H$, and the net longwave radiation, $R_{l,net}$. The accumulation of heat is thus also given by the integral of $H + R_{l,net}$ from early morning to solar noon (times $t_1$ and $t_2$ in Figure 4a). We can thus derive the warming rate of air temperature by combining the integrated warming rate with equation (1) and obtain

$$dT_a/dR_s = \sum_{t1}^{t2} \ \left(H + R_{l,net}\right) / \left(c_p \, \rho \, R_{s,\max} \, z_f\right) \tag{2}$$

where $R_{s,max}$ is the maximum solar radiation at solar noon and $\sum_{t1}^{t2} \ (H + R_{l,net})$ is calculated from the linear regressions shown in Figure 3c. Figure 4b (red line) shows the warming rate for this case, which shows a strong decrease with evaporative fraction that is inconsistent with observations (black line).

### 3.2.2. Growing Boundary Layer

The case of a growing boundary layer is shown by the gray shaded triangle in Figure 4a. The boundary layer grows by an increment $\Delta z$ against a background lapse rate $\Gamma_\theta$ due to the heat input from the surface. For simplicity, we assume that the background lapse rate remains constant for all evaporative fractions. The accumulation of heat in the boundary layer increases its potential temperature by $\Delta\theta$ (the width of the gray shaded triangle in Figure 4a), which is related to $\Delta z$ (the height of the triangle) by the background lapse rate by $\Gamma_\theta = \Delta\theta/\Delta z$. The growth in boundary layer height enlarges the total volume, and hence, the increase in heat storage ($\Delta U$) results from both the increase in temperature and in height:

$$\Delta U = c_p \, \rho \, \Delta\theta \, \Delta z/2 \tag{3}$$

Note that this expression is different from the mathematical derivative $\Delta U = c_p \, \rho \, \Delta \, (z\theta) = c_p \, \rho(z \, \Delta\theta + \theta \, \Delta z)$, which would imply that the growing boundary layer would heat the atmosphere from zero to $\theta$, rather than by $\Delta\theta$.

We obtain an expression for the warming rate of air temperature as in the fixed case, and get

$$dT_a/dR_s = \sum_{t1}^{t2} \ \left(H + R_{l,net}\right) / \left(c_p \, \rho \, R_{s,\max} \, \Delta z/2\right) \tag{4}$$

In the observations, $R_{s,max} \approx 950$ W/m$^2$. For consistency, $\Delta z$ is assumed to be equivalent to the difference between the maximum and minimum boundary layer height in the observations, and we use the linear regression from Figure 3b. The term $\sum_{t1}^{t2} \ (H + R_{l,net})$ is obtained from the linear regressions with evaporative fraction in the observations shown in Figure 3c.

The warming rate of air temperature with a growing boundary layer reproduces the observations very well (gray line in Figure 4b). Note that the uncertainty increases with higher evaporative fraction, which can be explained by comparatively fewer number of days with high evaporative fraction. This simple estimate supports our hypothesis that it is the difference in growth of the boundary layer that results in the weak response of the warming rate of near-surface air temperature to evaporative fraction.

### 3.3. Discussion

Although our estimate for the warming rate of air temperature is rather simple, it agrees very well with observations. This suggests that the changing heat capacity of the boundary layer is the main explanation for the differences in warming rates. It supports the notion of the boundary layer as a diurnal heat storage that buffers out the strong diurnal variations in solar radiation. This notion has previously been used to explain the difference in climate sensitivity of land and ocean (Kleidon & Renner, 2017).

While we only used one site in our evaluation because of the avilability of boundary layer measurements, we would expect our results and explanation to also hold in other regions as it is based on a simple, physical mechanism. The hysteretic behavior of air temperature was reported previously for a site in central Europe (Renner et al., 2019). Also, using four sites from the FluxNet data set, we found similar sensitivities of the warming rates to evaporative fraction for nonforested regions (see Figure S1 and Table S1 in the supporting information). This suggests that we describe a general phenomenon, although it would require additional research to better understand further factors that shape the sensitivities of warming rates.

Our result is also consistent with the study by Good et al. (2017), who showed the stronger coupling between global surface and air temperature at their minima. They attributed the weaker daytime coupling of the two temperatures to the influence of insolation. What we show here is that in addition to insolation, the evaporative fraction also governs the relationship of the two temperatures. Our observed decoupling of surface and

air temperatures during daytime agrees well with the findings by Sheng et al. (2017) for nonforested areas in southeastern China during the summer season.

Our findings are also consistent with a global study by Mildrexler et al. (2011), who analyzed the relationship between daily maximum air temperatures and remote sensing-derived land surface temperatures analogously to our Figure 2b. They found that all nonforested areas show good agreement at lower temperatures but a divergence toward higher surface temperatures. We show that this divergence can be attributed to drier conditions which enhance the response of surface temperature to solar radiation, while the increase of air temperature is suppressed by stronger boundary layer growth.

## 4. Conclusions

Our study demonstrates significant differences in the diurnal evolution and coupling of surface and air temperature under different surface evaporative conditions. We showed that the diurnal variation of surface temperatures respond much more strongly to evaporative conditions, using the relationship of its warming rate and evaporative fraction. This suggests that the warming rate of surface temperature is an important metric which can be used to estimate evapotranspiration. Contrary to this, we found that the warming rate of air temperature is much less related to the evaporative conditions, which would imply that evaporation cannot be inferred from diurnal variations in air temperature. Using heat storage considerations of the boundary layer, we then explained this lack of sensitivity in the warming rate of air temperature by the compensating role of boundary layer growth.

Temperature is widely used in the climate sciences, for instance in the detection and attribution of global warming, in estimating evaporation and in evaluating impacts of land cover change. Our findings imply that one cannot use surface and air temperature interchangeably when evaluating temperature records, as they convey different information about evaporation or boundary layer growth in land-atmosphere exchange.

## References

Benali, A., Carvalho, A. C., Nunes, J. P., Carvalhais, N., & Santos, A. (2012). Estimating air surface temperature in Portugal using MODIS LST data. *Remote Sensing of Environment*, *124*, 108–121. https://doi.org/10.1016/j.rse.2012.04.024

Betts, A. K., & Ball, J. H. (1995). The FIFE surface diurnal cycle climate. *Journal of Geophysical Research*, *100*(D12), 25679. https://doi.org/10.1029/94JD03121

Bristow, K. L., & Campbell, G. S. (1984). On the relationship between incoming solar radiation and daily maximum and minimum temperature. *Agricultural and Forest Meteorology*, *31*(2), 159–166. https://doi.org/10.1016/0168-1923(84)90017-0

Ferrare, R. (2012). *Raman lidar/AERI PBL Height Product* [data set]. Atmospheric Radiation Measurement (ARM) Archive, Oak Ridge National Laboratory (ORNL), Oak Ridge, TN. https://doi.org/10.5439/1169501

Fischer, M. L., Billesbach, D. P., Berry, J. A., Riley, W. J., & Torn, M. S. (2007). Spatiotemporal variations in growing season exchanges of $CO_2$, $H_2O$, and sensible heat in agricultural fields of the Southern Great Plains. *Earth Interactions*, *11*(17), 1–21. https://doi.org/10.1175/EI231.1

Gentine, P., Chhang, A., Rigden, A., & Salvucci, G. (2016). Evaporation estimates using weather station data and boundary layer theory: Evaporation from weather data. *Geophysical Research Letters*, *43*, 11,661–11,670. https://doi.org/10.1002/2016GL070819

Good, E. J., Ghent, D. J., Bulgin, C. E., & Remedios, J. J. (2017). A spatiotemporal analysis of the relationship between near-surface air temperature and satellite land surface temperatures using 17 years of data from the ATSR series: Global analysis of $T_{2 m}$ and satellite LST. *Journal of Geophysical Research: Atmospheres*, *122*, 9185–9210. https://doi.org/10.1002/2017JD026880

Hargreaves, G. H., & Samani, Z. A. (1985). Reference crop evapotranspiration from temperature. *Applied Engineering in Agriculture*, *1*(2), 96–99. https://doi.org/10.13031/2013.26773

Idso, S. B., Jackson, R. D., & Reginato, R. J. (1975). Estimating evaporation: A technique adaptable to remote sensing. *Science*, *189*(4207), 991–992. https://doi.org/10.1126/science.189.4207.991

Jin, M., & Dickinson, R. E. (2010). Land surface skin temperature climatology: Benefitting from the strengths of satellite observations. *Environmental Research Letters*, *5*(4), 044004. https://doi.org/10.1088/1748-9326/5/4/044004

Kalma, J. D., McVicar, T. R., & McCabe, M. F. (2008). Estimating land surface evaporation: A review of methods using remotely sensed surface temperature data. *Surveys in Geophysics*, *29*(4–5), 421–469. https://doi.org/10.1007/s10712-008-9037-z

Kawashima, S., Ishida, T., Minomura, M., & Miwa, T. (2000). Relations between surface temperature and air temperature on a local scale during winter nights. *Journal of Applied Meteorology*, *39*(9), 1570–1579. https://doi.org/10.1175/1520-0450(2000)039<1570:RBSTAA>2.0.CO;2

Kleidon, A., & Renner, M. (2017). An explanation for the different climate sensitivities of land and ocean surfaces based on the diurnal cycle. *Earth System Dynamics*, *8*(3), 849–864. https://doi.org/10.5194/esd-8-849-2017

Koster, R. D. (2004). Regions of strong coupling between soil moisture and precipitation. *Science*, *305*(5687), 1138–1140. https://doi.org/10.1126/science.1100217

Kustas, W. P., & Norman, J. M. (1996). Use of remote sensing for evapotranspiration monitoring over land surfaces. *Hydrological Sciences Journal*, *41*(4), 495–516. https://doi.org/10.1080/02626669609491522

Langbein, W. B. (1949). *Annual runoff in the United States (No.52)* (Circular).

Li, Z.-L., Tang, R., Wan, Z., Bi, Y., Zhou, C., Tang, B., et al. (2009). A review of current methodologies for regional evapotranspiration estimation from remotely sensed data. *Sensors*, *9*(5), 3801–3853. https://doi.org/10.3390/s90503801

Mildrexler, D. J., Zhao, M., & Running, S. W. (2011). A global comparison between station air temperatures and MODIS land surface temperatures reveals the cooling role of forests. *Journal of Geophysical Research*, *116*, G03025. https://doi.org/10.1029/2010JG001486

Oke, T. R. (1987). *Boundary Layer Climates*. London and New York: Methuen. [usw.]

Price, J. C. (1982). Estimation of regional scale evapotranspiration through analysis of satellite thermal-infrared data. *IEEE Transactions on Geoscience and Remote Sensing*, *GE-20*(3), 286–292. https://doi.org/10.1109/TGRS.1982.350445

Renner, M., Brenner, C., Mallick, K., Wizemann, H.-D., Conte, L., Trebs, I., et al. (2019). Using phase lags to evaluate model biases in simulating the diurnal cycle of evapotranspiration: A case study in Luxembourg. *Hydrology and Earth System Sciences*, *23*(1), 515–535. https://doi.org/10.5194/hess-23-515-2019

Santanello, J. A., Peters-Lidard, C. D., Kumar, S. V., Alonge, C., & Tao, W.-K. (2009). A modeling and observational framework for diagnosing local land–atmosphere coupling on diurnal time scales. *Journal of Hydrometeorology*, *10*(3), 577–599. https://doi.org/10.1175/2009JHM1066.1

Schwarz, N., Schlink, U., Franck, U., & Großmann, K. (2012). Relationship of land surface and air temperatures and its implications for quantifying urban heat island indicators—An application for the city of Leipzig (Germany). *Ecological Indicators*, *18*, 693–704. https://doi.org/10.1016/j.ecolind.2012.01.001

Seguin, B., & Itier, B. (1983). Using midday surface temperature to estimate daily evaporation from satellite thermal IR data. *International Journal of Remote Sensing*, *4*(2), 371–383. https://doi.org/10.1080/01431168308948554

Sellers, P. J., Hall, F. G., Asrar, G., Strebel, D. E., & Murphy, R. E. (1988). The first ISLSCP field experiment (FIFE). *Bulletin of the American Meteorological Society*, *69*(1), 22–27. https://doi.org/10.1175/1520-0477(1988)069<0022:TFIFE>2.0.CO;2

Sheng, Y., Liu, X., Yang, X., Xin, Q., Deng, C., & Li, X. (2017). Quantifying the spatial and temporal relationship between air and land surface temperatures of different land-cover types in southeastern China. *International Journal of Remote Sensing*, *38*(4), 1114–1136. https://doi.org/10.1080/01431161.2017.1280629

Shukla, J., & Mintz, Y. (1982). Influence of land-surface evapotranspiration on the Earth's climate. *Science*, *215*(4539), 1498–1501. https://doi.org/10.1126/science.215.4539.1498

Sisterson, D. L., Peppler, R. A., Cress, T. S., Lamb, P. J., & Turner, D. D. (2016). The ARM Southern Great Plains (SGP) site. *Meteorological Monographs*, *57*, 6.1–6.14. https://doi.org/10.1175/AMSMONOGRAPHS-D-16-0004.1

Stisen, S., Sandholt, I., Nørgaard, A., Fensholt, R., & Eklundh, L. (2007). Estimation of diurnal air temperature using MSG SEVIRI data in West Africa. *Remote Sensing of Environment*, *110*(2), 262–274. https://doi.org/10.1016/j.rse.2007.02.025

Stull, R. B. (Ed) (1988). *An Introduction to Boundary Layer Meteorology*. Dordrecht, Netherlands: Springer. https://doi.org/10.1007/978-94-009-3027-8

Sun, Y.-J., Wang, J.-F., Zhang, R.-H., Gillies, R. R., Xue, Y., & Bo, Y.-C. (2005). Air temperature retrieval from remote sensing data based on thermodynamics. *Theoretical and Applied Climatology*, *80*(1), 37–48. https://doi.org/10.1007/s00704-004-0079-y

Tennekes, H. (1973). A model for the dynamics of the inversion above a convective boundary layer. *Journal of the Atmospheric Sciences*, *30*(4), 558–567. https://doi.org/10.1175/1520-0469(1973)030<0558:AMFTDO>2.0.CO;2

Thornthwaite, C. W. (1948). An approach toward a rational classification of climate. *Geographical Review*, *38*(1), 55. https://doi.org/10.2307/210739

Troen, I. B., & Mahrt, L. (1986). A simple model of the atmospheric boundary layer; sensitivity to surface evaporation. *Boundary-Layer Meteorology*, *37*(1–2), 129–148. https://doi.org/10.1007/BF00122760

Zhu, W., Lü, A., & Jia, S. (2013). Estimation of daily maximum and minimum air temperature using MODIS land surface temperature products. *Remote Sensing of Environment*, *130*, 62–73. https://doi.org/10.1016/j.rse.2012.10.034

**@AGU**PUBLICATIONS

*Geophysical Research Letters*

Supporting Information for

# Do surface and air temperatures contain similar imprints of evaporative conditions?

**Annu Panwar, Axel Kleidon and Maik Renner**

Biospheric Theory and Modelling Group, Max Planck Institute for Biogeochemistry, Jena, 07745, Germany

**Contents of this file**

**Introduction**

This Supporting Information provides additional data analysis to support the generality of the results shown in the manuscript. We show data from four additional FLUXNET sites equivalent to Figure 3a in the manuscript in Figure S1. The data was processed for these sites as described in the Methods section of the manuscript. Information about the sites is provided in Table S1.
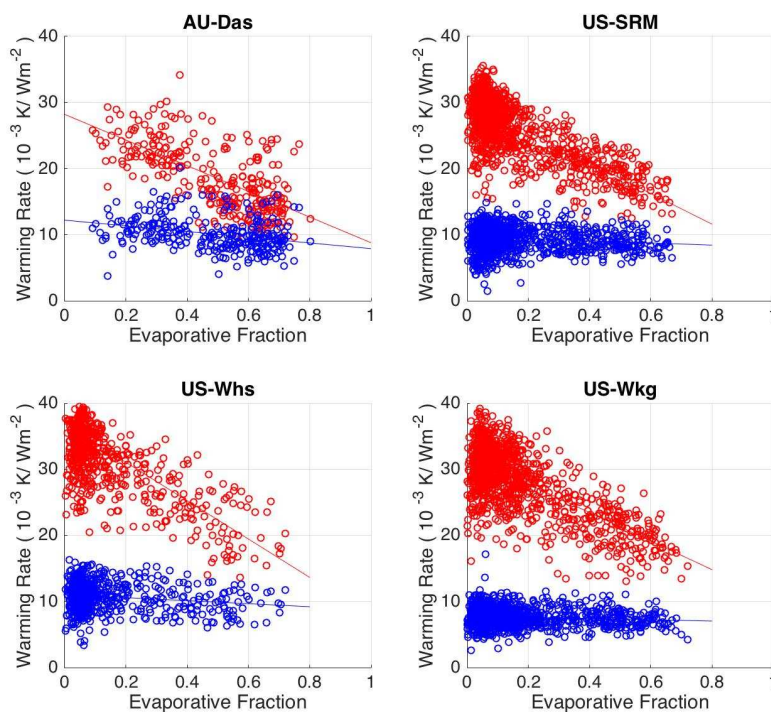
**Figure S1.** As Figure 3a, but for four additional FluxNet sites of different land cover types (See Table S1 for site information).

**Table S1.** Description of additional sites, data used, and regression equations for the trends shown in Figure S1.

| Site ID | Site Description | $dT_s/dR_s$ ($10^{-3}$ K/W m$^{-2}$) | $dT_a/dR_s$ ($10^{-3}$ K/W m$^{-2}$) | Reference |
|---|---|---|---|---|
| AU-Das | Savanna, Australia Daly river cleared 14.16° S, 131.39° E Time period: 2008-2014 | -(19.42 ± 1.45)×EF + 28.20 | -(4.30 ± 0.81)×EF +12.12 | https://doi.org/10.18140/FLX/1440122 |
| US-SRM | Woody Savanna, USA Santa Rita Mesquite 31.82° N, 110.86° W Time period: 2004-2014 | -(23.25 ± 2.03)×EF + 30.18 | -(1.68 ± 0.32)×EF + 9.77 | https://doi.org/10.18140/FLX/1440090 |
| US-Whs | Open Shrubland. USA Walnut Gulch Lucky Hills Shrub 31.74° N, 110.05° W Time period: 2007-2014 | -(29.00 ± 5.75)×EF + 36.85 | -(2.29 ± 0.54)×EF + 11.04 | https://doi.org/10.18140/FLX/1440097 |
| US-Wkg | Grassland, USA Walnut Gulch Kendall Grasslands 31.74° N, 109.94° W | -(21.57 ± 0.90)×EF + 32.07 | -(1.00 ± 0.24)×EF + 7.84 | https://doi.org/10.18140/FLX/1440096 |

# Chapter 4

# Imprints of Evaporative Conditions and Vegetation Type in Diurnal Temperature Variations

This chapter is originally published in

# Imprints of evaporative conditions and vegetation type in diurnal temperature variations

**Annu Panwar[1], Maik Renner[1,a], and Axel Kleidon[1]**

[1]Biospheric Theory and Modeling group, Max Planck Institute for Biogeochemistry, 07745 Jena, Germany
[a]now at: Brandenburg State Office for Environment, Flood Monitoring Centre, 15236 Frankfurt (Oder), Germany

**Correspondence:** Annu Panwar (apanwar@bgc-jena.mpg.de)

**Abstract.** Diurnal temperature variations are strongly shaped by the absorption of solar radiation, but evaporation, or the latent heat flux, also plays an important role. Generally, evaporation cools. Its relation to diurnal temperature variations, however, is unclear. This study investigates the diurnal response of surface and air temperatures to evaporative conditions for different vegetation types. We use the warming rate, defined as the increase in temperature in response to absorbed solar radiation in the morning, and evaluate how it changes with evaporative fraction, which is an indicator of the evaporative conditions. Results for 51 FLUXNET sites show that the warming rate of air temperature carries very weak imprints of evaporative fraction across all vegetation types. However, the warming rate of surface temperature is highly sensitive to evaporative fraction with a value of $\sim 23 \times 10^{-3}\,\mathrm{K\,(W\,m^{-2})^{-1}}$, indicating stronger evaporative cooling for moister conditions. Contrarily, the warming rates of surface and air temperatures are similar at forest sites and carry literally no imprints of evaporative fraction. We explain these contrasting patterns with an analytical surface energy balance model. The derived expressions reproduce the observed warming rates and their sensitivity to evaporative fraction in all vegetation types. Multiplying the warming rate with daily maximum solar radiation gives an approximation for the diurnal surface temperature range ($\mathrm{DT_sR}$). We use our model to compare the individual contributions of solar radiation, evaporative conditions, and vegetation (by its aerodynamic conductance) in shaping $\mathrm{DT_sR}$ and show that the high aerodynamic conductance of forests reduces $\mathrm{DT_sR}$ substantially more ($-56\,\%$) than evaporative cooling ($-22\,\%$). We further show that the strong diurnal variation in aerodynamic conductance ($\sim 2.5$ times of the mean across vegeta-

tion types) reduces $\mathrm{DT_sR}$ by $\sim 35\,\%$ in short vegetation and savanna but only by $\sim 22\,\%$ in forests. We conclude that diurnal temperature variations may be useful for predicting evaporation for short vegetation. In forests, however, the diurnal variations in temperatures are mainly governed by their high aerodynamic conductance, resulting in negligible imprints of evaporative conditions.

## 1 Introduction

Temperature is one of the most widely monitored variables in meteorology. Besides being important for our day-to-day activities, temperature serves as a primary attribute for understanding Earth system processes. The diurnal variation in temperature is considered to be informative in climate science, as described by the diurnal temperature range (DTR), which is basically the difference between daily maximum and minimum temperatures. Information on the diurnal temperature range has facilitated a broad spectrum of research including agriculture, health welfare, climate change, and ecological studies.

Over land, the diurnal variation in temperature is mainly driven by the solar energy input (Bristow and Campbell, 1984). Liu et al. (2004) show a high correlation of 0.88 between the annual solar radiation and the DTR in China. Likewise, Makowski et al. (2009) found their annual correlation to be 0.87 for Europe. Their obvious and still intricate association is also important for determining the influence of solar dimming and brightening on diurnal temperature variations (Wang and Dickinson, 2013; Wild, 2005).

Solar radiation is the dominant, but not the only, factor shaping the diurnal temperature. Available energy at the surface is partitioned into latent and sensible heat fluxes. A higher latent heat flux signifies higher evaporation, which reduces the temperature through evaporative cooling, an effect that can be seen in sensitivity simulations with a global climate model of land evaporation (Shukla and Mintz, 1982). Another climate-model-based analysis (Mearns et al., 1995) shows that differences in evaporation explain 52% of the variance in DTR in the summer season for the USA. Similarly, climate model simulations also show the high sensitivity of DTR to evaporation, especially in the summer season when evaporation is not energy limited (Lindvall and Svensson, 2015). Consequently, methods for estimating evaporation use air temperature (Blaney and Criddle, 1950; Hargreaves and Samani, 1985; Thornthwaite, 1948) and remotely sensed surface temperature (Anderson et al., 2012; Boegh et al., 2002; Jackson et al., 1999; Kustas and Norman, 1999; Price, 1982; Su et al., 2007). Most of the surface-energy-balance-based estimates of evaporation use DTR as an input (Baier and Robertson, 1965; Vinukollu et al., 2011; Yao et al., 2013).

Clouds and precipitation are also important factors that determine DTR (Dai et al., 1999; Stenchikov and Robock, 1995). One can exclude their contribution to some extent by considering only clear sky days in order to distinctly identify the role of evaporative conditions on DTR. Furthermore, the partitioning of the turbulent heat fluxes into sensible and latent heat is also influenced by vegetation type. Taller vegetation has a higher aerodynamic conductance that facilitates mass and heat exchange between the land and atmosphere (Jarvis and McNaughton, 1986). The greater aerodynamic conductance in forests reduces their DTR by reducing their maximum temperatures (Bevan et al., 2014; Gallo, 1996; Jackson and Forster, 2010). Few studies captured the impact of aerodynamic properties of vegetation on temperature, for example, in terms of the decomposed temperature metric theory (Juang et al., 2007; Luyssaert et al., 2014) and the theory of intrinsic biophysical mechanisms (Lee et al., 2011a; Zhao et al., 2014a). Generally, the lower temperatures of forests are associated with their mean evaporative environment, although this may be affected by periods of dry and moist conditions.

In this study, we investigate how the diurnal variation in surface and air temperature responds to changes in evaporative conditions in different vegetation types. Clearly, DTR is not independent of solar radiation, which is why we develop an alternative indicator, namely the warming rate (Panwar et al., 2019), that eliminates the contribution of solar radiation. To illustrate this, the observed normalized diurnal air and surface temperatures are plotted against absorbed solar radiation for a cropland and forest site in Fig. 1. Surface temperature is obtained from upwelling longwave radiation from the surface and air temperature above the canopy, which is usually measured at 2 m height. The diurnal evolution of tempera-

ture is mainly governed by the absorbed solar radiation ($R_s$); this is discernible from the linear increase in the morning ($20\,\mathrm{W\,m^{-2}} \leq R_s \leq R_{s,max}$), as described by the slope. This dependence is accounted for by what we refer to as the warming rate, defined as the increase in temperature due to a unit increase in the absorbed solar radiation and expressed as the derivative $dT_a/dR_s$ for air temperature and $dT_s/dR_s$ for surface temperature with units of $\mathrm{K\,(W\,m^{-2})^{-1}}$. One can approximate the warming rate by the ratio of DTR to maximum solar radiation, $R_{s,max}$, so that the warming rate can be seen as an efficient characteristic that captures the effects on DTR that are not caused by solar radiation. In this study, we use linear regressions of observed data from morning to noon to calculate warming rates.

The temperature warming rate provides insights on the effect of vegetation on the diurnal temperatures variation. Figure 1a shows a greater surface temperature warming compared to air temperature for a cropland site. Contrarily to the short vegetation site, the warming rates of the two temperatures are similar for a forest site (Fig. 1b). This indicates the strong aerodynamic coupling of diurnal air and surface temperatures in forests compared to short vegetation.

Certainly, it is intriguing to find out how evaporative conditions alter this coupling. In our earlier work (Panwar et al., 2019), we looked at the temperature warming rate for a cropland site in the Southern Great Plains (which is shown in Fig. 1a). We observed that the warming rate of surface temperature decreases from dry (less evaporative; sensible heat flux dominates) to moist (evaporative; latent heat flux dominates) conditions, but the warming rate of air temperature remained unaffected. Combining the boundary layer information and heat budget expression, we explained that the diurnal variation in air temperature does not contain the imprints of evaporative conditions due to the compensating role of boundary layer development. If this is a general finding, then the surface temperature warming rate can be used to estimate the evaporative conditions of short vegetation. Furthermore, it is also interesting to see how evaporative cooling competes with the cooling effect of a higher aerodynamic conductance of forests.

In this study, we approach the following two major questions to advance our understanding of diurnal temperature variations: (a) do the diurnal variations in surface and air temperature respond to evaporative conditions? And (b) what is the role of the aerodynamic conductance of vegetation in altering these responses? Our previous work (Panwar et al., 2019) shows the stronger imprints of evaporative conditions in diurnal surface temperature variations in a cropland site. Here, we examine the generality of this finding in short vegetation. Additionally, to understand the role of aerodynamic conductance in modifying these imprints, we analyze data from the taller and more complex vegetation like savanna and forests.

We first present a model based on the surface energy balance to provide an expression for the diurnal temperature
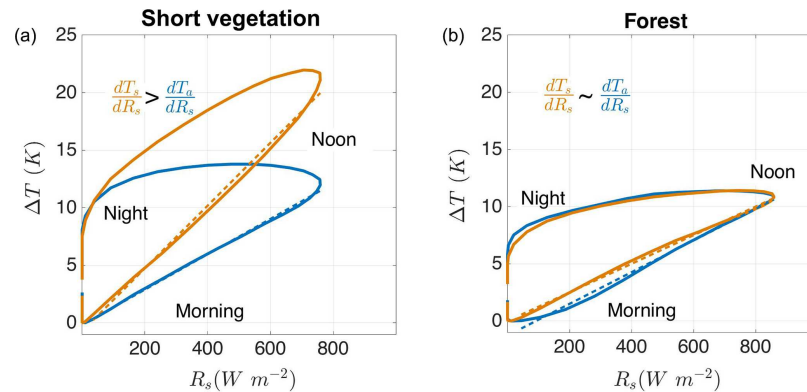
**Figure 1.** Mean diurnal hysteresis formed by plotting the normalized diurnal temperature ($\Delta T = T - T_{\min}$) against absorbed solar radiation ($R_s$) for summer clear sky days. Surface temperature ($T_s$) is depicted in orange and air temperature ($T_a$) in blue. **(a)** A short vegetation cropland site (US Atmospheric Radiation Measurement – ARM) in the Southern Great Plains, Lamont, OK, USA. **(b)** A forest site (CA-TP4) in Ontario, Canada. The dashed lines are the linear regression of the observations falling in the morning slope of the hysteresis that corresponds to the warming rate of air ($\mathrm{d}T_a/\mathrm{d}R_s$) and surface temperature ($\mathrm{d}T_s/\mathrm{d}R_s$).

variation and its response to changes in evaporative conditions and aerodynamic conductance (all variables used are summarized in Table A1). Previous studies (Mallick et al., 2013; Ronda et al., 2001; Steduto and Hsiao, 1998) show diurnal variations in aerodynamic conductance, which are also considered in our model. To evaluate our model, we used observations from 51 FLUXNET sites that include short vegetation, savanna, and forests. Surface and air temperature warming rates, and their response to evaporative conditions, are quantified for each site.

The observational analysis is followed by a demonstration of our model performance that reproduces observed temperature warming rates and their response to evaporative conditions. Using our model, we analyze the factors shaping the diurnal range of surface temperature ($DT_sR$). For this, the diurnal temperature range is obtained by combining the warming rates with the information on solar radiation. We conclude the study by demonstrating the contribution of solar radiation, evaporative fraction, aerodynamic conductance, and its diurnal variation in shaping $DT_sR$, using our observational analysis and model.

## 2 Modeling temperature warming rate

Surface and air temperatures possess a strong diurnal variation that is driven by the absorption of solar radiation. The amplitude of this variation is also affected by other components of the surface energy balance, among which the partitioning of turbulent heat fluxes into latent and sensible heat is important. Generally, the surface energy balance is written as follows:

$$R_s = R_{l,\text{net}} + LE + H + G. \tag{1}$$

Here, $R_s$ is the absorbed solar radiation at the surface, $R_{l,\text{net}}$ is the net longwave radiation, $LE$ is the latent heat flux (with $L$ being the latent heat of vaporization and $E$ the evaporation rate), $H$ is the sensible heat flux, and $G$ is the ground heat flux. For simplification of the surface energy balance, we linearize $R_{l,\text{net}}$ using the first-order terms, such that $R_{l,\text{net}} = R_o + k_r(T_s - T_{\text{ref}})$. Here, $R_o$ is the net radiation at a reference temperature $T_{\text{ref}}$. The second term, $k_r = 4\sigma T_{\text{ref}}^3$, is the linearization constant. Incorporating this simplification of $R_{l,\text{net}}$ in Eq. (1), the surface energy balance can be rearranged to yield an expression for $T_s$, as follows:

$$T_s = T_{\text{ref}} + \frac{R_s - R_o - LE - H - G}{k_r}. \tag{2}$$

The warming rate of surface temperature is obtained by taking the derivative of Eq. (2) with respect to absorbed solar radiation, $R_s$, such that, in the following:

$$\frac{\mathrm{d}T_s}{\mathrm{d}R_s} = \frac{1}{k_r} - \frac{1}{k_r} \cdot \frac{\mathrm{d}(H + LE)}{\mathrm{d}R_s}. \tag{3}$$

Since $R_o$ and $T_{\text{ref}}$ are assumed to be constants and do not vary diurnally with $R_s$, they disappear in Eq. (3). Additionally, it is assumed that the diurnal change in $G$, in response to $R_s$, is negligible ($\mathrm{d}G/\mathrm{d}R_s \sim 0$) compared to the other components of surface energy balance. This assumption is valid since we are considering vegetated sites for our study, although we are aware that, for nonvegetated surfaces, $G$ can represent a noticeable share of absorbed solar radiation (Clothier et al., 1986; Kustas and Daughtry, 1990).

We describe the evaporative conditions by the evaporative fraction ($f_e$), which is the ratio of the latent heat flux ($LE$) to the total turbulent heat fluxes ($H + LE$). Given this, the term $H + LE$ in Eq. (3) can be written as $H/(1 - f_e)$, which yields the following:

$$\frac{\mathrm{d}T_s}{\mathrm{d}R_s} = \frac{1}{k_r} - \frac{1}{k_r} \cdot \frac{1}{(1-f_e)} \cdot \frac{\mathrm{d}H}{\mathrm{d}R_s}. \tag{4}$$

Furthermore, the sensible heat flux can be expressed in terms of the aerodynamic conductance as $H = c_p \rho g_a (T_s - T_a)$, where $c_p = 1005 \, \mathrm{J\,kg^{-1}\,K^{-1}}$ is the specific heat capacity of air, $\rho = 1.23 \, \mathrm{kg\,m^{-3}}$ is air density, $g_a$ is the aerodynamic conductance, and $T_s - T_a$ is difference between surface and air temperature.

To use Eq. (4) to estimate warming rates, information is needed on $\mathrm{d}H/\mathrm{d}R_s$. Typically, $H$ increases linearly with $R_s$ in the morning so that the derivative $\mathrm{d}H/\mathrm{d}R_s$ is constant. Thus, the instantaneous response of $H$ to $R_s$ is equivalent to the mean response, such that $\mathrm{d}H/\mathrm{d}R_s$ can be expressed as follows:

$$\frac{\mathrm{d}H}{\mathrm{d}R_s} = c_p \cdot \rho \cdot \left[ \overline{(T_s - T_a)} \cdot \frac{\mathrm{d}g_a}{\mathrm{d}R_s} + \overline{g_a} \cdot \frac{\mathrm{d}.(T_s - T_a)}{\mathrm{d}R_s} \right]. \tag{5}$$

Here, $\overline{(T_s - T_a)}$ and $\overline{g_a}$ are the morning to noon means of $T_s - T_a$ and $g_a$. The diurnal variations in $g_a$ and $T_s - T_a$ are captured by the terms $\mathrm{d}g_a/\mathrm{d}R_s$ and $\mathrm{d}(T_s - T_a)/\mathrm{d}R_s$. When including Eq. (5) in Eq. (4), we obtain an approximation for the surface temperature warming rate, which is given by the following:

$$\frac{\mathrm{d}T_s}{\mathrm{d}R_s} =$$
$$\frac{(1-f_e) - c_p \cdot \rho \cdot \left[ \overline{(T_s - T_a)} \cdot \mathrm{d}g_a/\mathrm{d}R_s - \overline{g_a} \cdot (\mathrm{d}T_a/\mathrm{d}R_s) \right]}{k_r \cdot (1-f_e) + c_p \cdot \rho \cdot \overline{g_a}}. \tag{6}$$

Here, $\mathrm{d}T_a/\mathrm{d}R_s$ is the warming rate of air temperature. We can further simplify this expression by considering the two terms in the denominator of Eq. (6). Considering $T_{ref} \sim 288 \, \mathrm{K}$, the term $k_r(1-f_e)$ varies between $\sim 4.87$ and $\sim 0.54 \, \mathrm{W\,m^{-2}\,K^{-1}}$, from dry ($f_e = 0$) to moist ($f_e = 1$) conditions, which is much smaller in magnitude compared to the term $c_p \cdot \rho \cdot \overline{g_a}$ that is $\sim 60 \, \mathrm{W\,m^{-2}\,K^{-1}}$ for a typical cropland site ($\overline{g_a} = 0.05 \, \mathrm{m\,s^{-1}}$) and $250 \, \mathrm{W\,m^{-2}\,K^{-1}}$ for a typical forest site ($\overline{g_a} = 0.2 \, \mathrm{m\,s^{-1}}$). Because of these magnitudes, the term $k_r(1-f_e)$ can be neglected. This leads to a further simplification of the warming rate to the following:

$$\frac{\mathrm{d}T_s}{\mathrm{d}R_s} \approx \frac{(1-f_e)}{c_p \cdot \rho \cdot \overline{g_a}} + \frac{\mathrm{d}T_a}{\mathrm{d}R_s} - \frac{\overline{(T_s - T_a)}}{\overline{g_a}} \cdot \frac{\mathrm{d}g_a}{\mathrm{d}R_s}. \tag{7}$$

Equation (7) shows that the morning to noon warming rate of surface temperature is a function of evaporative fraction, the warming rate of air temperature, the mean difference in surface and air temperature, the mean aerodynamic conductance, and also the sensitivity of aerodynamic conductance to solar radiation. Multiplying Eq. (7) with the daily maximum solar radiation shall provide an approximation of the diurnal range of surface temperature ($DT_sR$) as follows:

$$DT_sR \approx \frac{(1-f_e)}{c_p \cdot \rho \cdot \overline{g_a}} \cdot R_{s,max} + DT_aR - \frac{\overline{T_s - T_a}}{\overline{g_a}} \cdot \frac{\mathrm{d}g_a}{\mathrm{d}R_s} \cdot R_{s,max}. \tag{8}$$

The $DT_sR$ approximation can be validated with the observational data. Using Eq. (8), the contribution of $f_e$, $\overline{g_a}$, and $\mathrm{d}g_a/\mathrm{d}R_s$ in shaping $DT_sR$ can be quantified.

Next, the sensitivity of the warming rate to changes in evaporative conditions is obtained by taking the derivative of Eq. (7) with respect to evaporative fraction ($f_e$). To express these derivatives with respect to evaporative fraction, we use the prime ($\mathrm{d}x/\mathrm{d}f_e = (x)'$). Therefore, $(\mathrm{d}T_s/\mathrm{d}R_s')$ and $(\mathrm{d}T_a/\mathrm{d}R_s')$ represent the change in surface and air temperature warming rates due to a unit change in the evaporative fraction. The sensitivity of the warming rate of surface temperature to evaporative fraction is as follows:

$$\left( \frac{\mathrm{d}T_s}{\mathrm{d}R_s}' \right) = -\frac{1}{c_p \cdot \rho \cdot \overline{g_a}} + \left( \frac{\mathrm{d}T_a}{\mathrm{d}R_s}' \right) - \left[ \frac{\overline{(T_s - T_a)}}{\overline{g_a}} \cdot \frac{\mathrm{d}g_a}{\mathrm{d}R_s}' \right]. \tag{9}$$

Equation (9) is a negative quantity that is provided ($\mathrm{d}T_a/\mathrm{d}R_s'$), and the third term response to evaporative fraction is small (or negative). The negative sign means that the warming rate decreases with an increase in evaporative fraction. The amplitude of this decrease mainly depends on the mean aerodynamic conductance ($\overline{g_a}$) and also on its diurnal sensitivity to solar radiation ($\mathrm{d}g_a/\mathrm{d}R_s$).

We next look into observations to obtain the values in Eq. (7) to predict the warming rate of surface temperature with $f_e$, $\overline{g_a}$, $\overline{T_s - T_a}$, and $\mathrm{d}g_a/\mathrm{d}R_s$. Likewise, using Eq. (9) requires the observations to quantify the sensitivities of the components of its third term ($\overline{T_s - T_a}$, $1/\overline{g_a}$, and $\mathrm{d}g_a/\mathrm{d}R_s$) to the evaporative fraction. We derive these quantities from observations to then show that Eq. (7) reproduces the warming rate of surface temperature and its sensitivity to evaporative fraction using Eq. (9). Lastly, using the values from observations and our model expression for $DT_sR$, as shown in Eq. (8), we estimate the contribution of the evaporative fraction and aerodynamic properties in shaping the magnitude of the diurnal surface temperature range.

## 3   Data and method

We use observations from 51 FLUXNET sites representing different vegetation types. The FLUXNET data consists of sensible and latent heat fluxes, using the standard eddy covariance method, and provides half-hourly radiation and meteorological data (Baldocchi et al., 2001). The selected 51 sites contain data of the surface energy balance components and temperatures for more than 4 years. To avoid the effect of energy limitation on evaporation, only summer days are considered. Summer is defined here as days having a greater daily mean incoming solar radiation at the surface than the median of the annual distribution. This approach standardizes the definition of summer days for sites at different latitudes and provides days with comparable solar energy input for the individual sites.

Furthermore, among summer days, only clear sky days are considered to avoid the influence of clouds on temperatures.

**Table 1.** Land cover types of the different sites considered here, and their grouping into the short vegetation, savanna, or forest types.

| Vegetation types | Land use type | Number of sites |
|---|---|---|
| Short vegetation | Cropland | 12 |
| | Grassland | 6 |
| | Shrubland | 5 |
| Savanna | Savanna | 4 |
| | Woody savanna | 5 |
| Forest | Deciduous broadleaf forest | 4 |
| | Evergreen broadleaf forest | 1 |
| | Evergreen needle leaf forest | 9 |
| | Mixed forest | 5 |

A filter to remove the cloudy days is applied, and it is based on the quantile regression method using surface solar radiation and potential solar radiation (Renner et al., 2019). This method was applied only from morning to noon so that the days with clouds in the evening were also considered as being clear sky days. This does not influence warming rates since they are calculated only from the morning to noontime variation in temperature.

The information on vegetation type is obtained from the FLUXNET land cover classification (Falge et al., 2017), which is based on the International Geosphere–Biosphere Programme (IGBP) data and information system. The IGBP land cover product is available at a 1 km resolution and was derived from the advanced very high-resolution radiometer (Loveland and Belward, 1997). Detailed information of each site with their location, number of days used in the analysis, land cover type, and references is provided in the Appendix (Table A2). Vegetation is classified into three types that are based on their typical height and coverage (see Table 1). Shorter vegetation, like croplands, grasslands, and shrublands, are grouped into the "short vegetation" type. Savanna ecosystems are complex, with heterogeneous vegetation height which basically delineates the transition of short vegetation to forests, and are grouped into the "savanna" type. All forest types, including deciduous broadleaf, evergreen broadleaf, evergreen needleleaf, and mixed, are grouped in the "forest" type.

The geographic location of the selected 51 sites is shown in Fig. 2. The color bar represents the mean annual evaporative fraction derived from FLUXCOM data (Jung et al., 2019; Tramontana et al., 2016). Selected sites represent a wide range of ecosystems that is ideal for studying the generality of the response of warming rates to differences in evaporative conditions and vegetation type.

Evaporative conditions are quantified by the evaporative fraction. One of the advantages of the evaporative fraction is its stability for daylight hours, such that it can be assumed to be constant over a day (Shuttleworth et al., 1989). The daily mean evaporative fraction is obtained by the linear regression of the half-hourly morning to noon values of the latent heat flux to the total turbulent heat fluxes. Similarly, a linear regression of the daily mean warming rates and daily mean evaporative fractions is used to quantify the sensitivity of the warming rate to the evaporative fraction.

We use the term air temperature for the temperature measured above the canopy, which is typically at a 2 m height. Surface temperature is calculated from the upwelling flux of longwave radiation using the Stefan–Boltzmann law, such that it represents the skin temperature of the vegetated surface. The aerodynamic conductance ($g_a$) is obtained from the observed sensible heat flux from $g_a = H/(c_p \cdot \rho \cdot (T_s - T_a))$. Since aerodynamic conductance is not constant over the day, its diurnal variation is described by $dg_a/dR_s$, which is estimated from a linear regression of the morning to noon half-hourly values of $g_a$ and $R_s$.

## 4 Results

### 4.1 Observational analysis

The primary advantage of the warming rate over DTR is its suitability for comparing sites with different solar energy input. This is apparent from Fig. 3, where we show the density distribution of the observed daily warming rates of (a) surface and (b) air temperatures for short vegetation, savanna, and forest. The warming rates of surface temperature for short vegetation, with a median value of $31.42 \times 10^{-3}\,\mathrm{K\,(W\,m^{-2})^{-1}}$, are larger by almost a factor of 2 compared to the respective warming rates of forests with a median value of $15.47 \times 10^{-3}\,\mathrm{K\,(W\,m^{-2})^{-1}}$. Savanna covers the range in warming rates of surface temperature, with a median value of $27.09 \times 10^{-3}\,\mathrm{K\,(W\,m^{-2})^{-1}}$, reflecting their characteristics due to being positioned between short vegetation and forests. Hence, the warming rates of surface temperature clearly show similar characteristics across different sites and a clear influence of vegetation type.

Surprisingly, this is not true for the warming rates of air temperature. All vegetation types show very similar distributions (Fig. 3b). For short vegetation, this distribution shifts markedly to smaller values, with a median of $12.32 \times 10^{-3}\,\mathrm{K\,(W\,m^{-2})^{-1}}$, compared to the respective distribution for the warming rates of surface temperature. Conversely, in forests, the distributions are similar (with a median of $11.13 \times 10^{-3}\,\mathrm{K\,(W\,m^{-2})^{-1}}$), indicating the strong aerodynamic coupling between surface and air temperatures. The distribution for savanna has a median of $14.43 \times 10^{-3}\,\mathrm{K\,(W\,m^{-2})^{-1}}$.

Within the short vegetation type, grassland and shrubland sites show much greater warming rates of surface temperature than cropland sites (site-specific information on warming rates is provided in Fig. A1). This distinction could be attributed to site-specific evaporative conditions. Most of the
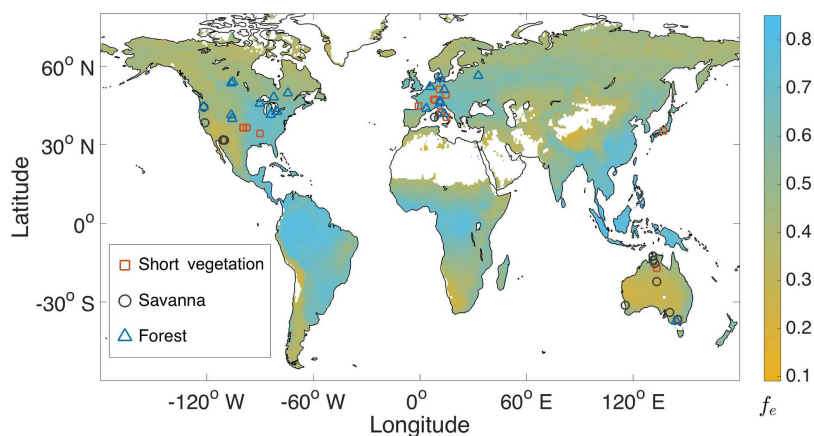
**Figure 2.** Geographical locations of FLUXNET sites used in this study. The vegetation type at each site is shown by the symbols. The color bar shows the mean annual evaporative fraction ($f_e$) derived from FLUXCOM data (2001 to 2013).
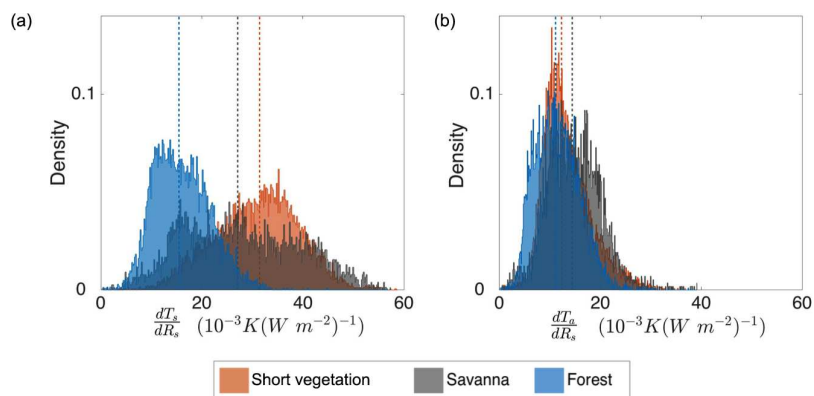


**Figure 3.** Density distribution of observed warming rates of **(a)** surface temperature and **(b)** air temperature for short vegetation, savanna, and forest. The vertical dashed lines indicate the median of each distribution in the respective colors of the vegetation types.

shrubland sites are drier, while cropland sites are generally moister. Such an uneven distribution of evaporative conditions could impact the estimation of warming rates, such that it is higher for dry sites and lower for moist sites. On the other hand, despite these differences in the mean evaporative conditions, the sites contain days with a good range of evaporative fractions (see Fig. A2). The range of evaporative fractions is important for the estimation of the sensitivity of the warming rates to the evaporative fraction.

Next, we quantify the sensitivity of warming rates to the evaporative fraction, $(dT/dR'_s)$ from the linear regression of the daily means. The value of this sensitivity represents the change in the warming rate from dry ($f_e = 0$) to moist ($f_e = 1$) conditions, although we should note that these extreme values for the evaporative fraction are hypothetical. Figure 4 shows the mean sensitivity of the warming rates of surface (orange) and air (blue) temperature to the evaporative fraction for short vegetation, savanna, and forest (for site-specific responses, see Fig. A2). The sensitivity in short vegetation shows a strong decrease of $\sim 23 \times 10^{-3}\,\mathrm{K\,(W\,m^{-2})^{-1}}$ for surface temperature, but a much smaller decrease by $\sim 5 \times 10^{-3}\,\mathrm{K\,(W\,m^{-2})^{-1}}$ for air temperature. In our earlier work, similar responses were found for a cropland site (Fig. A2, site no. 8). The savanna vegetation type shows a weaker decrease of $\sim 12 \times 10^{-3}\,\mathrm{K\,(W\,m^{-2})^{-1}}$ for surface temperature, but the warming rate of air temperature is almost insensitive to the evaporative fraction. In forests, both warming rates show very weak to almost no sensitivity to the evaporative fraction.

In addition to the evaporative fraction, the aerodynamic conductance also influences the diurnal variation in temperatures. The aerodynamic conductance governs the ventilation of energy and mass from the surface to the atmosphere (Thom, 1972). Figure 5a shows the density distribu-

**Table 2.** First quartile ($Q_1$), median, and third quartile ($Q_3$) for the distributions of $dT_s/dR_s$, $dT_a/dR_s$, $\overline{g_a}$, and $dg_a/dR_s$ for short vegetation, savanna, and forest.

| Vegetation | | $dT_s/dR_s$ $(10^{-3}\,\mathrm{K\,(W\,m^{-2})^{-1}})$ | $dT_a/dR_s$ $(10^{-3}\,\mathrm{K\,(W\,m^{-2})^{-1}})$ | $\overline{g_a}$ $(\mathrm{m\,s^{-1}})$ | $dg_a/dR_s$ $(10^{-3}\,\mathrm{m\,s^{-1}/W\,m^{-2}})$ |
|---|---|---|---|---|---|
| Short vegetation | $Q_1$ | 25.1 | 9.9 | 0.017 | 0.041 |
| | Median | 31.4 | 12.3 | 0.022 | 0.054 |
| | $Q_3$ | 36.7 | 15.7 | 0.032 | 0.078 |
| Savanna | $Q_1$ | 18.6 | 10.9 | 0.037 | 0.040 |
| | Median | 27.1 | 14.4 | 0.023 | 0.058 |
| | $Q_3$ | 36.8 | 18.1 | 0.060 | 0.137 |
| Forest | $Q_1$ | 11.8 | 8.1 | 0.093 | 0.229 |
| | Median | 15.5 | 11.1 | 0.135 | 0.321 |
| | $Q_3$ | 19.7 | 14.3 | 0.204 | 0.444 |
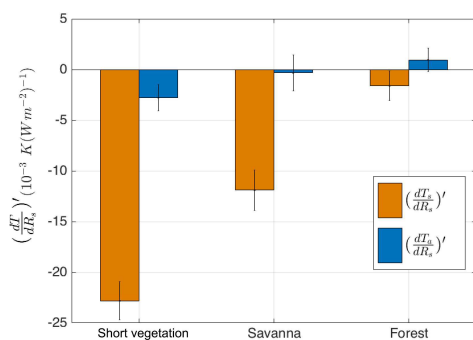


**Figure 4.** Bar plot of the sensitivity of warming rates of surface ($dT_s/dR_s'$) and air ($dT_a/dR_s'$) temperatures to evaporative fractions from observations for short vegetation, savanna, and forest. The error bars represent the standard error of the mean.

tion of morning to noon mean of the aerodynamic conductance for the short vegetation, savanna, and forest sites. The mean aerodynamic conductance is usually a characteristic of vegetation height (Jones, 1992). We find that the aerodynamic conductance of short vegetation is much lower (median $= 0.022\,\mathrm{m\,s^{-1}}$) than for forest (median $= 0.32\,\mathrm{m\,s^{-1}}$). Savanna sites have a similar aerodynamic conductance (median $= 0.023\,\mathrm{m\,s^{-1}}$) to short vegetation, but some woody savanna sites show relatively higher aerodynamic conductance (as shown by the second peak around $0.08\,\mathrm{m\,s^{-1}}$ in the distribution in Fig. 5a).

Aerodynamic conductance typically increases substantially during the day, increasing roughly linearly with absorbed solar radiation, which is captured by $dg_a/dR_s$ (Fig. 5b). The positive sign of $dg_a/dR_s$ reflects the increase in $g_a$ from morning to noon, which is found for all vegetation types. Forest sites show a stronger increase, but note that these sites also have a higher mean aerodynamic conductance. Overall, the aerodynamic conductance at noon is $\sim 2.5$ times the mean value across all vegetation types

(calculated with a $R_{s,\mathrm{max}} = 1000\,\mathrm{W\,m^{-2}}$), indicating similar relative diurnal variations (see Table 2). In other words, the relative sensitivity of aerodynamic conductance, $1/\overline{g_a} \cdot dg_a/dR_s \approx 2.5 \times 10^{-3}\,(\mathrm{W\,m^{-2}})^{-1}$ is about the same across the different sites. Because a greater aerodynamic conductance is expected to cool the surface more effectively, we expect that the diurnal increase in aerodynamic conductance shall reduce the warming rates of the surface temperature (which can also be seen in Eq. (7), where the last term on the right-hand side is negative). Thus, in addition to the mean aerodynamic conductance, its diurnal variation is another important factor which shapes the diurnal variation in temperatures.

To estimate the warming rate of surface temperature and its sensitivity to evaporative fraction using Eqs. (7)–(9), we also need to know the mean difference in surface and air temperature ($\overline{T_s - T_a}$). We find that $\overline{T_s - T_a}$ is higher in short vegetation and savanna compared to forest sites. Additionally, $\overline{T_s - T_a}$ decreases on days with a high evaporative fraction in short vegetation and savanna but not in forests. Betts and Ball (1995) showed a similar sensitivity of $\overline{T_s - T_a}$ to evaporative conditions in a grassland site. Unlike $\overline{T_s - T_a}$, we found no such sensitivity of $\overline{g_a}$ and $dg_a/dR_s$ to the evaporative fraction. This finding is different to the study by Rigden and Li (2017), who showed that the aerodynamic resistance depends on the Bowen ratio. This difference can be attributed to their method for estimating aerodynamic resistance from the frictional velocity and wind speeds, which assumes neutral conditions, whereas we obtain aerodynamic conductance from sensible heat flux.

Given that only the mean temperature difference, $\overline{T_s - T_a}$, is sensitive to the evaporative fraction, while $\overline{g_a}$ and $dg_a/dR_s$ are not, the last term in Eq. (9) reduces the sensitivity of this temperature difference to the evaporative fraction. This sensitivity is shown in Fig. 5c. The third term of Eq. (9) thus depends mostly on $\overline{(T_s - T_a)}'$ because the relative diurnal variation in aerodynamic conductance ($1/\overline{g_a} \cdot dg_a/dR_s$) is similar for all vegetation types.
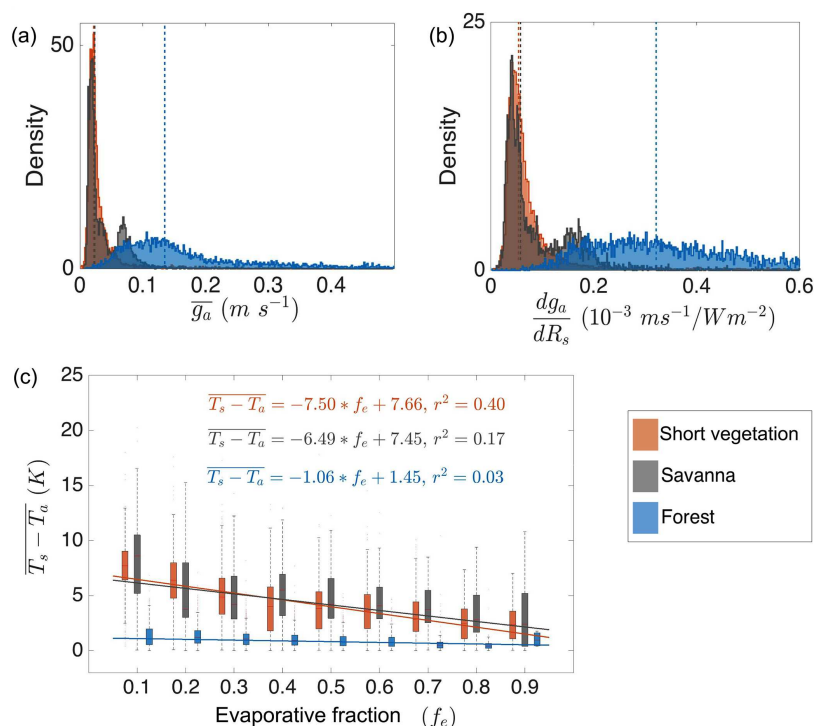
**Figure 5.** Density distributions inferred from the observations of the morning to noon **(a)** mean aerodynamic conductance ($\overline{g_a}$) and **(b)** its sensitivity to solar radiation ($dg_a/dR_s$). The vertical dashed lines show the medians of the distributions. Also shown in **(c)** is the sensitivity of the morning to noon mean surface and air temperature difference ($\overline{T_s - T_a}$) to evaporative fraction, which is a sensitivity needed for the estimation of how the warming rate of surface temperature responds to evaporative fraction, using Eq. (9). The bars indicate the 25th and 75th percentiles of the observations, respectively. The lines are the best fit for the linear regression of $\overline{T_s - T_a}$ and evaporative fraction for each vegetation type, with the equations and $r^2$ shown in the plot.

To summarize our analysis of the observations, we found that the diurnal variation in the surface temperature of short vegetation showed much stronger imprints of evaporative conditions than air temperature. In forests, the diurnal variations in both surface and air temperature were found to be insensitive to evaporative conditions. The mean aerodynamic conductance derived from observations confirms the characteristic high values for forests compared to short vegetation. Additionally, we found a strong diurnal variation in the aerodynamic conductance that, in relative terms, is comparable for all vegetation types.

To explain these findings, we hypothesize that the high aerodynamic conductance of forests lowers the diurnal increase in surface temperature as it provides greater ventilation. Since air temperatures do not respond to the evaporative fraction, we therefore expect the warming rate of the surface temperature of forests to be less sensitive. This can already be anticipated from Eq. (9), together with the values provided in Table 2 and the sensitivities shown in Fig. 5c. Using these values, Eq. (9) yields an estimate for the sensi-

tivity of the warming rate of surface temperature to the evaporative fraction for short vegetation of about $-24 \times 10^{-3}$ and $-4 \times 10^{-3}$ K (W m$^{-2}$)$^{-1}$ for forests, similar to what is shown in Fig. 4. In the following, we verify our model expression in greater detail.

## 4.2  Model application and interpretation

To estimate the warming rate of surface temperature using Eq. (7) in greater detail, we used daily values of observed $\overline{f_e g_a}$, $dT_a/dR_s$, $\overline{T_s - T_a}$, and $dg_a/dR_s$. Since $dT_a/dR_s$ is similar for all sites, the diurnal variation in air temperature does not seem to depend on the diurnal variation in surface temperature and vice versa. Figure 6a shows the comparison of the modeled warming rates to those derived from observations. The model performs very well for all sites for the given information, with coefficients of determination ($r^2$) of $r^2 = 0.69$ for short vegetation, $r^2 = 0.87$ for savanna, and $r^2 = 0.53$ for forests. Similarly, the slopes ($m$) of the regression between modeled and observed $dT_s/dR_s$ are close to 1 for short vegetation ($m = 0.85$) and savanna ($m = 0.90$),
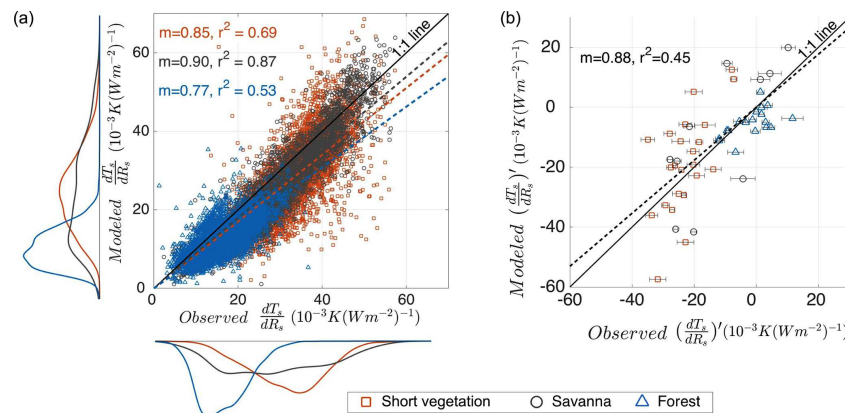
A. Panwar et al.: Imprints of evaporative conditions and vegetation type in diurnal temperature variations     **4931**



**Figure 6. (a)** Modeled versus observed warming rates, $\mathrm{d}T_s/\mathrm{d}R_s$ for each site, for the three vegetation types. The density distributions show the spread. The coefficient of the determination ($r^2$) and slope ($m$) of the linear fit (dashed lines) are depicted for each vegetation type. **(b)** Model evaluation of the sensitivity of the warming rates to the evaporative fraction ($\mathrm{d}T_s\mathrm{d}R_s'$) with those derived from observations for each site.

meaning the $\mathrm{d}T_s/\mathrm{d}R_s$ magnitudes are well captured by our model, although the slope is too low for forests ($m = 0.77$). However, at some sites with short vegetation, $\mathrm{d}T_s/\mathrm{d}R_s$ is underestimated. We speculate that these are the sites with non-vegetated surfaces where the ground heat flux contribution to diurnal surface temperature variations can be significant (Saltzman and Pollack, 1977), which is currently neglected in our model.

It is apparent from Fig. 6a, that the warming rates for surface temperature are higher for short vegetation compared to those of forests. This is mainly due to the relatively high aerodynamic conductance of forests, which reduces the magnitude of the first and third term on the right-hand side of Eq. (7).

The greater aerodynamic conductance of forests also reduces the sensitivity of warming rates to evaporative fraction compared to short vegetation, which can be seen in Eq. (9). Note that the diurnal variation in the aerodynamic conductance is included here by the term $\mathrm{d}g_a/\mathrm{d}R_s$ in our estimates. Equation (9) reproduces the response of the warming rates to evaporative fraction quite well for all vegetation types ($m = 0.88$, $r^2 = 0.45$, Fig. 6b), including their ranges. Certain deviations exist because there are some biases in the number of moist and dry days in the observations that are reflected in the horizontal error bars. The other possible cause for bias is the large variation in the sensitivity of $\overline{T_s - T_a}$ to $f_e$ in short vegetation and savanna (Fig. 5c).

We next link our estimates for warming rates back to the diurnal surface temperature range ($\mathrm{DT_sR}$) by multiplying the expression for the warming rate with the daily maximum of absorbed solar radiation, namely $R_{s,\max}$ (see Eq. 8). To understand how solar radiation, evaporative fraction, and the mean aerodynamic conductance and its diurnal variation contribute to $\mathrm{DT_sR}$ separately, we consider four cases. In

the first case, we assume that the diurnal variation in surface temperature is solely driven by solar radiation, such that there is no evaporation ($f_e = 0$), and the surface has a low and constant aerodynamic conductance of $g_a = 0.022\,\mathrm{m\,s^{-1}}$, which is the median of the aerodynamic conductance of short vegetation (see Table 2). Figure 7a shows that, in this case, $\mathrm{DT_sR}$ is overestimated for all vegetation types (regression slope $m > 1$), with a low $r^2 \leq 0.3$. This greater warming indicates that vegetation and evaporation cool surface temperatures and reduce the diurnal surface temperature range.

In the second case, we add the information on evaporative fraction (Fig. 7b). The $\mathrm{DT_sR}$ estimates for short vegetation ($m = 1.26$; $r^2 = 0.55$) and, to some extent, for savanna ($m = 1.37$, $r^2 = 0.46$) are considerably improved but not for forests ($m = 2.22$, $r^2 = 0.18$). Nevertheless, in this case, $\mathrm{DT_sR}$ is cooler and closer to the observed values than the previous case, indicating the importance of evaporation in cooling the diurnal temperature, although the values are still too high, as indicated by the regression slopes being $m > 1$.

However, in forests, the information on the evaporative fraction alone does not reduce $\mathrm{DT_sR}$ because their high aerodynamic conductance is not accounted for. Therefore, in the third case, in addition to the absorbed solar radiation and evaporative fraction, we added the information on the mean aerodynamic conductance ($\overline{g_a}$). The $\mathrm{DT_sR}$ in forests is now better captured ($r^2 = 0.35$), and the magnitude is closer to the observed ($m = 0.98$); see Fig. 7c. In short vegetation and savanna, however, $\mathrm{DT_sR}$ is still mostly overestimated. This can be attributed to the diurnal variation in the aerodynamic conductance, $\mathrm{d}g_a/\mathrm{d}R_s$, not being included in this case.

Finally, we add information on all components to our estimate (Fig. 7d). $\mathrm{DT_sR}$ estimates are much closer to the observation, with a good $r^2$ for all vegetation types, and regression slopes are reduced to values $m < 1$, indicating a slight cold
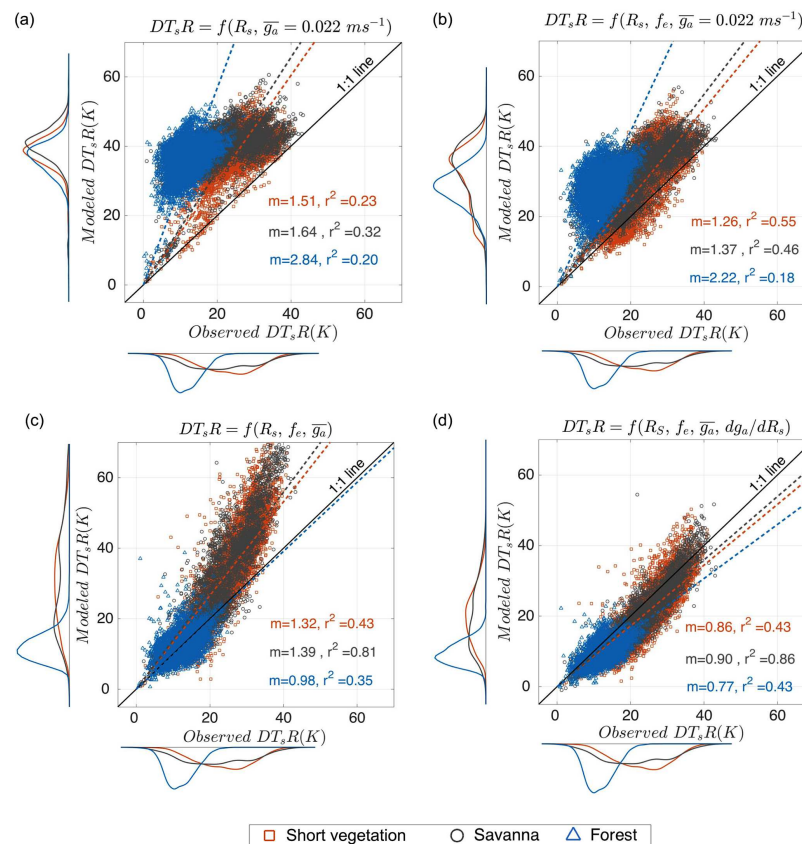
**Figure 7.** Comparison of the estimated diurnal surface temperature range ($DT_sR$) for short vegetation (red), savanna (gray), and forest (blue), with observations for the four scenarios. **(a)** $DT_sR$ is only a function of solar radiation ($R_s$). **(b)** $DT_sR$ including the effect of evaporative fraction ($f_e$). **(c)** $DT_sR$ with the additional effect of differences in the mean aerodynamic conductance between vegetation types ($\overline{g_a}$). **(d)** $DT_sR$ additionally includes the effect of the diurnal variation in aerodynamic conductance ($dg_a/dR_s$). Dashed lines show the linear regression between the model and observation with their slopes ($m$), and the coefficient of the determination is indicated ($r^2$) in the plots.

bias. Forest sites show a slight improvement in $r^2$, although the contribution of $dg_a/dR_s$ is comparatively small because $\overline{T_s - T_a}$ in the forest is small ($\sim 1$ K).

These four cases show that vegetation type and evaporative conditions play significant roles in modulating the diurnal variation in surface temperature. Evaporative fraction is important for reducing the spread and magnitude (as indicated by the lower values of $m$ and higher $r^2$), whereas differences in the mean aerodynamic conductance are important for capturing the different magnitudes of $DT_sR$ between short vegetation and forests.

The importance of these factors can be illustrated by how much they act to reduce the magnitude of $DT_sR$. This can be done by evaluating the extent to which the regression slope, $m$, is reduced by these factors, using the first case that only considers solar radiation as the reference case. Evaporation reduces $DT_sR$ by $\sim 18$ %

(short vegetation – $(1.26$–$1.51)/1.51 = -16.55$ %; savanna – $(1.37$–$1.64)/1.64 = -16.46$ %; forest – $(2.22$–$2.84)/2.84 = -21.83$ %). On comparing Fig. 7b and c, we found that the high aerodynamic conductance of forests reduces $DT_sR$ by 56 % ($(0.98$–$2.22)/2.22 = -56$ %). In other words, the higher aerodynamic conductance of forests causes substantially larger cooling than evaporation. The diurnal variation in the aerodynamic conductance then reduces the $DT_sR$ further, being stronger in short vegetation ($(0.86$–$1.32)/1.32 = -35$ %) and savanna ($(0.90$–$1.40)/1.75 = -35.25$ %) than in forests ($(0.77$–$0.98)/0.98 = -21$ %).

## 5   Discussion

We demonstrate a robust way of characterizing the diurnal variation in temperatures, using their morning to noon warming rates, which are derived from the half-hourly changes in

52

temperatures and absorbed solar radiation. Warming rates are suitable for the analysis of other factors that affect temperatures, such as evaporation and vegetation, because the most dominant variation in temperature caused by solar energy input is removed.

Our analytic surface energy balance model can reproduce the warming rates of the surface temperature derived from observations quite well and shows the physical significance of evaporative fraction, aerodynamic conductance, and its diurnal variation in shaping diurnal temperature variations. The approximations made in the derivation of Eqs. (7) and (9) can be further improved by a more detailed formulation of net longwave radiation (which could, for instance, include optical properties of the atmosphere) and the ground heat flux. Warming rates are also likely to be sensitive to clouds and might not capture the information of evaporative conditions and vegetation on cloudy days. These effects were not evaluated here because we focused the analysis on clear sky days. It may, however, very well be that the dominant effect of clouds is simply to reduce absorbed solar radiation, so that Eqs. (7) and (9) could also predict warming rates for those conditions. Also, we did not provide a way to estimate the warming rates of air temperature. These could be topics for future research.

One of the main findings of our study is the contrasting response of the warming rates of surface and air temperature to evaporative fraction. The warming rate of air temperature does not contain any imprints of evaporative fraction across all sites, irrespective of their aerodynamic conductance and evaporative conditions. This finding is consistent with our previous work (Panwar et al., 2019), where we explained this finding by showing how the effect of boundary layer growth compensates for the effects of different evaporative conditions. We anticipate that our hypothesis of the compensating effect of boundary layer growth might also hold for forests, but this would need further research.

The warming rate of surface temperature is highly sensitive to the evaporative fraction for short vegetation. The mean sensitivity of $\sim 23 \times 10^{-3}\,\mathrm{K\,(W\,m^{-2})^{-1}}$ is consistent with the reported sensitivity in Panwar et al. (2019). This decrease is comparable for all sites with short vegetation, and we anticipate that some of the spread is due to their somewhat different aerodynamic properties. Another source of uncertainty is the uneven distribution of the days of different evaporative fractions, which may affect the estimation of the sensitivity. This uncertainty could be reduced by a longer time series of observations to obtain a greater sampling range of evaporative conditions.

The notion that surface and air temperature variations respond differently to evaporative conditions was reported in previous research (Cresswell et al., 1999; Fu et al., 2011; Hengl et al., 2012; Jang et al., 2004; Kilibarda et al., 2014; Zhu et al., 2013) and is relevant when air temperature products are developed from remotely sensed surface temperature. Typically, these products are primarily based on the as-

sumption that surface temperature is a proxy of air temperature. Generally, these approaches overestimate daytime air temperature (Oyler et al., 2016; Zhang et al., 2011). This is consistent with our analysis, which shows markedly higher warming rates of surface temperature for nonforested vegetation than the warming rates of air temperature (see Fig. 3). This overestimate can also be understood by the first term on the right-hand side of Eq. (7), which causes the stronger response of surface temperature compared to air temperature to changes in absorbed solar radiation.

Our study shows that the warming rates of surface and air temperature are similar at forest sites, which indicates the strong coupling between the two temperatures. This finding is in agreement with the previous study by Li et al. (2015) and Mildrexler et al. (2011), where evaporative cooling and the high aerodynamic conductance of forests were identified as being the responsible factors for the strong coupling between surface and air temperature. Additionally, we show that the diurnal variation in surface and air temperature remains similar irrespective of the evaporative conditions in the forest. We can only speculate about the physical mechanism behind this finding. While it is well established that the greater aerodynamic roughness of the forest leads to a greater aerodynamic conductance for neutral conditions (Oke, 1978) we also find that the diurnal variation is much larger than the mean (the term $\mathrm{d}g_a/\mathrm{d}R_s$). This enhancement is most likely related to buoyancy, which is produced when the surface is heated by the absorption of solar radiation during the day. The finding that the relative enhancement of aerodynamic conductance between forests and nonforests is the same, and that this enhancement is insensitive to evaporative fraction, seems to be surprising and would need further investigations about their physical explanations.

We then applied our analytical model to estimate the diurnal surface temperature range $\mathrm{DT_sR}$ and attribute the dominant factors that influence this range. It attributed the low $\mathrm{DT_sR}$ of forests mostly to their high aerodynamic conductance ($\sim 56\,\%$), with evaporation playing only a secondary role ($\sim 22\,\%$). This finding is consistent with studies that showed that the warming induced by deforestation is mainly the consequence of changes in aerodynamic conductance rather than changes in evaporative conditions (Bright et al., 2017; Chen and Dirmeyer, 2016; Lee et al., 2011b; Zhao et al., 2014b). This aerodynamic effect is thus important for the cooling effect of forests (Ellison et al., 2017; Li et al., 2015; Tang et al., 2018), which our analysis and analytical model supports.

In addition to the role of the mean aerodynamic conductance, we find a strong diurnal variation in the aerodynamic conductance that is greater than the mean (as already reported by Mallick et al., 2013; Ronda et al., 2001; Steduto and Hsiao, 1998). This diurnal variation acts to reduce the diurnal variation in surface temperature further. While our findings show that the relative diurnal variation in aerodynamic conductance is about the same across the sites, this varia-

tion caused a stronger reduction in DT$_s$R ($\sim -35\%$) in short vegetation and savanna compared to forests ($\sim -21\%$). It indicates that in forests the greater mean aerodynamic conductance is much more important than its diurnal variation. This can be explained by $\overline{T_s - T_a}$ being small ($\sim 1$ K) in forests, although the reason for this small difference would need further evaluation.

Our model demonstrates a similar sensitivity of DT$_s$R to energy partitioning and aerodynamic conductance as per a previous study by Diak and Whipple (1993), who used simulations with a boundary layer model. Our model can capture this sensitivity solely with surface energy balance information, but it does not require information on the boundary layer (which is likely to be encapsulated in the warming rate of air temperature and its lack of sensitivity to evaporative fraction). This indicates that the diurnal variation in surface temperature is chiefly governed by the exchange at the surface, particularly regarding its aerodynamic conductance and the evaporative fraction.

To sum up this discussion, our findings are consistent with previously published research regarding the main factors that shape the diurnal variation in surface and air temperature across different vegetation types. The derived equations of the warming rate of surface temperature (Eq. 7) and its sensitivity to evaporative fraction (Eq. 9) appear to be useful for describing and quantifying the primary factors that cause differences in the diurnal variation in surface temperature across different land cover types.

## 6 Conclusions

We used warming rates, i.e., the change in temperatures with a change in absorbed solar radiation from morning to solar noon, to identify the influences of evaporative conditions and vegetation on diurnal temperature variations across 51 FLUXNET sites covering different vegetation types. We found that the warming rates of air temperature are similar across the sites and are insensitive to evaporative fraction. The warming rates of surface temperatures of sites with short vegetation decreased with greater evaporative fraction, representing a stronger evaporative cooling. For forests, warming rates of surface temperature are almost the same as those for air temperature, and they lacked sensitivity to the evaporative fraction. Using an analytical description of the surface energy balance, we reproduced these findings and attributed the different response of forests primarily to their higher aerodynamic conductance.

From our analysis, we can draw several conclusions. First, we found that diurnal variations in air temperature reflect very little information on evaporative conditions, implying that these observations cannot be used to infer evaporation. Second, the diurnal variation in surface temperature, however, shows a clear sensitivity to the evaporative fraction for short vegetation, so that evaporation may be inferred from surface temperature observations. Third, in forests, surface temperature is strongly aerodynamically coupled to air temperatures by their high aerodynamic conductance, so that these lack sensitivity to evaporative fraction. Hence, diurnal temperature variations in forested sites do not seem to carry a notable effect from evaporation. What this shows is that the effect of evaporative conditions on diurnal temperature variations delicately depends on the presence or absence of forests.

## Appendix A:  Observational analysis for each site

**Table A1.** Abbreviation used.

| Symbol | Full form | Unit |
|---|---|---|
| $\sigma$ | Stefan–Boltzmann constant | $\mathrm{W\,m^{-2}\,K^{-4}}$ |
| $\rho$ | Density of the lower atmosphere | $\mathrm{kg\,m^{-3}}$ |
| $LE$ | Latent heat flux | $\mathrm{W\,m^{-2}}$ |
| $H$ | Sensible heat flux | $\mathrm{W\,m^{-2}}$ |
| $G$ | Ground heat flux | $\mathrm{W\,m^{-2}}$ |
| $\mathrm{DT_sR}$ | Diurnal surface temperature range | K |
| DTR | Diurnal temperature range | K |
| $\mathrm{DT_aR}$ | Diurnal air temperature range | K |
| $\overline{(T_\mathrm{s} - T_\mathrm{a}}')$ | Derivative of $\overline{T_\mathrm{s} - T_\mathrm{a}}$ to evaporative fraction | K |
| $T_\mathrm{s}$ | Surface temperature obtained from longwave radiation | K |
| $T_\mathrm{ref}$ | Reference temperature | K |
| $T_\mathrm{a}$ | Air temperature, measured at 2 m height above the canopy | K |
| $R_\mathrm{s}$ | Surface solar radiation | $\mathrm{W\,m^{-2}}$ |
| $R_\mathrm{s,max}$ | Maximum of surface solar radiation | $\mathrm{W\,m^{-2}}$ |
| $R_\mathrm{o}$ | Net radiation at reference temperature | $\mathrm{W\,m^{-2}}$ |
| $R_\mathrm{l,net}$ | Net longwave radiation | $\mathrm{W\,m^{-2}}$ |
| $k_\mathrm{r}$ | Linearized constant | $\mathrm{W\,m^{-2}\,K^{-1}}$ |
| $g_\mathrm{a}$ | Aerodynamic conductance | $\mathrm{m\,s^{-1}}$ |
| $f_\mathrm{e}$ | Evaporative fraction | – |
| $\frac{\mathrm{d}T_\mathrm{s}}{\mathrm{d}R_\mathrm{s}}$ | Surface temperature warming rate | $\mathrm{K\,(W\,m^{-2})^{-1}}$ |
| $\frac{\mathrm{d}T_\mathrm{a}}{\mathrm{d}R_\mathrm{s}}$ | Air temperature warming rate | $\mathrm{K\,(W\,m^{-2})^{-1}}$ |
| $\frac{\mathrm{d}g_\mathrm{a}}{\mathrm{d}R_\mathrm{s}}$ | Morning ($20\,\mathrm{W\,m^{-2}} \leq R_\mathrm{s} \leq R_\mathrm{s,max}$) derivative of aerodynamic conductance to solar radiation | $\mathrm{m\,(W\,m^{-2}\,s)^{-1}}$ |
| $c_\mathrm{p}$ | Specific heat capacity of the lower atmosphere | $\mathrm{J\,(kg\,K)^{-1}}$ |
| $\overline{T_\mathrm{s} - T_\mathrm{a}}$ | Morning ($20\,\mathrm{W\,m^{-2}} \leq R_\mathrm{s} \leq R_\mathrm{s,max}$) mean surface and air temperature gradient | K |
| $\overline{g_\mathrm{a}}$ | Morning ($20\,\mathrm{W\,m^{-2}} \leq R_\mathrm{s} \leq R_\mathrm{s,max}$) mean aerodynamic conductance | $\mathrm{m\,s^{-1}}$ |
| $\left(\frac{\mathrm{d}T_\mathrm{s}}{\mathrm{d}R_\mathrm{s}}'\right)$ | Derivative of surface temperature warming rate to evaporative fraction | $\mathrm{K\,(W\,m^{-2})^{-1}}$ |
| $\left(\frac{\mathrm{d}T_\mathrm{a}}{\mathrm{d}R_\mathrm{s}}'\right)$ | Derivative of air temperature warming rate to evaporative fraction | $\mathrm{K\,(W\,m^{-2})^{-1}}$ |

Hydrol. Earth Syst. Sci., 24, 4923–4942, 2020

https://doi.org/10.5194/hess-24-4923-2020

**Table A2.** Description of the sites used for this study. For the definitions of the terms included herein, please see the corresponding DOI.

| Site no. | IGBP land use | Site ID | Site name | Location Latitude | Longitude | Number of days used | DOI |
|---|---|---|---|---|---|---|---|
| 1 | Croplands | AU-Rig | Riggs Creek | −36.65 | 145.57 | 237 | https://doi.org/10.18140/FLX/1440202 |
| 2 | (CRO) | CH-Oe1 | Oensingen1 grass | 47.28 | 7.73 | 182 | https://doi.org/10.18140/FLX/1440135 |
| 3 | | CZ-wet | CZECHWET | 49.02 | 14.77 | 184 | https://doi.org/10.18140/FLX/1440145 |
| 4 | | DE-Geb | Gebesee | 51.10 | 10.91 | 285 | https://doi.org/10.18140/FLX/1440146 |
| 5 | | IT-BCi | Borgo Cioffi | 40.52 | 14.95 | 274 | https://doi.org/10.18140/FLX/1440166 |
| 6 | | IT-CA2 | Castel d'Asso2 | 42.37 | 12.02 | 143 | https://doi.org/10.18140/FLX/1440231 |
| 7 | | JP-SMF | Seto mixed forest site | 35.25 | 137.06 | 164 | https://doi.org/10.18140/FLX/1440239 |
| 8 | | US-ARM | ARM Southern Great Plains site | 36.60 | −97.48 | 648 | https://doi.org/10.18140/FLX/1440066 |
| 9 | Croplands/ | CH-Cha | Chamau grassland | 47.21 | 8.41 | 188 | https://doi.org/10.18140/FLX/1440131 |
| 10 | natural | CH-Fru | Fruebuel grassland | 47.11 | 8.53 | 260 | https://doi.org/10.18140/FLX/1440133 |
| 11 | vegetation | FR-LBr | Le Bray (after 28 June 1998) | 44.71 | −0.76 | 265 | https://doi.org/10.18140/FLX/1440163 |
| 12 | (CRO/NV) | US-Goo | Goodwin Creek | 34.25 | −89.87 | 206 | https://doi.org/10.18140/FLX/1440070 |
| 13 | Grasslands | AU-Stp | Sturt Plains | −17.15 | 133.35 | 532 | https://doi.org/10.18140/FLX/1440204 |
| 14 | (GRA) | IT-MBo | Monte Bondone | 46.01 | 11.04 | 480 | https://doi.org/10.18140/FLX/1440170 |
| 15 | | US-AR1 | ARM USDA UNL OSU Woodward switchgrass 1 | 36.42 | −99.42 | 242 | https://doi.org/10.18140/FLX/1440103 |
| 16 | | US-AR2 | ARM USDA UNL OSU Woodward switchgrass 2 | 36.63 | −99.59 | 225 | https://doi.org/10.18140/FLX/1440104 |
| 17 | | US-SRG | Santa Rita grassland | 31.78 | −110.82 | 696 | https://doi.org/10.18140/FLX/1440114 |
| 18 | | US-Wkg | Walnut Gulch, Kendall grasslands | 31.73 | −109.94 | 1074 | https://doi.org/10.18140/FLX/1440097 |
| 19 | Shrublands | AU-ASM | Alice Springs | −22.28 | 133.24 | 477 | https://doi.org/10.18140/FLX/1440194 |
| 20 | (SH) | US-SRC | Santa Rita creosote | 31.90 | −110.83 | 621 | https://doi.org/10.18140/FLX/1440098 |
| 21 | | US-SRM | Santa Rita mesquite | 31.82 | −110.86 | 1121 | https://doi.org/10.18140/FLX/1440090 |
| 22 | | US-Whs | Walnut Gulch, Lucky Hills shrubland | 31.74 | −110.05 | 558 | https://doi.org/10.18140/FLX/1440097 |
| 23 | | AU-Cpr | Calperum | −34.00 | 140.58 | 284 | https://doi.org/10.18140/FLX/1440195 |
| 24 | Savanna | AU-DaP | Daly River pasture | −14.06 | 131.31 | 439 | https://doi.org/10.18140/FLX/1440123 |
| 25 | (SA) | AU-DaS | Daly River savanna | −14.15 | 131.38 | 504 | https://doi.org/10.18140/FLX/1440122 |
| 26 | | AU-Dry | Dry River | −15.25 | 132.37 | 466 | https://doi.org/10.18140/FLX/1440197 |
| 27 | | AU-How | Howard Springs | −12.49 | 131.15 | 355 | https://doi.org/10.18140/FLX/1440125 |
| 28 | Woody | AU-Gin | Gingin | −31.37 | 115.65 | 212 | https://doi.org/10.18140/FLX/1440199 |
| 29 | Savanna | AU-Whr | Whroo | −36.67 | 145.02 | 206 | https://doi.org/10.18140/FLX/1440206 |
| 30 | (WSA) | IT-Noe | Sardinia – Arca di Noe | 40.60 | 8.15 | 555 | https://doi.org/10.18140/FLX/1440171 |
| 31 | | US-Me6 | Metolius new young pine | 44.32 | −121.60 | 270 | https://doi.org/10.18140/FLX/1440099 |
| 32 | | US-Var | Vaira Ranch | 38.40 | −120.95 | 1091 | https://doi.org/10.18140/FLX/1440094 |

**Table A2.** Continued. For the definitions of the terms included herein, please see the corresponding DOI.

| Site no. | IGBP land use | Site ID | Site name | Location | | Number of days used | DOI |
|---|---|---|---|---|---|---|---|
| | | | | Latitude | Longitude | | |
| 33 | Deciduous | DK-Sor | Sorø – Lille Bøgeskov | 55.48 | 11.64 | 169 | https://doi.org/10.18140/FLX/1440155 |
| 34 | Broadleaf | IT-Col | Collelongo – Selva Piana | 41.84 | 13.58 | 343 | https://doi.org/10.18140/FLX/1440167 |
| 35 | Forest | US-Oho | Oak Openings | 41.55 | −83.84 | 408 | https://doi.org/10.18140/FLX/1440088 |
| 36 | (DBF) | US-WCr | Willow Creek | 45.80 | −90.07 | 237 | https://doi.org/10.18140/FLX/1440095 |
| 37 | Evergreen Broadleaf Forest | AU-Wom | Wombat | −37.42 | 144.09 | 180 | https://doi.org/10.18140/FLX/1440207 |
| 38 | Evergreen | CA-Obs | Saskatchewan southern old black spruce | 53.98 | −105.11 | 620 | https://doi.org/10.18140/FLX/1440044 |
| 39 | Needleleaf | CA-Qfo | Quebec eastern old black spruce (EOBS) | 49.69 | −74.34 | 194 | https://doi.org/10.18140/FLX/1440045 |
| 40 | Forest | DE-Tha | Tharandt – Anchor Station | 50.96 | 13.56 | 268 | https://doi.org/10.18140/FLX/1440152 |
| 41 | (ENF) | IT-Lav | Lavarone (after March 2002) | 45.95 | 11.28 | 557 | https://doi.org/10.18140/FLX/1440169 |
| 42 | | IT-Ren | Renon/Ritten (Bolzano) | 46.58 | 11.43 | 362 | https://doi.org/10.18140/FLX/1440173 |
| 43 | | NL-Loo | Loobos | 52.16 | 5.74 | 401 | https://doi.org/10.18140/FLX/1440178 |
| 44 | | US-GLE | GLEES | 41.36 | −106.23 | 514 | https://doi.org/10.18140/FLX/1440069 |
| 45 | | US-Me2 | Metolius intermediate pine | 44.45 | −121.55 | 450 | https://doi.org/10.18140/FLX/1440079 |
| 46 | | US-NR1 | Niwot Ridge (LTER NWT1) | 40.03 | −105.54 | 600 | https://doi.org/10.18140/FLX/1440087 |
| 47 | Mixed | CA-Gro | Ontario Groundhog River mixed wood | 48.21 | −82.15 | 339 | https://doi.org/10.18140/FLX/1440034 |
| 48 | Forest | CA-Oas | Saskatchewan – old Aspen | 53.62 | −106.19 | 688 | https://doi.org/10.18140/FLX/1440043 |
| 49 | (MF) | CA-TP4 | Ontario – Turkey Point 1939 white pine | 42.70 | −80.35 | 482 | https://doi.org/10.18140/FLX/1440053 |
| 50 | | FR-Pue | Puéchabon | 43.74 | 3.59 | 535 | https://doi.org/10.18140/FLX/1440164 |
| 51 | | RU-Fyo | Fedorovskoye – drained spruce stand | 56.46 | 32.92 | 257 | https://doi.org/10.18140/FLX/1440183 |
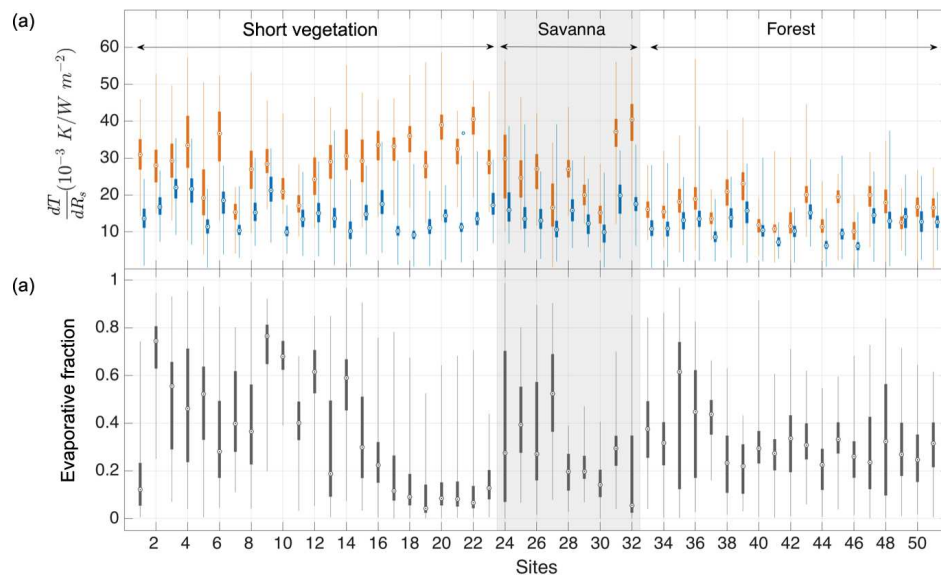
**Figure A1. (a)** Box plot of surface ($T_s$ – orange) and air ($T_a$ – blue) temperature warming rates ($dT/dR_s$). **(b)** Box plot of evaporative fractions. The vegetation types are separated by gray and white shading. The circle in the box plot indicates the median, and the top and bottom edges indicate the 75th and 25th percentiles, respectively. The whisker covers the range in the observation.
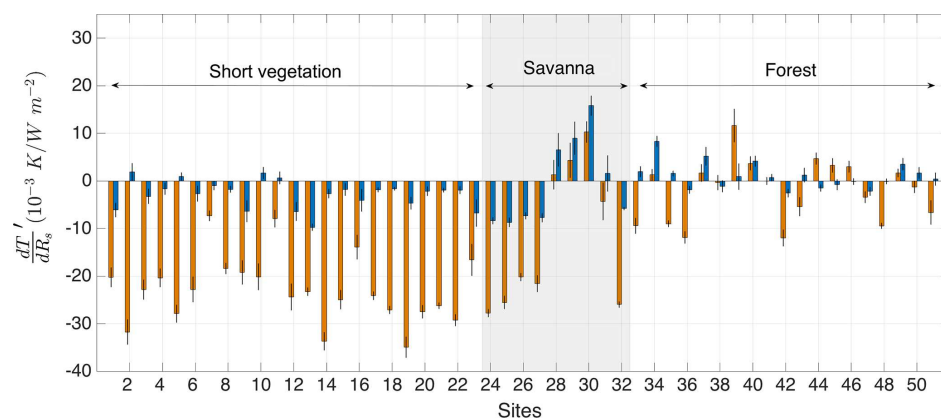


**Figure A2.** Warming rates response to evaporation ($dT/dR'_s$) for surface ($T_s$ – orange) and air ($T_a$ – blue) temperature. The vegetation types are separated by gray and white shading. The black bar represents the standard error in the linear regression of observed warming rate and evaporative fraction.
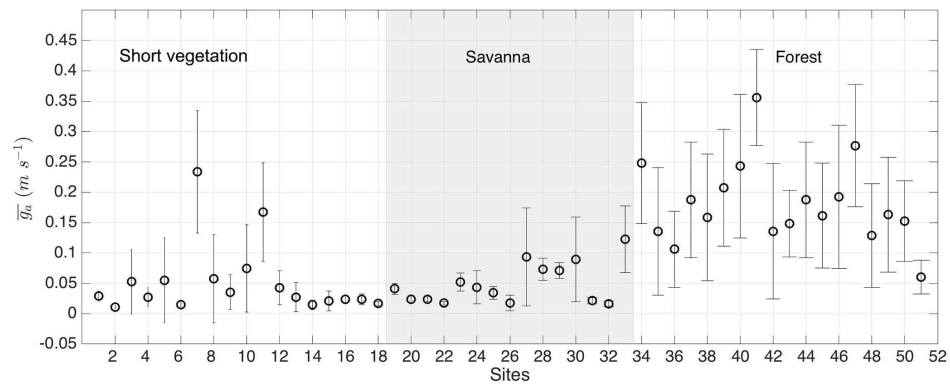
**Figure A3.** Morning time mean of aerodynamic conductance ($g_a$) for each site. The vegetation types are separated by gray and white shading. The error bar represents the standard deviation of the mean.

## References

Anderson, M. C., Allen, R. G., Morse, A., and Kustas, W. P.: Use of Landsat thermal imagery in monitoring evapotranspiration and managing water resources, Remote Sens. Environ., 122, 50–65, https://doi.org/10.1016/j.rse.2011.08.025, 2012.

Baier, W. and Robertson, G. W.: Estimation of latent evaporation from simple weather observations, Can. J. Plant Sci., 45, 276–284, https://doi.org/10.4141/cjps65-051, 1965.

Baldocchi, D., Falge, E., Gu, L., Olson, R., Hollinger, D., Running, S., Anthoni, P., Bernhofer, C., Davis, K., Evans, R., Fuentes, J., Goldstein, A., Katul, G., Law, B., Lee, X., Malhi, Y., Meyers, T., Munger, W., Oechel, W., Paw, K. T., Pilegaard, K., Schmid, H. P., Valentini, R., Verma, S., Vesala, T., Wilson, K., and Wofsy, S.: FLUXNET: A New Tool to Study the Temporal and Spatial Variability of Ecosystem–Scale Carbon Dioxide, Water Vapor, and Energy Flux Densities, B. Am. Meteorol. Soc., 82, 2415–2434, https://doi.org/10.1175/1520-0477(2001)082<2415:FANTTS>2.3.CO;2, 2001.

Betts, A. K. and Ball, J. H.: The FIFE surface diurnal cycle climate, J. Geophys. Res., 100, 25679, https://doi.org/10.1029/94JD03121, 1995.

Bevan, S. L., Los, S. O., and North, P. R. J.: Response of vegetation to the 2003 European drought was mitigated by height, Biogeosciences, 11, 2897–2908, https://doi.org/10.5194/bg-11-2897-2014, 2014.

Blaney, H. F. and Cridlle, W. D.: Determining Water Requirements in Irrigated Areas from Climatological Irrigation Data, Technical Paper No. 96, US Department of Agriculture, Soil Conservation Service, Washington, D.C., 48 pp., 1950.

Boegh, E., Soegaard, H., and Thomsen, A.: Evaluating evapotranspiration rates and surface conditions using Landsat TM to estimate atmospheric resistance and surface resistance, Remote Sens. Environ., 79, 329–343, https://doi.org/10.1016/S0034-4257(01)00283-8, 2002.

Bright, R. M., Davin, E., O'Halloran, T., Pongratz, J., Zhao, K., and Cescatti, A.: Local temperature response to land cover and management change driven by non-radiative processes, Nat. Clim. Change, 7, 296–302, https://doi.org/10.1038/nclimate3250, 2017.

Bristow, K. L. and Campbell, G. S.: On the relationship between incoming solar radiation and daily maximum and minimum temperature, Agr. Forest Meteorol., 31, 159–166, https://doi.org/10.1016/0168-1923(84)90017-0, 1984.

Chen, L. and Dirmeyer, P. A.: Adapting observationally based metrics of biogeophysical feedbacks from land cover/land use change to climate modeling, Environ. Res. Lett., 11, 034002, https://doi.org/10.1088/1748-9326/11/3/034002, 2016.

Clothier, B. E., Clawson, K. L., Pinter, P. J., Moran, M. S., Reginato, R. J., and Jackson, R. D.: Estimation of soil heat flux from net radiation during the growth of alfalfa, Agr. Forest Meteorol., 37, 319–329, https://doi.org/10.1016/0168-1923(86)90069-9, 1986.

Cresswell, M. P., Morse, A. P., Thomson, M. C., and Connor, S. J.: Estimating surface air temperatures, from Meteosat land surface temperatures, using an empirical solar zenith angle model, Int. J. Remote Sens., 20, 1125–1132, https://doi.org/10.1080/014311699212885, 1999.

Dai, A., Trenberth, K. E., and Karl, T. R.: Effects of Clouds, Soil Moisture, Precipitation, and Water Vapor on Diurnal Temperature Range, J. Climate, 12, 2451–2473, 1999.

Diak, G. R. and Whipple, M. S.: Improvements to models and methods for evaluating the land-surface energy balance and 'effective' roughness using radiosonde reports and satellite-measured 'skin' temperature data, Agr. Forest Meteorol., 63, 189–218, https://doi.org/10.1016/0168-1923(93)90060-U, 1993.

Ellison, D., Morris, C. E., Locatelli, B., Sheil, D., Cohen, J., Murdiyarso, D., Gutierrez, V., van Noordwijk, M., Creed, I. F., Pokorny, J., Gaveau, D., Spracklen, D. V., Tobella, A. B., Ilstedt, U., Teuling, A. J., Gebrehiwot, S. G., Sands, D. C., Muys, B., Verbist, B., Springgay, E., Sugandi, Y., and Sullivan, C. A.: Trees, forests and water: Cool insights for a hot world, Global Environ. Change, 43, 51–61, https://doi.org/10.1016/j.gloenvcha.2017.01.002, 2017.

Falge, E., Aubinet, M., Bakwin, P. S., Baldocchi, D., Berbigier, P., Bernhofer, C., Black, T. A., Ceulemans, R., Davis, K. J., Dolman, A. J., Goldstein, A., Goulden, M. L., Granier, A., Hollinger, D. Y., Jarvis, P. G., Jensen, N., Pilegaard, K., Katul, G., Kyawthapaw, P., Law, B. E., Lindroth, A., Loustau, D., Mahli, Y., Monson, R., Moncrieff, P., Moors, E., Munger, J. W., Meyers, T., Oechel, W., Schulze, E.-D., Thorgeirsson, H., Tenhunen, J., Valentini, R., Verma, S.

B., Vesala, T., and Wofsy, S. C.: FLUXNET Research Network Site Characteristics, Investigators, and Bibliography, 2016, 1459.4803539999996 MB, ORNL DAAC – Oak Ridge National Laboratory Distributed Active Archive Center, Oak Ridge, Tennessee, USA, https://doi.org/10.3334/ORNLDAAC/1530, 2017.

Fu, G., Shen, Z., Zhang, X., Shi, P., Zhang, Y., and Wu, J.: Estimating air temperature of an alpine meadow on the Northern Tibetan Plateau using MODIS land surface temperature, Acta Ecol. Sin., 31, 8–13, https://doi.org/10.1016/j.chnaes.2010.11.002, 2011.

Gallo, K. P.: The Influence of Land Use/Land Cover on Climatological Values of the Diurnal Temperature Range, J. Climate, 9, 2941–2944, 1996.

Hargreaves, G. H. and Samani, Z. A.: Reference Crop Evapotranspiration from Temperature, Appl. Eng. Agricult., 1, 96–99, https://doi.org/10.13031/2013.26773, 1985.

Hengl, T., Heuvelink, G. B. M., Perèec Tadiæ, M., and Pebesma, E. J.: Spatio-temporal prediction of daily temperatures using time-series of MODIS LST images, Theor. Appl. Climatol., 107, 265–277, https://doi.org/10.1007/s00704-011-0464-2, 2012.

Jackson, L. S. and Forster, P. M.: An Empirical Study of Geographic and Seasonal Variations in Diurnal Temperature Range, J. Climate, 23, 3205–3221, https://doi.org/10.1175/2010JCLI3215.1, 2010.

Jackson, T. J., Le Vine, D. M., Hsu, A. Y., Oldak, A., Starks, P. J., Swift, C. T., Isham, J. D., and Haken, M.: Soil moisture mapping at regional scales using microwave radiometry: the Southern Great Plains Hydrology Experiment, IEEE T. Geosci. Remote., 37, 2136–2151, https://doi.org/10.1109/36.789610, 1999.

Jang, J.-D., Viau, A. A., and Anctil, F.: Neural network estimation of air temperatures from AVHRR data, Int. J. Remote Sens., 25, 4541–4554, https://doi.org/10.1080/01431160310001657533, 2004.

Jarvis, P. G. and McNaughton, K. G.: Stomatal Control of Transpiration: Scaling Up from Leaf' to Region, Adv. Ecol. Res., 15, 1–49, 1986.

Jones, H. G.: Plants and Microclimate, Cambridge University Press, New York, USA, 47–67, 1992.

Juang, J.-Y., Katul, G., Siqueira, M., Stoy, P., and Novick, K.: Separating the effects of albedo from eco-physiological changes on surface temperature along a successional chronosequence in the southeastern United States, Geophys. Res. Lett., 34, L21408, https://doi.org/10.1029/2007GL031296, 2007.

Jung, M., Koirala, S., Weber, U., Ichii, K., Gans, F., Camps-Valls, G., Papale, D., Schwalm, C., Tramontana, G., and Reichstein, M.: The FLUXCOM ensemble of global land-atmosphere energy fluxes, Scient. Data, 6, 74, https://doi.org/10.1038/s41597-019-0076-8, 2019.

Kilibarda, M., Hengl, T., Heuvelink, G. B. M., Gräler, B., Pebesma, E., Perèec Tadiæ, M., and Bajat, B.: Spatio-temporal interpolation of daily temperatures for global land areas at 1 km resolution, J. Geophys. Res.-Atmos., 119, 2294–2313, https://doi.org/10.1002/2013JD020803, 2014.

Kustas, W. P. and Daughtry, C. S. T.: Estimation of the soil heat flux/net radiation ratio from spectral data, Agr. Forest Meteorol., 49, 205–223, https://doi.org/10.1016/0168-1923(90)90033-3, 1990.

Kustas, W. P. and Norman, J. M.: Evaluation of soil and vegetation heat flux predictions using a simple two-source model with radiometric temperatures for partial canopy cover, Agr. Forest Meteo-
rol., 94, 13–29, https://doi.org/10.1016/S0168-1923(99)00005-2, 1999.

Lee, X., Goulden, M. L., Hollinger, D. Y., Barr, A., Black, T. A., Bohrer, G., Bracho, R., Drake, B., Goldstein, A., Gu, L., Katul, G., Kolb, T., Law, B. E., Margolis, H., Meyers, T., Monson, R., Munger, W., Oren, R., Paw U, K. T., Richardson, A. D., Schmid, H. P., Staebler, R., Wofsy, S., and Zhao, L.: Observed increase in local cooling effect of deforestation at higher latitudes, Nature, 479, 384–387, https://doi.org/10.1038/nature10588, 2011a.

Lee, X., Goulden, M. L., Hollinger, D. Y., Barr, A., Black, T. A., Bohrer, G., Bracho, R., Drake, B., Goldstein, A., Gu, L., Katul, G., Kolb, T., Law, B. E., Margolis, H., Meyers, T., Monson, R., Munger, W., Oren, R., Paw U, K. T., Richardson, A. D., Schmid, H. P., Staebler, R., Wofsy, S., and Zhao, L.: Observed increase in local cooling effect of deforestation at higher latitudes, Nature, 479, 384–387, https://doi.org/10.1038/nature10588, 2011b.

Li, Y., Zhao, M., Motesharrei, S., Mu, Q., Kalnay, E., and Li, S.: Local cooling and warming effects of forests based on satellite observations, Nat. Commun., 6, 6603, https://doi.org/10.1038/ncomms7603, 2015.

Lindvall, J. and Svensson, G.: The diurnal temperature range in the CMIP5 models, Clim. Dynam., 44, 405–421, https://doi.org/10.1007/s00382-014-2144-2, 2015.

Liu, B., Xu, M., Henderson, M., Qi, Y., and Li, Y.: Taking China's Temperature: Daily Range, Warming Trends, and Regional Variations, 1955–2000, J. Climate, 17, 4453–4462, https://doi.org/10.1175/3230.1, 2004.

Loveland, T. R. and Belward, A. S.: The International Geosphere Biosphere Programme Data and Information System global land cover data set (DISCover), Acta Astronaut., 41, 681–689, https://doi.org/10.1016/S0094-5765(98)00050-2, 1997.

Luyssaert, S., Jammet, M., Stoy, P. C., Estel, S., Pongratz, J., Ceschia, E., Churkina, G., Don, A., Erb, K., Ferlicoq, M., Gielen, B., Grünwald, T., Houghton, R. A., Klumpp, K., Knohl, A., Kolb, T., Kuemmerle, T., Laurila, T., Lohila, A., Loustau, D., McGrath, M. J., Meyfroidt, P., Moors, E. J., Naudts, K., Novick, K., Otto, J., Pilegaard, K., Pio, C. A., Rambal, S., Rebmann, C., Ryder, J., Suyker, A. E., Varlagin, A., Wattenbach, M., and Dolman, A. J.: Land management and land-cover change have impacts of similar magnitude on surface temperature, Nat. Clim. Change, 4, 389–393, https://doi.org/10.1038/nclimate2196, 2014.

Makowski, K., Jaeger, E. B., Chiacchio, M., Wild, M., Ewen, T., and Ohmura, A.: On the relationship between diurnal temperature range and surface solar radiation in Europe, J. Geophys. Res., 114, D00D07, https://doi.org/10.1029/2008JD011104, 2009.

Mallick, K., Jarvis, A., Fisher, J. B., Tu, K. P., Boegh, E., and Niyogi, D.: Latent Heat Flux and Canopy Conductance Based on Penman–Monteith, Priestley–Taylor Equation, and Bouchet's Complementary Hypothesis, J. Hydrometeorol., 14, 419–442, https://doi.org/10.1175/JHM-D-12-0117.1, 2013.

Mearns, L. O., Giorgi, F., McDaniel, L., and Shields, C.: Analysis of variability and diurnal range of daily temperature in a nested regional climate model: comparison with observations and doubled $CO_2$ results, Clim. Dynam., 11, 193–209, https://doi.org/10.1007/BF00215007, 1995.

Mildrexler, D. J., Zhao, M., and Running, S. W.: A global comparison between station air temperatures and MODIS land surface temperatures reveals the cooling role of forests, J. Geophys. Res., 116, G03025, https://doi.org/10.1029/2010JG001486, 2011.

Oke, T. R.: Boundary layer climates, Methuen and Co., Ltd., London, Halsted Press, New York, p. 390, 1978.

Oyler, J. W., Dobrowski, S. Z., Holden, Z. A., and Running, S. W.: Remotely Sensed Land Skin Temperature as a Spatial Predictor of Air Temperature across the Conterminous United States, J. Appl. Meteorol. Clim., 55, 1441–1457, https://doi.org/10.1175/JAMC-D-15-0276.1, 2016.

Panwar, A., Kleidon, A., and Renner, M.: Do Surface and Air Temperatures Contain Similar Imprints of Evaporative Conditions?, Geophys. Res. Lett., 46, 3802–3809, https://doi.org/10.1029/2019GL082248, 2019.

Price, J. C.: Estimation of Regional Scale Evapotranspiration Through Analysis of Satellite Thermal-infrared Data, IEEE T. Geosci. Remote, GE-20, 286–292, https://doi.org/10.1109/TGRS.1982.350445, 1982.

Renner, M., Wild, M., Schwarz, M., and Kleidon, A.: Estimating Shortwave Clear-Sky Fluxes From Hourly Global Radiation Records by Quantile Regression, Earth Space Sci., 6, 1532–1546, https://doi.org/10.1029/2019EA000686, 2019.

Rigden, A. J. and Li, D.: Attribution of surface temperature anomalies induced by land use and land cover changes: Attribution of Temperature Anomalies, Geophys. Res. Lett., 44, 6814–6822, https://doi.org/10.1002/2017GL073811, 2017.

Ronda, R. J., de Bruin, H. A. R., and Holtslag, A. A. M.: Representation of the Canopy Conductance in Modeling the Surface Energy Budget for Low Vegetation, J. Appl. Meteorol., 40, 1431–1444, https://doi.org/10.1175/1520-0450(2001)040<1431:ROTCCI>2.0.CO;2, 2001.

Saltzman, B. and Pollack, J. A.: Sensitivity of the Diurnal Surface Temperature Range to Changes in Physical Parameters, J. Appl. Meteorol., 16, 614–619, https://doi.org/10.1175/1520-0450(1977)016<0614:SOTDST>2.0.CO;2, 1977.

Shukla, J. and Mintz, Y.: Influence of Land-Surface Evapotranspiration on the Earth's Climate, Science, 215, 1498–1501, https://doi.org/10.1126/science.215.4539.1498, 1982.

Shuttleworth, W. J., Gurney, R. J., Hsu, A. Y., and Ormsby, J. P.: FIFE: the variation in energy partition at surface flux sites, IAHS-AISH Publication, IAHS Publication – International Association of Hydrological Sciences, Belgium, 67–74, ISSN 0144-7815, 1989.

Steduto, P. and Hsiao, T. C.: Maize canopies under two soil water regimes, Agr. Forest Meteorol., 89, 169–184, https://doi.org/10.1016/S0168-1923(97)00085-3, 1998.

Stenchikov, G. L. and Robock, A.: Diurnal asymmetry of climatic response to increased $CO_2$ and aerosols: Forcings and feedbacks, J. Geophys. Res., 100, 26211, https://doi.org/10.1029/95JD02166, 1995.

Su, H., Wood, E. F., Mccabe, M. F., and Su, Z.: Evaluation of Remotely Sensed Evapotranspiration Over the CEOP EOP-1 Reference Sites, J. Meteorol. Soc. Jpn. A, 85, 439–459, https://doi.org/10.2151/jmsj.85A.439, 2007.

Tang, B., Zhao, X., and Zhao, W.: Local Effects of Forests on Temperatures across Europe, Remote Sens., 10, 529, https://doi.org/10.3390/rs10040529, 2018.

Thom, A. S.: Momentum, mass and heat exchange of vegetation, Q. J. Roy. Meteorol. Soc., 98, 124–134, https://doi.org/10.1002/qj.49709841510, 1972.

Thornthwaite, C. W.: An Approach toward a Rational Classification of Climate, Geogr. Rev., 38, 55–75, https://doi.org/10.2307/210739, 1948.

Tramontana, G., Jung, M., Schwalm, C. R., Ichii, K., Camps-Valls, G., Ráduly, B., Reichstein, M., Arain, M. A., Cescatti, A., Kiely, G., Merbold, L., Serrano-Ortiz, P., Sickert, S., Wolf, S., and Papale, D.: Predicting carbon dioxide and energy fluxes across global FLUXNET sites with regression algorithms, Biogeosciences, 13, 4291–4313, https://doi.org/10.5194/bg-13-4291-2016, 2016.

Vinukollu, R. K., Wood, E. F., Ferguson, C. R., and Fisher, J. B.: Global estimates of evapotranspiration for climate studies using multi-sensor remote sensing data: Evaluation of three process-based approaches, Remote Sens. Environ., 115, 801–823, https://doi.org/10.1016/j.rse.2010.11.006, 2011.

Wang, K. and Dickinson, R. E.: Contribution of solar radiation to decadal temperature variability over land, P. Natl. Acad. Sci. USA, 110, 14877–14882, https://doi.org/10.1073/pnas.1311433110, 2013.

Wild, M.: From Dimming to Brightening: Decadal Changes in Solar Radiation at Earth's Surface, Science, 308, 847–850, https://doi.org/10.1126/science.1103215, 2005.

Yao, Y., Liang, S., Cheng, J., Liu, S., Fisher, J. B., Zhang, X., Jia, K., Zhao, X., Qin, Q., Zhao, B., Han, S., Zhou, G., Zhou, G., Li, Y., and Zhao, S.: MODIS-driven estimation of terrestrial latent heat flux in China based on a modified Priestley–Taylor algorithm, Agr. Forest Meteorol., 171–172, 187–202, https://doi.org/10.1016/j.agrformet.2012.11.016, 2013.

Zhang, W., Huang, Y., Yu, Y., and Sun, W.: Empirical models for estimating daily maximum, minimum and mean air temperatures with MODIS land surface temperatures, Int. J. Remote Sens., 32, 9415–9440, https://doi.org/10.1080/01431161.2011.560622, 2011.

Zhao, L., Lee, X., Smith, R. B., and Oleson, K.: Strong contributions of local background climate to urban heat islands, Nature, 511, 216–219, https://doi.org/10.1038/nature13462, 2014a.

Zhao, L., Lee, X., Smith, R. B., and Oleson, K.: Strong contributions of local background climate to urban heat islands, Nature, 511, 216–219, https://doi.org/10.1038/nature13462, 2014b.

Zhu, W., Lû, A., and Jia, S.: Estimation of daily maximum and minimum air temperature using MODIS land surface temperature products, Remote Sens. Environ., 130, 62–73, https://doi.org/10.1016/j.rse.2012.10.034, 2013.

**Chapter 5**

# Evaluating the Response of Diurnal Variations in Surface and Air Temperature to Evaporative Conditions Across Vegetation Types in FLUXNET and ERA5

This chapter is originally published in

*"Panwar, A., Kleidon, A. (2022). Evaluating the response of diurnal variations in surface and air temperature to evaporative conditions across vegetation types in FLUXNET and ERA5. Journal of Climate, 35(19), 2701-2728."*

©American Meteorological Society. Used with permission.

# Evaluating the Response of Diurnal Variations in Surface and Air Temperature to Evaporative Conditions across Vegetation Types in FLUXNET and ERA5

ANNU PANWAR[a] AND AXEL KLEIDON[a]

[a] Max Planck Institute for Biogeochemistry, Jena, Germany

ABSTRACT: The diurnal variations of surface and air temperature are closely related, but their different responses to evaporative conditions can inform us about land–atmosphere interactions. Here, we evaluate the responses of the diurnal ranges in surface ($\Delta T_s$) and air ($\Delta T_a$) temperature to evaporative fraction at 160 FLUXNET sites and in the ERA5 reanalysis. We show that the sensitivity of $\Delta T_s$ to evaporative fraction depends on vegetation type, whereas $\Delta T_a$ does not. On days with low evaporative fraction, $\Delta T_s$ in FLUXNET is enhanced by up to ~20 K (~30 K in ERA5) in short vegetation, but only by up to ~10 K (~10 K in ERA5) in forests. Note that $\Delta T_a$ responds rather similarly to evaporative fraction irrespective of vegetation type (~5 K in FLUXNET, ~10 K in ERA5). We find a systematic bias in ERA5's $\Delta T$ response to evaporative conditions, showing a stronger sensitivity to evaporative fraction than in FLUXNET. We then demonstrate with a simple atmospheric boundary layer (SABL) model that the weak response of $\Delta T_a$ to evaporative fraction can be explained by greater boundary layer growth under dry conditions, which increases the heat storage capacity and reduces the response of air temperature to evaporative fraction. Additionally, using a simplified surface energy balance (SSEB) model we show that $\Delta T_s$ mainly responds to solar radiation, evaporative fraction, and aerodynamic conductance. We conclude that the dominant patterns of diurnal temperature variations can be explained by fundamental physical concepts, which should help us to better understand the main controls of land–atmosphere interactions.

SIGNIFICANCE STATEMENT: Generally, air temperature is used more widely than the surface temperature, and often they are assumed to be equivalent. However, we show that their responses to changes in vegetation type and evaporative conditions are quite different. Using FLUXNET observations, ERA5 reanalysis, and two simple physical models, we found that these responses are much stronger in surface temperature, especially in short vegetation, and relatively weaker in air temperature. Despite being measured just 2 m above the surface, air temperature carries lesser imprints of evaporation and vegetation than the surface temperature because of boundary layer dynamics. These findings suggest the importance of coupled land–atmosphere processes in shaping surface and air temperature differently and provide insights on their distinctive responses to global changes.

## 1. Introduction

The diurnal temperature range (DTR) is a vital index for describing how atmospheric conditions over land change during the day and is used as an indicator of global change (Karl et al. 1991; Easterling et al. 1997; Braganza et al. 2004; Lewis and Karoly 2013). Therefore, understanding the physical processes that shape DTR is crucial. Previous studies have shown that soil moisture, solar radiation, and vegetation types are among the leading controlling factors of DTR (Dai et al. 1997, 1999; Stone and Weaver 2002; Feddema et al. 2005; Zhou et al. 2009; Pyrgou et al. 2019). For instance, Mearns et al. (1995) showed that 52% of variance in DTR can be explained by evaporative cooling, while Makowski et al. (2009) demonstrate a strong correlation ($R^2 \approx 0.87$) between the annual mean of DTR and solar radiation. Recently, greater attention is given to quantify the consequences of deforestation and land use/land cover change on DTR (Gallo et al. 1996; Collatz et al. 2000; Zhou et al. 2007). For instance, Lobell and Bonfils (2008) estimated a mean decrease of DTR by 5°C due to irrigation in California.

Typically, in these studies, the diurnal range of air temperature (DTR of air temperature, hereafter $\Delta T_a$) is used due to the widespread availability of air temperature products, which are measured at ~2-m height above the ground at meteorological stations. However, advances in remote sensing and land surface modeling have encouraged the use of surface temperature, the radiative temperature of the surface or canopy, also known as skin temperature, which can be obtained using the Stefan–Boltzmann law. These products have stimulated discussions on the different responses of $\Delta T_a$ and the diurnal range of surface temperature (DTR of surface temperature, hereafter $\Delta T_s$) to changes in water availability and vegetation characteristics (Zhou et al. 2007; Jin and Dickinson 2010; Baldocchi and Ma 2013). In this study, we investigate the extent to which $\Delta T_s$ and $\Delta T_a$ respond differently to evaporative conditions, vegetation properties, and the physical constraints governing these responses across different climates.

---

Denotes content that is immediately available upon publication as open access.

---

*Corresponding author*: Annu Panwar, apanwar@bgc-jena.mpg.de
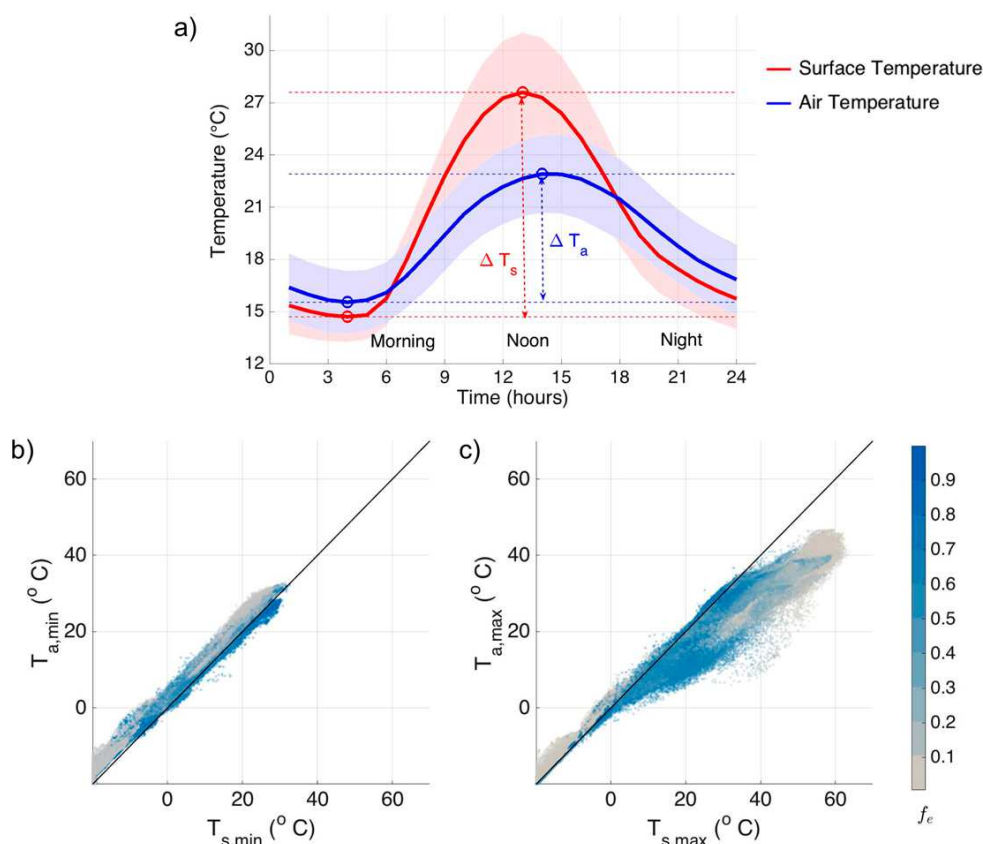
FIG. 1. (a) Mean diurnal variation of surface and air temperature for the summer season over the land surface in the ERA5 reanalysis (2000–15). The shaded regions show the standard error of the means. (b) The relationship between daily values of minimum surface ($T_{s,\min}$) and minimum air ($T_{a,\min}$) temperatures over the land surface in ERA5. (c) The relationship between daily maximum surface ($T_{s,\max}$) and maximum air ($T_{a,\max}$) temperatures over the land surface in ERA5. The color bar shows the mean evaporative fraction [$f_e = \mathrm{LE}/(\mathrm{LE} + H)$].

The diurnal evolution (or diel cycle) of surface and air temperature is dominantly shaped by the variation in solar energy input, but their amplitudes, or DTR, might respond differently to evaporative conditions. To illustrate this, we show in Fig. 1a the mean diurnal variation of surface and air temperature for the summer months (June–August for the Northern Hemisphere and December–February for Southern Hemisphere) for vegetated areas in the global ERA5 reanalysis (Copernicus Climate Change Service 2019). Figure 1b shows that the minimum surface ($T_{s,\min}$) and air ($T_{a,\min}$) temperatures are similar irrespective of the evaporative fraction ($f_e$, the ratio of the latent heat flux to the total turbulent heat flux). This is likely due to the absence of turbulent fluxes in the morning, although the latent heat release from dew formation might play a role in warming the minimum temperatures (Bourque and Arp 1994). The maximum surface temperature ($T_{s,\max}$), however, tends to be greater than the maximum air temperature ($T_{a,\max}$) on days with lower evaporative fraction (dry conditions) and to be more similar on the days with higher evaporative fraction (wet conditions), as shown in Fig. 1c. Since evaporation on land

occurs mainly during the daytime, the impact of evaporative cooling reduces the variation of daytime temperature. Hence, the effect of evaporative cooling can be quantified as the change in DTR from dry to wet conditions. In this study we quantify this reduction in $\Delta T_s$ and $\Delta T_a$ in response to evaporative fraction and examine the physical controls to obtain an explanation for the dominant processes shaping this reduction.

We also seek to explain the first-order responses of the diurnal temperature ranges using simple physical models to identify the major controls. Our previous study used a simple heat storage model (Panwar et al. 2019) to show that the diurnal warming rate of air temperature is strongly affected by the growth of the planetary boundary layer (PBL). Thus, the diurnal amplitude of air temperature could only be as high as the diurnal amplitude of surface temperature if the PBL height does not respond to the sensible heat flux. We then found that the weak response of air temperature to evaporative fraction in observations of a cropland site was due to the compensating effect of stronger boundary layer growth for drier conditions. In this study the warming rate is translated into

$\Delta T_a$ and then its relationship to boundary layer heat storage is obtained, primarily in the context of changing evaporative conditions. The heat storage in the boundary layer is calculated based on the maximum power limit (Kleidon and Renner 2017). The role of boundary layer growth on $\Delta T_a$ is accounted for by the lapse rate of potential temperature in the free atmosphere. We then investigate if these responses are independent of vegetation types and how they vary with energy availability for instance, from the tropics to extratropics.

Unlike air temperature, the diurnal variation of surface temperature is strongly governed by surface properties and its response to evaporative conditions can vary across vegetation types. Our recent study (Panwar et al. 2020), based on FLUXNET observations, shows that evaporation reduces $\Delta T_s$ similarly across vegetation types. In forests, however, the cooling due to their high aerodynamic conductance is more dominant, thus reducing the sensitivity to evaporative conditions. These findings were established using a surface energy balance–based expression of $\Delta T_s$. Here, we further simplify and develop this approach in order to capture the role of solar radiation, aerodynamic conductance, and evaporative fraction in explaining the spatial variation in $\Delta T_s$ across FLUXNET sites and across continents in ERA5. Even though the FLUXNET and ERA5 datasets represent quite different scales, we argue that the main drivers in shaping diurnal temperature variations and its buffering in the lower atmosphere are the same (as shown in our previous studies). Because these drivers are to first order independent of scale, we should find similar functional responses at local FLUXNET sites and at the coarser, corresponding grid cell in the ERA5 reanalysis. The sensitivities of $\Delta T_s$ and $\Delta T_a$ to evaporative fraction and vegetative cover should then also be similar and explainable by the same physical constraints.

To conduct this study, we use FLUXNET observations (Pastorello et al. 2020) across different vegetation types and the global ERA5 reanalysis (Copernicus Climate Change Service 2019). Both data sources have their benefits and drawbacks. FLUXNET provides in situ observations of near-surface meteorological variables but does not provide PBL height (Helbig et al. 2020). ERA5 provides information on PBL development that is required to explore the role of PBL dynamics in shaping $\Delta T_a$, but it is a modeled product. To identify potential biases, we compare the DTR responses to evaporative fraction in both datasets. The cooling effect of evaporation is expected for conditions that are not energy limited. Finally, we aim to extend our insights from the FLUXNET observations to the continental scale as well as to boundary layer dynamics by the combination of both data sources.

In the following section we present two simple models that explain the physical constraints of $\Delta T_a$ and $\Delta T_s$. The formulation of $\Delta T_a$ uses a simple PBL heat storage approach based on Panwar et al. (2019), and the formulation of $\Delta T_s$ uses a simple surface energy balance model based on Panwar et al. (2020). After describing the data sources and their preparation, we analyze and compare the $\Delta T_a$ and $\Delta T_s$ responses to evaporative fraction in FLUXNET and ERA5 in the results section. There, we also demonstrate how well our simple models can reproduce the geographical variation of $\Delta T_a$ and $\Delta T_s$ responses to evaporative fraction across vegetation types and across different climates. We then discuss and conclude with the implications of our study for a better understanding of land–vegetation–atmosphere interactions.

## 2. Methods

The diurnal variation of surface and air temperature is driven by absorbed solar radiation ($R_s$) and its partitioning into latent (LE) and sensible ($H$) heat flux. In this section we formulate $\Delta T_a$ and $\Delta T_s$, starting from the surface energy balance that is given as

$$R_s + R_{l,\text{net}} = \text{LE} + H + G. \tag{1}$$

Here, $R_{l,\text{net}}$ is the net longwave radiation and $G$ is the ground heat flux. For simplification, diurnal changes in $G$ are neglected (e.g., Betts and Ball 1995). The heat discharged from the surface cools the surface but contributes to the increase in heat storage in the atmospheric boundary layer.

We first use the components of the surface energy balance to formulate energy storage changes in the boundary layer, from which we infer $\Delta T_a$. We refer to this model for $\Delta T_a$ as the simple atmospheric boundary layer (SABL) model. We then derive an expression for $\Delta T_s$ by solving the surface energy balance for surface temperature, using a few simplifications. We refer to this model for $\Delta T_s$ as the simplified surface energy balance (SSEB) model.

### a. Formulating the $\Delta T_a$ response to evaporative fraction using SABL

Over land, the diurnal variation of air temperature $\Delta T_a$ reflects mostly the heat storage change ($\Delta U$) in the lower atmosphere due to strong variation in solar radiation. Part of the absorbed solar radiation is utilized in evaporation and does not contribute to a rise in air temperature. The increase in boundary layer heat storage is thus approximately given by $d(\Delta U)/dt = R_s - \text{LE}$. We use this energy balance constraint (Kleidon and Renner 2017) and the maximum power limit for turbulent fluxes (Kleidon and Renner 2018) to obtain the relationship of $\Delta U$ and evaporative fraction ($f_e$; see appendix B for the derivation):

$$\Delta U = \frac{2 - f_e}{2 + f_e} \Delta U_0. \tag{2}$$

Here, $\Delta U_0$ is the heat storage variation in the absence of evaporation, which depends on absorbed solar radiation and daylight length ($\Delta t_{\text{day}}$) by $\Delta U_0 = R_{s,\text{avg}} \Delta t_{\text{day}}$, or, rewritten in terms of maximum solar radiation ($R_{s,\text{max}}$), as $\Delta U_0 = (2 R_{s,\text{max}} \Delta t_{\text{day}})/\pi$.

The diurnal temperature range $\Delta T_a$ directly relates to this heat storage change, but the amplitude also depends on the PBL height. Figure 2a shows a simple depiction of the PBL heat storage and how it relates to $\Delta T_a$ for dry (orange) and wet (blue) conditions. The heat storage change is represented by the triangle, whose $y$ axis is the boundary layer height ($\Delta z$) and the $x$ axis is the change in potential temperature ($\theta$). Generally, the 2-m air temperature is similar to the potential
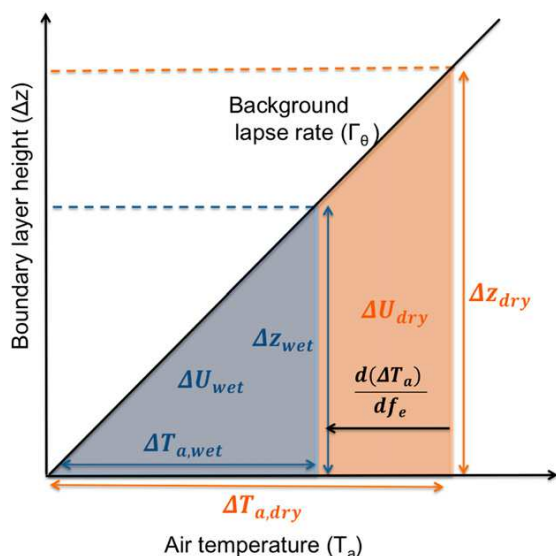
FIG. 2. A conceptual illustration of the heat storage change $\Delta U$ in the atmospheric boundary layer (colored areas) in relation to the diurnal temperature range $\Delta T_a$ and the change in boundary layer height $\Delta z$ for a given background lapse rate in potential temperature $\Gamma_\theta$. Two cases are shown for wet (blue) and dry (orange) evaporative conditions.

temperature (Stull et al. 2015), so we can assume that the morning to afternoon change in PBL potential temperature is equivalent to $\Delta T_a$. For dry conditions, both $\Delta U$ and $\Delta z$ increase in response to stronger buoyancy due to a higher sensible heat flux and less latent heating. In contrast, for wet conditions (blue triangle) $\Delta z$ and $\Delta U$ are lower, resulting in a lower response in $\Delta T_a$. The difference between the dry and wet $\Delta T_a$ depicted in the $x$ axis is a measure of the evaporative cooling effect of $\Delta T_a$ that is expressed as $d(\Delta T_a)/df_e$.

We can thus express $\Delta U$ in terms of $\Delta T_a$ and the planetary boundary layer height $\Delta z$ by [following Panwar et al. (2019)]

$$\Delta U = c_p \rho \Delta T_a \frac{\Delta z}{2}. \tag{3}$$

Here $c_p = 1005$ J kg$^{-1}$ is the specific heat capacity and $\rho$ is the density of air. Note that the air density changes with elevation but for simplification we consider a constant value of $\rho = 1.23$ kg m$^{-3}$.

During the day, the boundary layer height grows as per the background lapse rate of potential temperature ($\Gamma_\theta$). When we assume that $\Gamma_\theta$ is similar for dry and wet conditions, we can write $\Delta z = \Delta T_a/\Gamma_\theta$. Using $\Gamma_\theta$ and Eq. (2) for $\Delta U$, we can then express $\Delta T_a$ as

$$\Delta T_a = \left(\frac{2 - f_e}{2 + f_e}\right)^{1/2} \Delta T_{a0}. \tag{4}$$

Here $\Delta T_{a0}$ is the $\Delta T_a$ in the absence of evaporation that depends on solar radiation, background lapse rate, and

daylight length, given by $(\Delta T_{a0})^2 = (2\Gamma_\theta R_{s,\max} \Delta t_{\text{day}})/(\pi c_p \rho)$. By taking the derivative of Eq. (4) with respect to $f_e$ we get the response of $\Delta T_a$ to a change in evaporative fraction:

$$\frac{d(\Delta T_a)}{df_e} = -\frac{2}{[(2 - f)_e/(2 + f_e)]^{1/2}(2 + f_e)^2} \Delta T_{a0} \approx -0.4\Delta T_{a0}. \tag{5}$$

Note that this expression hardly depends on $f_e$, because the denominator in Eq. (5) varies only weakly from 4 for $f_e = 0$ to 5.2 for $f_e = 1$. The negative sign of $d(\Delta T_a)/df_e$ shows that $\Delta T_a$ decreases with greater evaporative fraction. This decrease is up to 40% of $\Delta T_{a0}$ over the range from $f_e = 0$ to $f_e = 1$. Because $\Delta T_{a0}$ depends on $R_{s,\max}$, $\Delta T_{a0}$ as well as $d(\Delta T_a)/df_e$ increase in regions with higher solar energy input. However, when calculating this sensitivity one needs to consider potential variations in $\Gamma_\theta$.

### b. Formulating the $\Delta T_s$ response to evaporative fraction using SSEB

The diurnal variation in surface temperature, $\Delta T_s$, mainly depends on the absorbed solar radiation, $R_s$, and its partitioning into surface energy balance components. It can be derived by linearizing net longwave radiation, expressing the latent heat flux by the evaporative fraction, and by expressing the sensible heat flux in terms of an aerodynamic conductance $g_a$ (Panwar et al. 2020). Then, the diurnal change in surface temperature in response to $R_s$ can be expressed as

$$\frac{dT_s}{dR_s} \approx \frac{dT_a}{dR_s} + \frac{1 - f_e}{c_p \rho g_a} - \frac{\overline{(T_s - T_a)}}{g_a} \frac{dg_a}{dR_s}. \tag{6}$$

Here, $\overline{T_s - T_a}$ is the morning time mean of the difference between surface and air temperature. The aerodynamic conductance, $g_a$, depends on vegetation type and its sensitivity to solar radiation is expressed as $dg_a/dR_s$. Note that the warming rates for surface and air temperature, $dT_s/dR_s$ and $dT_a/dR_s$, are related to each other and are more similar for higher values of $f_e$ and lower values of $\overline{T_s - T_a}$. On integrating Eq. (6) over the morning from $R_s = 0$ to $R_s = R_{s,\max}$, we get the expression for $\Delta T_s$ as follows:

$$\Delta T_s = \Delta T_a + \frac{(1 - f_e)}{c_p \rho \overline{g_a}} R_{s,\max} - \frac{\Delta g_a}{\overline{g_a}} \overline{(T_s - T_a)}. \tag{7}$$

Here $\Delta g_a$ is the morning to afternoon increase in aerodynamic conductance. Integrating $dT_s/dR_s$ to obtain $\Delta T_s$ is an approximation since $T_{s,\max}$ and $R_{s,\max}$ occur at a similar time during the day. The diurnal temperature range for air temperature, $\Delta T_a$, however, reflects a somewhat different integration because the maximum air temperature occurs in the afternoon (after $R_s = R_{s,\max}$; see also Fig. 1a). Hence, assuming that $(dT_a/dR_s)R_{s,\max} \approx \Delta T_a$ can lead to slight underestimation of $\Delta T_a$.

Equation (7) can further be simplified by assuming that $T_{s,\min} \approx T_{a,\min}$ (see Fig. 1b), such that $\Delta T_s$ can be expressed as $\Delta T_s = \Delta T_a + T_{s,\max} - T_{a,\max}$. Figure A1 in appendix A shows
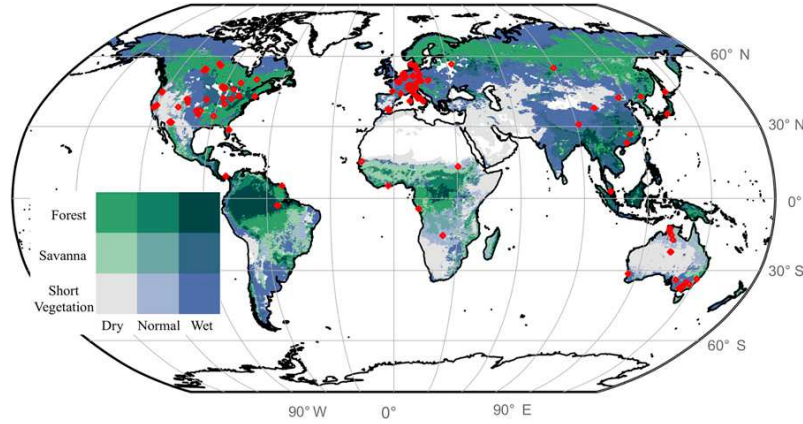
FIG. 3. Location of FLUXNET sites (red symbols) used for this study in relation to the vegetation type (green shades) and mean evaporative conditions (blue shades). The vegetation type is based on the IGBP classification. The mean evaporative conditions are defined as dry ($f_e \leq 0.35$), normal ($0.35 < f_e \leq 0.65$), and wet ($0.65 < f_e < 1$) and are obtained from the ERA5 reanalysis (2000–15).

that $T_{s,\max} - T_{a,\max} \approx 1.4(\overline{T_s - T_a})$. Based on these simplifications, we get $\Delta T_s$ as follows:

$$\Delta T_s \approx \Delta T_a + \frac{1.4(1 - f_e)}{c_p \rho (1.4\overline{g_a} + \Delta g_a)} R_{s,\max}. \tag{8}$$

To get the response of $\Delta T_s$ to evaporative fraction, we take the derivative of Eq. (8) with $f_e$ such that

$$\frac{d(\Delta T_s)}{df_e} \approx \frac{d(\Delta T_a)}{df_e} - \frac{1.4}{c_p \rho (1.4\overline{g_a} + \Delta g_a)} R_{s,\max}. \tag{9}$$

Equation (9) suggests that the sensitivity of $d(\Delta T_s)/df_e$ mainly depends on solar radiation, $R_{s,\max}$, and aerodynamic conductance, $g_a$, which depends on vegetation type, as we will see below. Since $d(\Delta T_a)/df_e$ as well as the second term of Eq. (9) is negative, $d(\Delta T_s)/df_e$ is also negative. Or, in other words, $\Delta T_s$ decreases with an increase in evaporative fraction. Additionally, $d(\Delta T_s)/df_e$ increases in regions with higher solar radiation.

## 3. Data

To evaluate the DTR responses to evaporative fraction, we use temperatures and surface energy balance components from FLUXNET observations and ERA5 reanalysis. The global FLUXNET network provides routine observations of local atmospheric state variables and surface energy balance components using the eddy covariance technique (Pastorello et al. 2020). Here, data from 160 FLUXNET sites with short vegetation (63), savanna (20), and forest (77) with observations for more than 2 years are used. Land cover types are assigned based on the International Geosphere–Biosphere Programme (IGBP) classification, as in Falge et al. (2017a). Short vegetation consists of croplands, grasslands and shrublands, and forest consists of mixed forest, deciduous, evergreen,

broadleaf, and needleleaf forests. Please refer to Table A1 in appendix A for site-specific land cover types. Figure 3 depicts the geographical locations of the FLUXNET sites used here, with the detailed description of each site provided in Table A1.

The FLUXNET data used in this study are gap-filled with the multidimensional scaling (MDS) method as described in Reichstein et al. (2005). Medium- to poor-quality gap-filled data are rejected and only measured and good quality gap-filled data are considered in this study. A more detailed description of the FLUXNET dataset processing is available at Pastorello et al. (2020).

Furthermore, we use the fifth-generation ERA5 reanalysis product by the European Centre for Medium-Range Weather Forecasts (ECMWF) (Copernicus Climate Change Service 2019) at a spatial resolution of 31 km (0.25° latitude–longitude grid) for the years 2000–15. We primarily use the temperature products as well as the boundary layer height product of the ERA5 reanalysis that is required to evaluate $\Gamma_\theta$ and thereby the $\Delta T_a$ response to evaporative fraction. Additionally, in order to identify and understand the biases between FLUXNET and ERA5, we compare DTR responses to evaporative fraction in ERA5 with the grid cells covering the FLUXNET sites. We then attribute possible biases to differences in the surface energy balance.

The responses of $\Delta T_s$ and $\Delta T_a$ to evaporative fraction from FLUXNET and ERA5 are obtained from the slope of their linear regressions against evaporative fraction that we describe as $d(\Delta T_s)/df_e$ and $d(\Delta T_a)/df_e$, respectively. In case of FLUXNET, we obtain these slopes as per vegetation type, using daily observations of DTR and $f_e$. In case of ERA5, we quantify $\Delta T_s$ and $\Delta T_a$ responses to evaporative fraction locally (i.e., at each grid cell), globally (i.e., by combining all vegetated land grid cells), and at FLUXNET sites. The ERA5 local response are based on daily values at each grid point,
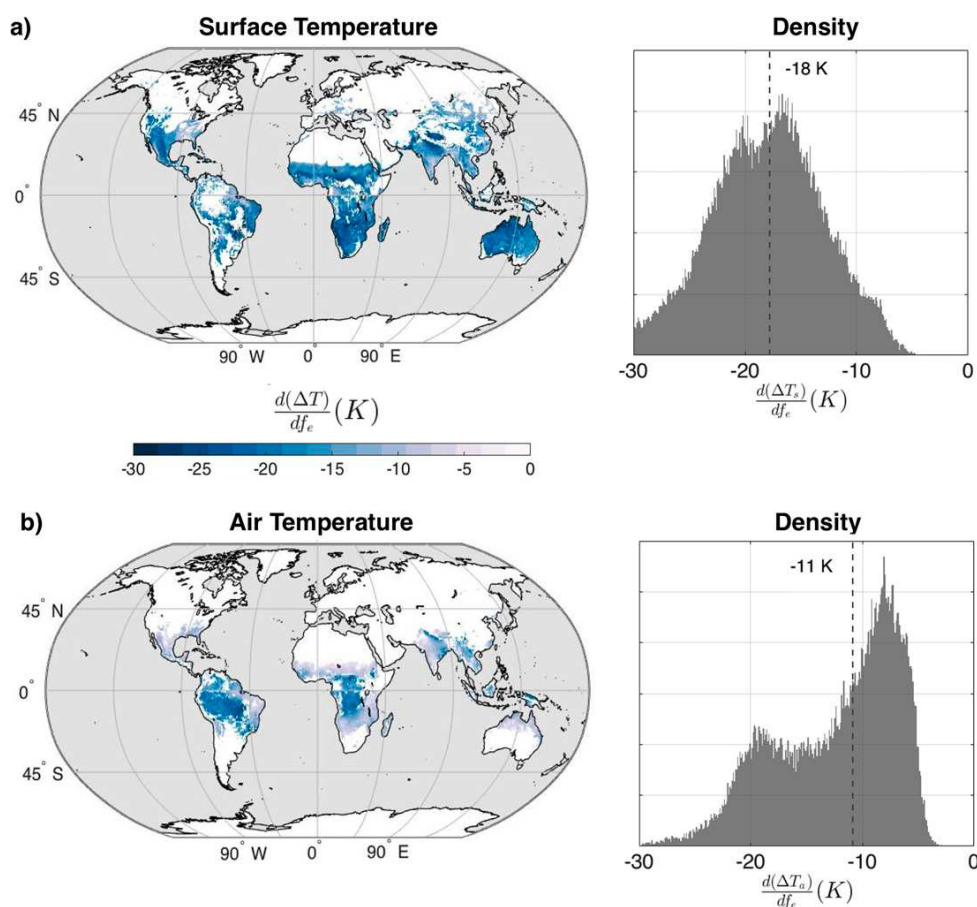
FIG. 4. Local responses of (a) $\Delta T_s$ and (b) $\Delta T_a$ to evaporative fraction obtained from the daily values of the summer season in ERA5 reanalyses for the years 2000–15. Only grid cells with $R^2 > 0.3$ for the regression of $\Delta T_a$ and $f_e$ are shown. The histograms show the density distribution of these responses with the median values indicated by the dashed lines.

and their analysis is aimed to identify regions with significant responses. Considering that not all the regions have a sufficiently large range in evaporative fraction, weaker and insignificant responses in those regions are expected. The limited range in evaporative fraction can be addressed by simply exploiting the natural occurrence of vegetation in different mean evaporative conditions. This is illustrated in Fig. 3, where the mean evaporative fraction is classified into three ranges for simplicity, as dry ($f_e \leq 0.35$), normal ($0.35 < f_e \leq 0.65$), and wet ($0.65 < f_e < 1$). In the global analysis we utilize this spatial combination of vegetation type and their mean evaporative fraction. Last, to compare the results from FLUXNET and ERA5, we estimate $d(\text{DTR})/df_e$ using the daily values of DTR and $f_e$ of the ERA5 grid points covering the FLUXNET sites.

We consider only time periods with non-energy-limited conditions to avoid the positive relationship of temperature and evaporation (Garcia et al. 2014; Sun et al. 2016) and to select days with a well-mixed convective boundary layer. We

selected summer days corresponding to June, July, and August (JJA) in the Northern Hemisphere and December, January, and February (DJF) in the Southern Hemisphere. Likewise, in ERA5, we only consider latitudes inside 66°S–66°N. In FLUXNET as well as in ERA5, air temperature is the temperature ~2 m above the ground or canopy. Since FLUXNET does not provide direct observations of surface temperature, we obtain it from the surface upwelling flux of longwave radiation using the Stefan–Boltzmann law. It should be noted that surface emissivity varies with surface moisture, vegetation, composition, and roughness, usually ranging from 0.8 to 1 (Humes et al. 1994; Valor and Caselles 1996; Nerry et al. 1988; Thome 2014). For simplicity we used a surface emissivity of 1. Surface temperature in ERA5 is available as skin temperature that is derived from the surface energy balance (ECMWF 2007). Additionally, daily minimum and maximum temperatures and DTR are calculated based on the half-hourly and hourly values in FLUXNET and ERA5, respectively. More information on the calculation of
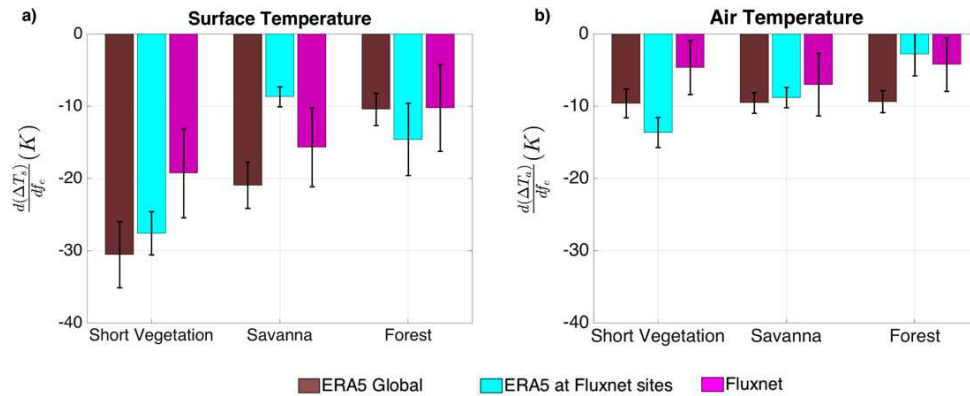
FIG. 5. Bar plots of (a) $\Delta T_s$ and (b) $\Delta T_a$ responses to evaporative fraction in ERA5 and FLUXNET for short vegetation, savanna, and forests. The ERA5 global estimate (brown bars) is obtained from all grid points falling into the respective vegetation type (except high latitudes). The cyan bars show the estimate obtained from ERA5 reanalyses at FLUXNET sites and the magenta bars using FLUXNET observations. The error bars represent the root-mean-square error for the respective estimates. The median values and regression statistics of these estimates are provided in Table 1.

different variables of FLUXNET and ERA5 is provided in Table A2 of appendix A.

The influence of vegetation type on $\Delta T_s$ and $\Delta T_a$ responses to evaporative fraction is evaluated through their aerodynamic conductance ($g_a$). To maintain consistency with the surface energy balance, the aerodynamic conductance is obtained from the observed sensible heat flux ($H$), such that $g_a = H/[c_p\rho(T_s - T_a)]$. Because $g_a$ is also sensitive to absorbed surface solar radiation ($R_s$) (Kumagai et al. 2004), we have also calculated the change in aerodynamic conductance ($\Delta g_a$) from morning ($R_s = 10$ W m$^{-2}$) to solar noon ($R_s = R_{s,\max}$) at FLUXNET sites.

## 4. Results

We start the presentation of the results with documenting the responses of the diurnal temperature ranges to evaporative fraction in ERA5 and FLUXNET and compare these to identify potential biases. We then use the models presented in section 2 to explain the responses of $\Delta T_a$ and $\Delta T_s$ separately. We recommend using our models mainly to evaluate surface and air temperature responses to evaporative conditions. Figure A2 in appendix A shows our models' performance in estimating diurnal range of surface and air temperature. The consistent underestimation of the diurnal temperature range occurs because of some simplified assumptions that are discussed in the method sections.

### a. The DTR responses to evaporative fraction in ERA5 and FLUXNET

Figures 4a and 4b show the local $d(\Delta T_s)/df_e$ and $d(\Delta T_a)/df_e$ obtained from the ERA5 reanalysis for summer months. These local responses are calculated from the linear regression of the daily values of $\Delta T$ and evaporative fraction (with a total of 1350 days) at each grid point for vegetated surfaces. We find that $\Delta T_s$ reduces more strongly than $\Delta T_a$ in response to higher

TABLE 1. The median values of $d(\Delta T_s)/df_e$ and $d(\Delta T_a)/df_e$ obtained from the global ERA5 reanalyses, ERA5 reanalyses at FLUXNET sites, and FLUXNET observations.

| Vegetation | $d(\Delta T_s)/df_e$ (K) | | | $d(\Delta T_a)/df_e$ (K) | | |
| | ERA5 Global | ERA5 at FLUXNET sites | FLUXNET | ERA5 | ERA5 at FLUXNET sites | FLUXNET |
|---|---|---|---|---|---|---|
| Short vegetation | −30.56 | −27.60 | −19.28 | −9.62 | −13.65 | −4.65 |
| $R^2$ | 0.64 | 0.60 | 0.28 | 0.49 | 0.42 | 0.06 |
| RMSE | 4.56 | 3.00 | 6.15 | 1.98 | 2.08 | 3.72 |
| | | | | | | |
| Savanna | −21.00 | −8.70 | −15.88 | −9.55 | −8.83 | −7.03 |
| $R^2$ | 0.46 | 0.56 | 0.25 | 0.47 | 0.56 | 0.12 |
| RMSE | 3.20 | 1.40 | 5.43 | 1.43 | 1.40 | 4.25 |
| | | | | | | |
| Forest | −10.44 | −14.60 | −10.25 | −9.38 | −2.80 | −4.24 |
| $R^2$ | 0.26 | 0.44 | 0.10 | 0.39 | 0.08 | 0.04 |
| RMSE | 2.24 | 5.00 | 6.00 | 1.51 | 3.00 | 3.71 |
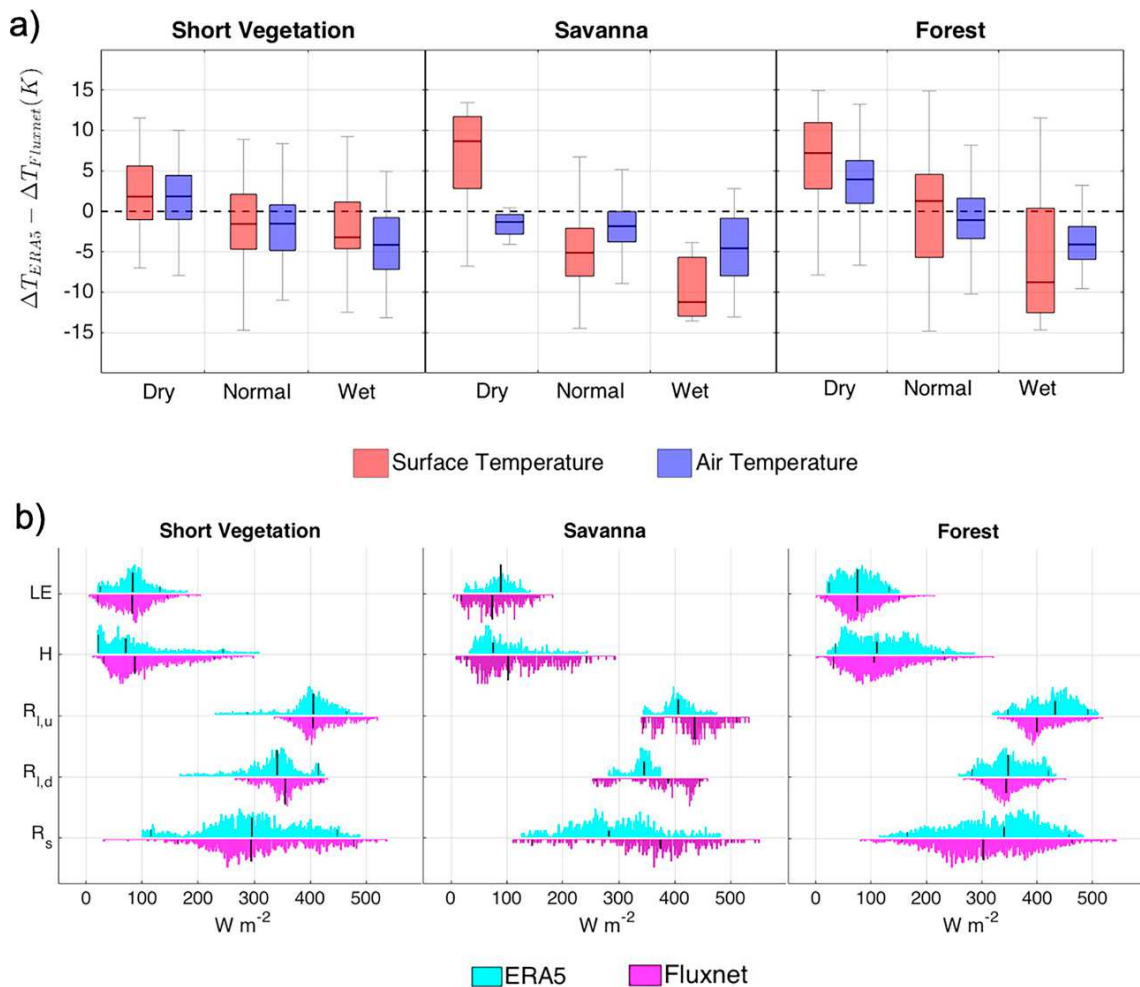
FIG. 6. Biases in ERA5 (a) diurnal temperature ranges and (b) surface energy balances in comparison to FLUXNET observations. The bias in the diurnal temperature range is expressed by the difference between the ERA5 and the FLUXNET values, separately for short vegetation, savanna, and forests for dry, normal, and wet conditions. The density plot of the surface energy balance components shows the latent (LE) and sensible ($H$) heat fluxes, upwelling ($R_{l,u}$) and downwelling ($R_{l,d}$) longwave radiation, and absorbed solar radiation ($R_s$) for ERA5 (cyan) and FLUXNET (magenta) for short vegetation, savanna, and forests. The nearest ERA5 grid points to the FLUXNET locations are used.

evaporative fractions. The frequency distribution of these responses shows a decrease in $\Delta T_s$ by 18 K (median) and in $\Delta T_a$ by 11 K (median) in response to an increase in evaporative fraction. Here only regions with correlation coefficients higher than $R^2 >$ 0.3 for the regression between $\Delta T$ and $f_e$ are shown. Local responses are sensitive to the range of evaporative fraction, which in turn depends on soil moisture dynamics and solar radiation (Nutini et al. 2014; Wang and Dickinson 2012). Consequently, the regression to estimate $d(\Delta T)/df_e$ is much more significant in the regions where evaporative fraction is variable (see Fig. A3). Additionally, these responses might vary across vegetation types, an aspect that we explore further and compare with FLUXNET data.

An alternative approach to obtain $d(\Delta T)/df_e$ is to simply utilize the existing spatial variation in vegetation and evaporative fraction that is shown in Fig. 3, using the summertime mean values. We refer to this estimate as the ERA5 global estimate. Figures 5a and 5b display $d(\Delta T_s)/df_e$ and $d(\Delta T_a)/df_e$ derived from the ERA5 reanalysis along with that from the FLUXNET observations for short vegetation, savanna, and forests. The responses derived from ERA5 are shown in terms of the global estimate (brown) as well as at FLUXNET sites (cyan), that uses only the grid cells closest to or at the FLUXNET sites. Despite the fact that surface and air temperature are closely related, their diurnal ranges respond remarkably different to evaporative fraction. Figure 5a shows that
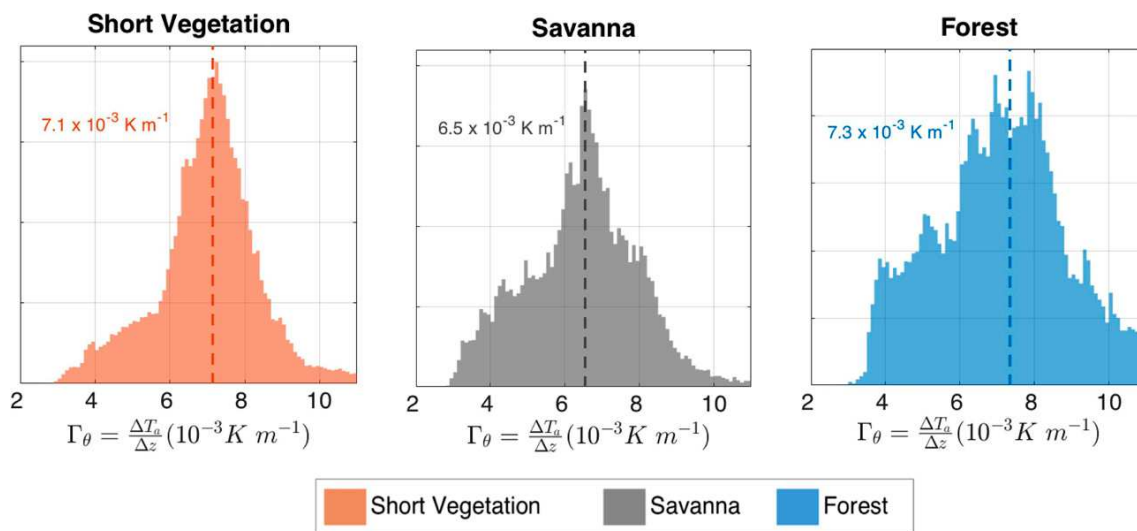
FIG. 7. The density distributions of the background lapse rate of potential temperature ($\Gamma_\theta = \Delta T_a/\Delta z$) in short vegetation, savanna, and forests obtained from ERA5 reanalyses. The dashed lines show the median values of the distribution that is also indicated in the figures.

$d(\Delta T_s)/df_e$ strongly differs among vegetation types, being higher in short vegetation ($\approx -20$ K in FLUXNET, $-30$ K in ERA5) and lower in forests ($\approx -10$ K in FLUXNET and ERA5). However, $d(\Delta T_a)/df_e$ is much lower than $d(\Delta T_s)/df_e$ and remains almost similar ($\approx -5$ K in FLUXNET and $-10$ K in ERA5) across vegetation types. Table 1 summarizes the statistics of $d(\Delta T_s)/df_e$ and $d(\Delta T_a)/df_e$ shown in Fig. 5.

Overall, the responses of $\Delta T$ to evaporative fraction in ERA5 and FLUXNET show similar patterns, even though these responses appear to be consistently stronger in ERA5 than in FLUXNET. This is mainly true for the ERA5 global responses that are more significant than the responses at FLUXNET sites, presumably due to larger data and a higher range in evaporative fraction. Additionally, this stronger response in ERA5 might result from systematic biases in the surface energy balance components that affect the $\Delta T$ responses.

To examine the disparity between the DTR responses in ERA5 and FLUXNET further, we directly look at the differences in $\Delta T$ in ERA5 at FLUXNET sites (Fig. 6a). These biases are obtained monthly and are aggregated based on the evaporative conditions, dry, normal, and wet, respectively. In general, ERA5's $\Delta T$ is higher in dry and lower in wet conditions when compared to FLUXNET observations. In short vegetation, ERA5 $\Delta T_s$ are slightly higher by $\approx 2$ K for dry conditions and considerably lower by $\approx 4$ K for wet conditions. When combined, these biases can explain the overestimation of $d(\Delta T_s)/df_e$ by $\approx 8$ K in ERA5 at FLUXNET sites (Fig. 5a). Similar biases in savanna are observed that explain the stronger ERA5 global $\Delta T$ response than in FLUXNET observations. However, it does not explain the lower ERA5 responses at FLUXNET sites. This may be because savannas are exceptionally heterogeneous, which causes high variability in temperatures between tree canopies and the surrounding open

land surface and hence a greater uncertainty in observations (Trigo et al. 2008, 2011; Ermida et al. 2014). Moreover, inaccuracies in vegetation cover in ERA5 can result in significant biases in diurnal temperature variations (Johannsen et al. 2019; Wang and Prigent 2020). In forests, $\Delta T_s$ in ERA5 on dry days is higher by $\approx 7$ K and lower by $\approx 10$ K on wet days than in FLUXNET observations that fairly explains the bias of $d(\Delta T_s)/df_e$ in ERA5 at FLUXNET sites. Similar biases are observed for ERA5's $\Delta T_a$, as shown in Fig. 6a, although these biases cannot be seen in the mean response in ERA5 at FLUXNET sites (see Fig. 5b). Overall, it appears that the ERA5 reanalysis overestimates the sensitivity of $\Delta T_a$ to evaporative conditions.

As shown in Fig. 6a, ERA5 has a systematic positive $\Delta T$ bias for dry conditions and negative bias for wet conditions. To find the sources of these biases, we compare the associated surface energy balance components for the summer months between ERA5 and FLUXNET in Fig. 6b. In short vegetation, overall ERA5's $\Delta T$ is lower than FLUXNET's $\Delta T$, which is also evident in comparatively lower values of sensible heat flux in ERA5. Similarly, in savanna ERA5's $\Delta T$ is overall considerably lower than FLUXNET's $\Delta T$, but in this case lower $R_s$ in ERA5 appears to be the main cause for the lower ERA5's $\Delta T$. In forests, however, $R_s$ is higher in ERA5 than in FLUXNET, but this does not lead to an overall positive bias in $\Delta T$, although it might explain the positive bias for dry conditions. The comparison of surface energy components does not directly convey the explicit source for the $\Delta T$ biases yet could be useful to understand how these biases in surface energy components propagate to biases in diurnal temperatures through inaccurate representation of surface process. In ERA5 the surface energy balance is satisfied by calculating surface temperature with a similar approach to the Penman–Monteith (Brutsaert 2013) and Best et al. (2004) methods. Here we use ERA5 fluxes accumulated hourly, which may be
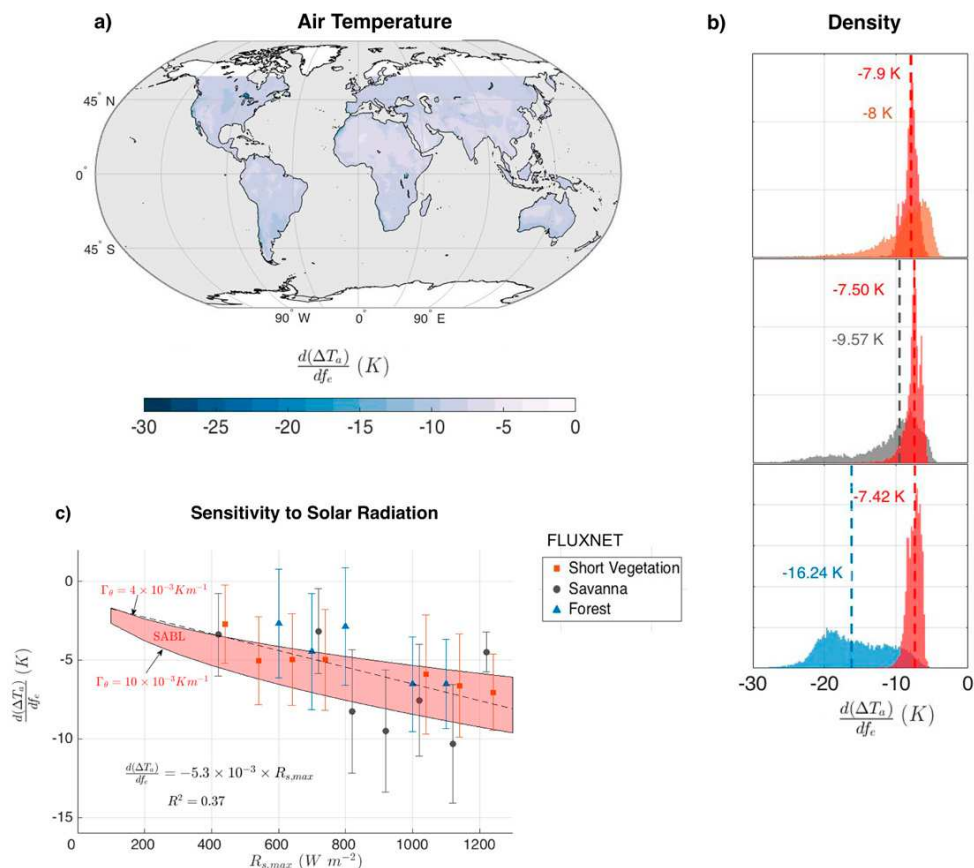
FIG. 8. The response of $\Delta T_a$ to evaporative fraction estimated from our SABL model using values of $\Gamma_\theta (\Delta T_a/\Delta z)$ and $R_{s,\max}$ from ERA5 in terms of (a) its mean geographic distribution, (b) its density distribution (red) compared to the one obtained from ERA5 for short vegetation, savanna, and forest (as shown in Fig. 4b), and (c) its sensitivity to maximum solar radiation $R_{s,\max}$ (red shaded area) compared to FLUXNET estimates for short vegetation, savanna, and forests. The dashed lines in (b) indicate the median values of the distribution. The error bars in (c) represent the RMSE and the black dashed line represents the linear regression of $d(\Delta T_a)/d(f_e)$ to $R_{s,\max}$.

different than the fluxes reported at FLUXNET sites due to solar zenith angle changes. Details of ERA5 model assimilation and physical parameterization (ECMWF 2007) are important when comparing ERA5 data to observations. The validation of the ERA5 reanalysis is not our primary objective, but it would seem that there are some systematic biases in the ERA5 surface energy balance components that would need to be considered when using and interpreting its temperature products, particularly when evaluating these in the context of water availability changes.

To summarize our ERA5- and FLUXNET-based findings, we found that even though diurnal surface and air temperature ranges are strongly related, they do not respond in the same way to evaporative fraction. Using FLUXNET observations and ERA5 reanalysis we find a strong decrease in $\Delta T_s$ in response to greater evaporative fraction, especially in short vegetation. $\Delta T_a$ has a weaker sensitivity to evaporative fraction that is similar across vegetation types. In the next two sections we use the physically

constrained models described in the Methods section (section 2) to reproduce and explain the $\Delta T_a$ and $\Delta T_s$ responses to $f_e$.

### b. Explaining the $\Delta T_a$ response to evaporative fraction

We first use the model presented in section 2a to reproduce the low $\Delta T_a$ sensitivity to evaporative fraction that is similar across vegetation types. According to Eq. (3), $\Delta T_a$ depends mainly on the change in PBL height ($\Delta z$ and $\Gamma_\theta$), evaporative fraction ($f_e$), and heat storage ($\Delta U$) from morning to afternoon, but the expression does not depend on vegetation type. This is consistent with our findings in the previous section. To solve for $d(\Delta T_a)/df_e$ [Eq. (5)], we require $R_{s,\max}$, $\Gamma_\theta$, and $\Delta t_{\text{day}}$, which we obtain from the summer mean values from ERA5. Figure 7a shows the value of $\Gamma_\theta$ for short vegetation, savanna, and forest from $\Gamma_\theta = \Delta T_a/\Delta z$. We found that $\Gamma_\theta$ is similar across vegetation types with a median value of $\approx 7 \times 10^{-3}$ K m$^{-1}$, with some notable variation in values between 4 and $10 \times 10^{-3}$ K m$^{-1}$.
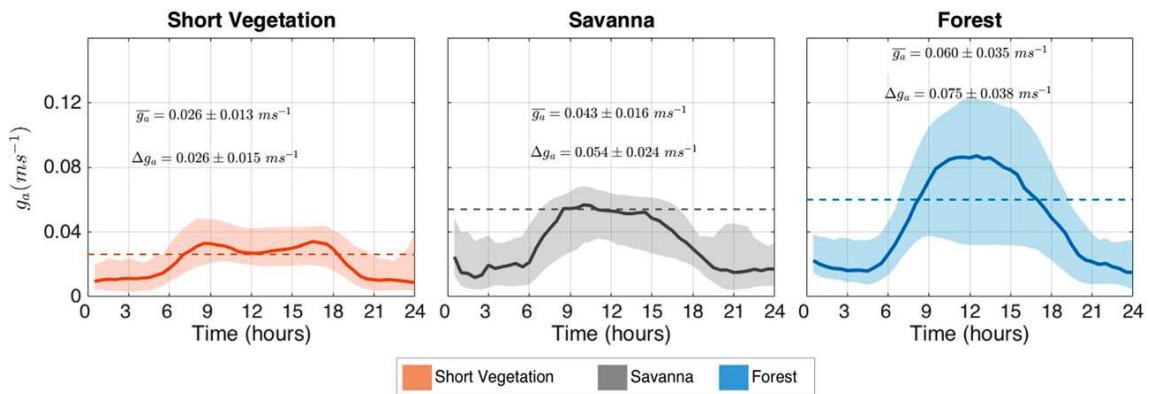
FIG. 9. The mean diurnal variation of aerodynamic conductance $g_a$ in short vegetation, savanna, and forests at FLUXNET sites. The shaded areas represent the standard deviations of the mean. The dashed lines mark the morning to afternoon mean values. The value for the morning to afternoon change, $\Delta g_a$, is also provided for each vegetation type. The numbers provide the mean and standard errors for $g_a$ and $\Delta g_a$.

We next use local values of $\Gamma_\theta$ obtained from ERA5 in our SABL model to reproduce $d(\Delta T_a)/df_e$ for each grid point.

Figure 8a shows that $d(\Delta T_a)/df_e$ obtained using the SABL model is reasonably invariant with a median value of $-8$ K, which is comparable to ERA5 (Fig. 4b). Likewise, the distributions of $d(\Delta T_a)/df_e$ in SABL for different vegetation types (Fig. 8b) are similar because of comparable $\Gamma_\theta$. Most of the spread in the distribution is due to variability in heat storage or incoming solar radiation. Note that in Fig. 4 the regions that do not show a significant response due to lower range and variability in $f_e$ are omitted. ERA5-derived $d(\Delta T_a)/df_e$ for forests is higher than the results from the SABL model. These higher values mainly correspond to tropical forests and can be connected to the variation in solar radiation due to clouds in those regions, which might alter $\Delta T_a$ and its response to $f_e$.

Next, we investigate the geographical variation of $d(\Delta T_a)/df_e$ observed in FLUXNET and modeled by SABL. Equation (5) indicates the dependency of $d(\Delta T_a)/df_e$ on solar radiation. Figure 8c shows the dependency of $d(\Delta T_a)/df_e$ to $R_{s,\max}$ observed in FLUXNET observations for the different vegetation types. These responses are sorted for different values of $R_{s,\max}$ ($x$ axis) and the error bar represents the RMSE of these responses. We find that $d(\Delta T_a)/df_e$ increases (becomes more negative) with $R_{s,\max}$ by similar magnitudes across vegetation types. The linear regression of these responses (dashed line) shows that $d(\Delta T_a)/df_e$ increases (becomes more negative) by $-6.5$ K for an increase in $R_{s,\max}$ by 1000 W m$^{-2}$. We evaluate this sensitivity of $\Delta T_a$ to $R_{s,\max}$ in our SABL model (red area) by varying the value of $\Gamma_\theta$ between 4 and $10 \times 10^{-3}$ K m$^{-1}$. We find that SABL produces a similar sensitivity as obtained using FLUXNET observations. Note that the daylight length is kept the same (12 h) in all cases for simplicity. The daylight length during summer is, however, longer, and increasingly so at higher latitudes, which introduces some bias into our results.

To conclude, our SABL model can reproduce global values of $d(\Delta T_a)/df_e$ similar to ERA5 and its sensitivity to solar radiation that is in agreement with FLUXNET observations.

The sensitivity analysis shows that the $\Delta T_a$ response to evaporative fraction is amplified in regions with high solar radiation, and this amplification is similar across vegetation types.

### c. Explaining the $\Delta T_s$ response to evaporative fraction

We next use the SSEB model presented in section 2b to reproduce the response of $\Delta T_s$ to evaporative fraction. To do so, we use Eq. (9), which shows that $d(\Delta T_s)/df_e$ strongly depends on the aerodynamic conductance ($g_a$) and its diurnal amplitude ($\Delta g_a$). We derive these two quantities from the FLUXNET observations, and show the mean diurnal cycle of $g_a$ for short vegetation, savanna, and forests in Fig. 9. Note that the mean aerodynamic conductance, $g_a$, is about twice as large for forests than for short vegetation. Additionally, $g_a$ substantially increases during daytime, which is indicative of strong heat transfer from the surface to the atmosphere. The shaded region shows the standard deviation of $g_a$ among vegetation types that is taken into account when formulating sensitivity of $d(\Delta T_s)/df_e$ to $R_{s,\max}$.

To estimate $d(\Delta T_s)/df_e$ across regions, we use $R_{s,\max}$ from ERA5 and $d(\Delta T_a)/df_e$ from observations. For $g_a$ and $\Delta g_a$, we use the values shown in Fig. 9. Figure 10a shows the estimated response of $\Delta T_s$ to evaporative fraction. On comparing Figs. 10a and 8a we find that $d(\Delta T_s)/df_e$ is higher in magnitude and shows more geographical variability than $d(\Delta T_a)/df_e$, which is consistent with Figs. 4 and 5. Figure 10b shows the probability distributions of $d(\Delta T_s)/df_e$ from the SSEB model (red) and ERA5 for each vegetation type. In short vegetation, the SSEB model seems to reproduce the mean responses in ERA5. In savanna and forest, SSEB shows some slightly different distributions than ERA5, which might be simply because we used the observed mean of $g_a$ and $\Delta g_a$. The consequence of using mean values of $g_a$ from FLUXNET is evident in the biases in forests and savanna due to their high aerodynamic conductances and larger deviations from the mean (Fig. 9). In forests, the stronger responses of surface temperatures of the SSEB model are mainly because of the high values of $d(\Delta T_a)/df_e$ in ERA5, which is one of the inputs to the model (Fig. 8b).
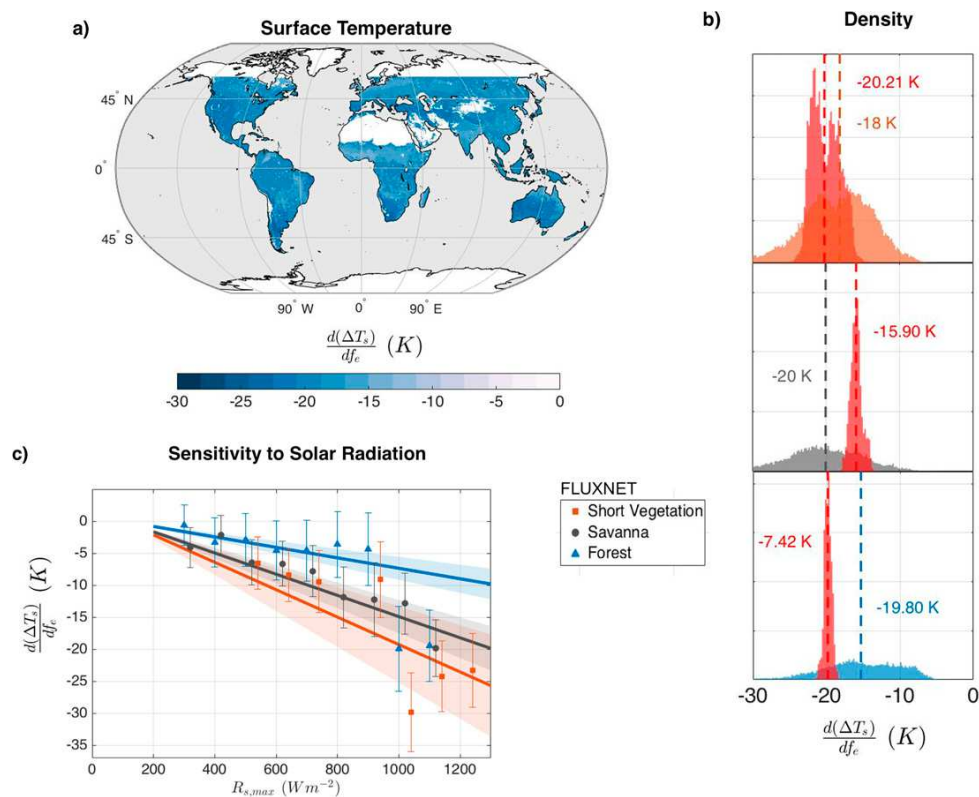
FIG. 10. The response of $\Delta T_s$ to evaporative fraction estimated from the SSEB model using values of $g_a$ and $\Delta g_a$ from FLUXNET and $R_{s,\max}$ from ERA5 in terms of (a) its mean geographic distribution, (b) its density distribution (red) compared to the one obtained from ERA5 for short vegetation, savanna, and forest (as shown in Fig. 4a), and (c) its sensitivity to maximum solar radiation, $R_{s,\max}$ (lines and shaded areas) compared to FLUXNET estimates (symbols) for short vegetation, savanna, and forests. The dashed lines in (b) indicate the median values of the distribution. The error bars in (c) represent the RMSE. The shaded area represents the standard error that mostly corresponds to $g_a$ variations as shown in Fig. 9.

In addition to aerodynamic conductance, $d(\Delta T_s)/df_e$ is also sensitive to $R_{s,\max}$, which is visible in FLUXNET observations as shown in Fig. 10c. We find that the $\Delta T_s$ response to $f_e$ increases in regions with stronger solar radiation, or greater $R_{s,\max}$. This sensitivity is larger for short vegetation than for forests. Our SSEB model also reproduces this sensitivity (shaded areas in Fig. 10c), matching the sensitivity from FLUXNET observations quite well. The shaded region shows the variation in these sensitivities due to the variation in $g_a$ within each vegetation type.

Overall, the SSEB model captures most of the observed sensitivity of $\Delta T_s$ to $f_e$ and $R_{s,\max}$. Our results emphasize the dominating role of aerodynamic conductance in cooling $\Delta T_s$ in forests. In contrast, in short vegetation, variations in $f_e$ alter $\Delta T_s$ comparably to greater extent because of the lower aerodynamic conductance, and increasingly so in regions with greater solar radiation.

## 5. Discussion

In this work we evaluated $\Delta T_s$ and $\Delta T_a$ responses to evaporation in FLUXNET observations and ERA5 reanalyses. We found stronger responses of $\Delta T_s$ to evaporative fraction in short vegetation than in forests. Notably, the $\Delta T_a$ response to evaporative fraction is similar for short vegetation, savanna, and forests. ERA5 and FLUXNET-derived sensitivities show similar trends, being slightly stronger in ERA5. We demonstrate that this is due to systematic biases in ERA5's $\Delta T$ on dry (positive) and wet (negative) conditions, which also relates to the representation of surface energy components. The comparison of FLUXNET and ERA5's surface energy balance components show an overestimation of shortwave and net longwave radiative fluxes especially in short vegetation and forests. These biases are in agreement with the results shown by Urraca et al. (2018) and Jiang et al. (2020). Even though we used the finest spatial resolution of ERA5, these biases to some degree might represent blended information of the larger scale (31 km) in ERA5 and the MODIS IGBP vegetation classification than the local information provided by FLUXNET. Studies evaluating ERA5 products are currently limited (Martens et al. 2020; Bell et al. 2021; Simmons et al. 2021), and our study advocates investigating such biases

when employing ERA5's products in climate and hydrology research.

To explain the FLUXNET- and ERA5-based findings, we present two simple models that are based on fundamental physical concepts. Our SABL and SSEB models reproduce the local responses of $\Delta T_a$ and $\Delta T_s$ to evaporative fraction in ERA5 and their sensitivity to solar radiation in FLUXNET reasonably well.

The SABL model demonstrates that the change in boundary layer growth reduces the response of $\Delta T_a$ to evaporative fraction. Overall, the diurnal variation of air temperature is mainly constrained by the total solar radiation input into the boundary layer (reduced by the latent heat flux). This is in agreement with our previous interpretation (Panwar et al. 2019) where we showed that in absence of boundary layer growth, the diurnal amplitude of air temperature would be as large as the diurnal amplitude of surface temperature.

Our SABL model is rather simple because it only requires information on solar radiation and background lapse rate to estimate $d(\Delta T_a)/df_e$. Using ERA5 we show some variation in $\Gamma_\theta$. For further understanding of PBL processes, it would be interesting to explore the factors shaping $\Gamma_\theta$. Furthermore, it should be possible to obtain better estimates of the heat storage changes in the boundary layer by integrating the information of the vertical profile of temperature and humidity. Generally, studies to investigate the sensitivity of the boundary layer to soil moisture use more sophisticated boundary layer models and observations as shown by Santanello et al. (2011), Wouters et al. (2019), and Denissen et al. (2021). Such modeling approaches provide critical insights on controls of soil moisture in shaping boundary layer dynamics and air temperature (Dirmeyer and Brubaker 2007; Koster et al. 2011; Green et al. 2017; Gentine et al. 2019). What our results show is that the non-latent energy input into the boundary layer is the dominant factor that explains its dynamics, resulting in weaker responses of $\Delta T_a$ to $f_e$.

Our SSEB model shows that the $\Delta T_s$ response to evaporative fraction strongly depends on the aerodynamic conductance (which depends on vegetation type) and solar radiation. Our model assumes negligible effects of the ground heat flux and biomass heat storage (Gu et al. 2007; Lindroth et al. 2010; Swenson et al. 2019). Meier et al. (2019) showed that the heat stored in the forest biomass is relatively small (25–80 W m$^{-2}$) and dampens the diurnal temperature variation only by 1 K, which justifies our assumptions. Some variance in our model can likely to be further reduced by improving the calculation of aerodynamic conductance, that is currently based on the sensible heat flux. Additionally, to estimate the $\Delta T_s$ sensitivity we do not require information on the boundary layer that was otherwise integrated in earlier models (Diak 1990; Norman et al. 1995; Anderson et al. 1997; Kustas and Norman 1999). One might argue that the estimation of $d(\Delta T_s)/df_e$ requires $d(\Delta T_a)/df_e$ that depends on boundary layer dynamics. However, we also show that $d(\Delta T_a)/df_e$ has very small, comparatively uniform value that can be obtained from the solar energy input (reduced by the latent heat flux), so consequently, $d(\Delta T_s)/df_e$ does not need information on boundary layer dynamics. Therefore, it can be argued that surface temperature is more strongly coupled to surface properties rather than boundary layer processes.

The SSEB model and data analysis shows that $d(\Delta T_s)/df_e$ is higher in short vegetation than in forests. The lower value of $d(\Delta T_s)/df_e$ in forests appears to contradict the known cooling effect of evaporation. Clearly, forests can maintain high evaporation via their deep root system (Kleidon and Heimann 2000), which maintains water availability in dry episodes. However, our SSEB model shows that in addition to evaporation, their high aerodynamic conductance is the primary cooling agent. In our model aerodynamic conductance represents vegetation effects at the ecosystem scale. To examine the leaf scale response and its impact on diurnal temperature variation, one could potentially look at the stomata–atmosphere coupling that is widely quantified by the decoupling factor (Jarvis and McNaughton 1986). In general, short vegetation is expected to be more strongly decoupled from the atmosphere than forests (Meinzer et al. 1993; Lee and Black 1993; Whitehead et al. 1984; Jarvis 1985), meaning that transpiration in short vegetation is mainly controlled by solar radiation and less by changes in stomatal conductance. However, previous studies have also shown high degree of variation in the decoupling factor for different ecosystems (Lin et al. 2015; Miner et al. 2017; Kauwe et al. 2017). Our study considers water limitation as the main control of evaporation, rather than stomatal conductance. Hence, further studies on stomatal controls on evaporative fraction and its relevance to global change could be beneficial.

Model sensitivities as well as FLUXNET observations show that $d(\Delta T)/df_e$ depends on solar radiation, indicating stronger impact of drought or dryness in regions with high solar radiation. For instance, in the tropics, $\Delta T_s$ of short vegetation is more sensitive to evaporation than in forests. Therefore, it can be anticipated that in the tropics, the increase in $\Delta T_s$ would be higher due to tropical deforestation than in the higher latitudes. This notion is in line with previous studies that show similar findings based on climate model simulations (Davin and de Noblet-Ducoudré 2010; Pitman et al. 2012; Lawrence et al. 2012; Li et al. 2018; Chen and Dirmeyer 2019b). We suggest that the lower response of temperature to deforestation-induced dryness in higher latitudes is mainly due to lower solar energy as also indicated by previous studies (Claussen et al. 2001; Brovkin et al. 2006; Mahmood et al. 2014; Longobardi et al. 2016).

Our findings are broadly consistent with previous studies. Surface temperature can be a good proxy for evaporative conditions (Su 2002; Kalma et al. 2008), but it also depends on vegetation type. The diurnal variation in surface temperature may be useful to quantify the impact of land use and land cover change, which has also been proposed by Li et al. (2015) and Bright et al. (2017). Similarly, Chen and Dirmeyer (2019a) show stronger daytime warming of surface temperature due to deforestation but discrepancies in air temperature due to differing turbulent characteristics. The distinction between surface and air temperature is also important because they are usually considered to be a proxy of each other, especially in developing temperature products (Zhang et al. 2011; Oyler et al. 2016). Similar observations were made by Mildrexler

et al. (2011), who looked at the relationship between remotely sensed land surface and in situ air temperatures data and interpreted this as the cooling effect of forests.

Finally, our simple models can be useful tools to analyze the different sensitivity of surface and air temperature trends to global changes, especially associated to drought and deforestation. The differences in surface and air temperature could be used to understand the different controls on land–atmosphere interactions. For instance, the diurnal variation of air temperature could be used to obtain the boundary layer height, and surface temperature to obtain aerodynamic conductance of vegetation. It would also be intriguing to evaluate how the compensating effect of boundary layer dynamics would adjust the response of the diurnal variation of air temperature in global warming scenarios. Which role could vegetation and altered water availability play in modulating the diurnal temperatures? So far, our study shows that it is mainly the solar energy input and not the vegetation type that controls the dynamics of the land–atmosphere system. Previous studies (Dai et al. 2006; Zhou et al. 2009; Lauritsen and Rogers 2012) show that the effect of clouds combined with soil moisture effect can reduce $\Delta T$ by 50%. Our approach can further be extended for cloudy versus clear-sky conditions to incorporate the radiative effects of clouds (see Fig. A4).

## 6. Summary and conclusions

Our study evaluated the response of $\Delta T_s$ and $\Delta T_a$ to changes in evaporative fraction in FLUXNET observations and ERA5 reanalyses and examined the underlying physical constraints that can explain these responses. We found that $\Delta T_s$ decreases strongly in response to changes in evaporative fraction, particularly in short vegetation. Contrarily, the $\Delta T_a$ response to evaporative fraction is weaker and similar across vegetation types. We also found that ERA5 appears to overestimate the sensitivity of the diurnal temperature range to evaporative fraction compared to FLUXNET.

We used two models based on physical constraints to explain these trends found in FLUXNET and ERA5. We found that $\Delta T_s$ is related to the surface energy partitioning and the aerodynamic conductance, which differs among vegetation types, whereas $\Delta T_a$ is primarily determined by the total, non-latent energy input into the lower atmosphere. Based on the surface energy balance we provide an expression for $d(\Delta T_s)/df_e$ that mainly depends on the aerodynamic conductance of vegetation and absorbed solar radiation. Similarly, $d(\Delta T_a)/df_e$ is obtained from a simple heat storage model of the lower atmosphere and it mainly depends on solar radiation and the background lapse rate of potential temperature. Our simple models also capture the observed sensitivity of $d(\Delta T_s)/df_e$ and $d(\Delta T_a)/df_e$ to solar radiation that can explain the geographical variation of these responses.

Since our energy balance-based models are able to reproduce the identified responses in FLUXNET and ERA5 datasets, we can draw the following conclusions. The main patterns of diurnal temperature ranges mainly reflect how solar radiation is being partitioned at the surface, and how the non-latent energy components are then buffered in the lower atmosphere.
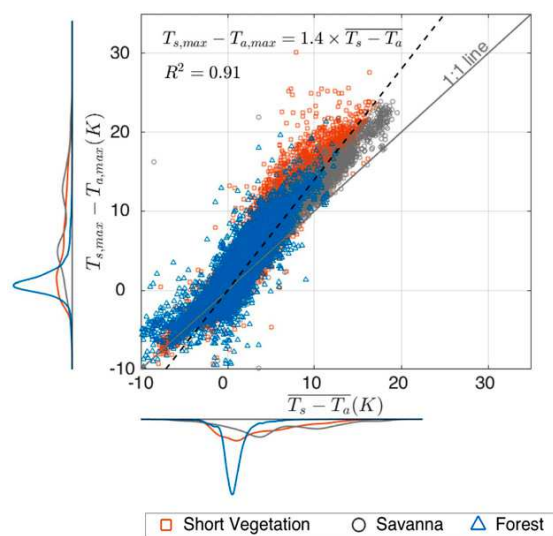


FIG. A1. The relationship between $T_{s,\max} - T_{a,\max}$ and $\overline{T_s - T_a}$ in FLUXNET sites of short vegetation, savanna, and forests. Each data point shows the value for one day at a site during the time period considered. The dotted line represents the linear regression of the relationship between $T_{s,\max} - T_{a,\max}$ and $\overline{T_s - T_a}$.

Both aspects reflect the constraints imposed by the energy balances of the surface and of the lower atmosphere. What this implies is that the main coupling between the land surface and the atmosphere is represented by the strongly constrained response of the convective boundary layer to surface heating, as it is the dominant buffer that levels out the strong variation of solar radiation during the diurnal cycle.

Our findings suggests that surface temperature is a robust metric for evaporative conditions and vegetation properties, whereas air temperature provides unique information on boundary layer dynamics and heat storage changes. The different physical constraints of surface and air temperature shall be considered when using them as proxies of each other. Our results imply that surface temperature is better suited to detect impacts of deforestation than the more commonly used air temperature.

To summarize, our findings clearly show that land–atmosphere processes shape the diurnal variation of surface and air temperature differently. This distinction between diurnal surface and air temperature is important when analyzing trends in climate science. Our study can be used for further exploring the process-based sensitivities of diurnal surface and air temperatures to land cover change and global climate change.

## Surface Temperature
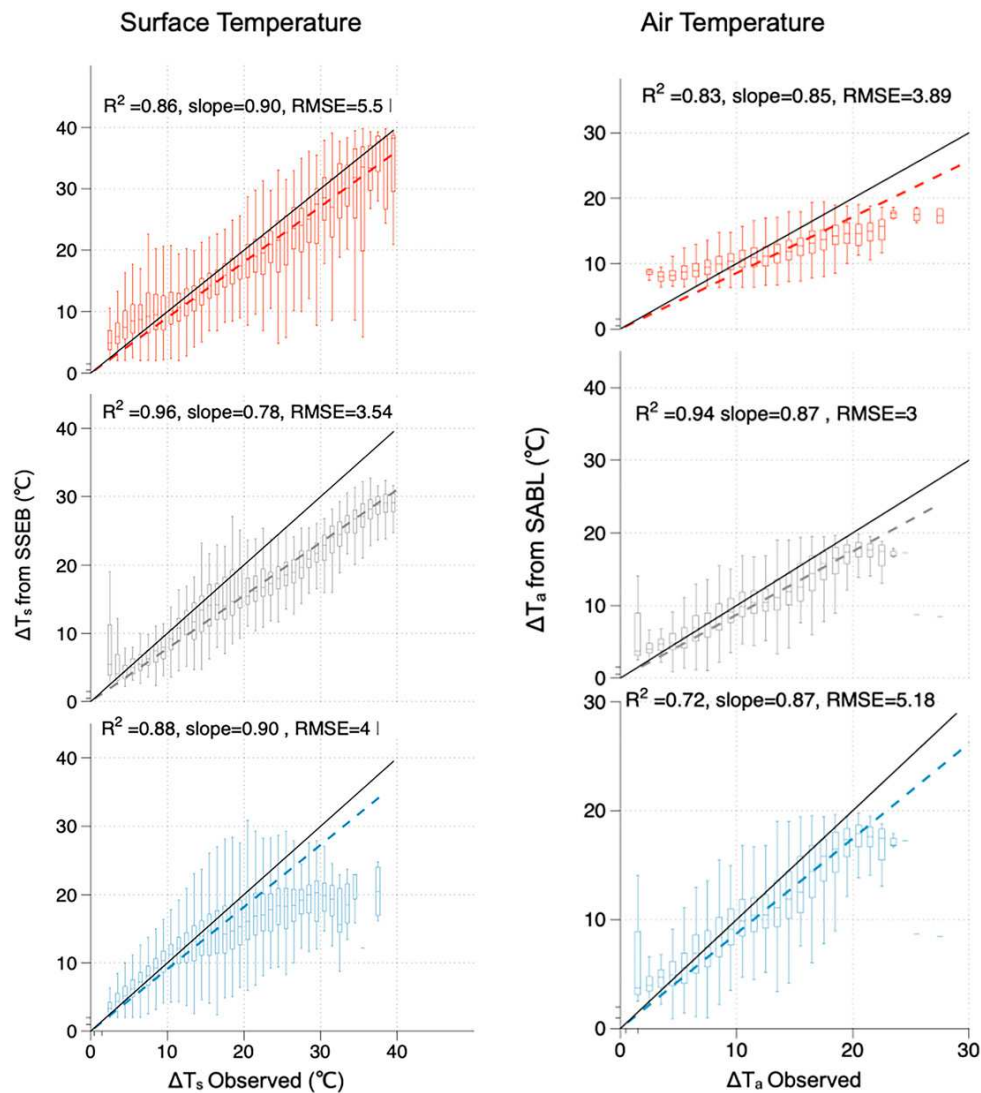
## Air Temperature



FIG. A2. Comparison of diurnal surface ($\Delta T_s$) and air ($\Delta T_a$) temperature range obtained from the SSEB and SABL models ($y$ axis), respectively, to the observed values at FLUXNET ($x$ axis) for short vegetation (red), savanna (gray), and forests (blue). The correlation coefficient ($R^2$), the slope of the linear regression, and root-mean-square values (RMSE) are provided for the corresponding plots.

use R and Matlab programming languages for analysis and plotting.

*Data availability statement.* The FLUXNET data are available at https://FLUXNET.fluxdata.org/; all of the FLUXNET data cited herein were downloaded on 23 October 2020. More descriptions of each FLUXNET site (160 sites) used in this study are provided in appendix A. The ERA5 reanalysis data are available on the Copernicus Climate Change Service (C3S) Climate Data Store at https://cds.climate.copernicus.eu/

doi/10.24381/cds.e2161bac. The IGBP land cover class used for vegetation classification for FLUXNET sites is available at https://doi.org/10.3334/ORNLDAAC/1530.

### APPENDIX A

#### Appendix Figures and Tables

Figure A1 shows the relationship between the differences in mean ($x$ axis) and maximum ($y$ axis) temperatures between the
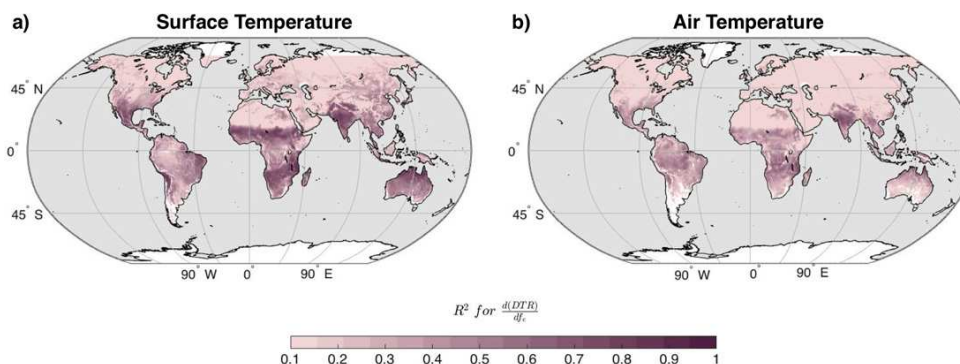
Fig. A3. The correlation coefficient ($R^2$) for the local responses of $\Delta T_s$ and $\Delta T_a$ to evaporative fraction in ERA5. The local responses are obtained from the linear regression of daily values of DTR and $f_e$.

surface and at 2-m height. Each point represents the daily values obtained at FLUXNET sites of short vegetation, savanna, and forests. The dashed line represents the linear regression of their relationship. We found that the differences of their maximum is about 1.4 times the differences of their mean values across vegetation types. This relationship is used to simplify Eq. (7) into Eq. (8).

Figure A2 shows the comparison of the observed diurnal range of surface and air temperature (x axis) with the one estimated using the SSEB and SABL models (y axis). The observations and input to the models are obtained from FLUXNET sites of short vegetation (red), savanna (gray) and forests (blue).

The SABL and SSEB models predict the diurnal variation of temperatures quite well with high correlation coefficient. The slopes of the estimates are lower than one, meaning the diurnal variations predicted by the models are lower than the observed one, especially for warmer and/or high solar radiation conditions. This is likely due to the simplifications of physical processes in SABL and SSEB models that have been discussed in detail in the methods and discussion sections. It should be noted that our models are mainly developed to obtain temperatures sensitivities to evaporation and therefore they include some assumptions that may lead to biases when using them to estimate diurnal range of temperature.

Figure A3 shows the correlation coefficient of local responses of the diurnal temperature ranges to changes in evaporative conditions. These responses are calculated using daily data from the ERA5 reanalysis for years 2000–15. High $R^2$ values indicate stronger responses of diurnal temperature ranges to changes in evaporative fractions. Not all regions have high $R^2$. Lower $R^2$ values can be linked to limited variations of evaporative fraction in the grid cell, for instance in deserts due to limited water or at high latitudes due to limited energy input. Only a few regions have high $R^2$ that are also shown in Figs. 4a and 4b.

Table A1 provides the description of each FLUXNET site used in the study, and Table A2 describes the variables used from FLUXNET observations and ERA5 reanalyses.

Figure A4 evaluates the effect of clouds on our results. It shows that under cloudy conditions, solar radiation is reduced, which lowers the sensitivities of the diurnal temperature ranges to evaporative fraction. These values are obtained for short vegetation FLUXNET sites. Cloudy days are here taken as days when the observed solar radiation is less than 30% of the potential solar radiation. It is observed that the diurnal range of surface temperature reduces by 15 K on cloudy days but only by 3 K for the diurnal range of air temperature.

Cloud effects on diurnal temperature ranges can also be estimated by the SABL and SSEB models. Based on Eq. (5), $d(\Delta T_a)/df_e$ for cloudy conditions ($R_s = 100$ W m$^{-2}$) is only $-2.8$ K, and for noncloudy conditions ($R_s = 220$ W m$^{-2}$) it is $-4.2$ K. Similarly, based on Eq. (9), the sensitivity of the diurnal range of surface temperature [$d(\Delta T_s)/df_e$] for noncloudy conditions ($R_s = 220$ W m$^{-2}$) is $-17$ K whereas for cloudy conditions ($R_s = 100$ W m$^{-2}$) it is $-8$ K. These values are similar to the values obtained from observations (Fig. A4).

### APPENDIX B

### Derivation of $\Delta U$

We derive an expression for the diurnal heat storage change $\Delta U$ in the boundary layer using the energy balance constraint as described in (Kleidon and Renner 2017). We seek the input of nonlatent energy into the lower atmosphere, so we need to subtract the latent heat flux, LE, from the solar energy input by absorption at the surface, $R_s$. We use the maximum power limit of the cold heat engine (Kleidon and Renner 2018) to get an expression of the turbulent heat fluxes, and then use the evaporative fraction $f_e$ to infer LE.

The optimum heat flux from maximum power is given by

$$J_{\text{opt}} = \frac{1}{2}\left(R_s + \frac{dU}{dt}\right), \qquad (B1)$$

where $R_s$ is absorbed solar radiation at the surface and $dU/dt$ is the heat storage variation in the boundary layer (assuming

Table A1. Description of FLUXNET sites used in this study.

| Site No. | IGBP Land use | Site ID | Site name | Location Lat (°) | Location Lon (°) | Data citation |
|---|---|---|---|---|---|---|
| 1 | Open shrublands | AU-ASM | Alice Springs | −22.28 | 133.25 | Cleverly and Eamus (2016a) |
| 2 | Closed shrublands | AU-Cpr | Calperum | −34.00 | 140.59 | Meyer et al. (2016) |
| 3 | Croplands | AU-Rig | Riggs Creek | −36.66 | 145.58 | Beringer et al. (2016a) |
| 4 | Grasslands | AU-Stp | Sturt Plains | −17.15 | 133.35 | Beringer and Hutley (2016f) |
| 5 | Open shrublands | AU-TTE | Ti Tree East | −22.29 | 133.64 | Cleverly and Eamus (2016b) |
| 6 | Croplands | AU-Ync | Australia Yanco site | −34.99 | 146.29 | Beringer and Walker (2016) |
| 7 | Croplands | BE-Lon | Lonzee | 50.55 | 4.75 | De Ligne et al. (2016b) |
| 8 | Croplands | CA-TP1 | ON-Turkey Point 2002 White Pine | 42.66 | −80.56 | Arain (2016a) |
| 9 | Croplands | CA-TP2 | ON-Turkey Point 1989 White Pine | 42.77 | −80.46 | Arain (2016b) |
| 10 | Croplands | CH-Cha | Chamau grassland | 47.21 | 8.41 | Merbold et al. (2020) |
| 11 | Croplands | CH-Fru | Fruebuel grassland | 47.12 | 8.54 | Hörtnagl et al. (2016c) |
| 12 | Croplands | CH-Oe1 | Oensingen1 grass | 47.29 | 7.73 | Ammann (2016) |
| 13 | Croplands | CH-Oe2 | Oensingen2 crop | 47.29 | 7.73 | Hörtnagl et al. (2016d) |
| 14 | Grasslands | CN-Dan | Damxung | 30.85 | 91.08 | Shi et al. (2016) |
| 15 | Grasslands | CN-Du2 | Duolun-grassland | 42.05 | 116.28 | Chen (2016) |
| 16 | Grasslands | CN-Ha2 | Haibei Shrubland | 37.67 | 101.33 | Li (2016) |
| 17 | Croplands | CZ-wet | CZECHWET | 49.02 | 14.77 | Dusek et al. (2016) |
| 18 | Croplands | DE-Geb | Gebesee | 51.10 | 10.91 | Brümmer et al. (2016) |
| 19 | Croplands | DE-Kli | Klingenberg | 50.89 | 13.52 | Bernhofer et al. (2016b) |
| 20 | Grasslands | DE-RuR | Rollesbroich | 50.62 | 6.30 | Schmidt and Graf (2016) |
| 21 | Croplands | DE-Seh | Selhausen | 50.87 | 6.45 | Schneider and Schmidt (2016) |
| 22 | Croplands | DE-Zrk | Zarnekow | 53.88 | 12.89 | Sachs et al. (2016) |
| 23 | Croplands | DK-Eng | Enghave | 55.69 | 12.19 | Pilegaard and Ibrom (2016) |
| 24 | Croplands | DK-Fou | Foulum | 56.48 | 9.59 | Olesen (2016) |
| 25 | Closed shrublands | ES-Amo | Amoladeras | 36.83 | −2.25 | Poveda et al. (2016) |
| 26 | Closed shrublands | ES-LJu | Llano de los Juanes | 36.93 | −2.75 | Cañete et al. (2016) |
| 27 | Croplands | FR-Gri | Grignon | 48.84 | 1.95 | Buysse et al. (2016) |
| 28 | Croplands | FR-LBr | Le Bray (after 28 Jun 1998) | 44.72 | −0.77 | Berbigier and Loustau (2016) |
| 29 | Croplands | IT-BCi | Borgo Cioffi | 40.52 | 14.96 | Magliulo et al. (2016) |
| 30 | Croplands | IT-CA1 | Castel d'Asso1 | 42.38 | 12.03 | Sabbatini et al. (2016c) |
| 31 | Croplands | IT-CA2 | Castel d'Asso2 | 42.38 | 12.03 | Sabbatini et al. (2016a) |
| 32 | Croplands | IT-CA3 | Castel d'Asso 3 | 42.38 | 12.02 | Sabbatini et al. (2016b) |
| 33 | Grasslands | IT-MBo | Monte Bondone | 46.01 | 11.05 | Gianelle et al. (2016a) |
| 34 | Croplands | IT-PT1 | Zerbolo-Parco Ticino-Canarazzo | 45.20 | 9.06 | Manca and Goded (2016) |
| 35 | Croplands | IT-Ro1 | Roccarespam pani1 | 42.41 | 11.93 | Valentini et al. (2016c) |
| 36 | Croplands | IT-Ro2 | Roccarespam pani2 | 42.39 | 11.92 | Papale et al. (2016) |
| 37 | Croplands | JP-SMF | Seto Mixed Forest Site | 35.25 | 137.07 | Kotani (2016b) |
| 38 | Croplands | PA-SPn | Sardinilla Plantation | 9.32 | −79.63 | Wolf et al. (2016a) |
| 39 | Croplands | PA-SPs | Sardinilla Pasture | 9.31 | −79.63 | Wolf et al. (2016b) |
| 40 | Grasslands | RU-Ha1 | Ubs Nur-Hakasija–grassland | 54.73 | 90.00 | Belelli et al. (2016) |
| 41 | Grasslands | SD-Dem | Demokeya | 13.28 | 30.48 | Ardö et al. (2016) |
| 42 | Grasslands | SN-Dhr | Dahra | 15.40 | −15.43 | Tagesson et al. (2016) |
| 43 | Grasslands | U.S.-AR1 | ARM USDA UNL OSU Woodward Switchgrass 1 | 36.43 | −99.42 | Billesbach et al. (2016a) |
| 44 | Grasslands | U.S.-AR2 | ARM USDA UNL OSU Woodward Switchgrass 2 | 36.64 | −99.60 | Billesbach et al. (2016b) |
| 45 | Croplands | U.S.-ARM | ARM Southern Great Plains site | 36.61 | −97.49 | Biraud et al. (2016) |
| 46 | Croplands | U.S.-ARb | ARM Southern Great Plains burn site | 35.55 | −98.04 | Torn (2016a) |
| 47 | Grasslands | U.S.-ARc | ARM Southern Great Plains control site | 35.55 | −98.04 | Torn (2016b) |
| 48 | Grasslands | U.S.-Cop | Corral Pocket | 38.09 | −109.39 | Bowling (2016) |
| 49 | Croplands | U.S.-Goo | Goodwin Creek | 34.25 | −89.87 | Meyers (2016a) |
| 50 | Croplands | U.S.-IB2 | Fermi National Accelerator Laboratory | 41.84 | −88.24 | Matamala (2016) |

TABLE A1. (*Continued*)

| Site No. | IGBP Land use | Site ID | Site name | Location Lat (°) | Location Lon (°) | Data citation |
|---|---|---|---|---|---|---|
| 51 | Grasslands | U.S.-LWW | Little Washita Watershed | 34.96 | −97.98 | Meyers (2016b) |
| 52 | Croplands | U.S.-Me1 | Metolius Eyerly Burn | 44.58 | −121.50 | Law (2016a) |
| 53 | Croplands | U.S.-Ne1 | Mead–irrigated continuous maize site | 41.17 | −96.48 | Suyker (2016a) |
| 54 | Croplands | U.S.-Ne2 | Mead–irrigated maize-soybean rotation site | 41.16 | −96.47 | Suyker (2016b) |
| 55 | Croplands | U.S.-Ne3 | Mead–rainfed maize-soybean rotation site | 41.18 | −96.44 | Suyker (2016c) |
| 56 | Open shrublands | U.S.-SRC | Santa Rita Creosote | 31.91 | −110.84 | Kurc (2016) |
| 57 | Grasslands | U.S.-SRG | Santa Rita Grassland | 31.79 | −110.83 | Scott (2016a) |
| 58 | Open shrublands | U.S.-SRM | Santa Rita Mesquite | 31.82 | −110.87 | Scott (2016b) |
| 59 | Open shrublands | U.S.-Sta | Saratoga | 41.40 | −106.80 | Ewers and Pendall (2016) |
| 60 | Croplands | U.S.-Twt | Twitchell Island | 38.11 | −121.65 | Baldocchi (2016) |
| 61 | Open shrublands | U.S.-Whs | Walnut Gulch Lucky Hills Shrubland | 31.74 | −110.05 | Scott (2016c) |
| 62 | Croplands | U.S.-Wi6 | Pine barrens 1 (PB1) | 46.62 | −91.30 | Chen (2016c) |
| 63 | Grasslands | U.S.-Wkg | Walnut Gulch Kendall Grasslands | 31.74 | −109.94 | Scott (2016d) |
| 64 | Savannas | AU-Ade | Adelaide River | −13.08 | 131.12 | Beringer and Hutley (2016a) |
| 65 | Woody Savannas | AU-Cum | Cumberland Plains | −33.61 | 150.72 | Pendall and Griebel (2016) |
| 66 | Savannas | AU-DaP | Daly River Pasture | −14.06 | 131.32 | Beringer and Hutley (2016b) |
| 67 | Savannas | AU-DaS | Daly River Savanna | −14.16 | 131.39 | Beringer and Hutley (2016g) |
| 68 | Savannas | AU-Dry | Dry River | −15.26 | 132.37 | Beringer and Hutley (2016c) |
| 69 | Savannas | AU-Fog | Fogg Dam | −12.55 | 131.31 | Beringer and Hutley (2016d) |
| 70 | Woody savannas | AU-Gin | Gingin | −31.38 | 115.65 | Macfarlane et al. (2016) |
| 71 | Savannas | AU-How | Howard Springs | −12.5 | 131.15 | Beringer and Hutley (2016e) |
| 72 | Woody savannas | AU-Whr | Whroo | −36.67 | 145.03 | Beringer et al. (2016b) |
| 73 | Woody savannas | CG-Tch | Tchizalamou | −4.29 | 11.66 | Nouvellon (2016) |
| 74 | Woody savannas | CN-Qia | Qianyanzhou | 26.73 | 115.07 | Wang and Fu (2016) |
| 75 | Woody savannas | ES-LgS | Laguna Seca | 37.1 | −2.97 | Reverter et al. (2016) |
| 76 | Woody savannas | IT-Isp | Ispra ABC-IS | 45.81 | 8.63 | Gruening et al. (2016a) |
| 77 | Woody savannas | IT-Noe | Sardinia/Arca di Noe | 40.61 | 8.15 | Spano et al. (2016) |
| 78 | Woody savannas | U.S.-KS2 | Kennedy Space Center (scrub oak) | 28.61 | −80.67 | Drake and Hinkle (2016b) |
| 79 | Woody savannas | U.S.-Me6 | Metolius New Young Pine | 44.32 | −121.6 | Law (2016f) |
| 80 | Woody savannas | U.S.-Myb | Mayberry Wetland | 38.05 | −121.77 | Sturtevant et al. (2016) |
| 81 | Woody savannas | U.S.-Ton | Tonzi Ranch | 38.43 | −120.97 | Baldocchi and Ma (2016) |
| 82 | Woody savannas | U.S.-Var | Vaira Ranch | 38.41 | −120.95 | Baldocchi et al. (2016) |
| 83 | Savannas | ZM-Mon | Mongo | −15.44 | 23.25 | Kutsch et al. (2016) |
| 84 | Mixed forests | AT-Neu | Neustift/Stubai Valley | 47.12 | 11.32 | Wohlfahrt et al. (2016) |
| 85 | Evergreen broadleaf forest | AU-Tum | Tumbarumba | −35.66 | 148.15 | Woodgate et al. (2016) |
| 86 | Evergreen broadleaf forest | AU-Wac | Wallaby Creek | −37.43 | 145.19 | Beringer et al. (2016c) |
| 87 | Evergreen broadleaf forest | AU-Wom | Wombat | −37.42 | 144.09 | Arndt et al. (2016) |
| 88 | Mixed forests | BE-Bra | Brasschaat (De Inslag Forest) | 51.31 | 4.52 | Neirynck et al. (2016) |
| 89 | Mixed forests | BE-Vie | Vielsalm | 50.31 | 6.00 | De Ligne et al. (2016a) |
| 90 | Evergreen broadleaf forest | BR-Sa1 | Santarem-Km67-Primary Forest | −2.86 | −54.96 | Saleska (2016) |
| 91 | Evergreen broadleaf forest | BR-Sa3 | Santarem-Km83-Logged Forest | −3.02 | −54.97 | Goulden (2016a) |
| 92 | Mixed forests | CA-Gro | ON-Groundhog River Mixedwood | 48.22 | −82.16 | McCaughey (2016) |
| 93 | Evergreen needleleaf forest | CA-Man | MB-Northern Old Black Spruce | 55.88 | −98.48 | Amiro (2016a) |
| 94 | Evergreen needleleaf forest | CA-NS1 | UCI 1850 | 55.88 | −98.48 | Goulden (2016b) |
| 95 | Evergreen needleleaf forest | CA-NS2 | UCI 1930 | 55.91 | −98.52 | Goulden (2016c) |
| 96 | Evergreen needleleaf forest | CA-NS3 | UCI 1964 | 55.91 | −98.38 | Goulden (2016d) |
| 97 | Evergreen needleleaf forest | CA-NS4 | UCI 1964 wet | 55.91 | −98.38 | Goulden (2016e) |
| 98 | Evergreen needleleaf forest | CA-NS5 | UCI 1981 | 55.86 | −98.49 | Goulden (2016f) |

TABLE A1. (*Continued*)

| Site No. | IGBP Land use | Site ID | Site name | Lat (°) | Lon (°) | Data citation |
|---|---|---|---|---|---|---|
| 99 | Evergreen needleleaf forest | CA-NS6 | UCI 1989 | 55.92 | −98.96 | Goulden (2016g) |
| 100 | Evergreen needleleaf forest | CA-NS7 | UCI 1998 | 56.64 | −99.95 | Goulden (2016h) |
| 101 | Mixed forests | CA-Oas | SK-Old Aspen | 53.63 | −106.20 | Black (2016a) |
| 102 | Evergreen needleleaf forest | CA-Obs | SK-Southern Old Black Spruce | 53.99 | −105.12 | Black (2016b) |
| 103 | Evergreen needleleaf forest | CA-Qfo | QC-Eastern Old Black Spruce (EOBS) | 49.69 | −74.34 | Margolis (2016) |
| 104 | Evergreen needleleaf forest | CA-SF1 | SK-1977 Fire | 54.48 | −105.82 | Amiro (2016b) |
| 105 | Mixed forests | CA-SF2 | SK-1989 Fire | 54.25 | −105.88 | Amiro (2016c) |
| 106 | Evergreen needleleaf forest | CA-SF3 | SK-1998 Fire | 54.09 | −106.01 | Amiro (2016d) |
| 107 | Mixed forests | CA-TP3 | ON-Turkey Point 1974 White Pine | 42.71 | −80.35 | Arain (2016c) |
| 108 | Deciduous broadleaf forest | CA-TPD | ON-Turkey Point Deciduous | 42.64 | −80.56 | Arain (2016d) |
| 109 | Evergreen needleleaf forest | CH-Dav | Davos–Seehorn forest | 46.82 | 9.86 | Hörtnagl et al. (2016b) |
| 110 | Mixed forests | CH-Lae | Laegeren | 47.48 | 8.37 | Hörtnagl et al. (2016a) |
| 111 | Mixed forests | CN-Cha | Changbaishan | 42.40 | 128.10 | Zhang and Han (2016) |
| 112 | Evergreen broadleaf forest | CN-Din | Dinghushan | 23.17 | 112.53 | Zhou and Yan (2016) |
| 113 | Mixed forests | CZ-BK2 | Bily Kriz-grassland | 49.49 | 18.54 | Sigut et al. (2016) |
| 114 | Mixed forests | DE-Gri | Grillenburg-grass station | 50.95 | 13.51 | Bernhofer et al. (2016a) |
| 115 | Mixed forests | DE-Hai | Hainich | 51.08 | 10.45 | Knohl et al. (2016b) |
| 116 | Evergreen needleleaf forest | DE-Lkb | Lackenberg | 49.10 | 13.30 | Lindauer et al. (2016) |
| 117 | Deciduous broadleaf forest | DE-Lnf | Leinefelde | 51.33 | 10.37 | Knohl et al. (2016a) |
| 118 | Evergreen needleleaf forest | DE-Obe | Oberbarenburg | 50.78 | 13.72 | Bernhofer et al. (2016c) |
| 119 | Evergreen needleleaf forest | DE-SfN | Schechenfilz Nord | 47.81 | 11.33 | Klatt et al. (2016) |
| 120 | Mixed forests | DE-Spw | Spreewald | 51.89 | 14.03 | Bernhofer et al. (2016d) |
| 121 | Evergreen needleleaf forest | DE-Tha | Tharandt-Anchor Station | 50.96 | 13.57 | Bernhofer et al. (2016e) |
| 122 | Deciduous broadleaf forest | DK-Sor | Soroe-LilleBogeskov | 55.49 | 11.64 | Ibrom and Pilegaard (2016) |
| 123 | Deciduous broadleaf forest | FR-Fon | Fontainebleau | 48.48 | 2.78 | Berveiller et al. (2016) |
| 124 | Mixed forests | FR-Pue | Puechabon | 43.74 | 3.60 | Ourcival (2016) |
| 125 | Evergreen broadleaf forest | GF-Guy | Guyaflux | 5.28 | −52.92 | Bonal and Burban (2016) |
| 126 | Evergreen broadleaf forest | GH-Ank | Ankasa | 5.27 | −2.69 | Valentini et al. (2016b) |
| 127 | Deciduous broadleaf forest | IT-Col | Collelongo-Selva Piana | 41.85 | 13.59 | Matteucci (2016) |
| 128 | Evergreen needleleaf forest | IT-Cp2 | Castelporziano2 | 41.70 | 12.36 | Fares et al. (2016) |
| 129 | Evergreen needleleaf forest | IT-Cpz | Castelporziano | 41.71 | 12.38 | Valentini et al. (2016a) |
| 130 | Evergreen needleleaf forest | IT-La2 | Lavarone2 | 45.95 | 11.29 | Cescatti et al. (2016) |
| 131 | Evergreen needleleaf forest | IT-Lav | Lavarone (after March 2002) | 45.96 | 11.28 | Gianelle et al. (2016b) |
| 132 | Evergreen needleleaf forest | IT-Ren | Renon/Ritten (Bolzano) | 46.59 | 11.43 | Montagnani and Minerbi (2016) |
| 133 | Mixed forests | IT-SR2 | San Rossore 2 | 43.73 | 10.29 | Gruening et al. (2016b) |
| 134 | Evergreen needleleaf forest | IT-Tor | Torgnon | 45.84 | 7.58 | Cremonese et al. (2016) |
| 135 | Mixed forests | JP-MBF | Moshiri Birch Forest Site | 44.38 | 142.32 | Kotani (2016a) |
| 136 | Evergreen broadleaf forest | MY-PSO | Pasoh Forest Reserve | 2.97 | 102.31 | Kosugi and Takanashi (2016) |
| 137 | Mixed forests | NL-Hor | Horstermeer | 52.24 | 5.07 | Dolman et al. (2016) |
| 138 | Evergreen needleleaf forest | NL-Loo | Loobos | 52.17 | 5.74 | Moors and Elbers (2016) |
| 139 | Mixed forests | RU-Fyo | Fedorovskoje-drained spruce stand | 56.46 | 32.92 | Varlagin et al. (2016) |
| 140 | Evergreen needleleaf forest | U.S.-Blo | Blodgett Forest | 38.90 | −120.63 | Goldstein (2016) |
| 141 | Evergreen needleleaf forest | U.S.-GBT | GLEES Brooklyn Tower | 41.37 | −106.24 | Massman (2016a) |
| 142 | Evergreen needleleaf forest | U.S.-GLE | GLEES | 41.36 | −106.24 | Massman (2016b) |
| 143 | Mixed forests | U.S.-Ha1 | Harvard Forest EMS Tower (HFR1) | 42.54 | −72.17 | Munger (2016) |
| 144 | Mixed forests | U.S.-KS1 | Kennedy Space Center (slash pine) | 28.46 | −80.67 | Drake and Hinkle (2016a) |
| 145 | Mixed forests | U.S.-Los | Lost Creek | 46.08 | −89.98 | Desai (2016a) |
| 146 | Deciduous broadleaf forest | U.S.-MMS | Morgan Monroe State Forest | 39.32 | −86.41 | Novick and Phillips (2016) |
| 147 | Evergreen needleleaf forest | U.S.-Me2 | Metolius Intermediate Pine | 44.45 | −121.56 | Law (2016b) |
| 148 | Evergreen needleleaf forest | U.S.-Me3 | Metolius Second Young Pine | 44.32 | −121.61 | Law (2016c) |
| 149 | Evergreen needleleaf forest | U.S.-Me4 | Metolius Old Pine | 44.50 | −121.62 | Law (2016d) |

TABLE A1. (*Continued*)

| Site No. | IGBP Land use | Site ID | Site name | Location Lat (°) | Location Lon (°) | Data citation |
|---|---|---|---|---|---|---|
| 150 | Evergreen needleleaf forest | U.S.-Me5 | Metolius First Young Pine | 44.44 | −121.57 | Law (2016e) |
| 151 | Evergreen needleleaf forest | U.S.-NR1 | Niwot Ridge (LTER NWT1) | 40.03 | −105.55 | Blanken et al. (2016) |
| 152 | Deciduous broadleaf forest | U.S.-Oho | Oak Openings | 41.55 | −83.84 | Chen et al. (2016) |
| 153 | Mixed forests | U.S.-PFa | Park Falls | 45.95 | −90.27 | Desai (2016b) |
| 154 | Mixed forests | U.S.-Syv | Sylvania Wilderness Area | 46.24 | −89.35 | Desai (2016c) |
| 155 | Deciduous broadleaf forest | U.S.-UMB | Univ. of Mich. Biological Station | 45.56 | −84.71 | Gough et al. (2016a) |
| 156 | Mixed forests | U.S.-UMd | Univ. of Mich. Biological Station Disturbance | 45.56 | −84.70 | Gough et al. (2016b) |
| 157 | Deciduous broadleaf forest | U.S.-WCr | Willow Creek | 45.81 | −90.08 | Desai (2016d) |
| 158 | Deciduous broadleaf forest | U.S.-Wi3 | Mature hardwood (MHW) | 46.63 | −91.10 | Chen (2016a) |
| 159 | Mixed forests | U.S.-Wi4 | Mature red pine (MRP) | 46.74 | −91.17 | Chen (2016b) |
| 160 | Mixed forests | U.S.-Wi9 | Young Jack pine (YJP) | 46.62 | −91.08 | Chen (2016d) |

that the heat storage change in the soil is negligible). The heat storage increase during the day is given by

$$\frac{dU}{dt} = R_s - \mathrm{LE} = R_s - f_e J_{\mathrm{opt}}. \tag{B2}$$

When Eqs. (B1) and (B2) are combined, we obtain

$$\frac{dU}{dt} = \frac{2 - f_e}{2 + f_e} R_s. \tag{B3}$$

TABLE A2. Description of data used.

| Variable name | Unit | Data source | Description | Resolution Spatial | Resolution Temporal |
|---|---|---|---|---|---|
| Surface temperature ($T_s$) | K | FLUXNET | Calculated from the upwelling flux of longwave radiation emitted by the surface (Stefan–Boltzmann law) | Site level | Half hourly |
| | | ERA5 | Temperature of the uppermost surface layer, which has no heat capacity. Available as skin temperature (Copernicus Climate Change Service 2019) | 0.25° lat–lon grid | Hourly |
| Air temperature ($T_a$) | K | FLUXNET | Usually measured 2 m above the canopy. For more details please refer to the site descriptions. | Site level | Half hourly |
| | | ERA5 | Air temperature 2 m above the surface calculated by interpolating between the lowest model level and Earth's surface (Copernicus Climate Change Service 2019) | 0.25° lat–lon grid | Hourly |
| Evaporative fraction ($f_e$) | — | FLUXNET | The slope of the linear regression between the half hourly observations of latent heat flux (LE) and total turbulent heat flux (LE + H) | Site level | Half hourly |
| | | ERA5 | | 0.25° lat–lon grid | Hourly |
| Aerodynamic conductance ($g_a$) | m s$^{-1}$ | FLUXNET | From the sensible heat flux, $g_a = H/[c_p\rho(T_s - T_a)]$ | Site level | — |
| Vegetation type | — | IGBP-MODIS | Vegetation is classified into short vegetation (croplands, grasslands, and shrublands), savanna, and forests (decidous broadleaf, evergreen broadleaf, evergreen needleleaf, and mixed forests). For details on individual sites see Table A1 and Falge et al. (2017b) | Site level and 0.25° lat–lon grid | — |
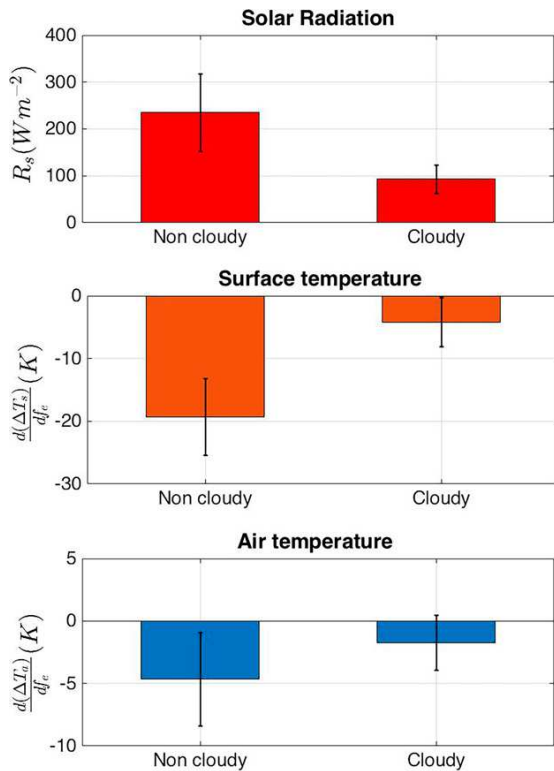
FIG. A4. The impact of clouds on solar radiation and on the sensitivities of the diurnal temperature ranges to evaporative fraction. These relations are obtained from the FLUXNET observations for short vegetation sites.

Integrated over the daytime of solar energy input, this yields a magnitude of heat storage change, $\Delta U$, in the lower atmosphere of

$$\Delta U = \frac{2 - f_e}{2 + f_e} \Delta U_0, \tag{B4}$$

where the heat storage variation in the absence of evaporation is given by the total absorbed solar energy during the day, $\Delta U_0 = R_{s,\text{avg}} \Delta t = (2/\pi) R_{s,\text{max}} \Delta t_{\text{day}}$ with $\Delta t$ being 24 h, $\Delta t_{\text{day}}$ being the daytime length, and $R_{s,\text{max}}$ being the maximum in solar absorption at the surface during the day at solar noon.

## REFERENCES

Amiro, B., 2016a: FLUXNET2015 CA-Man Manitoba - Northern old black spruce (former BOREAS northern study area). FluxNet, University of Manitoba, https://www.osti.gov/dataexplorer/biblio/dataset/1440035.

——, 2016b: FLUXNET2015 CA-SF1 Saskatchewan - Western Boreal, forest burned in 1977. FluxNet, University of Manitoba, https://www.osti.gov/servlets/purl/1440046.

——, 2016c: FLUXNET2015 CA-SF2 Saskatchewan - Western Boreal, forest burned in 1989. FluxNet, University of Manitoba, https://www.osti.gov/servlets/purl/1440047.

——, 2016d: FLUXNET2015 CA-SF3 Saskatchewan - Western Boreal, forest burned in 1998. FluxNet, University of Manitoba; Canadian Forest Service, https://www.osti.gov/servlets/purl/1440048.

Ammann, C., 2016: FLUXNET2015 CH-Oe1 Oensingen Grassland. FluxNet, Agroscope Zuerich, https://www.osti.gov/servlets/purl/1440135.

Anderson, M., J. Norman, G. Diak, W. Kustas, and J. Mecikalski, 1997: A two-source time-integrated model for estimating surface fluxes using thermal infrared remote sensing. *Remote Sens. Environ.*, **60**, 195–216, https://doi.org/10.1016/S0034-4257(96)00215-5.

Arain, M. A., 2016a: FLUXNET2015 CA-TP1 Ontario - Turkey point 2002 plantation white pine. FluxNet, McMaster University, https://www.osti.gov/servlets/purl/1440050.

——, 2016b: FLUXNET2015 CA-TP2 Ontario - Turkey point 1989 plantation white pine. FluxNet, McMaster University, https://www.osti.gov/servlets/purl/1440051.

——, 2016c: FLUXNET2015 CA-TP3 Ontario - Turkey point 1974 plantation white pine. FluxNet, McMaster University, https://www.osti.gov/servlets/purl/1440052.

——, 2016d: FLUXNET2015 CA-TPD Ontario - Turkey point mature deciduous. FluxNet, McMaster University, https://www.osti.gov/servlets/purl/1440112.

Ardö, J., B. Tahir, and H. ElKhidir, 2016: FLUXNET2015 SD-Dem Demokeya. FluxNet, Lund University, https://www.osti.gov/servlets/purl/1440186.

Arndt, S., N. Hinko-Najera, A. Griebel, J. Beringer, and S. Livesley 2016: FLUXNET2015 AU-Wom Wombat. FluxNet, University of Melbourne, https://www.osti.gov/servlets/purl/1440207.

Baldocchi, D., 2016: FLUXNET2015 US-Twt Twitchell Island. FluxNet, University of California, Berkeley, https://www.osti.gov/servlets/purl/1440106.

——, and S. Ma, 2013: How will land use affect air temperature in the surface boundary layer? Lessons learned from a comparative study on the energy balance of an oak savanna and annual grassland in California, USA. *Tellus*, **65B**, 19994, https://doi.org/10.3402/tellusb.v65i0.19994.

——, and ——, 2016: FLUXNET2015 US-Ton Tonzi Ranch. FluxNet, University of California, Berkeley, https://www.osti.gov/servlets/purl/1440092.

——, ——, and L. Xu, 2016: FLUXNET2015 US-Var Vaira Ranch- Ione. FluxNet, University of California, Berkeley, https://www.osti.gov/servlets/purl/1440094.

Belelli, L., D. Papale, and R. Valentini, 2016: FLUXNET2015 RU-Ha1 Hakasia Steppe. FluxNet, University of Tuscia - Viterbo, https://www.osti.gov/servlets/purl/1440184.

Bell, B., and Coauthors, 2021: The ERA5 global reanalysis: Preliminary extension to 1950. *Quart. J. Roy. Meteor. Soc.*, **147**, 4186–4227, https://doi.org/10.1002/qj.4174.

Berbigier, P., J. Bonnefond, A. Bosc, P. Trichet, and D. Loustau, 2016: FLUXNET2015 Fr-Lbr Le Bray. FluxNet, INRA - UMR ISPA, https://www.osti.gov/servlets/purl/1440163.

Beringer, J., and L. Hutley, 2016a: FLUXNET2015 AU-Ade Adelaide River. FluxNet, Monash University, Charles Darwin University, https://www.osti.gov/servlets/purl/1440193.

——, and ——, 2016b: FLUXNET2015 AU-DaP Daly River Savanna. FluxNet, Monash University, Charles Darwin University, https://www.osti.gov/servlets/purl/1440123.

——, and ——, 2016c: FLUXNET2015 Au-Dry Dry River. FluxNet, Monash University, University of Western Australia, Charles Darwin University, https://www.osti.gov/servlets/purl/1440197.

——, and ——, 2016d: FLUXNET2015 AU-Fog Fogg Dam. FluxNet, Monash University, Charles Darwin University, https://www.osti.gov/servlets/purl/1440124.

——, and ——, 2016e: FLUXNET2015 AU-How Howard Springs. FluxNet, Charles Darwin University, University of Western Australia, Monash University, https://www.osti.gov/servlets/purl/1440125.

——, and ——, 2016f: FLUXNET2015 AU-Stp Sturt Plains. FluxNet, University of Western Australia, Charles Darwin University, Monash University, https://www.osti.gov/servlets/purl/1440204.

——, and ——, 2016g: FLUXNET2015 AU-DaS daly river cleared. FluxNet, University of Western Australia, https://www.osti.gov/servlets/purl/1440122.

——, and J. Walker, 2016: FLUXNET2015 Au-Ync Jaxa. FluxNet, University of Western Australia, Monash University, https://www.osti.gov/servlets/purl/1440208.

——, S. Cunningham, P. Baker, T. Cavagnaro, R. MacNally, R. Thompson, and I. McHugh, 2016a: FLUXNET2015 AU-Rig Riggs Creek. FluxNet, Monash University, https://www.osti.gov/servlets/purl/1440202.

——, ——, ——, ——, ——, ——, and ——, 2016b: FLUXNET2015 AU-Whr Whroo. FluxNet, Monash University, https://www.osti.gov/servlets/purl/1440206.

——, L. Hutley, D. McGuire, U. Paw, and I. McHugh, 2016c: FLUXNET2015 AU-WaC Wallaby Creek. FluxNet, Monash University, https://www.osti.gov/servlets/purl/1440127.

Bernhofer, C., T. Grünwald, U. Moderow, M. Hehn, U. Eichelmann, H. Prasse, and U. Postel, 2016a: FLUXNET2015 DE-Gri Grillenburg. FluxNet, TU Dresden, https://www.osti.gov/servlets/purl/1440147.

——, ——, ——, ——, ——, ——, and ——, 2016b: FLUXNET2015 DE-Kli Klingenberg. FluxNet, TU Dresden, https://www.osti.gov/servlets/purl/1440149.

——, ——, ——, ——, ——, ——, and ——, 2016c: FLUXNET2015 DE-Obe Oberbärenburg. FluxNet, TU Dresden, https://www.osti.gov/servlets/purl/1440151.

——, ——, ——, ——, ——, ——, and ——, 2016d: FLUXNET2015 DE-Spw Spreewald. FluxNet, TU Dresden, https://www.osti.gov/servlets/purl/1440220.

——, ——, ——, ——, ——, ——, and ——, 2016e: FLUXNET2015 DE-Tha Tharandt. FluxNet, TU Dresden, https://www.osti.gov/servlets/purl/1440152.

Berveiller, D., N. Delpierre, E. Dufrêne, J.-Y. Pontailler, L. Vanbostal, B. Janvier, L. Mottet, and K. Cristinacce, 2016: FLUXNET2015 FR-Fon Fontainebleau-Barbeau. FluxNet, CNRS, https://www.osti.gov/servlets/purl/1440161.

Best, M. J., A. Beljaars, J. Polcher, and P. Viterbo, 2004: A proposed structure for coupling tiled surfaces with the planetary boundary layer. *J. Hydrometeor.*, **5**, 1271–1278, https://doi.org/10.1175/JHM-382.1.

Betts, A. K., and J. Ball, 1995: The FIFE surface diurnal cycle climate. *J. Geophys. Res.*, **100**, 25 679–25 693, https://doi.org/10.1029/94JD03121.

Billesbach, D., J. Bradford, and M. Torn, 2016a: FLUXNET2015 US-AR1 ARM USDA UNL OSU Woodward Switchgrass 1. FluxNet, Lawerence Berkeley National Lab, U.S. Department of Agriculture, University of Nebraska, https://www.osti.gov/servlets/purl/1440103.

——, ——, and ——, 2016b: FLUXNET2015 US-AR2 ARM USDA UNL OSU Woodward Switchgrass 2. FluxNet, Lawrence Berkeley National Lab, U.S. Department of Agriculture, University of Nebraska, https://www.osti.gov/servlets/purl/1440104.

Biraud, S., M. Fischer, S. Chan, and M. Torn, 2016: FLUXNET2015 US-ARM ARM Southern Great Plains site - Lamont. FluxNet, Lawrence Berkeley National Laboratory, https://www.osti.gov/servlets/purl/1440066.

Black, T. A., 2016a: FLUXNET2015 CA-OAS Saskatchewan - Western Boreal, mature aspen. FluxNet, The University of British Columbia, https://www.osti.gov/servlets/purl/1440043.

——, 2016b: FLUXNET2015 CA-OBS Saskatchewan - Western Boreal, mature black spruce. FluxNet, The University of British Columbia, https://www.osti.gov/servlets/purl/1440044.

Blanken, P. D., R. K. Monson, S. P. Burns, D. R. Bowling, and A. A. Turnipseed, 2016: FLUXNET2015 US-NR1 Niwot Ridge forest (LTER NWT1). FluxNet, University of Colorado, https://www.osti.gov/servlets/purl/1440087.

Bonal, D., and B. Burban, 2016: FLUXNET2015 GF-Guy Guyaflux (French Guiana). FluxNet, https://www.osti.gov/servlets/purl/1440165.

Bourque, C.-A., and P. Arp, 1994: Dawn-to-dusk evolution of air turbulence, temperature and sensible and latent heat fluxes above a forest canopy: Concepts, model and field comparisons. *Atmos.–Ocean*, **32**, 299–334, https://doi.org/10.1080/07055900.1994.9649500.

Bowling, D., 2016: FLUXNET2015 US-Cop Corral Pocket. FluxNet, University of Utah, https://www.osti.gov/servlets/purl/1440100.

Braganza, K., D. J. Karoly, and J. M. Arblaster, 2004: Diurnal temperature range as an index of global climate change during the twentieth century. *Geophys. Res. Lett.*, **31**, L13217, https://doi.org/10.1029/2004GL019998.

Bright, R. M., E. Davin, T. O'Halloran, J. Pongratz, K. Zhao, and A. Cescatti, 2017: Local temperature response to land cover and management change driven by non-radiative processes. *Nat. Climate Change*, **7**, 296–302, https://doi.org/10.1038/nclimate3250.

Brovkin, V., and Coauthors, 2006: Biogeophysical effects of historical land cover changes simulated by six Earth system models of intermediate complexity. *Climate Dyn.*, **26**, 587–600, https://doi.org/10.1007/s00382-005-0092-6.

Brümmer, C., A. M. Lucas-Moffat, M. Herbst, O. Kolle, and J.-P. Delorme 2016: FLUXNET2015 DE-GEB Gebesee. FluxNet, Thünen Institute of Climate-Smart Agriculture, Braunschweig, https://www.osti.gov/servlets/purl/1440146.

Brutsaert, W., 2013: *Evaporation into the Atmosphere: Theory, History and Applications*, Vol. 1. Springer, 409 pp.

Buysse, P., B. Durand, J.-C. Gueudet, N. Mascher, E. Larmanou, P. Cellier, and B. Loubet, 2016: FLUXNET2015 FR-Gri Grignon. FluxNet, French National Institute for Agricultural Research, https://www.osti.gov/servlets/purl/1440162.

Cañete, E., P. Ortiz, M. Jimenez, F. Poveda, O. Priego, A. Ballesteros, and A. Kowalski, 2016: FLUXNET2015 ES-LJu Llano De Los Juanes. FluxNet, University of Granada, https://www.osti.gov/servlets/purl/1440157.

Cescatti, A., B. Marcolla, R. Zorer, and D. Gianelle, 2016: FLUXNET2015 IT-La2 Lavarone2. FluxNet, Centro di Ecologia Alpina, https://www.osti.gov/servlets/purl/1440235.

Chen, J., 2016a: FLUXNET2015 US-Wi3 Mature Hardwood (MHW). FluxNet, Michigan State University, https://www.osti.gov/servlets/purl/1440057.

——, 2016b: FLUXNET2015 US-Wi4 Mature Red Pine (MRP). FluxNet, Michigan State University, https://www.osti.gov/servlets/purl/1440058.

——, 2016c: FLUXNET2015 US-Wi6 Pine Barrens. FluxNet, Michigan State University, https://www.osti.gov/servlets/purl/1440060.

——, 2016d: FLUXNET2015 US-Wi9 Young Jack Pine (YJP). FluxNet, Michigan State University, https://www.osti.gov/servlets/purl/1440063.

——, H. Chu, and A. Noormets, 2016: FLUXNET2015 UU-Oho Oak Openings. FluxNet, University of Toledo/Michigan State University, https://www.osti.gov/servlets/purl/1440088.

Chen, L., and P. A. Dirmeyer, 2019a: Differing responses of the diurnal cycle of land surface and air temperatures to deforestation. *J. Climate*, **32**, 7067–7079, https://doi.org/10.1175/JCLI-D-19-0002.1.

——, and ——, 2019b: The relative importance among anthropogenic forcings of land use/land cover change in affecting temperature extremes. *Climate Dyn.*, **52**, 2269–2285, https://doi.org/10.1007/s00382-018-4250-z.

Chen, S., 2016: FLUXNET2015 CN-Du2 Duolun grassland (d01). FluxNet, Institute of Botany, Chinese Academy of Sciences, https://www.osti.gov/servlets/purl/1440140.

Claussen, M., V. Brovkin, and A. Ganopolski, 2001: Biogeophysical versus biogeochemical feedbacks of large-scale land cover change. *Geophys. Res. Lett.*, **28**, 1011–1014, https://doi.org/10.1029/2000GL012471.

Cleverly, J., D. Eamus, and P. Isaac, 2016a: FLUXNET2015 AU-ASM Alice Springs. FluxNet, University of Technology Sydney, https://www.osti.gov/servlets/purl/1440194.

——, ——, and ——, 2016b: FLUXNET2015 AU-TTE Ti Tree East. FluxNet, University of Technology Sydney, https://www.osti.gov/servlets/purl/1440205.

Collatz, G. J., L. Bounoua, S. O. Los, D. A. Randall, I. Y. Fung, and P. J. Sellers, 2000: A mechanism for the influence of vegetation on the response of the diurnal temperature range to changing climate. *Geophys. Res. Lett.*, **27**, 3381–3384, https://doi.org/10.1029/1999GL010947.

Copernicus Climate Change Service, 2019: ERA5-land hourly data from 2001 to present. ECMWF, downloaded 1 November 2020, https://cds.climate.copernicus.eu/doi/10.24381/cds.e2161bac.

Cremonese, E., M. Galvagno, U. M. Di Cella, and M. Migliavacca, 2016: FLUXNET2015 IT-Tor Torgnon. FluxNet, Environmental Protection Agency of Aosta Valley, https://www.osti.gov/servlets/purl/1440237.

Dai, A., A. D. Del Genio, and I. Y. Fung, 1997: Clouds, precipitation and temperature range. *Nature*, **386**, 665–666, https://doi.org/10.1038/386665b0.

——, K. E. Trenberth, and T. R. Karl, 1999: Effects of clouds, soil moisture, precipitation, and water vapor on diurnal temperature range. *J. Climate*, **12**, 2451–2473, https://doi.org/10.1175/1520-0442(1999)012<2451:EOCSMP>2.0.CO;2.

——, T. R. Karl, B. Sun, and K. E. Trenberth, 2006: Recent trends in cloudiness over the United States: A tale of monitoring inadequacies. *Bull. Amer. Meteor. Soc.*, **87**, 597–606, https://doi.org/10.1175/BAMS-87-5-597.

Davin, E. L., and N. de Noblet-Ducoudré, 2010: Climatic impact of global-scale deforestation: Radiative versus nonradiative processes. *J. Climate*, **23**, 97–112, https://doi.org/10.1175/2009JCLI3102.1.

De Kauwe, M. G., B. E. Medlyn, J. Knauer, and C. A. Williams, 2017: Ideas and perspectives: How coupled is the vegetation to the boundary layer? *Biogeosciences*, **14**, 4435–4453, https://doi.org/10.5194/bg-14-4435-2017.

De Ligne, A., T. Manise, B. Heinesch, M. Aubinet, and C. Vincke, 2016a: FLUXNET2015 BE-Vie Vielsalm. FluxNet, University of Liege - Gembloux Agro-Bio Tech, University catholic of Louvain-la-Neuve, https://www.osti.gov/servlets/purl/1440130.

——, ——, C. Moureaux, M. Aubinet, and B. Heinesch, 2016b: FLUXNET2015 BE-Lon Lonzee. FluxNet, University of Liege - Gembloux Agro-Bio Tech, https://www.osti.gov/servlets/purl/1440129.

Denissen, J. M., R. Orth, H. Wouters, D. G. Miralles, C. C. van Heerwaarden, J. V.-G. de Arellano, and A. J. Teuling, 2021: Soil moisture signature in global weather balloon soundings. *npj Climate Atmos. Sci.*, **4**, 13, https://doi.org/10.1038/s41612-021-00167-w.

Desai, A., 2016a: FLUXNET2015 US-Los Lost Creek. FluxNet, University of Wisconsin, https://www.osti.gov/servlets/purl/1440076.

——, 2016b: FLUXNET2015 US-PFa Park Falls/Wlef. FluxNet, University of Wisconsin, https://www.osti.gov/servlets/purl/1440089.

——, 2016c: FLUXNET2015 US-Syv Sylvania Wilderness Area. FluxNet, University of Wisconsin, https://www.osti.gov/servlets/purl/1440091.

——, 2016d: FLUXNET2015 US-WCr Willow Creek. FluxNet, University of Wisconsin, https://www.osti.gov/servlets/purl/1440095.

Diak, G. R., 1990: Evaluation of heat flux, moisture flux and aerodynamic roughness at the land surface from knowledge of the pbl height and satellite-derived skin temperatures. *Agric. For. Meteor.*, **52**, 181–198, https://doi.org/10.1016/0168-1923(90)90105-F.

Dirmeyer, P. A., and K. L. Brubaker, 2007: Characterization of the global hydrologic cycle from a back-trajectory analysis of atmospheric water vapor. *J. Hydrometeor.*, **8**, 20–37, https://doi.org/10.1175/JHM557.1.

Dolman, H., D. Hendriks, F.-J. Parmentier, L. B. Marchesini, J. Dean, and K. Van Huissteden, 2016: FLUXNET2015 NL-Hor horstermeer. FluxNet, Vrije Universiteit Amsterdam, https://www.osti.gov/servlets/purl/1440177.

Drake, B., and R. Hinkle, 2016a: FLUXNET2015 US-KS1 Kennedy Space Center (Slash Pine). FluxNet, Smithsonian Environmental Research Center, University of Central Florida, https://www.osti.gov/servlets/purl/1440074.

——, and ——, 2016b: FLUXNET2015 US-KS2 Kennedy Space Center (Scrub Oak). FluxNet, Smithsonian Environmental Research Center, University of Central Florida, URL https://www.osti.gov/servlets/purl/1440075.

Dusek, J., D. Janous, and M. Pavelka, 2016: FLUXNET2015 Cz-Wet Trebon (Czechwet). FluxNet, Global Change Research Institute CAS, https://www.osti.gov/servlets/purl/1440145.

Easterling, D. R., and Coauthors, 1997: Maximum and minimum temperature trends for the globe. *Science*, **277**, 364–367, https://doi.org/10.1126/science.277.5324.364.

ECMWF, 2007: IFS documentation CY31R1 - Part IV: Physical processes. ECMWF, https://www.ecmwf.int/node/9221.

Ermida, S. L., I. F. Trigo, C. C. DaCamara, F. M. Gottsche, F. S. Olesen, and G. Hulley, 2014: Validation of remotely sensed surface temperature over an oak woodland landscape—The problem of viewing and illumination geometries. *Remote Sens. Environ.*, **148**, 16–27, https://doi.org/10.1016/j.rse.2014.03.016.

Ewers, B., and E. Pendall, 2016: FLUXNET2015 US-Sta Saratoga. FluxNet, University of Wyoming, https://www.osti.gov/servlets/purl/1440115.

Falge, E., and Coauthors, 2017a: FLUXNET research network site characteristics, investigators, and bibliography, 2016. ORNL DAAC, https://doi.org/10.3334/ORNLDAAC/1530.

——, and Coauthors, 2017b: FLUXNET research network site characteristics, investigators, and bibliography, 2016. ORNL Distributed Active Archive Center, https://daac.ornl.gov/cgi-bin.

Fares, S., F. Savi, and A. Conte, 2016: FLUXNET2015 IT-Cp2 Castelporziano 2. FluxNet, Council for Agricultural Research and Economics, https://www.osti.gov/servlets/purl/1440233.

Feddema, J. J., K. W. Oleson, G. B. Bonan, L. O. Mearns, L. E. Buja, G. A. Meehl, and W. M. Washington, 2005: The importance of land-cover change in simulating future climates. *Science*, **310**, 1674–1678, https://doi.org/10.1126/science.1118160.

Gallo, K. P., D. R. Easterling, and T. C. Peterson, 1996: The influence of land use/land cover on climatological values of the diurnal temperature range. *J. Climate*, **9**, 2941–2944, https://doi.org/10.1175/1520-0442(1996)009<2941:TIOLUC>2.0.CO;2.

Garcia, M., N. Fernández, L. Villagarcía, F. Domingo, J. Puigdefábregas, and I. Sandholt, 2014: Accuracy of the Temperature–Vegetation Dryness Index using MODIS under water-limited vs. energy-limited evapotranspiration conditions. *Remote Sens. Environ.*, **149**, 100–117, https://doi.org/10.1016/j.rse.2014.04.002.

Gentine, P., A. Massmann, B. R. Lintner, S. H. Alemohammad, R. Fu, J. K. Green, D. Kennedy, and J. V.-G. de Arellano, 2019: Land–atmosphere interactions in the tropics—A review. *Hydrol. Earth Syst. Sci.*, **23**, 4171–4197, https://doi.org/10.5194/hess-23-4171-2019.

Gianelle, D., M. Cavagna, R. Zampedri, and B. Marcolla, 2016a: FLUXNET2015 IT-MBo Monte Bondone. FluxNet, Edmund Mach Foundation, https://www.osti.gov/servlets/purl/1440170.

——, R. Zampedri, M. Cavagna, and M. Sottocornola, 2016b: FLUXNET2015 IT-Lav Lavarone. FluxNet, Edmund Mach Foundation, https://www.osti.gov/servlets/purl/1440169.

Goldstein, A., 2016: FLUXNET2015 US-Blo Blodgett Forest. FluxNet, University of California, Berkeley, https://www.osti.gov/servlets/purl/1440068.

Gough, C., G. Bohrer, and P. Curtis, 2016a: FLUXNET2015 US-UMB Univ. of Mich. Biological Station. FluxNet, Ohio State University, Virginia Commonwealth University, https://www.osti.gov/servlets/purl/1440093.

——, ——, and ——, 2016b: FLUXNET2015 US-UMd UMBS disturbance. FluxNet, Ohio State University, Virginia Commonwealth University, https://www.osti.gov/servlets/purl/1440101.

Goulden, M., 2016a: FLUXNET2015 BR-Sa3 Santarem-Km83-logged forest. FluxNet, University of California, Irvine, https://www.osti.gov/servlets/purl/1440033.

——, 2016b: FLUXNET2015 CA-Ns1 UCI-1850 burn site. FluxNet, University of California, Irvine, https://www.osti.gov/servlets/purl/1440036.

——, 2016c: FLUXNET2015 CA-Ns2 UCI-1930 burn site. FluxNet, University of California, Irvine, https://www.osti.gov/servlets/purl/1440037.

——, 2016d: FLUXNET2015 CA-Ns3 UCI-1964 burn site. FluxNet, University of California, Irvine, https://www.osti.gov/servlets/purl/1440038.

——, 2016e: FLUXNET2015 CA-Ns4 UCI-1964 burn site wet. FluxNet, University of California, Irvine, https://www.osti.gov/servlets/purl/1440039.

——, 2016f: FLUXNET2015 CA-Ns5 UCI-1981 burn site. FluxNet, University of California, Irvine, https://www.osti.gov/servlets/purl/1440040.

——, 2016g: FLUXNET2015 CA-Ns6 UCI-1989 burn site. FluxNet, University of California, Irvine, https://www.osti.gov/servlets/purl/1440041.

——, 2016h: FLUXNET2015 CA-Ns7 UCI-1998 burn site. FluxNet, University of California, Irvine, https://www.osti.gov/servlets/purl/1440042.

Green, J. K., A. G. Konings, S. H. Alemohammad, J. Berry, D. Entekhabi, J. Kolassa, J.-E. Lee, and P. Gentine, 2017: Regionally strong feedbacks between the atmosphere and terrestrial biosphere. *Nat. Geosci.*, **10**, 410–414, https://doi.org/10.1038/ngeo2957.

Gruening, C., I. Goded, A. Cescatti, and O. Pokorska, 2016a: FLUXNET2015 IT-Isp Ispra ABC-IS. FluxNet, European Commission, Joint Research Centre, https://www.osti.gov/servlets/purl/1440234.

——, ——, ——, and ——, 2016b: FLUXNET2015 IT-SR2 San Rossore 2. FluxNet, European Commission, Joint Research Centre, https://www.osti.gov/servlets/purl/1440236.

Gu, L., and Coauthors, 2007: Influences of biomass heat and biochemical energy storages on the land surface fluxes and radiative temperature. *J. Geophys. Res.*, **112**, D02107, https://doi.org/10.1029/2006JD007425.

Helbig, M., and Coauthors, 2020: Whitepaper: Understanding land–atmosphere interactions through tower-based flux and continuous atmospheric boundary layer measurements. Ameriflux, 45 pp., http://ameriflux.lbl.gov/community/highlight/whitepaper-understanding-land-atmosphere-interactions-through-tower-based-flux-and-continuous-atmospheric-boundary-layer-measurements/.

Hörtnagl, L., W. Eugster, N. Buchmann, E. Paul-Limoges, S. Etzold, M. Haeni, and P. Pluess, and T. Baur, 2016a: FLUXNET2015 CH-Lae Laegern. FluxNet, ETH Zurich, https://www.osti.gov/servlets/purl/1440134.

——, and Coauthors, 2016b: FLUXNET2015 CH-Dav Davos. FluxNet, ETH Zurich, https://www.osti.gov/servlets/purl/1440132.

——, and Coauthors, 2016c: FLUXNET2015 CH-Fru Früebüel. FluxNet, ETH Zurich, https://www.osti.gov/servlets/purl/1440133.

——, and Coauthors, 2016d: FLUXNET2015 CH-Oe2 Oensingen Crop. FluxNet, ETH Zurich, https://www.osti.gov/servlets/purl/1440136.

Humes, K. S., W. P. Kustas, M. S. Moran, W. D. Nichols, and M. A. Weltz, 1994: Variability of emissivity and surface temperature over a sparsely vegetated surface. *Water Resour. Res.*, **30**, 1299–1310, https://doi.org/10.1029/93WR03065.

Ibrom, A., and K. Pilegaard, 2016: FLUXNET2015 DK-Sor Soroe. FluxNet, Technical University of Denmark (DTU), https://www.osti.gov/servlets/purl/1440155.

Jarvis, P. G., 1985: Transpiration and assimilation of tree and agricultural crops: The omega factor. *Attributes of Trees as Crop Plants*, M. G. R. Cannell and J. E. Jackson, Eds., Institute of Terrestrial Ecology, 460–480.

——, and K. G. McNaughton, 1986: Stomatal control of transpiration: Scaling up from leaf to region. *Adv. Ecol. Res.*, **15**, 1–49, https://doi.org/10.1016/S0065-2504(08)60119-1.

Jiang, H., Y. Yang, Y. Bai, and H. Wang, 2020: Evaluation of the total, direct, and diffuse solar radiations from the ERA5 reanalysis data in China. *IEEE Geosci. Remote Sens. Lett.*, **17**, 47–51, https://doi.org/10.1109/LGRS.2019.2916410.

Jin, M., and R. E. Dickinson, 2010: Land surface skin temperature climatology: Benefitting from the strengths of satellite observations. *Environ. Res. Lett.*, **5**, 044004, https://doi.org/10.1088/1748-9326/5/4/044004.

Johannsen, F., S. Ermida, J. P. A. Martins, I. F. Trigo, M. Nogueira, and E. Dutra, 2019: Cold bias of ERA5 summertime daily maximum land surface temperature over Iberian Peninsula. *Remote Sens.*, **11**, 2570, https://doi.org/10.3390/rs11212570.

Kalma, J. D., T. R. McVicar, and M. F. McCabe, 2008: Estimating land surface evaporation: A review of methods using remotely sensed surface temperature data. *Surv. Geophys.*, **29**, 421–469, https://doi.org/10.1007/s10712-008-9037-z.

Karl, T. R., G. Kukla, V. N. Razuvayev, M. J. Changery, R. G. Quayle, R. R. Heim, Jr., D. R. Easterling, and C. B. Fu, 1991: Global warming: Evidence for asymmetric diurnal temperature change. *Geophys. Res. Lett.*, **18**, 2253–2256, https://doi.org/10.1029/91GL02900.

Klatt, J., H. P. Schmid, M. Mauder, and R. Steinbrecher, 2016: FLUXNET2015 DE-Sfn Schechenfilz Nord. FluxNet, Karlsruhe Institute of Technology, IMK-IFU, https://www.osti.gov/servlets/purl/1440219/.

Kleidon, A., and M. Heimann, 2000: Assessing the role of deep rooted vegetation in the climate system with model simulations: Mechanism, comparison to observations and implications for Amazonian deforestation. *Climate Dyn.*, **16**, 183–199, https://doi.org/10.1007/s003820050012.

——, and M. Renner, 2017: An explanation for the different climate sensitivities of land and ocean surfaces based on the diurnal cycle. *Earth Syst. Dyn.*, **8**, 849–864, https://doi.org/10.5194/esd-8-849-2017.

——, and ——, 2018: Diurnal land surface energy balance partitioning estimated from the thermodynamic limit of a cold heat engine. *Earth Syst. Dyn.*, **9**, 1127–1140, https://doi.org/10.5194/esd-9-1127-2018.

Knohl, A., F. Tiedemann, O. Kolle, E.-D. Schulze, P. Anthoni, W. Kutsch, M. Herbst, and L. Siebicke, 2016a: FLUXNET2015 DE-Lnf Leinefelde. FluxNet, University of Goettingen, Bioclimatology, https://www.osti.gov/servlets/purl/1440150/.

——, ——, ——, ——, W. Kutsch, M. Herbst, and L. Siebicke, 2016b: FLUXNET2015 DE-Hai Hainich. FluxNet, University of Goettingen, Bioclimatology, https://www.osti.gov/servlets/purl/1440148.

Koster, R., and Coauthors, 2011: The second phase of the Global Land-Atmosphere Coupling Experiment: Soil moisture contributions to subseasonal forecast skill. *J. Hydrometeor.*, **12**, 805–822, https://doi.org/10.1175/2011JHM1365.1.

Kosugi, Y., and S. Takanashi, 2016: FLUXNET2015 MY-PSO Pasoh Forest Reserve (PSO). FluxNet, FRIM (Forest Research Institute of Malaysia), Kyoto University, https://www.osti.gov/servlets/purl/1440240.

Kotani, A., 2016a: FLUXNET2015 JP-MBF Moshiri Birch Forest Site. FluxNet, Nagoya University, https://www.osti.gov/servlets/purl/1440238.

——, 2016b: FLUXNET2015 JP-SMF Seto Mixed Forest Site. FluxNet, Nagoya University, https://www.osti.gov/servlets/purl/1440239.

Kumagai, T., T. M. Saitoh, Y. Sato, T. Morooka, O. J. Manfroi, K. Kuraji, and M. Suzuki, 2004: Transpiration, canopy conductance and the decoupling coefficient of a lowland mixed dipterocarp forest in Sarawak, Borneo: Dry spell effects. *J. Hydrol.*, **287**, 237–251, https://doi.org/10.1016/j.jhydrol.2003.10.002.

Kurc, S., 2016: FLUXNET2015 US-SRC Santa Rita Creosote. FluxNet, University of Arizona, https://www.osti.gov/servlets/purl/1440098

Kustas, W. P., and J. M. Norman, 1999: Evaluation of soil and vegetation heat flux predictions using a simple two-source model with radiometric temperatures for partial canopy cover. *Agric. For. Meteor.*, **94**, 13–29, https://doi.org/10.1016/S0168-1923(99)00005-2.

Kutsch, W. L., L. Merbold, and O. Kolle, 2016: FLUXNET2015 ZM-Mon Mongu. FluxNet, Max-Planck Institute for Biogeochemistry, https://www.osti.gov/servlets/purl/1440189.

Lauritsen, R. G., and J. C. Rogers, 2012: U.S. diurnal temperature range variability and regional causal mechanisms, 1901–2002. *J. Climate*, **25**, 7216–7231, https://doi.org/10.1175/JCLI-D-11-00429.1.

Law, B., 2016a: FLUXNET2015 US-Me1 Metolius - Eyerly Burn. FluxNet, Oregon State University, https://www.osti.gov/servlets/purl/1440078.

——, 2016b: FLUXNET2015 US-Me2 Metolius Mature Ponderosa Pine. FluxNet, Oregon State University, https://www.osti.gov/servlets/purl/1440079.

——, 2016c: FLUXNET2015 US-Me3 Metolius-Second Young Aged Pine. FluxNet, Oregon State University, https://www.osti.gov/servlets/purl/1440080.

——, 2016d: FLUXNET2015 US-Me4 Metolius-Old Aged Ponderosa Pine. FluxNet, Oregon State University, https://www.osti.gov/servlets/purl/1440081.

——, 2016e: FLUXNET2015 US-Me5 Metolius-First Young Aged Pine. FluxNet, Oregon State University, https://www.osti.gov/servlets/purl/1440082.

——, 2016f: FLUXNET2015 US-Me6 Metolius Young Pine Burn. FluxNet, Oregon State University, https://www.osti.gov/servlets/purl/1440099.

Lawrence, P. J., and Coauthors, 2012: Simulating the biogeochemical and biogeophysical impacts of transient land cover change and wood harvest in the Community Climate System Model (CCSM4) from 1850 to 2100. *J. Climate*, **25**, 3071–3095, https://doi.org/10.1175/JCLI-D-11-00256.1.

Lee, X., and T. A. Black, 1993: Atmospheric turbulence within and above a douglas-fir stand. Part II: Eddy fluxes of sensible heat and water vapour. *Bound.-Layer Meteor.*, **64**, 369–389, https://doi.org/10.1007/BF00711706.

Lewis, S. C., and D. J. Karoly, 2013: Evaluation of historical diurnal temperature range trends in CMIP5 models. *J. Climate*, **26**, 9077–9089, https://doi.org/10.1175/JCLI-D-13-00032.1.

Li, X., H. Chen, J. Wei, W. Hua, S. Sun, H. Ma, X. Li, and J. Li, 2018: Inconsistent responses of hot extremes to historical land use and cover change among the selected CMIP5 models. *J. Geophys. Res. Atmos.*, **123**, 3497–3512, https://doi.org/10.1002/2017JD028161.

Li, Y., 2016: FLUXNET2015 CN-Ha2 Haibei Shrubland. FluxNet, NWIPB Chinese Academy of Sciences, https://www.osti.gov/servlets/purl/1440211.

——, M. Zhao, S. Motesharrei, Q. Mu, E. Kalnay, and S. Li, 2015: Local cooling and warming effects of forests based on satellite observations. *Nat. Commun.*, **6**, 6603, https://doi.org/10.1038/ncomms7603.

Lin, Y.-S., and Coauthors, 2015: Optimal stomatal behaviour around the world. *Nat. Climate Change*, **5**, 459–464, https://doi.org/10.1038/nclimate2550.

Lindauer, M., R. Steinbrecher, B. Wolpert, M. Mauder, and H. P. Schmid, 2016: FLUXNET2015 DE-Lkb Lackenberg. FluxNet, Karlsruhe Institute of Technology, IMK-IFU, https://www.osti.gov/servlets/purl/1440214.

Lindroth, A., M. Mölder, and F. Lagergren, 2010: Heat storage in forest biomass improves energy balance closure. *Biogeosciences*, **7**, 301–313, https://doi.org/10.5194/bg-7-301-2010.

Lobell, D. B., and C. Bonfils, 2008: The effect of irrigation on regional temperatures: A spatial and temporal analysis of trends in California, 1934–2002. *J. Climate*, **21**, 2063–2071, https://doi.org/10.1175/2007JCLI1755.1.

Longobardi, P., A. Montenegro, H. Beltrami, and M. Eby, 2016: Deforestation induced climate change: Effects of spatial scale. *PLOS ONE*, **11**, e0153357, https://doi.org/10.1371/journal.pone.0153357.

MacFarlane, C., P. Lambert, J. Byrne, C. Johnstone, and N. Smart, 2016: FLUXNET2015 AU-Gin Gingin. FluxNet, Edith Cowan University (Centre for Ecosystem Management), https://www.osti.gov/servlets/purl/1440199.

Magliulo, V., and Coauthor, 2016: FLUXNET2015 IT-BCI BORGO CIOFFI. FluxNet, CNR ISAFOM, https://www.osti.gov/servlets/purl/1440166.

Mahmood, R., and Coauthors, 2014: Land cover changes and their biogeophysical effects on climate. *Int. J. Climatol.*, **34**, 929–953, https://doi.org/10.1002/joc.3736.

Makowski, K., E. B. Jaeger, M. Chiacchio, M. Wild, T. Ewen, and A. Ohmura, 2009: On the relationship between diurnal temperature range and surface solar radiation in Europe. *J. Geophys. Res.*, **114**, D00D07, https://doi.org/10.1029/2008JD011104.

Manca, G., and I. Goded, 2016: FLUXNET2015 IT-PT1 Parco Ticino forest. FluxNet, European Commission - DG Joint Research Centre, https://www.osti.gov/servlets/purl/1440172.

Margolis, H. A., 2016: FLUXNET2015 CA-QFO Quebec - Eastern boreal, mature black spruce. FluxNet, Universite Laval, https://www.osti.gov/servlets/purl/1440045.

Martens, B., D. L. Schumacher, H. Wouters, J. Muñoz-Sabater, N. E. C. Verhoest, and D. G. Miralles, 2020: Evaluating the land-surface energy partitioning in ERA5. *Geosci. Model Dev.*, **13**, 4159–4181, https://doi.org/10.5194/gmd-13-4159-2020.

Massman, B., 2016a: FLUXNET2015 US-GBT Glees Brooklyn tower. FluxNet, USDA Forest Service, https://www.osti.gov/servlets/purl/1440118.

——, 2016b: FLUXNET2015 US-GLE Glees. FluxNet, USDA Forest Service, https://www.osti.gov/servlets/purl/1440069.

Matamala, R., 2016: FLUXNET2015 US-IB2 Fermi National Accelerator Laboratory- Batavia (Prairie site). FluxNet, Argonne National Laboratory, https://www.osti.gov/servlets/purl/1440072.

Matteucci, G., 2016: FLUXNET2015 IT-COL Collelongo. FluxNet, Istituto di Ecologia e Idrologia Forestale CNR, https://www.osti.gov/servlets/purl/1440167

McCaughey, H., 2016: FLUXNET2015 CA-GRO Ontario - Groundhog River, boreal mixedwood forest. FluxNet, Queen's University, https://www.osti.gov/servlets/purl/1440034.

Mearns, L. O., F. Giorgi, L. McDaniel, and C. Shields, 1995: Analysis of variability and diurnal range of daily temperature in a nested regional climate model: Comparison with observations and doubled $CO_2$ results. *Climate Dyn.*, **11**, 193–209, https://doi.org/10.1007/BF00215007.

Meier, R., E. L. Davin, S. C. Swenson, D. M. Lawrence, and J. Schwaab, 2019: Biomass heat storage dampens diurnal temperature variations in forests. *Environ. Res. Lett.*, **14**, 084026, https://doi.org/10.1088/1748-9326/ab2b4e.

Meinzer, F. C., G. Goldstein, N. M. Holbrook, P. Jackson, and J. Cavelier, 1993: Stomatal and environmental control of transpiration in a lowland tropical forest tree. *Plant Cell Environ.*, **16**, 429–436, https://doi.org/10.1111/j.1365-3040.1993.tb00889.x.

Merbold, L., K. Fuchs, N. Buchmann, and L. Hörtnagl, 2020: FLUXNET-CH4 CH-Cha Chamau. FluxNet, ETH Zurich, https://www.osti.gov/servlets/purl/1669629.

Meyer, W., P. Cale, G. Koerber, C. Ewenz, and Q. Sun, 2016: Fluxnet2015 AU-CPR Calperum. FluxNet;, University of Adelaide, https://www.osti.gov/servlets/purl/1440195/.

Meyers, T., 2016a: FLUXNET2015 US-GOO Goodwin creek. FluxNet, NOAA/ARL, https://www.osti.gov/servlets/purl/1440070/.

——, 2016b: FLUXNET2015 US-LWW little Washita watershed. FluxNet, NOAA/ARL, https://www.osti.gov/servlets/purl/1440077/.

Mildrexler, D. J., M. Zhao, and S. W. Running, 2011: A global comparison between station air temperatures and modis land surface temperatures reveals the cooling role of forests. *J. Geophys. Res.*, **116**, G03025, https://doi.org/10.1029/2010JG001486.

Miner, G. L., W. L. Bauerle, and D. D. Baldocchi, 2017: Estimating the sensitivity of stomatal conductance to photosynthesis: A review. *Plant Cell Environ.*, **40**, 1214–1238, https://doi.org/10.1111/pce.12871.

Montagnani, L., and S. Minerbi, 2016: FLUXNET2015 IT-REN renon. FluxNet, Autonomous Province of Bolzano, Forest Services, https://www.osti.gov/servlets/purl/1440173.

Moors, E., and J. Elbers, 2016: FLUXNET2015 NL-LOO Loobos. FluxNet, ALTERRA/Wageningen Environmental Research, https://www.osti.gov/servlets/purl/1440178.

Munger, J. W., 2016: FLUXNET2015 US-HA1 Harvard forest EMS tower (HFR1). FluxNet, Harvard University, https://www.osti.gov/servlets/purl/1440071.

Neirynck, J., H. Verbeeck, A. Carrara, A. S. Kowalski, R. Ceulemans, I. A. Janssens, B. Gielen, and M. Roland, 2016: FLUXNET2015 BE-Bra Brasschaat. FluxNet, University of Antwerp, https://doi.org/10.18140/FLX/1440128.

Nerry, F., J. Labed, and M.-P. Stoll, 1988: Emissivity signatures in the thermal IR band for remote sensing: Calibration procedure and method of measurement. *Appl. Opt.*, **27**, 758–764, https://doi.org/10.1364/AO.27.000758.

Norman, J. M., W. P. Kustas, and K. S. Humes, 1995: Source approach for estimating soil and vegetation energy fluxes in observations of directional radiometric surface temperature. *Agric. For. Meteor.*, **77**, 263–293, https://doi.org/10.1016/0168-1923(95)02265-Y.

Nouvellon, Y., 2016: FLUXNET2015 CG-Tch Tchizalamou. FluxNet, Centre de cooperation internationale en recherche agronomique pour le developpement, https://www.osti.gov/servlets/purl/1440142.

Novick, K., and R. Phillips, 2016: FLUXNET2015 US-MMS Morgan Monroe state forest. FluxNet, Indiana University, https://www.osti.gov/servlets/purl/1440083.

Nutini, F., M. Boschetti, G. Candiani, S. Bocchi, and P. Brivio, 2014: Evaporative fraction as an indicator of moisture condition and water stress status in semi-arid rangeland ecosystems. *Remote Sens.*, **6**, 6300–6323, https://doi.org/10.3390/rs6076300.

Olesen, J., 2016: FLUXNET2015 DK-Fou Foulum. FluxNet, Danish Institute of Agricultural Sciences, https://www.osti.gov/servlets/purl/1440154.

Ourcival, J.-M., K. Piquemal, R. Joffre, and L. Jean-Marc, 2016: FLUXNET2015 Fr-Pue puechabon. FluxNet, CNRS, https://www.osti.gov/servlets/purl/1440164.

Oyler, J. W., S. Z. Dobrowski, Z. A. Holden, and S. W. Running, 2016: Remotely sensed land skin temperature as a spatial predictor of air temperature across the conterminous United States. *J. Appl. Meteor. Climatol.*, **55**, 1441–1457, https://doi.org/10.1175/JAMC-D-15-0276.1.

Panwar, A., A. Kleidon, and M. Renner, 2019: Do surface and air temperatures contain similar imprints of evaporative

conditions? *Geophys. Res. Lett.*, **46**, 3802–3809, https://doi.org/10.1029/2019GL082248.

——, M. Renner, and A. Kleidon, 2020: Imprints of evaporative conditions and vegetation type in diurnal temperature variations. *Hydrol. Earth Syst. Sci.*, **24**, 4923–4942, https://doi.org/10.5194/hess-24-4923-2020.

Papale, D., and Coauthors, 2016: FLUXNET2015 IT-RO2 Roccarespampani 2. FluxNet, University of Tuscia - Viterbo, https://www.osti.gov/servlets/purl/1440175.

Pastorello, G., and Coauthors, 2020: The FLUXNET2015 dataset and the ONEFlux processing pipeline for eddy covariance data. *Sci. Data*, **7**, 225, https://doi.org/10.1038/s41597-020-0534-3.

Pendall, E., A. Griebel, D. Metzen, and C. Barton, 2016: FLUXNET2015 AU-Cum Cumberland Plains. FluxNet, Western Sydney University, https://www.osti.gov/servlets/purl/1440196.

Pilegaard, K., and A. Ibrom, 2016: FLUXNET2015 DK-Eng enghave. FluxNet, Technical University of Denmark (DTU), https://www.osti.gov/servlets/purl/1440153.

Pitman, A., and Coauthors, 2012: Effects of land cover change on temperature and rainfall extremes in multi-model ensemble simulations. *Earth Syst. Dyn.*, **3**, 213–231, https://doi.org/10.5194/esd-3-213-2012.

Poveda, F. D., A. L. Ballesteros, E. P. S. Cañete, P. S. Ortiz, M. R. M. Jiménez, O. P. Priego, and A. S. Kowalski, 2016: FLUXNET2015 ES-Amo Amoladeras. FluxNet, Estacion Experimental de Zona aridas (EEZA, CSIC), https://www.osti.gov/servlets/purl/1440156.

Pyrgou, A., M. Santamouris, and I. Livada, 2019: Spatiotemporal analysis of diurnal temperature range: Effect of urbanization, cloud cover, solar radiation, and precipitation. *Climate*, **7**, 89, https://doi.org/10.3390/cli7070089.

Reichstein, M., and Coauthors, 2005: On the separation of net ecosystem exchange into assimilation and ecosystem respiration: Review and improved algorithm. *Global Change Biol.*, **11**, 1424–1439, https://doi.org/10.1111/j.1365-2486.2005.001002.x.

Reverter, B. R., E. S. Perez-Canete, and A. S. Kowalski, 2016: FLUXNET2015 ES-LGS Laguna Seca. FluxNet, Universidad de Granada, https://www.osti.gov/servlets/purl/1440225.

Sabbatini, S., N. Arriga, B. Gioli, and D. Papale, M. Tomassucci, and A. Boschi, 2016a: FLUXNET2015 IT-CA2 Castel d'asso2. FluxNet, CNR IBIMET, University of Tuscia - Viterbo, https://www.osti.gov/servlets/purl/1440231.

——, ——, G. Matteucci, D. Papale, M. Tomassucci, and A. Boschi, 2016b: FLUXNET2015 IT-CA3 Castel d'asso 3. FluxNet, University of Tuscia - Viterbo, CNR IBAF, https://www.osti.gov/servlets/purl/1440232.

——, ——, D. Papale, M. Tomassucci, and A. Boschi, 2016c: FLUXNET2015 IT-CA1 Castel d'asso1. FluxNet, University of Tuscia - Viterbo, https://www.osti.gov/servlets/purl/1440230.

Sachs, T., C. Wille, E. Larmanou, and D. Franz, 2016: FLUXNET2015 DE-Zrk Zarnekow. FluxNet, GFZ German Research Centre for Geosciences, https://www.osti.gov/servlets/purl/1440221.

Saleska, S., 2016: FLUXNET2015 BR-SA1 Santarem-km67-primary forest. FluxNet, University of Arizona, https://www.osti.gov/servlets/purl/1440032.

Santanello, J. A., Jr., C. D. Peters-Lidard, and S. V. Kumar, 2011: Diagnosing the sensitivity of local land–atmosphere coupling via the soil moisture-boundary layer interaction. *J. Hydrometeor.*, **12**, 766–786, https://doi.org/10.1175/JHM-D-10-05014.1.

Schmidt, M., and A. Graf, 2016: FLUXNET2015 DE-RuR rollesbroich. FluxNet, IBG-3 Agrosphäre, Research Centre Jülich GmbH, https://www.osti.gov/servlets/purl/1440215.

Schneider, K., and M. Schmidt, 2016: FLUXNET2015 DE-SEH selhausen. FluxNet, University of Cologne, https://www.osti.gov/servlets/purl/1440217.

Scott, R., 2016a: FLUXNET2015 US-SRG Santa Rita Grassland. FluxNet, U.S. Department of Agriculture, https://www.osti.gov/servlets/purl/1440114.

——, 2016b: FLUXNET2015 US-SRM Santa Rita Mesquite. FluxNet, U.S. Department of Agriculture, https://www.osti.gov/servlets/purl/1440090.

——, 2016c: FLUXNET2015 US-Whs walnut gulch lucky hills shrub. FluxNet, U.S. Department of Agriculture, https://www.osti.gov/servlets/purl/1440097.

——, 2016d: FLUXNET2015 US-WKg Walnut Gulch Kendall grasslands. FluxNet, U.S. Department of Agriculture, https://www.osti.gov/servlets/purl/1440096.

Shi, P., X. Zhang, and Y. He, 2016: FLUXNET2015 Cn-Dan Dangxiong. FluxNet, IGSNRR Chinese Academy of Sciences, https://www.osti.gov/servlets/purl/1440138.

Sigut, L., K. Havrankova, G. Jocher, M. Pavelka, D. Janouš, K. Stanik, J. Trusina, and R. Czerny, 2016: FLUXNET2015 CZ-BK2 Bily Kriz grassland. FluxNet, Global Change Research Institute CAS, https://www.osti.gov/servlets/purl/1440144.

Simmons, A., and Coauthors, 2021: Low frequency variability and trends in surface air temperature and humidity from ERA5 and other datasets. Tech. Memo. 881, European Centre for Medium-Range Weather Forecasts, 99 pp., https://www.ecmwf.int/sites/default/files/elibrary/2021/19911-low-frequency-variability-and-trends-surface-air-temperature-and-humidity-era5-and-other.pdf.

Spano, D., and Coauthors, 2016: FLUXNET2015 IT-Noe arca di noe - le prigionette. FluxNet, University of Sassari, CNR-Ibimet Sassari, https://www.osti.gov/servlets/purl/1440171.

Stone, D. A., and A. J. Weaver, 2002: Daily maximum and minimum temperature trends in a climate model. *Geophys. Res. Lett.*, **29**, 1356, https://doi.org/10.1029/2001GL014556.

Stull, R. B., and Coauthors, 2015: *Practical Meteorology: An Algebra-Based Survey of Atmospheric Science.* University of British Columbia, 940 pp., https://www.eoas.ubc.ca/books/Practical_Meteorology/.

Sturtevant, C., D. Szutu, D. Baldocchi, J. H. Matthes, P. Oikawa, and S. D. Chamberlain, 2016: FLUXNET2015 US-MyB mayberry wetland. FluxNet, University of California, Berkeley, https://www.osti.gov/servlets/purl/1440105.

Su, Z., 2002: The Surface Energy Balance System (SEBS) for estimation of turbulent heat fluxes. *Hydrol. Earth Syst. Sci.*, **6**, 85–100, https://doi.org/10.5194/hess-6-85-2002.

Sun, Z., Q. Wang, O. Batkhishig, and Z. Ouyang, 2016: Relationship between evapotranspiration and land surface temperature under energy- and water-limited conditions in dry and cold climates. *Adv. Meteor.*, **2016**, 1835487, https://doi.org/10.1155/2016/1835487.

Suyker, A., 2016a: FLUXNET2015 US-Ne1 mead - irrigated continuous maize site. FluxNet, University of Nebraska, Lincoln, https://www.osti.gov/servlets/purl/1440084.

——, 2016b: FLUXNET2015 US-Ne2 mead - irrigated maize-soybean rotation site. FluxNet, University of Nebraska, Lincoln, https://www.osti.gov/servlets/purl/1440085.

——, 2016c: FLUXNET2015 US-Ne3 mead - rainfed maize-soybean rotation site. FluxNet, University of Nebraska, Lincoln, https://www.osti.gov/servlets/purl/1440086.

Swenson, S. C., S. P. Burns, and D. M. Lawrence, 2019: The impact of biomass heat storage on the canopy energy balance and atmospheric stability in the Community Land Model.

*J. Adv. Model. Earth Syst.*, **11**, 83–98, https://doi.org/10.1029/2018MS001476.

Tagesson, T., J. Ardö, and R. Fensholt, 2016: FLUXNET2015 SN-Dhr Dahra. FluxNet, Lund University, https://www.osti.gov/servlets/purl/1440246.

Thome, K., 2014: ASTER global emissivity database: 100 times more detailed than its predecessors. NASA, https://terra.nasa.gov/news/aster-global-emissivity-database-100-times-more-detailed-than-its-predecessors.

Torn, M., 2016a: FLUXNET2015 US-ARb ARM Southern Great Plains burn site- lamont. FluxNet, Lawrence Berkeley National Laboratory, https://osti.gov/servlets/purl/1440064.

——, 2016b: FLUXNET2015 US-ARc ARM Southern Great Plains control site- lamont. FluxNet, Lawrence Berkeley National Laboratory, https://www.osti.gov/servlets/purl/1440065.

Trigo, I. F., L. F. Peres, C. C. DaCamara, and S. C. Freitas, 2008: Thermal land surface emissivity retrieved from SEVIRI/Meteosat. *IEEE Trans. Geosci. Remote Sens.*, **46**, 307–315, https://doi.org/10.1109/TGRS.2007.905197.

——, and Coauthors, 2011: The Satellite Application Facility for Land Surface Analysis. *Int. J. Remote Sens.*, **32**, 2725–2744, https://doi.org/10.1080/01431161003743199.

Urraca, R., T. Huld, A. Gracia-Amillo, F. J. Martinez-de Pison, F. Kaspar, and A. Sanz-Garcia, 2018: Evaluation of global horizontal irradiance estimates from ERA5 and COSMO-REA6 reanalyses using ground and satellite-based data. *Sol. Energy*, **164**, 339–354, https://doi.org/10.1016/j.solener.2018.02.059.

Valentini, R., S. Dore, F. Mazzenga, S. Sabbatini, P. Stefani, G. Tirone, and D. Papale, 2016a: FLUXNET2015 IT-Cpz Castelporziano. FluxNet, University of Tuscia - Viterbo, https://www.osti.gov/servlets/purl/1440168.

——, G. Nicolini, P. Stefani, A. De Grandcourt, and S. Stivanello, 2016b: FLUXNET2015 GH-Ank Ankasa. FluxNet, Euro Mediterranean Center for Climate Change - Viterbo, University of Tuscia - Viterbo, https://www.osti.gov/servlets/purl/1440229

——, and Coauthors, 2016c: FLUXNET2015 IT-Ro1 roccarespampani 1. FluxNet, University of Tuscia - Viterbo, https://www.osti.gov/servlets/purl/1440174.

Valor, E., and V. Caselles, 1996: Mapping land surface emissivity from NDVI: Application to European, African, and South American areas. *Remote Sens. Environ.*, **57**, 167–184, https://doi.org/10.1016/0034-4257(96)00039-9.

Varlagin, A., J. Kurbatova, and N. Vygodskaya, 2016: FLUXNET2015 RU-Fyo Fyodorovskoye. FluxNet, A.N. Severtsov Institute of Ecology and Evolution, https://www.osti.gov/servlets/purl/1440183.

Wang, H., and X. Fu, 2016: FLUXNET2015 CN-Qia Qianyanzhou. FluxNet, IGSNRR Chinese Academy of Sciences, https://www.osti.gov/servlets/purl/1440141.

Wang, K., and R. E. Dickinson, 2012: A review of global terrestrial evapotranspiration: Observation, modeling, climatology, and climatic variability. *Rev. Geophys.*, **50**, RG2005, https://doi.org/10.1029/2011RG000373.

Wang, X., and C. Prigent, 2020: Comparisons of diurnal variations of land surface temperatures from numerical weather prediction analyses, infrared satellite estimates and in situ measurements. *Remote Sens.*, **12**, 583, https://doi.org/10.3390/rs12030583.

Whitehead, D., P. G. Jarvis, and R. H. Waring, 1984: Stomatal conductance, transpiration, and resistance to water uptake in a *Pinus sylvestris* spacing experiment. *Can. J. For. Res.*, **14**, 692–700, https://doi.org/10.1139/x84-124.

Wohlfahrt, G., A. Hammerle, and L. Hörtnagl, 2016: FLUXNET2015 AT-NEU Neustift. FluxNet, University of Innsbruck, https://www.osti.gov/servlets/purl/1440121.

Wolf, S., W. Eugster, and N. Buchmann, 2016a: FLUXNET2015 Pa-Spn Sardinilla plantation. FluxNet, ETH Zurich, https://www.osti.gov/servlets/purl/1440180.

——, ——, and ——, 2016b: FLUXNET2015 Pa-Sps Sardinilla-Pasture. FluxNet, ETH Zurich, https://www.osti.gov/servlets/purl/1440179.

Woodgate, W., E. Van Gorsel, and R. Leuning, 2016: FLUXNET2015 AU-Tum Tumbarumba. FluxNet, CSIRO, https://www.osti.gov/servlets/purl/1440126.

Wouters, H., I. Y. Petrova, C. C. Heerwaarden, J. Vila-Guerau de Arellano, A. J. Teuling, V. Meulenberg, J. A. Santanello, and D. G. Miralles, 2019: Atmospheric boundary layer dynamics from balloon soundings worldwide: CLASS4GL v1.0. *Geosci. Model Dev.*, **12**, 2139–2153, https://doi.org/10.5194/gmd-12-2139-2019.

Zhang, J., and S. Han, 2016: FLUXNET2015 CN-Cha changbaishan. FluxNet, IAE Chinese Academy of Sciences, https://www.osti.gov/servlets/purl/1440137.

Zhang, W., Y. Huang, Y. Yu, and W. Sun, 2011: Empirical models for estimating daily maximum, minimum and mean air temperatures with MODIS land surface temperatures. *Int. J. Remote Sens.*, **32**, 9415–9440, https://doi.org/10.1080/01431161.2011.560622.

Zhou, G., and J. Yan, 2016: FLUXNET2015 CN-Din Dinghushan. FluxNet, SCIB Chinese Academy of Sciences, https://www.osti.gov/servlets/purl/1440139.

Zhou, L., R. E. Dickinson, Y. Tian, R. S. Vose, and Y. Dai, 2007: Impact of vegetation removal and soil aridation on diurnal temperature range in a semiarid region: Application to the Sahel. *Proc. Natl. Acad. Sci. USA*, **104**, 17 937–17 942, https://doi.org/10.1073/pnas.0700290104.

——, A. Dai, Y. Dai, R. S. Vose, C.-Z. Zou, Y. Tian, and H. Chen, 2009: Spatial dependence of diurnal temperature range trends on precipitation from 1950 to 2004. *Climate Dyn.*, **32**, 429–440, https://doi.org/10.1007/s00382-008-0387-5.

# Chapter 6

# Synthesis

This chapter first summarizes the key findings from the preceding chapters via answering the three research questions raised in the objectives. Next, limitations and the interpretations of the results are discussed in the context of the broader research, literature and their implications. Finally, based on the results and discussion last section outlines the key outcomes of the study in reference to future prospects and research directions.

## 6.1 Main findings

The study found that surface and air temperature respond quite differently to changes in evaporative conditions and vegetation types and these responses can be justified by fundamental physical constraints. Responses of surface and air temperature were quantified in terms of diurnal warming rates and DTR. In order to accomplish our three objectives the analyses was extended from a single FLUXNET site to multiple FLUXNET sites and finally to global scale using ERA5 reanalysis data. The main findings of the thesis objectives are summarised as the followings:

- Does diurnal surface and air temperature variation respond differently to changes in evaporative conditions, if so why?

  Yes, the diurnal variation of surface and air temperature respond differently to changes in evaporative conditions. The findings of chapter 3 suggests that the warming rate of surface temperature decreases strongly by about $14 \times 10^{-3} K (Wm^{-2})^{-1}$, whereas warming rate of air temperature only by about $1.7 \times 10^{-3} K (Wm^{-2})^{-1}$. This study was conducted for a cropland ecosystem to capture the first order responses. Boundary layer height observation shows strong increase in PBL height on dry days. It was hypothesized that the diurnal variation of boundary layer height compensates for the warming of air temperature. The growth in boundary layer height increases its heat capacity such that the higher heat on dry day distributes in a larger volume, resulting in lower diurnal amplitude of air temperature. To illustrate this, a sensitivity experiment of air temperature to boundary layer growth using a simple

planetary boundary layer model was employed. In the absence of the boundary layer diurnal variation, air temperature would have similar warming rates as of surface temperature.

- How do these responses vary across vegetation types?

  Based on the findings of chapter 4 the aerodynamic conductance of vegetation impacts the diurnal warming of surface and air temperature and their responses to evaporation quite differently. In short vegetation (23 FLUXNET sites), the warming rate of surface temperature decreases strongly by about $23 \times 10^{-3} K (Wm^{-2})^{-1}$, similar to the findings of chapter 3. However, surface temperature warming rate in forests (19 FLUXNET sites), decreases weakly by about $4 \times 10^{-3} K (Wm^{-2})^{-1}$ on days with higher evaporative fraction. To explain this, a simple surface energy model was developed that demonstrates the dominant role of the aerodynamic conductance of forest in cooling temperatures. Based on the observational analysis and model based findings, it is concluded that the variability in evaporative conditions does not influence diurnal surface temperature because their high aerodynamic conductance causes the maximum cooling. On multiplying these responses with the maximum solar radiation, these responses can be interpreted in terms of reduced $DTR$. Using this model a sensitivity analyses of $DT_sR$ to solar radiation, evaporative fraction and aerodynamic conductance was presented to illustrate their individual contributions.

- What are the dominant physical constraints that shape the diurnal variation of surface and air temperatures?

  Findings from chapter 3 and chapter 4 demonstrate different mechanisms shaping diurnal variation of surface and air temperature. These approaches were further developed in chapter 5 to create two simple models, SABL for $DT_aR$ and SSEB for $DT_sR$, based on fundamental physical constraints. Here the responses of surface and air temperatures were quantified in terms of $DTR$ that is the product of warming rate and solar radiation. The responses of $DTR$ to changes in evaporative fraction and vegetation types were similar to the findings of chapter 3 and chapter 4. In short vegetation (63 FLUXNET sites), $DT_sR$ decreases by 30 K in response to increase in evaporative fraction, whereas in forest (79 FLUXNET sites) only by 10 K. $DT_aR$ however, decreases only by 10 K and these responses were found very similar in all vegetation. SABL model shows that $DT_aR$ response to evaporative cooling is mainly constrained by the solar radiation and boundary layer dynamics but not by aerodynamic conductance of vegetation. SSEB model shows that $DT_sR$ on the other hand is a function of solar radiation, aerodynamic conductance and evaporative conditions. Both the models reproduces $DTR$ sensitivities to solar

radiation, vegetation and evaporative fraction in FLUXNET and ERA5 reanalysis data.

## 6.2   Limitations

The estimates of warming rate depend on hourly to sub-hourly values of temperatures, that are often not available or computationally expensive to obtain when extended to global scale. Although, this limitation can be resolved by using $DTR$ that requires only daily maximum and minimum temperatures. When using $DTR$ it is assumed that surface and air temperatures are in phase with solar radiation. However, generally the maximum of air temperature occurs in the afternoon and maximum of surface temperature around solar noon. Not accounting for phase differences can lead to some deviations when approximating warming rates from $DTR$ and vice versa.

Calculation of the warming rate is also sensitive to clouds that reduces the daytime solar radiation. Short duration cloudy events can alter the linear relationship between temperature and solar radiation, which would eventually influence the warming rate. In chapter 3 and chapter 4 cloudy days were excluded from the analyses. However, in chapter 5 $DTR$ and its sensitivity to evaporation were obtained for all sky conditions. Despite this, the findings in chapter 3, chapter 4 and chapter 5 were in agreement to each other, indicating that during daytime the cooling effect of clouds can be indirectly accounted through reduced solar radiation. Our models can be further improved in order to include the warming effect of clouds especially on minimum temperatures.

To understand the role of boundary layer height in shaping diurnal variation of air temperature the observations of boundary layer heights are required. Currently, at FLUXNET sites PBL observations are limited. In chapter 3 and chapter 5 it is shown that PBL height decreases by about 2000 meters in response to increase in evaporative fraction. However, one can approximate PBL height from $DT_aR$ and lapse rate of potential temperature of free atmosphere that is similar across vegetation types. These calculation were based on ERA5 that is a model but not observations. It should also be considered that ERA5 is not independent of systematic biases related to energy, heat and water fluxes.

Our SABL and SSEB models are rather simple but can reproduce the observed sensitivities of diurnal surface and air temperature to evaporative conditions and solar radiation quite well. In SABL model we quantify the heat storage in the PBL based on maximum power. It is assumed that only heat released in form of sensible heat flux is stored in the atmosphere, however in reality PBL moisture and cloud condensation can also influence

the heat storage differently. Similarly, the responses in SSEB model are sensitive to the aerodynamic conductance of vegetation, and calculation of aerodynamic conductance is not easy to obtain for a typical weather station.

In this thesis I also compare FLUXNET based findings with those obtained from ERA5 reanalysis. In general, both the datasets agree with the sensitivities of diurnal variation of surface and air temperature to evaporation. The slight overestimation of ERA5 is due to its $DTR$ biases on dry and wet conditions. However, one needs to take into account that ERA5 is derived from a model, whereas FLUXNET is observation. Additionally, ERA5 represent blended information in larger area (31 km) whereas FLUXNET represent the local information. Similar local and regional scale conversion issue might influence the IGBP vegetation classification that was used in chapter 4 and chapter 5.

## 6.3    Interpretations and implications

This research uses a robust index called warming rate to quantify the diurnal variation of temperatures using their half-hourly morning to noon variation in response to solar radiation. It is shown that the morning to afternoon warming of surface and air temperature are mainly controlled by solar radiation and variation of warming rate can provide useful insights on evaporation, vegetation and planetary boundary layer dynamics. The diurnal observations of temperature, in combination with boundary layer modelling have been used before to approximate surface energy partitioning (Betts, 1992; Betts and Ball, 1995; Santanello Jr et al., 2009; Gentine et al., 2016). However, warming rate is different since it normalizes the warming effect of solar radiation and enables the comparison of regions receiving different solar energy input. Alternatively, $DTR$ can be used but it contains the information on solar radiation, therefore, it shall be interpreted discreetly while carrying out a global analysis. In this thesis, a first order approximation of $DTR$ from warming rate is shown that accounts for the relation of $DTR$ and solar radiation.

The Warming rate of surface and air temperature usually decreases due to evaporative cooling and these responses are quite consistent across multiple FLUXNET sites. Data analysis and SSEB model shows that the surface temperature responses to evaporative condition are reasonably distinctive across vegetation types. In short vegetation, it reduces strongly in response to evaporative fraction, suggesting that evaporative cooling is the dominant cooling agent. This also indicates that surface temperature in short vegetation can be a good indicator of evaporative conditions. This notion has been addressed in previous studies that were attributed to the relationship of radiometric surface temperatures and evaporation (Kustas and Norman, 1996; Mu et al., 2007; Kalma, McVicar,

and McCabe, 2008). This thesis elaborates for the physical mechanism leading to their relationship. Based on these findings one can conclude that surface temperature is a better proxy for evaporation than air temperature as also mentioned by Su, 2002.

Contrarily, in forest the diurnal variation of surface temperature respond weakly to evaporative fraction. Usually, the lower surface temperature in forest is associated to their higher rate of evaporation. Our findings and the sensitivity analysis using SSEB model shows that lower diurnal variation of surface temperature in forest is mainly due to their high aerodynamic conductance, whereas evaporative cooling is the secondary cause. Therefore, it can be speculated that the warming in the event of deforestation is mainly connected to the reduced aerodynamic conductance leading to changes in biophysical properties rather than decreased evaporation, as also argued by previous studies (Bright et al., 2017; Chen and Dirmeyer, 2016; Tang, Zhao, and Zhao, 2018). The high aerodynamic conductance could also be one of the contributing factor for the tolerance of tall vegetation to drought, in addition to their shading effect and deep root system (Kleidon and Heimann, 1998; Teuling et al., 2010; Bevan, Los, and North, 2014).

Besides the mean aerodynamic conductance of vegetation, its sensitivity to solar radiation was also noted to have an impact on the diurnal variation of surface temperature. However, the relative sensitivity of aerodynamic conductance to solar radiation were found similar across vegetation types. This enhancement is apparently connected to greater buoyancy of the air parcels during the noon. The complexity in obtaining aerodynamic conductance and its diurnal behaviour is discussed in previous researches (Roberts, Cabral, and De Aguiar, 1990; Tan et al., 2019; Trebs et al., 2015; Mallick et al., 2016). Overall, aerodynamic conductance is not purely a vegetation characteristics and it might also contain information on surface energy conversion. Further investigation on their relationship could benefit the understanding of controlling environment factors that explain the aerodynamic conductance.

Our findings show that the diurnal variation of air temperature respond weakly to changes in evaporative conditions and moreover similarly across vegetation types. These responses are quite consistent in FLUXNET sites across vegetation, and global ERA5 reanalysis data. Historically, air temperature products have been used to approximate evaporation (Blaney et al., 1952; Hargreaves and Samani, 1985). But my findings support that, the imprints of evaporation in diurnal variation of air temperature is reduced by the compensating effects of diurnal growth of boundary layer height. This hypothesis is novel, but is implicitly included in earlier studies while discussing the controls of energy partitioning in shaping PBL height (Dirmeyer and Brubaker, 2007; Koster et al., 2006;

Green et al., 2017; Gentine et al., 2019). Here, the impact of this mechanism is quantified and modelled for diurnal varaition of air temperature. To support this argument, SABL model quantifies the impact of boundary layer dynamics in weakening air temperature's response to evaporative conditions.

In the SABL model, the boundary layer growth and its relation to $DT_a R$ is expressed in terms of $\Gamma_\theta$ that has similar values (calculated using ERA5) across vegetation types. This indicates that the boundary layer responses to energy partitioning is insensitive to vegetation characteristics. Certainly, mean values of air temperature depends on vegetation properties but these insights should be considered when using diurnal variation of air temperature as an index of deforestation. Based on the sensitivies of the SSEB and the SABL models, it can be speculated that surface and air temperatures would response differently to deforestation, that is also in agreement with the findings of the recent studies by Schultz, Lawrence, and Lee, 2017 and Winckler et al., 2019.

Differences between diurnal variation of surface and air temperature is also important while using them as proxy of each other (Zhang et al., 2011; Oyler et al., 2016). Surface and air temperature are similar in the morning when the turbulent heat fluxes are minimum (Panwar, Kleidon, and Renner, 2019; Good et al., 2017), but their maximum values during noon depends on the turbulent heat flux partitioning and vegetation types. Similar to our findings, Mildrexler, Zhao, and Running, 2011 showed decoupling between surface and air temperature on days with higher solar radiation. In this thesis it is explained that this decoupling is mainly due to higher sensible heat flux that on one hand increases the surface temperature, but on the other hand also increases the boundary layer height and hence suppresses the warming of air temperature. Li et al., 2015, explained that high evaporation in the forest results in similar values of surface and air temperature. However, findings from chapter 4 and chapter 5 suggests that the strong coupling of surface and air temperature in forest is mainly due to its high aerodynamic conductance, and this coupling would remain persistent even in dry conditions.

To summarise, the findings of this thesis has several implications in understanding the land atmosphere system from diurnal variation of temperatures. First, the diurnal variation of air temperature shall not be used to infer evaporation and to access the impact of land use land cover changes, since it is strongly adjusted by the boundary layer dynamics. Diurnal variation of air temperature however can be a useful tool to investigate the PBL heat storage and boundary layer dynamics. Second, the diurnal variation of surface temperature holds important information on evaporation but only in short vegetation types. In forest, the aerodynamic conductance is the dominant

cooling factor whereas evaporation is secondary. These physical constraints shall be considered particularly when using surface and air temperature in quantifying the impact of deforestation and draught.

## 6.4 Future prospects

The fact that surface and air temperature respond differently to evaporative cooling has several future prospects. Their different physical constraints suggest that responses of surface and air temperatures to global climate changes can be also different. Our simple SSEB and SABL model can be further used in obtaining their first order sensitivities, specially to changes in solar radiation, evaporation and vegetation types. These fundamental models could further be developed to include the impact of greenhouse warming by incorporating the information on atmospheric moisture and emissivity. I think to understand the longwave heating and greenhouse effect one can look into evening warming rate. I speculate that evening warming rates will be lower for moist and warm environment. The whole concept of warming rate is based on incoming solar radiation being the main driver of diurnal temperature. One can change the x-axis in figure 2.1 with longwave radiation to understand how temperature respond to other components of surface energy balance.

Going forward, temperature sensitivities to evaporation and vegetation obtained in this thesis can be applied and compared to global satellite observations, reanalysis data and different climate model outputs. In my research surface temperature is derived from upwelling longwave radiation that might have some drawbacks. This can be verified with the surface temperature data estimated from satellites. Since the estimation of LST in satellite products depend on the albedo, the vegetation cover and the soil moisture one can formulate these sensitivities from the methodology used in developing these products.

Our findings show quite consistent increase in surface temperature warming rates on dry days, specially in croplands. Given the high expansion of agricultural land, the impact of these responses in altering local and global climate can be investigated. High surface temperature results in increased erosion, soil drying, increased runoff and nutrient losses (DeBano, Rice, and Eugene, 1979). One strategic measure is the dissipation of solar radiation into evaporation that would keep the surroundings near agricultural field cool. Our findings imply that the diurnal variation of surface temperature can be used as an indicator of draught and water stress. Eventually, monitoring surface temperature warming rates and its spatial variation can support landscape management and help in

determining the impacts of extremes on crop yields.

Even though weak responses of diurnal temperature variations to evaporation were reported in forest, it is still intriguing to determine what does it signify on the importance of forest's structure. Clearly, evaporation and aerodynamic conductance of forest are associated but using our SSEB model one can evaluate their individual contributions in cooling surface and air temperatures. This approach can be extended towards time based trend analyses of regions witnessing events of deforestation and afforestation. Moreover, the high aerodynamic conductance of forest cools the surface temperature but at the expense of heating the atmosphere. It is certainly stimulating to uncover how this process would effect the vertical energy transport and water cycle in the atmosphere. To explore these unknowns one can potentially use vertical profiles of meteorological variables retrieved from radiosondes in combination with the surface flux observations.

One of the important aspects highlighted in our study was the potential use of FLUXNET data to capture the footprints of land atmosphere interaction in ecosystem scales. In regard to this, a recent research by Horst et al., 2019 have discussed the representation of measurements of surface fluxes and responses of vegetation during temperature extremes, which were otherwise heavily depended on climate models (Eyring et al., 2016). Based on our findings, vegetation's response to changing climate can be estimated using different sets of FLUXNET sites spread across different evaporative and vegetation regimes. In future, this approach can be better validated for individual sites by including information on the site specific sensor's height, main research objective and observation's standards. Previous studies have found that lower sensor heights reduced the energy flux footprint significantly (Haniff et al., 2018; Chen et al., 2009). Collaboration among different FLUXNET regional network and principal investigator of sites would benefit in accomplishing this goal.

Findings from chapter 5 shows the relationship of diurnal surface and air temperature variation to solar radiation. The SSEB model and the SABL model found that the sensitivity of temperatures to evaporation and deforestation increases in region with high solar radiation. Based on these findings one would expect stronger changes in temperatures in tropics than in high latitudes. Previous studies based on climate model simulations (Davin and Noblet-Ducoudré, 2010; Pitman et al., 2012; Lawrence et al., 2012; Li et al., 2018; Chen, Liang and Dirmeyer, 2019) also found similar results. Using our physical models, the first order contribution of deforestation-induced dryness and its relation to solar radiation can be analyzed to understand the physical mechanisms of the responses observed in the previous studies (Claussen, Brovkin, and Ganopolski, 2001; Brovkin

et al., 2006; Mahmood et al., 2014; Longobardi et al., 2016).

Finally, the diurnal variation of surface and air temperature contains unique information on land atmosphere processes. They are associated to each other and are dominantly constrained by the surface and atmospheric energy balance but respond quite differently to variation in evaporative conditions and vegetation types. Fundamental physical approaches presented in this thesis allows for the interpretation of their diurnal variation in understanding these processes, that mainly include boundary layer dynamics, aerodynamic conductance and evaporative cooling. The growing use of remotely sensed surface temperature over air temperature is visible in current studies related to land use and land cover change. Meanwhile, global values of air temperature is an equally crucial input variable for climate and weather forecast models. Therefore, both, surface and air temperatures, are essential variables for climate science. Further understanding of their diurnal variation requires more research in order to gain a better understanding of their responses to global change and its consequences on climate system.

# Bibliography

Anderson, Martha C et al. (2012). "Use of Landsat thermal imagery in monitoring evapotranspiration and managing water resources". In: *Remote Sensing of Environment* 122, pp. 50–65.

Baldocchi, Dennis et al. (2001). "FLUXNET: A new tool to study the temporal and spatial variability of ecosystem-scale carbon dioxide, water vapor, and energy flux densities". In: *Bulletin of the American Meteorological Society* 82.11, pp. 2415–2434.

Barnett, Tim P et al. (1999). "Detection and attribution of recent climate change: A status report". In: *Bulletin of the American Meteorological Society* 80.12, pp. 2631–2660.

Barry, Roger Graham (1992). *Mountain weather and climate*. Psychology Press.

Benali, A et al. (2012). "Estimating air surface temperature in Portugal using MODIS LST data". In: *Remote Sensing of Environment* 124, pp. 108–121.

Betts, AK (1992). "FIFE atmospheric boundary layer budget methods". In: *Journal of Geophysical Research: Atmospheres* 97.D17, pp. 18523–18531.

Betts, Alan K and JH Ball (1995). "The FIFE surface diurnal cycle climate". In: *Journal of Geophysical Research: Atmospheres* 100.D12, pp. 25679–25693.

Betts, Alan K and John H Ball (1997). "Albedo over the boreal forest". In: *Journal of Geophysical Research: Atmospheres* 102.D24, pp. 28901–28909.

Bevan, SL, SO Los, and PRJ North (2014). "Response of vegetation to the 2003 European drought was mitigated by height". In: *Biogeosciences* 11.11, pp. 2897–2908.

Biraud, Sebastien et al. (2016). *FLUXNET2015 US-ARM ARM Southern Great Plains site-Lamont*. Tech. rep. FluxNet; Lawrence Berkeley National Lab.(LBNL), Berkeley, CA (United States).

Blaney, Harry French et al. (1952). "Determining water requirements in irrigated areas from climatological and irrigation data". In.

Boisier, JP et al. (2012). "Attributing the impacts of land-cover changes in temperate regions on surface temperature and heat fluxes to specific causes: Results from the first LUCID set of simulations". In: *Journal of Geophysical Research: Atmospheres* 117.D12.

Bonan, Gordon (2015). *Ecological climatology: concepts and applications*. Cambridge University Press.

Bonan, Gordon B (2008). "Forests and climate change: forcings, feedbacks, and the climate benefits of forests". In: *science* 320.5882, pp. 1444–1449.

Braganza, Karl, David J Karoly, and Julie M Arblaster (2004). "Diurnal temperature range as an index of global climate change during the twentieth century". In: *Geophysical research letters* 31.13.

Bright, Ryan M et al. (2017). "Local temperature response to land cover and management change driven by non-radiative processes". In: *Nature Climate Change* 7.4, pp. 296–302.

Bristow, Keith L and Gaylon S Campbell (1984). "On the relationship between incoming solar radiation and daily maximum and minimum temperature". In: *Agricultural and forest meteorology* 31.2, pp. 159–166.

Brovkin, Victor et al. (2006). "Biogeophysical effects of historical land cover changes simulated by six Earth system models of intermediate complexity". In: *Climate Dynamics* 26.6, pp. 587–600.

Buma, B and CA Wessman (2013). "Forest resilience, climate change, and opportunities for adaptation: a specific case of a general problem". In: *Forest Ecology and Management* 306, pp. 216–225.

Camillo, PJ, RJ Gurney, and TJ Schmugge (1983). "A soil and atmospheric boundary layer model for evapotranspiration and soil moisture studies". In: *Water Resources Research* 19.2, pp. 371–380.

Cellier, Pierre, G Richard, and P Robin (1996). "Partition of sensible heat fluxes into bare soil and the atmosphere". In: *Agricultural and forest meteorology* 82.1-4, pp. 245–265.

Chen, Baozhang et al. (2009). "Assessing tower flux footprint climatology and scaling between remotely sensed and eddy covariance measurements". In: *Boundary-Layer Meteorology* 130.2, pp. 137–167.

Chen, Liang and Paul A Dirmeyer (2016). "Adapting observationally based metrics of biogeophysical feedbacks from land cover/land use change to climate modeling". In: *Environmental Research Letters* 11.3, p. 034002.

Chen, Liang and Paul A Dirmeyer (2019). "The relative importance among anthropogenic forcings of land use/land cover change in affecting temperature extremes". In: *Climate Dynamics* 52.3, pp. 2269–2285.

Claussen, Martin, Victor Brovkin, and Andrey Ganopolski (2001). "Biogeophysical versus biogeochemical feedbacks of large-scale land cover change". In: *Geophysical research letters* 28.6, pp. 1011–1014.

Collins, Fred C (1995). "A comparison of spatial interpolation techniques in temperature estimation". PhD thesis. Virginia Tech.

Copernicus (2019). *Surface air temperature maps*. URL: https://climate.copernicus.eu/surface-air-temperature-maps (visited on 05/05/2020).

Crago, Richard D (1996). "Conservation and variability of the evaporative fraction during the daytime". In: *Journal of Hydrology* 180.1-4, pp. 173–194.

Culf, AD, G Fisch, and MG Hodnett (1995). "The albedo of Amazonian forest and ranch land". In: *Journal of Climate* 8.6, pp. 1544–1554.

Dai, Aiguo, Kevin E Trenberth, and Thomas R Karl (1999). "Effects of clouds, soil moisture, precipitation, and water vapor on diurnal temperature range". In: *Journal of Climate* 12.8, pp. 2451–2473.

Davies, F, DR Middleton, and KE Bozier (2007). "Urban air pollution modelling and measurements of boundary layer height". In: *Atmospheric environment* 41.19, pp. 4040–4049.

Davin, Edouard L and Nathalie de Noblet-Ducoudré (2010). "Climatic impact of global-scale deforestation: Radiative versus nonradiative processes". In: *Journal of Climate* 23.1, pp. 97–112.

DeBano, Leonard F, Raymond M Rice, and Conrad C Eugene (1979). "Soil heating in chaparral fires: effects on soil properties, plant nutrients, erosion, and runoff". In: *Res. Paper PSW-RP-145. Berkeley, CA: US Department of Agriculture, Forest Service, Pacific Southwest Forest and Range Experiment Station. 21 p* 145.

Devaraju, N et al. (2018). "Quantifying the relative importance of direct and indirect biophysical effects of deforestation on surface temperature and teleconnections". In: *Journal of Climate* 31.10, pp. 3811–3829.

Dickinson, Robert E and Ann Henderson-Sellers (1988). "Modelling tropical deforestation: A study of GCM land-surface parametrizations". In: *Quarterly Journal of the Royal Meteorological Society* 114.480, pp. 439–462.

Dirmeyer, Paul A and Kaye L Brubaker (2007). "Characterization of the global hydrologic cycle from a back-trajectory analysis of atmospheric water vapor". In: *Journal of Hydrometeorology* 8.1, pp. 20–37.

Eliasson, Ingegärd (1990). "Urban geometry, surface temperature and air temperature". In: *Energy and buildings* 15.1-2, pp. 141–145.

Ellison, David et al. (2017). "Trees, forests and water: Cool insights for a hot world". In: *Global Environmental Change* 43, pp. 51–61.

Eltahir, Elfatih AB (1998). "A soil moisture–rainfall feedback mechanism: 1. Theory and observations". In: *Water resources research* 34.4, pp. 765–776.

Emamifar, Saeed, Ali Rahimikhoob, and Ali Akbar Noroozi (2013). "Daily mean air temperature estimation from MODIS land surface temperature products based on M5 model tree". In: *International Journal of Climatology* 33.15, pp. 3174–3181.

ESA (2020). "Land Surface Temperature". In: URL: https://climate.esa.int/en/projects/land-surface-temperature.

Eyring, Veronika et al. (2016). "Overview of the Coupled Model Intercomparison Project Phase 6 (CMIP6) experimental design and organization". In: *Geoscientific Model Development* 9.5, pp. 1937–1958.

Feddes, Reinder A et al. (2001). "Modeling root water uptake in hydrological and climate models". In: *Bulletin of the American meteorological society* 82.12, pp. 2797–2810.

Federer, CA (1968). "Spatial variation of net radiation, albedo and surface temperature of forests". In: *Journal of Applied Meteorology and Climatology* 7.5, pp. 789–795.

Ferrare, Richard (2012). *Raman lidar/AERI PBL Height Product*. Tech. rep. Oak Ridge National Lab.(ORNL), Oak Ridge, TN (United States). Atmospheric . . .

Findell, Kirsten L and Elfatih AB Eltahir (2003). "Atmospheric controls on soil moisture–boundary layer interactions. Part I: Framework development". In: *Journal of Hydrometeorology* 4.3, pp. 552–569.

Findell, Kirsten L, Thomas R Knutson, and PCD Milly (2006). "Weak simulated extratropical responses to complete tropical deforestation". In: *Journal of Climate* 19.12, pp. 2835–2850.

Flerchinger, Gerald N et al. (2015). "Modeling temperature and humidity profiles within forest canopies". In: *Agricultural and Forest Meteorology* 213, pp. 251–262.

GCOS (n.d.). *Global Climate Observing System (GCOS)*. URL: https://gcos.wmo.int/en/home. (accessed: 05.05.2020).

Gentine, P et al. (2016). "Evaporation estimates using weather station data and boundary layer theory". In: *Geophysical Research Letters* 43.22, pp. 11–661.

Gentine, Pierre et al. (Oct. 2019). "Land–atmosphere interactions in the tropics – a review". In: *Hydrology and Earth System Sciences* 23.10, pp. 4171–4197. DOI: 10.5194/hess-23-4171-2019. URL: https://doi.org/10.5194/hess-23-4171-2019.

Good, Elizabeth (2015). "Daily minimum and maximum surface air temperatures from geostationary satellite data". In: *Journal of Geophysical Research: Atmospheres* 120.6, pp. 2306–2324.

Good, Elizabeth J et al. (2017). "A spatiotemporal analysis of the relationship between near-surface air temperature and satellite land surface temperatures using 17 years of data from the ATSR series". In: *Journal of Geophysical Research: Atmospheres* 122.17, pp. 9185–9210.

Green, Julia K. et al. (May 2017). "Regionally strong feedbacks between the atmosphere and terrestrial biosphere". In: *Nature Geoscience* 10.6, pp. 410–414. DOI: 10.1038/ngeo2957. URL: https://doi.org/10.1038/ngeo2957.

Guo, Zhichang et al. (2006). "GLACE: the global land–atmosphere coupling experiment. Part II: analysis". In: *Journal of Hydrometeorology* 7.4, pp. 611–625.

Haniff, MH et al. (2018). "Influence of eddy covariance sensor height above the oil palm canopy on CO2 and energy fluxes." In: *Journal of Oil Palm Research* 30.1, pp. 94–100.

Hargreaves, George H and Zohrab A Samani (1985). "Reference crop evapotranspiration from temperature". In: *Applied engineering in agriculture* 1.2, pp. 96–99.

Hartmann, Dennis L and David A Short (1980). "On the use of earth radiation budget statistics for studies of clouds and climate". In: *Journal of Atmospheric Sciences* 37.6, pp. 1233–1250.

Hassan, Gasser E et al. (2016). "New temperature-based models for predicting global solar radiation". In: *Applied energy* 179, pp. 437–450.

Ho, Hung Chak et al. (2014). "Mapping maximum urban air temperature on hot summer days". In: *Remote Sensing of Environment* 154, pp. 38–45.

Hoffmann, Lars et al. (2019). "From ERA-Interim to ERA5: the considerable impact of ECMWF's next-generation reanalysis on Lagrangian transport simulations". In: *Atmospheric Chemistry and Physics* 19.5, pp. 3097–3124.

Horst, Sophie VJ van der et al. (2019). "How representative are FLUXNET measurements of surface fluxes during temperature extremes?" In: *Biogeosciences* 16.8, pp. 1829–1844.

Huete, A, C Justice, and H Liu (1994). "Development of vegetation and soil indices for MODIS-EOS". In: *Remote Sensing of environment* 49.3, pp. 224–234.

Irvine, Peter J, Andy Ridgwell, and Daniel J Lunt (2011). "Climatic effects of surface albedo geoengineering". In: *Journal of Geophysical Research: Atmospheres* 116.D24.

Jackson, Ray D, Sherwood B Idso, and J Otterman (1975). "Surface albedo and desertification". In: *Science* 189.4207, pp. 1012–1015.

Jackson, Robert B et al. (2008). "Protecting climate with forests". In: *Environmental Research Letters* 3.4, p. 044006.

Jackson, Thomas J et al. (1999). "Soil moisture mapping at regional scales using microwave radiometry: The Southern Great Plains Hydrology Experiment". In: *IEEE transactions on geoscience and remote sensing* 37.5, pp. 2136–2151.

Janatian, Nasime et al. (2017). "A statistical framework for estimating air temperature using MODIS land surface temperature data". In: *International Journal of Climatology* 37.3, pp. 1181–1194.

Jang, J-D, AA Viau, and F Anctil (2004). "Neural network estimation of air temperatures from AVHRR data". In: *International Journal of Remote Sensing* 25.21, pp. 4541–4554.

Jin, Menglin and Robert E Dickinson (2010). "Land surface skin temperature climatology: Benefitting from the strengths of satellite observations". In: *Environmental Research Letters* 5.4, p. 044004.

Jin, Menglin and Shunlin Liang (2006). "An improved land surface emissivity parameter for land surface models using global remote sensing observations". In: *Journal of Climate* 19.12, pp. 2867–2881.

Juang, Jehn-Yih et al. (2007). "Separating the effects of albedo from eco-physiological changes on surface temperature along a successional chronosequence in the southeastern United States". In: *Geophysical Research Letters* 34.21.

Kalma, Jetse D, Tim R McVicar, and Matthew F McCabe (2008). "Estimating land surface evaporation: A review of methods using remotely sensed surface temperature data". In: *Surveys in Geophysics* 29.4-5, pp. 421–469.

Kan, Haidong et al. (2007). "Diurnal temperature range and daily mortality in Shanghai, China". In: *Environmental research* 103.3, pp. 424–431.

Karl, Thomas R et al. (1991). "Global warming: Evidence for asymmetric diurnal temperature change". In: *Geophysical Research Letters* 18.12, pp. 2253–2256.

Kawashima, Shigeto et al. (2000). "Relations between surface temperature and air temperature on a local scale during winter nights". In: *Journal of Applied Meteorology and Climatology* 39.9, pp. 1570–1579.

Kleidon, Axel and Martin Heimann (1998). "A method of determining rooting depth from a terrestrial biosphere model and its impacts on the global water and carbon cycle". In: *Global Change Biology* 4.3, pp. 275–286.

Kleidon, Axel and Maik Renner (2017). "An explanation for the different climate sensitivities of land and ocean surfaces based on the diurnal cycle". In: *Earth System Dynamics* 8.3, pp. 849–864.

Kleidon, Axel and Martin Heimann (2000). "Assessing the role of deep rooted vegetation in the climate system with model simulations: mechanism, comparison to observations and implications for Amazonian deforestation". In: *Climate Dynamics* 16.2-3, pp. 183–199.

Kloog, Itai et al. (2014). "Predicting spatiotemporal mean air temperature using MODIS satellite surface temperature measurements across the Northeastern USA". In: *Remote sensing of environment* 150, pp. 132–139.

Koster, Randal D et al. (2006). "GLACE: the global land–atmosphere coupling experiment. Part I: overview". In: *Journal of Hydrometeorology* 7.4, pp. 590–610.

Krayenhoff, E Scott and James A Voogt (2010). "Impacts of urban albedo increase on local air temperature at daily–annual time scales: Model results and synthesis of previous work". In: *Journal of Applied Meteorology and Climatology* 49.8, pp. 1634–1648.

Kustas, William P and John M Norman (1999). "Evaluation of soil and vegetation heat flux predictions using a simple two-source model with radiometric temperatures for partial canopy cover". In: *Agricultural and Forest Meteorology* 94.1, pp. 13–29.

Kustas, WP and JM Norman (1996). "Use of remote sensing for evapotranspiration monitoring over land surfaces". In: *Hydrological Sciences Journal* 41.4, pp. 495–516.

Lambin, E F and D Ehrlich (1996). "The surface temperature-vegetation index space for land cover and land-cover change analysis". In: *International journal of remote sensing* 17.3, pp. 463–487.

Law, BE et al. (2002). "Environmental controls over carbon dioxide and water vapor exchange of terrestrial vegetation". In: *Agricultural and Forest Meteorology* 113.1-4, pp. 97–120.

Lawrence, Peter J et al. (2012). "Simulating the biogeochemical and biogeophysical impacts of transient land cover change and wood harvest in the Community Climate System Model (CCSM4) from 1850 to 2100". In: *Journal of Climate* 25.9, pp. 3071–3095.

Lee, Whan-Hee et al. (2017). "An investigation on attributes of ambient temperature and diurnal temperature range on mortality in five East-Asian Countries". In: *Scientific reports* 7.1, pp. 1–9.

Lee, Xuhui (1998). "On micrometeorological observations of surface-air exchange over tall vegetation". In: *Agricultural and Forest Meteorology* 91.1-2, pp. 39–49.

Lee, Xuhui and T Andrew Black (1993). "Atmospheric turbulence within and above a Douglas-fir stand. Part II: Eddy fluxes of sensible heat and water vapour". In: *Boundary-Layer Meteorology* 64.4, pp. 369–389.

Lejeune, Quentin, Sonia I Seneviratne, and Edouard L Davin (2017). "Historical land-cover change impacts on climate: Comparative assessment of LUCID and CMIP5 multimodel experiments". In: *Journal of Climate* 30.4, pp. 1439–1459.

Li, Xing et al. (2018). "Inconsistent responses of hot extremes to historical land use and cover change among the selected CMIP5 models". In: *Journal of Geophysical Research: Atmospheres* 123.7, pp. 3497–3512.

Li, Yan et al. (2015). "Local cooling and warming effects of forests based on satellite observations". In: *Nature communications* 6.1, pp. 1–8.

Li, Zhao-Liang et al. (2013). "Satellite-derived land surface temperature: Current status and perspectives". In: *Remote sensing of environment* 131, pp. 14–37.

Lobell, David B (2007). "Changes in diurnal temperature range and national cereal yields". In: *Agricultural and forest meteorology* 145.3-4, pp. 229–238.

Lobell, DB, G Bala, and PB Duffy (2006). "Biogeophysical impacts of cropland management changes on climate". In: *Geophysical Research Letters* 33.6.

Longobardi, Patrick et al. (2016). "Deforestation induced climate change: effects of spatial scale". In: *PloS one* 11.4, e0153357.

Loveland, Thomas R et al. (1999). "An analysis of the IGBP global land-cover characterization process". In: *Photogrammetric engineering and remote sensing* 65, pp. 1021–1032.

Lutz, David A and Richard B Howarth (2014). "Valuing albedo as an ecosystem service: implications for forest management". In: *Climatic change* 124.1, pp. 53–63.

Luyssaert, Sebastiaan et al. (2014). "Land management and land-cover change have impacts of similar magnitude on surface temperature". In: *Nature Climate Change* 4.5, pp. 389–393.

Mahmood, Rezaul et al. (2014). "Land cover changes and their biogeophysical effects on climate". In: *International journal of climatology* 34.4, pp. 929–953.

Mallick, Kaniska et al. (2016). "Canopy-scale biophysical controls of transpiration and evaporation in the Amazon Basin". In: *Hydrology and Earth System Sciences* 20.10, pp. 4237–4264.

McBean, Gordon A et al. (1979). "The planetary boundary layer". In: *WMO Technical Note-WMO*.

Mildrexler, David J, Maosheng Zhao, and Steven W Running (2011). "A global comparison between station air temperatures and MODIS land surface temperatures reveals the cooling role of forests". In: *Journal of Geophysical Research: Biogeosciences* 116.G3.

Monteith, JL (1972). "Latent heat of vaporization in thermal physiology". In: *Nature New Biology* 236.64, pp. 96–96.

Morrison, Travis et al. (2021). "The impact of surface temperature heterogeneity on near-surface heat transport". In: *Boundary-Layer Meteorology*, pp. 1–26.

Mu, Qiaozhen et al. (2007). "Development of a global evapotranspiration algorithm based on MODIS and global meteorology data". In: *Remote sensing of Environment* 111.4, pp. 519–536.

Nepstad, Daniel C et al. (1994). "The role of deep roots in the hydrological and carbon cycles of Amazonian forests and pastures". In: *Nature* 372.6507, pp. 666–669.

Nicholls, Neville (1997). "Increased Australian wheat yield due to recent climate trends". In: *Nature* 387.6632, pp. 484–485.

Noblet-Ducoudré, Nathalie de et al. (2012). "Determining robust impacts of land-use-induced land cover changes on surface climate over North America and Eurasia: Results from the first set of LUCID experiments". In: *Journal of Climate* 25.9, pp. 3261–3281.

Oleson, Keith W et al. (2010). "Technical description of version 4.0 of the Community Land Model (CLM)". In.

Olson, RJ et al. (2004). *FLUXNET. Database of fluxes, site characteristics, and flux-community information*. Tech. rep. Oak Ridge National Lab.(ORNL), Oak Ridge, TN (United States).

Oyler, Jared W et al. (2016). "Remotely sensed land skin temperature as a spatial predictor of air temperature across the conterminous United States". In: *Journal of Applied Meteorology and Climatology* 55.7, pp. 1441–1457.

Panwar, Annu and Axel Kleidon (2022). "Evaluating the response of diurnal variations in surface and air temperature to evaporative conditions across vegetation types in FLUXNET and ERA5". In: *Journal of Climate* 35.19, pp. 2701–2728.

Panwar, Annu, Axel Kleidon, and Maik Renner (2019). "Do surface and air temperatures contain similar imprints of evaporative conditions?" In: *Geophysical Research Letters* 46.7, pp. 3802–3809.

Panwar, Annu, Maik Renner, and Axel Kleidon (2020). "Imprints of evaporative conditions and vegetation type in diurnal temperature variations". In: *Hydrology and Earth System Sciences* 24.10, pp. 4923–4942.

Parker, Wendy S (2016). "Reanalyses and observations: What's the difference?" In: *Bulletin of the American Meteorological Society* 97.9, pp. 1565–1572.

Pastorello, Gilberto et al. (July 2020). "The FLUXNET2015 dataset and the ONEFlux processing pipeline for eddy covariance data". In: *Scientific Data* 7.1, p. 225. ISSN: 2052-4463. DOI: 10.1038/s41597-020-0534-3. URL: https://doi.org/10.1038/s41597-020-0534-3.

Pauluis, Olivier and Isaac M Held (2002). "Entropy budget of an atmosphere in radiative–convective equilibrium. Part II: Latent heat transport and moist processes". In: *Journal of Atmospheric Sciences* 59.2, pp. 140–149.

Pecl, Gretta T et al. (2017). "Biodiversity redistribution under climate change: Impacts on ecosystems and human well-being". In: *Science* 355.6332.

Philip, Rich and Kim Novick (2016). *AmeriFlux US-MMS Morgan Monroe State Forest*. Tech. rep. Lawrence Berkeley National Lab.(LBNL), Berkeley, CA (United States . . .

Pitman, AJ et al. (2012). "Effects of land cover change on temperature and rainfall extremes in multi-model ensemble simulations". In: *Earth System Dynamics* 3.2, pp. 213–231.

Pitman, Andrew J et al. (2009). "Uncertainties in climate responses to past land cover change: First results from the LUCID intercomparison study". In: *Geophysical Research Letters* 36.14.

Pongratz, Julia et al. (2010). "Biogeophysical versus biogeochemical climate response to historical anthropogenic land cover change". In: *Geophysical Research Letters* 37.8.

Prescott, JA and Joyce A Collins (1951). "The lag of temperature behind solar radiation". In: *Quarterly Journal of the Royal Meteorological Society* 77.331, pp. 121–126.

Prihodko, Lara and Samuel N Goward (1997). "Estimation of air temperature from remotely sensed surface observations". In: *Remote Sensing of Environment* 60.3, pp. 335–346.

Pulliainen, Jouni T, Jochen Grandell, and Martti T Hallikainen (1997). "Retrieval of surface temperature in boreal forest zone from SSM/I data". In: *IEEE Transactions on Geoscience and Remote Sensing* 35.5, pp. 1188–1200.

Rigor, Ignatius G, Roger L Colony, and Seelye Martin (2000). "Variations in surface air temperature observations in the Arctic, 1979–97". In: *Journal of Climate* 13.5, pp. 896–914.

Roberts, John, Osvaldo MR Cabral, and Leandro Ferreira De Aguiar (1990). "Stomatal and boundary-layer conductances in an Amazonian terra firme rain forest". In: *Journal of Applied Ecology*, pp. 336–353.

Sailor, David J (1995). "Simulated urban climate response to modifications in surface albedo and vegetative cover". In: *Journal of Applied Meteorology and Climatology* 34.7, pp. 1694–1704.

Sandeep, A et al. (2014). "Differences in atmospheric boundary-layer characteristics between wet and dry episodes of the Indian summer monsoon". In: *Boundary-layer meteorology* 153.2, pp. 217–236.

Santanello Jr, Joseph A and Mark A Friedl (2003). "Diurnal covariation in soil heat flux and net radiation". In: *Journal of Applied Meteorology* 42.6, pp. 851–862.

Santanello Jr, Joseph A, Mark A Friedl, and William P Kustas (2005). "An empirical investigation of convective planetary boundary layer evolution and its relationship with the land surface". In: *Journal of Applied Meteorology* 44.6, pp. 917–932.

Santanello Jr, Joseph A et al. (2009). "A modeling and observational framework for diagnosing local land–atmosphere coupling on diurnal time scales". In: *Journal of Hydrometeorology* 10.3, pp. 577–599.

Saunders, Peter M (1967). "Aerial measurement of sea surface temperature in the infrared". In: *Journal of Geophysical Research* 72.16, pp. 4109–4117.

Schultz, Natalie M, Peter J Lawrence, and Xuhui Lee (2017). "Global satellite data highlights the diurnal asymmetry of the surface temperature response to deforestation". In: *Journal of Geophysical Research: Biogeosciences* 122.4, pp. 903–917.

Sebastien, Biraud (2016). *US-ARM*. URL: http://www.arm.gov/sites/sgp. (accessed: 05.05.2020).

Sheil, Douglas and Daniel Murdiyarso (2009). "How forests attract rain: an examination of a new hypothesis". In: *Bioscience* 59.4, pp. 341–347.

Shukla, Jagadish, Carlos Nobre, and Piers Sellers (1990). "Amazon deforestation and climate change". In: *Science* 247.4948, pp. 1322–1325.

Shukla, Jagdish and Yale Mintz (1982). "Influence of land-surface evapotranspiration on the earth's climate". In: *Science* 215.4539, pp. 1498–1501.

Stephens, Graeme L et al. (2012). "An update on Earth's energy balance in light of the latest global observations". In: *Nature Geoscience* 5.10, pp. 691–696.

Stewart, John B et al. (1994). "Sensible heat flux-radiometric surface temperature relationship for eight semiarid areas". In: *Journal of Applied Meteorology and Climatology* 33.9, pp. 1110–1117.

Stoll, Matthew J and Anthony J Brazel (1992). "Surface-air temperature relationships in the urban environment of Phoenix, Arizona". In: *Physical Geography* 13.2, pp. 160–179.

Stull, Roland B (1988). *An introduction to boundary layer meteorology*. Vol. 13. Springer Science & Business Media.

Su, Zhongbo (2002). "The Surface Energy Balance System (SEBS) for estimation of turbulent heat fluxes". In: *Hydrology and earth system sciences* 6.1, pp. 85–100.

Sugita, Michiaki and Wilfried Brutsaert (1991). "Daily evaporation over a region from lower boundary layer profiles measured with radiosondes". In: *Water Resources Research* 27.5, pp. 747–752.

Sun, Y-J et al. (2005). "Air temperature retrieval from remote sensing data based on thermodynamics". In: *Theoretical and applied climatology* 80.1, pp. 37–48.

Takagi, Kentaro, Taro Tsuboya, and Hidenori Takahashi (1998). "Diurnal hystereses of stomatal and bulk surface conductances in relation to vapor pressure deficit in a cool-temperate wetland". In: *Agricultural and Forest Meteorology* 91.3-4, pp. 177–191.

Tan, Zheng-Hong et al. (2019). "Surface conductance for evapotranspiration of tropical forests: Calculations, variations, and controls". In: *Agricultural and Forest Meteorology* 275, pp. 317–328.

Tang, Bijian, Xiang Zhao, and Wenqian Zhao (2018). "Local effects of forests on temperatures across Europe". In: *Remote Sensing* 10.4, p. 529.

Teuling, Adriaan J et al. (2010). "Contrasting response of European forest and grassland energy exchange to heatwaves". In: *Nature geoscience* 3.10, pp. 722–727.

Tomlinson, Charlie J et al. (2011). "Remote sensing land surface temperature for meteorology and climatology: A review". In: *Meteorological Applications* 18.3, pp. 296–306.

Träumner, K et al. (2011). "Convective boundary-layer entrainment: Short review and progress using Doppler lidar". In: *Boundary-layer meteorology* 141.3, pp. 369–391.

Trebs, Ivonne et al. (2015). "Stomatal and Aerodynamic Controls of Transpiration and Evaporation over Amazonian Landscapes". In: *AGU Fall Meeting Abstracts*. Vol. 2015, H31A–1405.

Trenberth, Kevin E, John T Fasullo, and Jeffrey Kiehl (2009). "Earth's global energy budget". In: *Bulletin of the American Meteorological Society* 90.3, pp. 311–324.

Turner, DD, EJ Mlawer, and HE Revercomb (2016). "Water vapor observations in the ARM Program". In: *Meteorological Monographs* 57, pp. 13–1.

Vancutsem, Christelle et al. (2010). "Evaluation of MODIS land surface temperature data to estimate air temperature in different ecosystems over Africa". In: *Remote Sensing of Environment* 114.2, pp. 449–465.

Wang, Jinfeng et al. (2018). "Global land surface air temperature dynamics since 1880". In: *International Journal of Climatology* 38, e466–e474.

Wang, Kaicun and Robert E Dickinson (2013). "Global atmospheric downward longwave radiation at the surface from ground-based observations, satellite retrievals, and reanalyses". In: *Reviews of Geophysics* 51.2, pp. 150–185.

Wang, XY and KC Wang (2014). "Estimation of atmospheric mixing layer height from radiosonde data". In: *Atmospheric Measurement Techniques* 7.6, pp. 1701–1709.

Wickham, James D, Timothy G Wade, and Kurt H Riitters (2013). "Empirical analysis of the influence of forest extent on annual and seasonal surface temperatures for the continental U nited S tates". In: *Global Ecology and Biogeography* 22.5, pp. 620–629.

Wilber, Anne C (1999). *Surface emissivity maps for use in satellite retrievals of longwave radiation*. NASA.

Winckler, Johannes et al. (2019). "Different response of surface temperature and air temperature to deforestation in a climate model". In: *Earth System Dynamics* 10, pp. 473–484.

WMO (2020). "State of the Global Climate 2020". In: WMO- No. 1264. URL: https://gcos.wmo.int/en/global-climate-indicators.

Xu, Liukang, Dennis D Baldocchi, and Jianwu Tang (2004). "How soil moisture, rain pulses, and growth alter the response of ecosystem respiration to temperature". In: *Global Biogeochemical Cycles* 18.4.

Yi, Yu-jun et al. (2018). "The influence of climate change on an endangered riparian plant species: The root of riparian Homonoia". In: *Ecological Indicators* 92, pp. 40–50.

Zhang, Quan et al. (2020). "Reforestation and surface cooling in temperate zones: mechanisms and implications". In: *Global change biology* 26.6, pp. 3384–3401.

Zhang, Renhua et al. (2015). "A remote sensing method for estimating surface air temperature and surface vapor pressure on a regional scale". In: *Remote Sensing* 7.5, pp. 6005–6025.

Zhang, Wen et al. (2011). "Empirical models for estimating daily maximum, minimum and mean air temperatures with MODIS land surface temperatures". In: *International Journal of Remote Sensing* 32.24, pp. 9415–9440.

Zhu, Wenbin, Aifeng Lǚ, and Shaofeng Jia (2013). "Estimation of daily maximum and minimum air temperature using MODIS land surface temperature products". In: *Remote Sensing of Environment* 130, pp. 62–73.

# Declaration of authorship

**Declaration of authorship and copyright in a cumulative doctoral thesis**

Reprint permissions have been obtained for all manuscripts used as part of the doctoral thesis.

The co-authors of the manuscripts used in the present cumulative doctoral thesis have been informed about the use of the manuscripts and about the declared individual contributions; they have given their consent. The declared individual contributions of the doctoral candidate and the other participate as co-authors in the publications are listed in this chapter.

Jena, 28.05.2021
Place, Date

_____
Annu Panwar

I give my consent to the submission of a cumulative doctoral thesis and confirm the correctness of the information provided above.

Jena, 2.6.21
Place, Date

_____
Prof. Dr. Christiane Schmuillius

Jena, 28.05.2021
Place, Date

_____
PD Dr. Axel Kliedon

**Publication 1**

Citation: Panwar, Kleidon, and Renner, 2019 :

Panwar Annu, Axel Kleidon, and Maik Renner (2019). "Do surface and air temperatures contain similar imprints of evaporative conditions?" In: Geophysical Research Letters 46.7, pp.3802-3809 .URL: `https://doi.org/10.1029/2019GL082248`

| Involved in | Panwar Annu | Maik Renner | Axel Kleidon |
|---|---|---|---|
| **Conceptual research design** | ✓ | ✓ | ✓ |
| **Data collection** | ✓ | | |
| **Data analysis** | ✓ | | |
| **Manuscript writing** | ✓ | | |
| **Final interpretations and inputs** | ✓ | ✓ | ✓ |
| **Suggested publication equivalence value** | 1 | n.a. | n.a. |

All authors conceived the study. Axel Kleidon and Maik Renner developed the concept of temperature and solar radiation hysteresis. Annu Panwar identified the index warming rate, and its relation to evaporative fraction. Annu Panwar did the data analysis. Annu Panwar built the hypothesis of boundary layer dynamics and air temperature relationship. Annu Panwar conducted the experiment using the simple boundary layer model developed by Axel Kleidon. Annu Panwar wrote the paper with inputs from Maik Renner and Axel Kleidon.

**Publication 2**

Citation: Panwar, Renner, and Kleidon, 2020 :

Panwar Annu, Maik Renner, and Axel Kleidon (2020). "Imprints of evaporative conditions and vegetation type in diurnal temperature variations". In: Hydrology and Earth System Sciences 24.10, pp. 4923-4942.URL: `https://doi.org/10.5194/hess-24-4923-2020`

| Involved in | Annu Panwar | Maik Renner | Axel Kleidon |
|:---:|:---:|:---:|:---:|
| Conceptual research design | ✓ | ✓ | ✓ |
| Data collection | ✓ | ✓ | |
| Data analysis | ✓ | | |
| Manuscript writing | ✓ | | |
| Final interpretations and inputs | ✓ | ✓ | ✓ |
| Suggested publication equivalence value | 1 | n.a. | n.a. |

All authors conceived the study. Annu Panwar analyzed data, and Axel Kleidon derived the energy-balance model that was further developed by Annu Panwar. Maik Renner provided classification of cloud-free conditions. All authors interpreted the results. Annu Panwar wrote the paper with input from Maik Renner and Axel Kleidon.

## Publication 3

Citation: Panwar and Kleidon, 2022 :

Panwar, A., Kleidon, A. (2022). Evaluating the response of diurnal variations in surface and air temperature to evaporative conditions across vegetation types in FLUXNET and ERA5. Journal of Climate, 35(19), 2701-2728.

| Involved in | Annu Panwar | Axel Kleidon |
|:---:|:---:|:---:|
| Conceptual research design | ✓ | ✓ |
| Data collection | ✓ | |
| Data analysis | ✓ | |
| Manuscript writing | ✓ | |
| Final interpretations and inputs | ✓ | ✓ |
| Suggested publication equivalence value | 1 | n.a. |

All authors conceived the study. Annu Panwar analyzed the data. Annu Panwar developed SSEB model. Axel Kleidon added maximum power approach in SABL model. All authors interpreted the results. Annu Panwar wrote the paper with inputs from Axel Kleidon.

# Selbständigkeitserklärung

Ich erkläre, dass ich die vorliegende Arbeit selbständig und unter Verwendung der angegebenen Hilfsmittel, persönlichen Mitteilungen und Quellen angefertigt habe.

Jena, 02·06·2021

Place, Date

Annu Panwar